LASER INDUCED PHOTOCATALYTIC APPLICATIONS OF NANOSCALE MATERIALS FOR DEGRADATION OF DYES AND PHENOL

BY

KHIZAR HAYAT

A Dissertation Presented to the

DEANSHIP OF GRADUATE STUDIES

KING FAHD UNIVERSITY OF PETROLEUM & MINERALS

DHAHRAN, SAUDI ARABIA

In Partial Fulfillment of the

Requirements for the Degree of

DOCTOR OF PHILOSOPHY

In

CHEMISTRY

January, 2011

KING FAHD UNIVERSITY OF PETROLEUM & MINERALS
DHAHRAN 31261, SAUDI ARABIA
DEANSHIP OF GRADUATE STUDIES

This thesis, written by **KHIZAR HAYAT** under the direction of his thesis advisor and approved by his thesis committee, has been presented to and accepted by the Dean of Graduate Studies, in partial fulfillment of the requirements for the degree of

DOCTOR OF PHILOSOPHY IN CHEMISTRY.

Thesis Committee

Dr. Mazen M.Khaled Chairman

Dr. M.A.Gondal Co-Chairman

Dr. A. M. Abulkibash
(Member)

Dr. B. El Ali
(Member)

Dr. Shakeel Ahmed
(Member)

Dr. Abdullah J. Al-Hamdan
Department Chairman

Dr. Salam S. Zummo
Dean of Graduate Studies

15/1/11
[Date]

DEDICATED TO

MY PARENTS

BROTHERS, SISTER

WIFE, DAUGHTER AND SON

Acknowledgement

In the name of Allah who alone is the Most Beneficent and the Most Merciful. First and foremost thanks to Allah who gave me strength, patience and ability to accomplish this research. Praise and blessings be upon the last Prophet SAW, his family and noble companions.

I wish to express my appreciation to Associate Professor Dr. Mazen Mohammad Khaled and Professor Dr. Mohammad Ashraf Gondal, who served as my major advisor and co-advisor, for their guidance, patience, continuous, unforgettable support and encouragement through the Ph.D. Dissertation. I would like to thank Professor Dr.Abdulla Abulkibash, Professor Dr. Bassam El Ali, and Dr. Shakeel Amhed for their help, suggestions and valuable comments. Thanks are also due to the Chairman of Chemistry Department Dr. Abdullah Al-Hamdan for providing all the available facilities.

I am also grateful to all faculty members for their encouragement and their direct or indirect help. I also acknowledge their assistance to complete this work. I would like to pay my special thanks and wishes to Dr. Ahsan M.Shemsi., Dr. Atif Fazal, Monim-ul-Mehboob, Tawfik A.S., Muhammad Jamal Khan, Muhammad Sabeeh, Izzat Qazi, Kashif Hussain, Asif Siddique, Dr. M. Qamar, Khurram Masood, Haider, Walliuddin Farooqi, Aiman, Bahauddin, M. Dastgeer, Arab, Inayat, Arif, M. Saleem, and all other staff members and Friends for their help, efforts and encouragement during whole period of my study. I am also thankful to all staff members, all of my friends and colleagues for their help and support.

I would like to pay my special thanks to Dr.Shafique Ahmed Awan, Dr. Abdul Khalique, and Zafar Iqbal and all other colleagues and Friends in Pakistan who helped me directly or indirectlyduring my studies.

I offer my sincere thanks to the KACST for helping me in FESEM and TEM of our synthesized nanomaterials. Acknowledgment is due to the King Fahd University of Petroleum & Minerals for supporting this research. The support and assistanship by King Fahd University of Petroleum and Minerals (KFUPM) under Center of Excellence in Nanotechnology is gratefully acknowledged.

I am always grateful to my mother and family members for their moral support, encouragement and prayers without which this research work would not have been possible. Thanks to my wife, daughter (Jawaria) and son (Muhammad Omar Farooq) for their love and help during my Ph.D.studies.

TABLE OF CONTENTS

LIST OF TABLES

LIST OF FIGURES

Ph.D. Dissertation Abstract

Name: Khizar Hayat
Title: Laser Induced Photocatalytic Applications of nanoscale materials for degradation of dyes and phenol

Major Field: Chemistry
Date of Degree: October, 2010

This Ph.D. dissertation deals with the photocatalytic degradation of toxic dyes and phenol in aqueous suspension of pure and doped semiconductor metal oxides. The nanoparticles such as Pure $WO_{3,}$ ZnO and NiO were synthesized by precipitation and sol gel while noble metal doped semiconductor oxides were prepared using wet incipient impregnation method. The synthesized nanomaterials were characterized by high-resolution transmission electron microscopy (HRTEM), field emission scanning electron microscopy (FESEM) and X-ray diffraction (XRD). These studies revealed that the synthesized metal oxide nanoparticles were having the range of 7 to 50 nm. The nano-catalysts were applied for removal of carcinogenic organic pollutants (phenol and dyes). The effect of different experimental parameters like calcination temperature, dopants content, laser energy, catalyst concentration, pH and exposure time on photo-catalytic removal of dyes and phenol from aqueous solutions was investigated. The experimental results demonstrated that various parameters mentioned above have strong influence on the photocatalytic degradation process of dyes and phenol. The reaction kinetics for these degradation processes was also discussed.

ملخص الرسالة

الاســـــــــم: **خضر حيات**

عنوان الرسالة: **التحفيز الضوئي المحفز بالليزر وتطبيقات المواد النانوية المحفزة لتفكيك الاصباغ والفينول**

التخصـــــص: **كيمياء**

تاريخ التخـرج: **اكتوبر 2010**

تتناول هذه الدراسة إنتاج المواد النانوية النقية والملقحة باستخدام طرق كيميائية ثم توصيفها وتطبيقاتها. المواد النانوية مثل اكاسيد الزنك و اكاسيد النيكل و اكاسيد التنجستن انتجت خلال الدراسة بواسطة طرق الترسيب. هذه المحفزات اشباه الموصلات تم تلقيحها بطريقة التلقيح أو الاشباع الكيميائية في أوساط سائلة. تأثير الظروف التفاعلية المختلفة مثل درجة الحرارة على حجم المواد المنتجة تم دراسته. تركيب وشكل المواد المنتجة تم توصيفه باستخدام ميكرسكوب الانتقالات الالكترونية عالي الدقة وجهاز ميكرسكوب الفحص الالكتروني وجهاز تشتت اشعة اكس. اوضحت النتائج ان حجم المواد النانوية المنتجة تتراوح ما بين 7 الى 50 نانو متر.هذه النتائج تتفق مع معدل حجم المواد كما تم قياسه باشعة اكس وحسابة باستخدام معادلة شرر .

تم تطبيق فعالية هذه المواد كمواد حفازة واستخدامها في تفكيك مواد ملوثة سامة مثل محاليل الاصباغ والفينول تحت اشعة الليزر. تمت دراسة تاثير متغيرات عملية متعددة مثل درجة الحرارة وكمية المواد المستخدمة للتلقيح وطاقة الليزر وتركيز او كمية الحفازات ودرجة حموضة المحاليل وزمن التعريض على معدل التفكيك . اوضحت النتائج ان الليزر حفز عملية التفكيك وبينت ان الطريقة فعالة جدا. تمت دراسة ميكانيكية التفكيك ايضا واوضحت النتائج ان متغيرات مثل درجة الحموضة والمواد المؤكسدة ودرجة الحرارة تلعب دورا هاما في التفكيك. كل هذه العوامل تمت دراستها ودراسة تاثيرها على التفكيك الضوئي للاصباغ في المحاليل بتراكيز مختلفة.

CHAPTER 1

INTRODUCTION

Water is used in agriculture, construction, transport, chemical industry, and in numerous other activities of the human beings. Most advanced industrialized nations in the world are faced with a tremendous set of environmental problems related to the remediation of hazardous wastes, contaminated groundwater and the control of toxic air contaminants [1]. According to the United Nations, the first priority of poor countries should not be financial support or technological knowledge but clean water supply to the population [2]. One of the most vital worldwide concerns is the current deterioration of the water supply due to economic and industrial growth. A diversity of refractory contaminants due to human activity, from heavy metals to emerging micropollutants is being identified in water in increasing numbers. Conventional methods for remediation of these pollutants [3] are aeration, extraction, filtration, reverse osmosis, ion exchange, absorption, biological treatment, chemical treatment, high-temperature incineration, evaporation, distillation, chlorination and ozonation. However, these methods have some disadvantages such as generation of intermediate products which requires further processing .The removal of these by products increases the overall cost of the process.

Various chemical oxidation techniques have emerged in the last decades, in particular for the treatment of industrial wastewaters to overcome the inconvenience of conventional treatment methods. Among these techniques, advanced oxidation processes (AOPs) appear to be a promising field of study which has been reported to be effective for

the degradation of soluble organic contaminants in waters and soils. Actually, they can often provide an almost total degradation under reasonably mild conditions of temperature and pressure [4–6]. AOPs leads to the complete mineralization of compounds, their oxidation at very low concentration, the generation of environmentally friendly byproducts and the low consumption of energy as compared to other conventional methods. These processes utilize chemical reactions, electron beams and UV light or ultrasound pulses to obtain high oxidation rates through the generation of free radicals (mainly hydroxyl radicals). Actually, highly reactive hydroxyl radicals ($HO^{\bullet}$) are thought to be the main active species responsible for the destruction of the pollutants [7–9].

Recently the research focus on photocatalysis has shifted to use nanosized particles. The main advantage is that nanoparticles exhibit novel properties that extensively differ from those of corresponding bulk solid state as a result of different behaviour in terms of small size, surface area, quantum size and macroscopic quantum tunnel effects [10]. In recent years, metal oxide nanoparticles have been extensively studied due to their novel optical, electronic, magnetic, thermal and mechanical properties and potential application in catalysis, gas sensors, photo-electronic devices [11, 12]. The high proportion of surface to bulk atoms in nanoscale materials greatly influences their properties. The very high surface area of nanoscale particles gives rise to a number of defect sites. The catalytic properties and the electronic structure of the nanomaterials can be tailored by changing the cluster size, composition and structure [13, 14].

The synthesis approach must fulfill good yields and high crystallinity as the main requirements. Nanoparticles could be obtained by two general approaches, `top down' and `bottom up'. In `top down' methods bulk metals are mechanically ground to the nanometer

size and stabilized by using a suitable stabilizer [15]. The problem with this method is difficulty in achieving the narrow size distribution and control over the shape of the particles. Moreover, bimetallic nanoparticles with core shell structures cannot be obtained by this method. In `bottom up' approach nanoparticles are obtained by starting with molecular precursors and building-up from nature's smallest building blocks like atoms and molecules. Precipitation and sol gel methods are related to bottom up approach. Sol–gel preparation of solid catalysts has been reported by many research groups since 1980 [16–20]. Within the broad family of functional materials, metal oxides are particularly attractive with respect to applications in catalysis, sensing, energy storage and conversion, optics, and electronics [21]. In contrast to high-temperature processes, sol–gel procedures offer advantages such as the possibility of obtaining metastable materials, achieving superior purity and compositional homogeneity of the products at moderate temperatures with simple laboratory equipment, and affecting the particle morphology during the chemical transformation of the molecular precursor to the final metal oxides [22].

In 1972, Fujishima and Honda [23] discovered that water can be photo catalytically split into O_2 and H_2 on TiO_2 electrodes. Application of the heterogeneous photocatalysis to environmental decontamination has been inspired by the TiO_2-based photocatalyst ability for the abatement of different classes of pollutants [24] and even inorganic ions [25]. Semiconductor photocatalysis is very promising to solve the environmental problems in the most economic way. Semiconductor photocatalysis utilizes only light and the pollutants are completely decomposed into CO_2, water and inorganic acids [26-28]. However, TiO_2 photocatalysis is limited for its widespread applications because of the

band gap of TiO_2 which absorbs light in UV region and the requirement of removal of TiO_2 catalysts after their applications in case of TiO_2 particles in suspension.

Semiconductors such as TiO_2, ZnO, Fe_2O_3, CdS, and ZnS can act as catalysts for light-induced redox processes due to their electronic structure, which is characterized by a filled valence band and an empty conduction band [29]. Zinc sulfide and cadmium sulfide are not good catalysts as they suffer from photocorrosion induced by self-oxidation [30]. The most commonly studied photocatalysts are TiO_2, ZnO, CdS, WO_3, ZnS, In_2O_3, Fe_3O_4 and $SrTiO_3$.

The general mechanism of photocatalysis is illustrated in Figure 1.1**.** In heterogeneous photocatalysis, photocatalysts capture photons with energies greater than the band gap energy of the semiconductor to create electron–hole pairs, subsequently, the charge carriers interact with water and oxygen to produce oxidizing intermediates as hydroxyl radicals ($OH^{\bullet}$) or $OH_2^{\bullet}$, $O_2^{\bullet}$, which have the ability to oxidize pollutants to an inorganic compound [31].

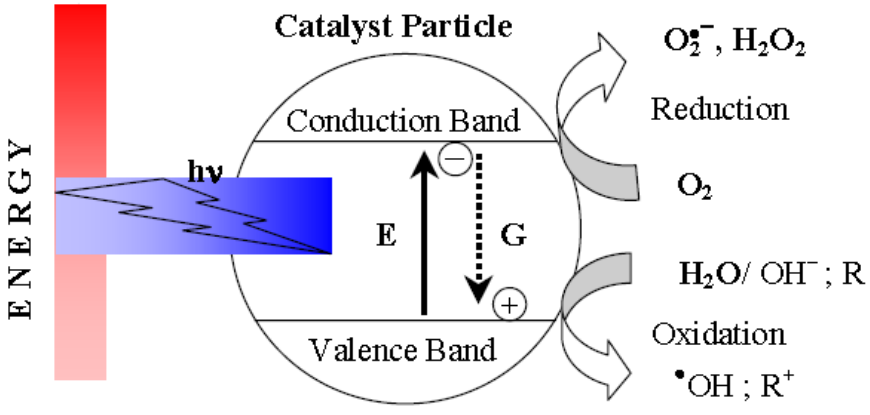

Figure 1.1 Schematic diagram of photocatalytic process initiated by photon acting on the semiconductor

When the semiconductors are photo excited with energy greater than their band gap energy (*E*g), electron and hole pairs are generated. These generated species can either recombine and dissipate the energy as heat or react with oxygen or water molecules as mentioned below:

$$SC + h\nu \longrightarrow SC\ (h^{+}_{vb}, e^{-}_{cb}) \longrightarrow \text{Recombination} \qquad (1)$$

$$O_2^{-} + H^{+} \longrightarrow HO_2 \qquad (2)$$

$$HO_2 + HO_2 \longrightarrow H_2O_2 + O_2 \qquad (3)$$

$$H_2O_2 + h\nu \longrightarrow 2OH^{\bullet} \qquad (4)$$

$$H_2O_2 + e^{-} \longrightarrow OH^{-} + OH^{\bullet} \qquad (5)$$

The $OH^{\bullet}$ radicals react with the adsorbed phenol forming the products CO_2 and H_2O [32-34] where the intermediate products such as catechol, hydroquinone, hydroxyhydroquinone and benzoquinone may be formed [35].

In this Ph.D. dissertation, an attempt was made to study the photocatalytic degradation of organic pollutants such as toxic dyes and phenol using nano sized semiconductor metal oxides e.g. WO_3, ZnO, NiO and noble metal doped metal oxides synthesized. Thirty four samples (undoped and noble metal doped metal oxides) were synthesized by these methods. The nanosized metal oxide and doped materials were

applied for removal of hazardous materials from the aqueous solutions using UV laser irradiation. Photocatalysis gradually breaks down the contaminant molecule, no wastes of the original material remain which reduce cost of the process tremendously. The catalyst itself is unchanged during the process and no consumable chemicals are required. The degradation of dyes and phenol at very low concentrations was achieved because the contaminant is attracted strongly to the surface of the catalyst. Innovative use of nanoparticles for treatment of polluted water is potentially a useful application.

The main challenge at present in photo-catalysis is to enhance the efficiency of photo- catalytic process, to prohibit the e_{cb}^{-}/h_{vb}^{+} recombination rate and to extend its light absorption ability to the visible spectral region. These challenges could be overcome by using the nano-scale semiconductors catalysts (ZnO, WO_3 etc.) and using special doped materials in conjunction with lasers. In Laser induced photo-catalytic process, the e_{cb}^{-}/h_{vb}^{+} recombination rate may be decreased. The photon energy, wavelength, photonic efficiency and delivery of photon to the reaction zone can be easily controlled using laser which is not possible with conventional setups like lamps. The efficient photo-reduction of different organic and inorganic pollutants inside water is highly desirable. Photo-catalytic removal of phenol and hazardous dyes was investigated. The influence of calcination temperature, laser irradiation time, catalyst concentration, substrate concentration and pH on the photodegradation of pollutants was also studied.

Most of the previous work on photo-catalysis has been carried out with micron size metal oxides by using lamps having emission over broad spectral ranges. As laser radiations have unique properties over the conventional light sources and at present the

commercial availability of tunable lasers in the visible range at moderate cost is possible, the use of lasers in heterogeneous photo-catalysis will be very attractive.

The aim of this study was to apply nanoparticles of metal oxide catalysts (WO_3, ZnO and NiO) in pure and doped form for treatment of polluted water with toxic organic compounds such as dyes and phenol. Nano metal oxides and doped materials were synthesized using the sol gel method .The surface modification of semiconductor metal oxides (WO_3, ZnO) was carried out by the addition of noble metals (Pt, Pd, Ag and Rh). The Incipient wetness impregnation method was used to synthesize the noble metal doped metal oxides. The morphology of the synthesized nanocrystalline metal oxides and transition metal doped oxides was investigated using various analytical techniques like XRD, FESEM and HRTEM. The photo catalytic activity of the synthesized nanomaterials was investigated for model pollutants i.e. Phocatalytic degradation of dyes, phocatalytic degradation of phenol.

The synthesized nanomaterials were applied to study the photocatalytic degradation of alizarin yellow GG, safranin O, methyl red and acid red 87, cyanosine dyes and phenol. The effect of different operational parameters on photocatalytic degradation of the dyes like calcination temperature, laser energy, and amount of photocatalyst, the initial dye concentration and pH was also studied. It was observed that under given experimental conditions, the photocatalytic degradation of investigated dyes exhibited pseudo first-order kinetics.

1.1. Overview of Dissertation

The Ph.D Dissertation consists of eight chapters.

The first chapter deals with the introduction of the advanced oxidation processes. The study of photocatalytic degradation of dyes and phenol using nano photocatalysts synthesized by the precipitation, sol gel and incipient wetness impregnation methods was also discussed.

The second chapter deals with the literature review regarding the synthesis of nanomaterials, heterogeneous photocatalysis and its applications on photocatalytic degradation of hazardous dyes and phenol. In addition, a review on the role of noble metals for surface modifications of semiconductor nanosized materials in photocatalysis for various processes is presented in this chapter 2.

All the experimental details regarding synthesis of nanopaticles using different methods such as precipitation sol gel and incipient wetness impregnation methods and procedure to test the photocatalytic activity of photocatalysts are presented in chapter 3.

The experimental techniques which are used for the characterization of nanomaterials and the results obtained for characterization of undoped and doped metal oxide photocatalysts are discussed in Chapter 4. Chapter 5 presents results on laser induced photocatalytic degradation of hazardous dyes using nanocrystalline WO_3, Nano ZnO and nano NiO and their discussion.

Chapter 6 describes the photoctalytic degradation of phenol by different nano photocatalysts like nano ZnO and nano NiO. Discussion regarding the photocatalytic activity after surface modification of nanosized metal oxides by noble metals is given in Chapter 7. The conclusions and future prospects of this study are discussed in chapter 8.

1.2. Objectives

The overall objective of this dissertation is to study the photocatalytic activity of novel nano-materials for environmental applications. However the specific objecticves are as follows:

- Synthesis of nano scale pure and transition metal doped metal oxides (WO_3, ZnO) using sol gel method locally and pretreatment of nanosized procured metal oxides for utilization in environmental cleanup.
- Characterization of the synthesized materials using SEM, XRD, TEM
- Development of an experimental setup for laser-based photo-catalytic process for removal of toxic pollutants such as hazardous dyes and phenol for waste water treatment.
- Study the effect of catalyst loading, laser energy, pH and exposure time
- Analysis of products by UV Visible spectro-photometry and High Performance Liquid Chromatography.

CHAPTER 2

LITERATURE REVIEW

2.1. Heterogeneous Photocatalysis

Studies in photocatalysis started in the early 1930s by the observation that the pigment “titanium white” (TiO_2) was responsible for fading and chalking in paints. [36-38].The first definition of photocatalysis was then given by Plotnikow who entitled every chemical reaction which was caused by light, a photocatalytic reaction [39]. The initial interest in the heterogeneous photocatalysis was started when Fujishima and Honda discovered the photochemical splitting of water into hydrogen and oxygen with TiO_2 in 1972 [23]. This exceptional discovery was the initial point for many investigations concerning heterogeneous photocatalysis.

Fueled by the first oil crisis in 1973, the interests in research were mainly focused on solar energy conversion into chemical or electrical energy. However, heterogeneous photocatalysis became also a rapidly expanding technology for water and air treatment. In 1976 degradation of environmentally harmful polychlorobiphenyls using semiconductor photocatalysis was discussed for the first time [40]. In the early 1980s, the oxidative photomineralization of pollutants using titanium dioxide and UV light was observed by Ollis et al. [41, 42]. They investigated mineralization of trichloroethylene, dichloromethane, chloroform and carbon tetrachloride using TiO_2.

Early studies were focused on the utilization of solar energy for the production of hydrogen as a clean fuel from water. However, various groups also found that illuminated semiconductor particles could catalyze a wide range of interesting and useful redox reactions of organic and inorganic substrates. In particular, such particles were found to completely decompose a variety of organic or inorganic compounds that were known as environmental pollutants. Thenceforth, extensive studies were initiated on the environmental applications of heterogeneous photocatalysis [43].

Serpone et al. [44] mentioned critically that many reactions which involve illuminated semiconductors belong to the class of photogenerated catalysis. Thereby a photochemical transformation of a substance is due to initial photon absorption of the photosensitizer. The general description of photocatalysis indicates that light and photocatalyst are necessary to influence the reaction. The research on photocatalysis changed from UV light to visible light absorbing materials. First Grätzel developed a photovoltaic system which uses visible light by the utilization of a dye sensitizer [45] Recently visible light sensitization was reached by modifying TiO_2 with various materials like $PtCl_6^{2-}$,[46] nitrogen or carbon[47-57]. During the last decade, practical applications of TiO_2 photo catalysts have been carried out in both indoor and outdoor environments. The photocatalytic activity of TiO_2 along with its excellent physicochemical properties has propelled the development of new technologies for environmental and other applications [58]. In recent years, it was found that the nano-material of the narrower band gap (such as ZnO, NiO, Fe_2O_3, and MnO_2) could be used to harvest the energy in the visible region [59].

When the semiconductor oxide photocatalyst is provided with sufficient energy (UV radiation with above the band gap, electrons and holes are generated in the

conduction and valence bands, respectively [60].Redox reactions at the catalytic surface involve the formation of superoxide radical anion ($O_2^{-\bullet}$) via the reduction of oxygen adsorbed at the catalytic sites and the formation of hydroxyl radicals ($^{\bullet}OH$) via the interaction of holes with surface hydroxyl groups. The hydroxyl radicals readily attack organic compounds to transform their molecular structure to simpler organics, then finally to carbon dioxide, water and other inorganic species.

Most of the earlier work on heterogeneous photo-catalysis has been carried out with custom made setups using broad spectral lamps and TiO_2 semiconductor catalyst [61-68] at micro-scale. The important factors that control the efficiency of photo-catalysis are (a) rapid recombination of photo-generated electrons and holes in semi-conductor particles, (b) decomposition of water into hydrogen and oxygen is an energy increasing process, thus backward reaction (recombination of hydrogen and oxygen into water) easily proceeds;(c) Inability to utilize visible light: The band gaps of most of the catalysts are (2.8 - 3.2 eV) which limits the photocatalytic activity to only UV light. Since the UV light only accounts for about 4% of the solar radiation energy while the visible light contributes about 50%, the inability to utilize visible light limits the efficiency of solar photo-catalytic for many of the above mentioned applications. By synthesizing special nano materials or by doping the pure metal oxides (likeWO_3, ZnO) which are not readily available from shelf will enhance our capability to apply a radiation source in the visible region and eventually the use of solar radiations for commercial or field applications [69].

2.2. Synthesis of Nanomaterials

Nanomaterials research has witnessed an exponential growth during the last decade [70-72].In the nanometric range, metallic and small band gap semiconducting materials exhibit fascinating quantum phenomena. Large band gap materials such as oxides stabilize in their high temperature phases and reveal enhanced surface phenomena like catalysis and reduced reaction barriers for solid-state reactions [73, 74]. In fact, in the nanometric range, materials may be expected to behave quite differently from both molecular and bulk states since the ratio of the number of surface atoms to the number of bulk atoms is quite high. There is thus a curiosity to understand the behaviour of materials in the nano-scale and if possible to take advantage of the new properties exhibited by materials purely as a consequence of the small size.

Nano oxide materials have found wide range applications particularly as catalysts and as starting materials for making advanced structural ceramics. During sintering and shaping of oxidic materials for practical applications, use of nano- sized particles as starting materials can be of great advantage because of the availability of large surface areas of the nanoparticles. Therefore, several methods have been developed for the preparation of nanomaterials [75, 76]. It was reported recently that the trend is moving more towards preparation of ordered, crystalline nanoscale metal oxides (mono- and mixed-metal oxides) as well as surface decoration or modification of one metal oxide on another on an atomic scale.

Techniques for the preparation of metal nanocluster/nanoparticles can be classified into three primary categories; condensed phase, gas phase and vacuum methods. In condensed phase synthesis, metal and semiconductor nanoparticles are prepared by means

of chemical synthesis, which is also known as wet chemical preparation. In gas phase synthesis, metal is vaporized and the vaporized atoms are condensed in the presence or absence of an inert gas. In vacuum methods, the metal of interest is vaporized with high energy Ar, Kr ions, or laser beam in a vacuum and thus generated metal vapor is deposited on a support.

One of the conventional methods to prepare nanoparticles of metal oxide ceramics is the precipitation method. This process involves dissolving a salt precursor, usually a chloride, oxychloride or nitrate, such as $AlCl_3$ to make Al_2O_3, Y $(NO_3)_3$ to make Y_2O_3, and $ZrOCl_2$ to make ZrO_2 [77]. The corresponding metal hydroxides usually form and precipitate in water by adding a base solution such as sodium hydroxide or ammonium hydroxide to the solution. The resulting chloride salts, i.e. NaCl or NH_4Cl, are then washed away and the hydroxide is calcined after filtration and washing to obtain the final oxide powder. This method is useful in preparing composites of different oxides by co-precipitation of the corresponding hydroxides in the same solution. One of the disadvantages of this method is the difficulty to control the particle size and size distribution. In contrast to the traditional high temperature preparation of bulk metal oxides, involving the reaction of a mixture of powders, the use of liquid-phase routes bears the advantage that it is possible to obtain metastable materials, to achieve superior compositional homogeneity, and to influence the particle morphology during the chemical transformation of the molecular precursor to the final oxidic network [78].

Especially aqueous sol–gel chemistry was highly successful in the synthesis of bulk metal oxides [79]. This synthesis involves the single-stage high-temperature hydrolysis of the metal alkoxide precursors to obtain crystalline, uniform, organically coated nanoparticles which are well-dispersed in an organic solvent. Other oxides like

V_2O_5 MoO_3, Fe_2O_3, MnO_2 and TiO_2 aerogels have also been prepared. [80-84]. Microemulsion-mediated hydrothermal method was used to synthesize TiO_2 .The advantage of using this route is the significant reduction in reaction time and temperatures as compared with the conventional hydrothermal process. The oil/water emulsion ratio significantly affected the particle sizes of the obtained TiO_2 powders. The specific surface area of TiO_2 powders was increased with the oil/water ratio, thereby leading to enhanced photocatalytic activity of TiO_2 powders.

Xingxue Wang et. al. [85] prepared nanosized dark brown C doped TiO_2 which are highly crystalline and visible-light responsive. These nanomaterials were prepared by means of a controlled nonhydrolytic sol–gel process followed by the thermal treatment at 400 ^{0}C. C doped TiO_2 nanoparticles exhibit significant photo response from UV to near infrared region in excess of 950 nm which results from the multi-type carbon doping and the subsequent complex midgap formation. This multi-carbon doping of TiO_2 would be beneficial to allow the more efficient use of sunlight in photocatalysis and photochemistry. Nonaqueous solvothermal method was used to prepare $NiFe_2O_4$; Monodispersed nanoparticles of $NiFe_2O_4$ have been synthesized using different precursors, namely, Iron (III) and Nickel (II) acetylacetonates as well as Iron (III) and Nickel (II) nitrates. Oleic acid is used as the surfactant to stabilize the particles. Oleylamine provides the essential basic condition for the formation of spinel oxides. The long chain alcohol is essential for the nucleation and growth process since it probably makes ferric cations available] that particularly facilitate the formation of ferrites.

The results obtained by Kudo and his coworkers indicate that although the activity of the Ni-doped ZnS photocatalyst was lower in contrast to the Cu-doped ZnS photocatalyst, it was thermally and chemically stable than the Cu-doped ZnS

photocatalyst,. The Ni-doped ZnS photocatalyst can produce H_2 using reducing reagents of sulfur compounds which are formed as by-products in petrochemical industries. Therefore, the Ni-doped photocatalyst is expected to be a practically useful photocatalyst [86]. A novel Pd/$BiVO_4$ composite photocatalysts with visible light photoactivity were synthesized by impregnation method. The authors observed that the Pd/$BiVO_4$ composite samples have monoclinic phase and consist of quatrefoil-like particles.

After Pd species was doped, the ability of visible light absorption is enhanced greatly, the absorption edge of the composite powders shifts to red light It was also found that the 1.0 wt% Pd/$BiVO_4$ sample shows the best photocatalytic activity when compared with other samples [87]. The coupling between titanium dioxide with other semi-conductors (MOx and MSx).mainly intend to the limitation of the charge recombination phenomena; extend photocatalyst light response in the visible region; prepare stable, effective materials easy to implement. Boron and Nitrogen doped TiO_2 nanopowders were prepared by sol-gel method. The obtained results suggest the formation of nanostructured powders with a high surface area, characterized by lowered crystallite sizes and a progressive anatase to rutile phase transition upon increasing the B-doping level. A significant enhancement in photocatalytic degradation of Methyl orange was observed upon doping, especially when B and N species were introduced together into the TiO_2 network [88, 89].

2.3. Photocatalytic Degradation of Dyes

The industrial and agricultural effluents, gaseous or liquid, are harmful to the health and general well-being of man. Because undesirable substances are present in liquid effluents, their presence poses severe threat to the immediate recipients. Wastewaters from various industries, factories, laboratories, etc. are serious problems to the environment. The discharged wastes containing dyes are toxic to microorganisms, aquatic life and human beings [90]. These deleterious effects of chemicals on the earth ecosystems are a cause for serious concern. Several of these chemicals such as azo dyes, herbicides, and pesticides are actually present in rivers and lakes, and are suspected of being endocrine-disrupting chemicals (EDCs) [91–95].

Konstantinou and Albanis [96] reported that textile dyes and other industrial dyestuffs comprise one of the largest groups of organic compounds that represent an increasing environmental danger. About 1–20% of the total world production of dyes is lost during the dyeing process and is released in the textile effluents [97]. The release of those colored wastewaters in the environment is a considerable source of non-aesthetic pollution and eutrophication.This can originate dangerous byproducts through oxidation, hydrolysis, or other chemical reactions taking place in the wastewater phase. It should be noted that dyes can present toxic effects and reduce light penetration in contaminated waters [98].

Degradation of dyes in industrial wastewaters has therefore received increasing attention and some methods of remediation have been proffered. Traditional physical techniques (adsorption on activated carbon, ultrafiltration, reverse osmosis, coagulation by chemical agents, ion exchange on synthetic adsorbent resins, etc.) have been used for

the removal of dye pollutants [99].These methods only succeed in transferring organic compounds from water to another phase, thus creating secondary pollution. This will require a further treatment of solid-wastes and regeneration of the adsorbent which will add more cost to the process. Microbiological or enzymatic decomposition [100], biodegradation [101], ozonation [102], and advanced oxidation processes such as Fenton and photo-Fenton catalytic reactions [103], H_2O_2/UV processes [104] have also been used for dyes removal from wastewaters.

Forgacs E. et al. [105] noted that traditional wastewater treatment technologies have proven to be markedly ineffective for handling wastewater of synthetic textile dyes because of the chemical stability of these pollutants, most of the azo dyes can pass through the activated sludge process practically untreated. Most textile dyes are photo catalytically stable and refractory towards chemical oxidation [106], and these characteristics render them resistant towards decolorization by conventional biochemical and physico-chemical methods.

Adsorption techniques have potential for removing organics from water due to their high efficiency and ability to separate a wide range of chemical compounds. Activated carbon has been widely used as an adsorbent in wastewater treatment to remove organic and inorganic pollutants [107]. Possessing high surface area, activated carbon frequently exhibits high removal efficiency for most dissolved compounds. It has a good capacity for the adsorption of many organic molecules. In spite of this it suffers from few disadvantages. Activated carbon is quite expensive, and its regeneration produces additional effluent and results in considerable loss (10–15%) of the adsorbent.

Over the years, waste materials from agricultural products, such as rice straw, coconut husk, peat moss, etc., have been exploited as possible alternatives to activated

carbon to remove hazardous chemicals from wastewater [108]. All the aforementioned processes have a wide range of their deficiencies in the removal of dyes from wastewaters. Recent studies [109-111] have been devoted to the use of photocatalysis in the removal of dyes from wastewaters, particularly, because of the ability of this method to completely mineralize the target pollutants.

Photocatalytic oxidation using a semiconductor such as TiO_2 as photocatalyst is one of the various advanced oxidation processes used nowadays. As TiO_2 is illuminated by light with a wavelength below 380 nm, the photons excite valence band electrons across the band gap into the conduction band, leaving holes behind in the valence band. It was suggested that hydrogen peroxide absorbs only UV light with a wavelength <300 nm [112]. The holes in TiO_2 react with water molecules or hydroxide ions (OH^-) producing hydroxyl radicals $OH^\bullet$ .The generation of $OH^\bullet$.depends on the solution pH. Organic pollutants which are adsorbed on the surface of the catalyst will then be oxidized by $OH^\bullet$.

Photocatalytic oxidation processes can oxidize a wide variety of toxic and persistent organic compounds to harmless inorganics such as mineral acids, carbon dioxide and water [113]. The color of dyes results from conjugated chains or rings which absorb light at visible wavelengths. UV degradation by the cleavage of conjugated chains was achieved [114]. The results obtained show that the photocatalytic oxidation process is more efficient in the removal of pollutants from pretreated wastewater.

The photocatalytic degradation of Basic Red 46 and Basic Yellow 28 was studied using UV/TiO_2/Periodate.This study demonstrated that the UV/TiO_2/Periodate system constituted an effective process for the treatment of BR46 and BY28, in a single solution or binary mixture[115].The S-doped Zn_2SnO_4 showed enhanced photocatalytic activity for photodegradation of Rhodamine B (RhB) in aqueous solution under visible light

irradiation.[116] The results obtained by Lei Ge indicate that the visible light absorption of the $Pt/BiVO_4$ photocatalyst is greatly enhanced [117]. It was found that complete degradation of all the solutions of the dyes (Methyl orange, Rhodamine B, Thymol blue and Bromocresol green) was achieved more efficiently with the composition with x = 0.005 as compared to all other compositions of $Fe_xTi_{1-x}O_2$, and degussa P25. The decolorization rate of different dyes decreases with the increase in Fe (III) concentration in TiO_2 increases.

Sampa Chakrabarti et al. [118] observed that the experimental parameters such as the amount of semi-conductor film (PVC–ZnO composite), intensity of UV radiation and the amount of dye present effect greatly the photodegradation of Eosin Y .The observations made by M.R. Sohrabi clearly demonstrate that the dye decomposition rate increases with the TiO_2 suspension concentration up to 4.0 g L^{-1}, and then decreases with increasing TiO_2 suspension concentration for the degradation of Direct Red 23 [119]. Chung-Hsin studied for the photodegradation of Methyl orange by Sulfate-modified titania [120]. He observed the increase in the removal of Reactive Red 198 increased with ZnO dosage.

Analytical results obtained by Parida et. al. [121] demonstrated that TiO_2 is mesoporous in nature, and sulfate modification could inhibit the phase transformation and enhance the thermal stability of TiO_2. It was also observed by him that sulfate modification could reduce the crystallite size and increase the specific surface area of the catalysts. Some researchers show that the photocatalytic degradation of real textile effluents was carried out using $UV/TiO_2/H_2O_2$ and $UV/Fe^{2+}/H_2O_2$ systems, the association of TiO_2 and H_2O_2 was found to be the most efficient treatment for removing organic pollutants from textile effluents.

In spite of their efficiency, Fenton reactions based treatment proved to be slower [122,123]. It was also observed that the catalyst loading, pH values and the initial dye concentration affected the degradation efficiency of ZnO powders for photodegradation of methyl orange .The photodegradation efficiency is enhanced with the increase of catalyst loading and the reverse effect is obtained with the increase of initial dye concentration in our experiments [124].Recent studies present the significant enhancement of the photocatalytic activity of the Ag–TiO_2 under visible light irradiation which could be ascribed to simultaneous effects of Ag deposits, which act as electron traps and enhanced adsorption of Reactive Yellow-17 on Ag–TiO_2 surface. The effect of pH noted in this study and neutral pH was found to be the best for carrying out the photocatalytic degradation of RY-17. The addition of hydrogen peroxide and potassium per sulphate improves the photodegradation rate [125].

The photosensitized catalytic activity of as-prepared TiO_2 was investigated upon its degradation of Rhodamine B under visible light irradiation. The experimental results demonstrate the as prepared TiO_2 can degrade of RhB more efficiently than TiO_2 P-25 under visible light irradiation due to its higher activity in both the de-ethylation and cleavage of RhB chromophore ring structure reaction [126]. Photocatalytic degradation of Disperse Blue 79 by Gold/iron oxide was investigated. It was observed that the photocatalytic activity enhanced with increasing Au loading up to 8 wt%, and the activity increase was dependent upon catalyst pretreatment. The dye degradation was accelerated remarkably when carried out in alkaline media or in the presence of hydrogen peroxide [127].

The Pt–TiO_2–SiO_2 mesoporous materials were used for the degradation of Methyl orange by Theodora Papadama et. al .which shows higher photocatalytic activity for the

photodegradation of methyl orange in the illumination of visible light than TiO_2 alone. They attributed the improved activity to the charge-transfer on the TiO_2–SiO_2 composites and an enhanced ability to trap photogenerated electrons on the Pt-derived states that adsorbed on the TiO_2 surface [128]. The photocatalytic degradation of Acidic Black 10B was studied using CeO_2. It was found that the decolorizing rate increases with the dosage of CeO_2 and the maximum decolorizing rate is obtained when the dosage is 80 mg. After that the decolorizing rate decreases with the dosage. This might be due to the reason that the excess catalyst leads to the decreasing transmission of the solution which makes the photocatalytic oxidation–reduction reaction not proceed effectively [129]. It was also observed by some researchers that TiO_2 and Pt-modified titania catalysts oxidize Acid Orange 7 more efficiently than P-25 Degussa TiO_2 [130].

Photocatalytic degradation of Methyl Orange and Rhodamine 6G has been investigated by means of TiO_2, ZnO, SnO_2, ZnS and CdS Mohamed Mokhtar and coworkers. The results obtained indicate that the ZnO is the most active photocatalyst for decolorization of MO and R6G. Moreover, photocatalytic activity of ZnO is greater in the presence of solar light as compared to UV light [131]. Zhiyong et al reported that the activity of the Zn-doped catalyst was found to be higher than of the pure Degussa P25 (TiO_2) during the photodegradation of organic compounds. They also observed in this study that the most suitable doping level of TiO_2 for Zn was 4 mol% during the degradation of azo-dye Orange II and of the transparent 2- propanol solutions [132].

Titanium dioxide nanoparticle (Degussa P-25) was applied for the removal of Reactive Orange 107 and Reactive Red 152 by Niyaz Mohammad and his co-workers [133]. They also investigated the effects of operational parameters such as H_2O_2, dye concentration, anions (NO_3^-, Cl^-, SO_4^{2-}, HCO_3^- and CO_3^{2-}) and pH. They found that

Na_2CO_3 exhibited the strongest inhibition effect followed by $NaHCO_3$. The decolorization rate for all the dyes studied goes through a maximum when the concentration of the hydrogen peroxide increases from 0 to 300 mg $L^{-1}$and then it does not show appreciable change. The photocatalytic decolorization kinetics follows a zero-order model for RO 107 and first-order model for RR 152. The significant decrease in the decolorization of Orange II in the presence of ZnO photocatalyst and UV light and the enhancement of decolorization of Orange II with increasing aeration rate was found by Muruganandham and Swaminathan [134]. Neppolian and his coworkers [135] reported that TiO_2 catalyses photodegradation of Reactive blue 4 using solar irradiation. They found that the oxidising agents such as hydrogen peroxide and persulphate ion have major role in the degradation efficiency of the dye. The additives such as sodium carbonate and sodium chloride were found to hinder the rate of photocatalytic degradation.

ZnO nanopowder appears to be a suitable alternative to TiO_2 since its photo degradation mechanism has been proven to be similar to that of TiO_2 [136]. ZnO nanopowder has been reported, sometimes, to be more efficient than TiO_2. Its higher efficiency has been reported in the advanced oxidation of pulp mill bleaching wastewater, the photo oxidation of 2-phenylphenol and photocatalysed oxidation of phenol [137,138]. A lot of studies have been reported on the photocatalytic degradation of refractory organics. Degussa P-25 TiO_2 has been used for many systems either in suspended or in supported forms [139,140]. In few studies, other semiconductors, such as ZnO [141] and WO_3 [142] have been used. The biggest advantage of ZnO in comparison with TiO_2 is it adsorbs over a larger fraction of UV spectrum and the corresponding threshold of ZnO is 425 nm [143]. For this reason, ZnO and WO_3 photocatalyst might be the most suitable for photocatalytic degradation in the presence of sunlight.

2.4. Photocatalytic Degradation of Phenol

Phenol and Phenolic compounds are widely used in industry and daily life. The presence of phenol and phenolic compounds in the resulting wastewaters is an issue of environmental concern. Their high toxicity, even at low concentration, has motivated the search and improvement of many treatment techniques. They have caused considerable damage and threat to the ecosystem in water bodies and human health due to their high stability, high toxicity and carcinogenicity. Removal of phenol and phenolics in wastewater effectively is an urgent demand.

Semiconductor photocatalysts offer huge potential for elimination of toxic chemicals [144]. The photocatalytic degradation of organic pollutants in water and air, using semiconductors such as TiO_2 and ZnO have attracted more attention due to their unique ability in the environmental detoxification [145–147]. Traditional wastewater treatment techniques include activated carbon adsorption, chemical oxidation and biological digestion are not effective .More research has been focused on the Photocatalytic degradation assisted by titanium dioxide under ultraviolet light and modification of the catalyst, the photocatalytic principles, the factors influencing photocatalytic rate and the reaction kinetics [148-150]. It was shown that photodegradation using $H_2O_2/TiO_2/UV$ process was much more effective than using either H_2O_2/UV or TiO_2/UV process for phenol degradation [151]. Phenol degradation by NiO was studied and it was observed that laser induced photo-catalytic process is highly efficient in removal of phenol in water over a short period of time (in minutes) as compared to conventional methods using lamps (hours) [152].

TiO_2 was used for the removal of phenol in this study and found that photocatalysis was capable of removing phenol toxicity, generating an effluent much less toxic. With the highest salinity and extended irradiation periods, a virtually nontoxic effluent was produced [153] .The results obtained using (activated sludge+TiO_2) for phenol removal indicated that the photocatalytic step was able to add the capacities of totally removing phenol and practically mineralizing the organic matter to the biological treatment [154] .

Catalysts of the Zr-doped TiO_2 prepared by the homogenous co-precipitation method show that catalysts annealed between 800 and 900 ^{0}C are more efficient than the standard photocatalyst Degussa P25 for the degradation of 4-chlorophenol. The most photoactive catalyst annealed at 900 ^{0}C contains 87 wt % of anatase and 13 wt. % of rutile [155]. J. Arana et. al. investigated the removal of catechol, resorcinol, phenol, m-cresol and o-cresol using TiO_2 Degussa P-25. The obtained results indicated that catechol adsorption is much higher than those of the other phenolics and its interaction occurs preferentially through the formation of a catecholate monodentate. Resorcinol and the cresols interact by means of hydrogen bonds through the hydroxyl group, and their adsorption is much lower than that of catechol [156].

The Pr-doped TiO_2 nanoparticles that were annealed at 600 ^{0}C revealed the highest phenol photodegradation efficiency, primarily because they included both anatase and rutile structures [157]. Phenol degradation by CdS/TiO_2 Nanocomposite was studied by Zhifeng Guo and his coworkers. It was found that the surface-coated CdS and TiO_2 anatase nanocomposite extends the absorption band edge in the visible region as observed from the UV-Vis measurements. The as-synthesized nanocomposite materials exhibit better photoactivity under visible light irradiation than that of pure TiO_2 [158].It was

investigated that the photocatalytic activity of N-doped TiO_2 under various irradiation conditions and found the photocatalytic activity of the N-doped TiO_2 with anatase phases is higher than that of the commercial TiO_2 photocatalyst Degussa P25 for phenol decomposition under visible light irradiation [159].

Comparison of photocatalytic activity of TiO_2 and Degussa P-25 for phenol degradation show that under identical conditions of catalyst loading, pH and phenol concentration the most of photocatalysts presented a global efficiency much lower than that for a TiO_2standard photocatalyst named Degussa P-25. However, two photocatalysts prepared by different methods showed approximately the same global efficiency than the commercial material. [160].It was shown by the author that phenol and its dihydroxy derivatives undergo destruction in the presence of illuminated TiO_2 according to 1st order kinetics. Hence, in a mixture their reactions are competitive. It is therefore proposed that initial reaction rates should be taken into account for reaction kinetic studies. P-benzoquinone, six hydroxylated aromatics and four aliphatic compounds have been found to be intermediates of phenol full photocatalytic mineralisation [161].

A few studies about photooxidation of phenol reported in the literature [162,163]. Highly efficient catalysts are still needed to eliminate these toxic materials. Thus, development of new photocatalysts for pollution treatment is of current interest [164]. ZnO, with bang gap = 3.4 eV, has become promising in the past few years because of its distinctive optoelectronic, catalytic, and photochemical properties [165]. The quantum efficiency of ZnO is also significantly larger than that of TiO_2. In some cases, ZnO has revealed better activity than TiO_2 [166]. The ZnO-mediated photocatalytic process has been successfully used to degrade organic pollutants. ZnO is available at low cost and it absorbs over a larger fraction of the solar spectrum than TiO_2 [167]. For this reason, ZnO

is thought to be more suitable material for photocatalytic degradation of organic pollutants.

Narayanasamy et al. [168] studied the photocatalytic degradation of 4-acetylphenol by Activated Carbon –ZnO, It was observed that AC–ZnO are much higher than bare ZnO. The higher efficiency of this photocatalyst is due to the synergistic effect between ZnO and activated carbon. The catalyst is found to be reusable. A synergic affect between platinisation and sulphate pretreatment of TiO_2 was found for the photocatalytic activity of sol–gel prepared TiO_2.The results reveal that samples simultaneously sulphated and platinised obtained a remarkable improvement of the photocatalytic activity for phenol degradation [169].

Comparative Photocatalytic activity of ZnO and TiO_2 was studied by N. Hadj Salah et. al. They observed that ZnO presented photocatalytic activity comparable to TiO_2 and Degussa P25. The Degussa P25 shows better activity than TiO_2 but because Degussa P25 is formed from only one crystallite. All the grains are active that is the main reason that it is better than the other two TiO_2catalysts [170].

The application of catalytic techniques to waste treatment demands a deep knowledge of catalyst surface features, such as surface area, hydroxylation degree, crystallinity or pore size. Additionally, in photocatalytic processes, the proximity between adsorption and photoactive centres also determines reaction rate [171]. For more efficient utilization of sunlight and indoor light, visible-light-responsive photocatalysts are indispensable. Tungsten oxide (WO_3) is a visible-light-responsive photocatalyst and an n-type semiconductor photocatalyst for O_2 generation using sacrificial reagents [172,173], but reports on the degradation of organic substances by WO_3 are limited [174].

In the present work, nano ZnO catalysts were prepared using two different methods and characterized by XRD, FESEM and TEM, The photocatalytic activity of catalysts was evaluated for the degradation of phenol under ultraviolet laser irradiation. The influence of various parameters such as calcination temperature, the amount of the catalyst, laser exposure time, initial pH and initial phenol concentration on the rat of photocatalytic degradation of phenol using nano ZnO and UV laser was also investigated.

CHAPTER 3

EXPERIMENTAL METHODS AND TECHNIQUES

In this chapter, all the experimental details related to synthesis of pure and noble metal doped nanoparticles using precipitation, sol gel method and incipient impregnation method are explained.The experimental set up design and the procedure to test the photocatalytic activity of the synthesized samples was also discussed.

3.1. Synthesis of WO_3 by Precipitation Method

The WO_3 nanostructures were synthesized by precipitation technique from aqueous solution of ammonium tungstate pentahydrate ($(NH_4)_{10}\,W_{12}O_{41}.5H_2O$) and nitric acid ($HNO_3$, Merck). A pre-determined amount of the tungstate salt was dissolved in de-ionized water and the resulting solution was heated up to 85 ^{0}C slowly. Appropriate amount of a warm, concentrated nitric acid was dripped to this solution with continuous vigorous stirring. The mixed solution was kept at 85 ^{0}C for 25 min under continuous stirring conditions. The precipitate was allowed to settle for 24 hours at room temperature.

$$(NH_4)_{10}\,W_{12}O_{41}.5H_2O) + 10HNO_3 + 2H_2O \rightarrow 10\,WO_3.H_2O + 10\,NH_4^+ + 10\,NO_3^- \quad (7)$$

$$10\,WO_3.H_2O + \text{heat} \rightarrow 10\,WO_3 \quad (8)$$

The precipitate was washed by addition of a large amount of de-ionized water followed by stirring for about 10 min and allowing the precipitates to settle down for 24

hours before decanting the liquid. This washing procedure was carried out three times. Finally, the precipitates were separated by ultra-filtration procedure by using a polymer membrane (pore size = 0.2 µm). Then, the precipitate was dried at 100 ^{0}C for 12 hours. After drying, it was calcined at 500 ^{0}C for 7 hours at the rate of 1^{0}C/minute. The synthesized nano structure WO_3 in powder form was then characterized. The flowchart for synthesis of WO_3 is presented in Figure 3.1.

3.2. Sol Gel Method

Sol-gel method consists of hydrolysis and polycondensation steps.

3.2.1. Synthesis of Nano ZnO Modified Sol Gel Method

Zinc oxide nanoparticles were prepared by modified sol gel method from aqueous precursor solutions. The conditions used for synthesis such as aging, drying temperature, calcination time and temperatures are different. The zinc nitrate and polyvinyl alcohol (PVA) solutions of desired molar ratio were prepared.

A stoichiometric amount of zinc nitrate hexahydrate [Zn $(NO_3)_2$•$6H_2O$] and PVA were accurately weighed and dissolved in deionized water. The two prepared solutions mixed in a beaker and stirred with a magnetic stirrer at room temperature for three hours. Subsequently, the mixed solution was heated at a temperature of 80 ºC for 60 hours to obtain the gel. The obtained gel was dried at 100 °C for 24 hours then ground into a fine powder. The temperature of the dried precursor powder was increased at the rate of 1 °C /minute to attain the required temperature and then allowed the sample to stay at that temperature for seven hours to obtain the final product (i.e., ZnO nanoparticles).

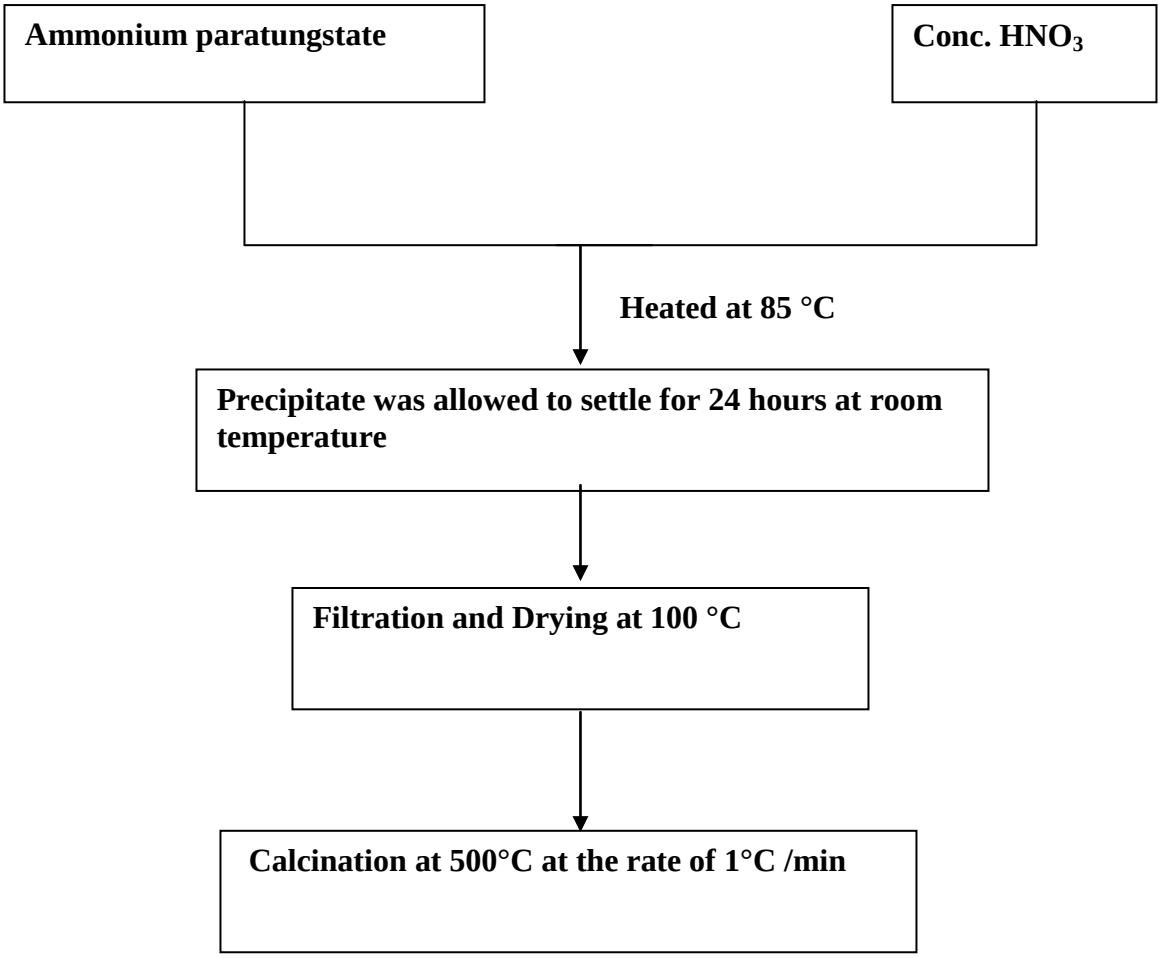

Figure 3.1 Schematic Flowchart showing the steps for the synthesis of nano metal oxides by precipitation method

Thermal treatment was performed 500 ^{0}C. The ZnO powder obtained from calcination was grounded for more than one hour to obtain homogenous nano powder. The calcined ZnO nano powders were then characterized by micrographic techniques. The flow chart scheme was shown in Figure 3.2.

3.2.2. Synthesis of Nano NiO by Modified Sol Gel Method

Nickel oxide nanoparticles were prepared using the following process. Appropriate molar ratio of nickel nitrate hexahydrate [Ni $(NO_3)_2$•$6H_2O$] to citric acid monohydrate were accurately weighed and dissolved in deionized water, respectively. Then the two solutions were mixed in a breaker and stirred with a magnetic stirrer at room temperature for three hours. Subsequently the mixed solution was heated at a temperature of 80 ºC for 60 hours. In this process, a green gel was formed. The gel so obtained was dried at 100 °C for 24 hours. Finally, the precursors were calcined in a programmable furnace at 400°C for 6 h.The temperature of the precursor was increased at the rate of 1 °C /minute to attain the temperature of 400°C and then allowed the sample at this temperature to obtain the products (i.e., NiO nanoparticles) whose color was extremely dark. The calcined products were then collected for further analysis.

3.2.3. Incipient Impregnation Method for Doping of Noble Metals

The Pt, Pd, Ag and Rh doped semiconductor metal oxide (WO_3, ZnO and NiO) photocatalysts were prepared by incipient wetness impregnation method. The required amount of metal precursor salt was dissolved in de-ionized water to obtain an incipient volume of solution. Then the calculated amount metal oxide to be impregnated was added

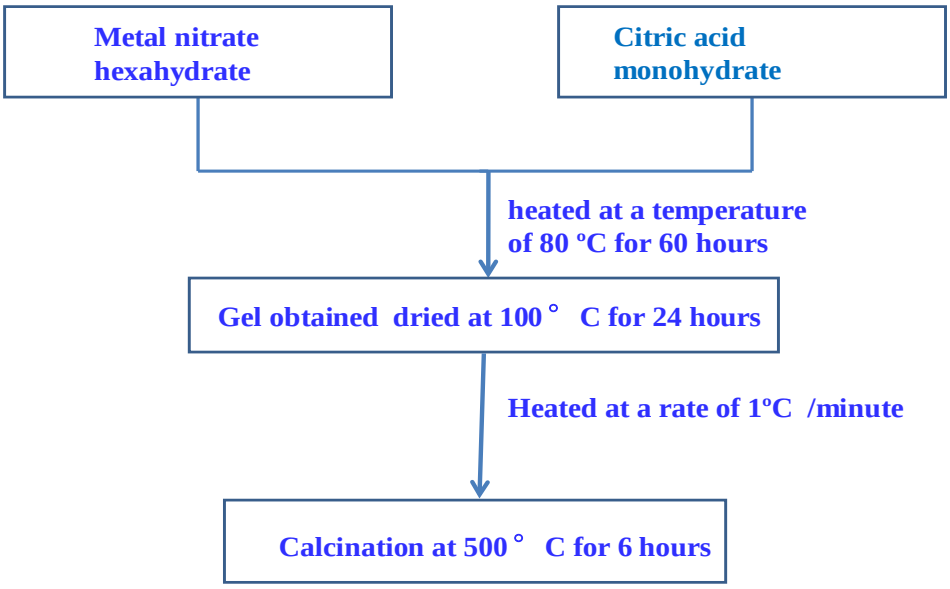

Figure 3.2 Schematic Flowchart showing the steps for the synthesis of nano metal oxides by sol method

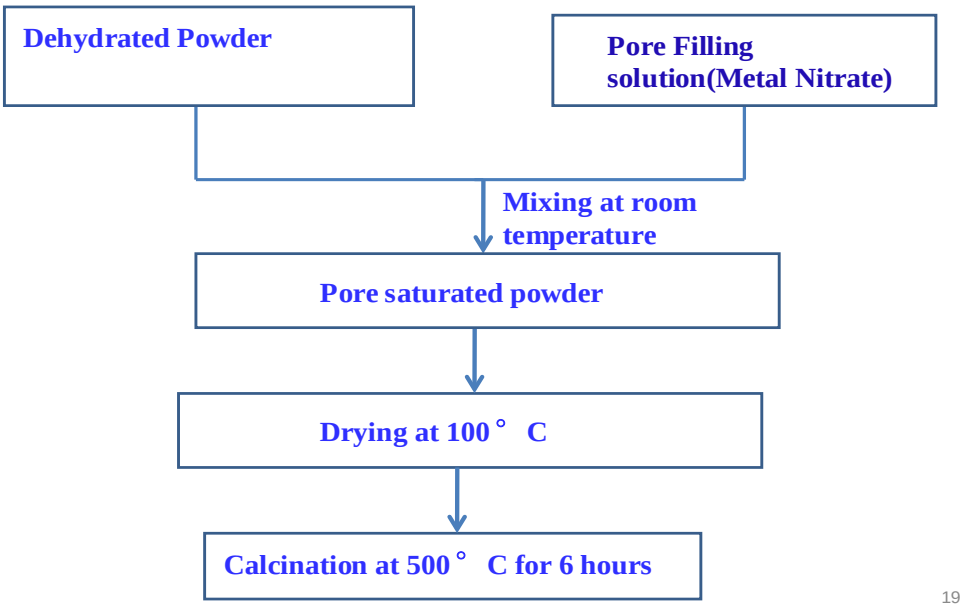

Figure 3.3 Incipient Impregnation Method for doping of noble metals

under continuous mixing. After drying at 100 °C over night, sample was calcined at 500 °C for 6 h and then cooled to room temperature to obtain the final catalyst. The schematic diagram is shown in Figure 3.3.

3.3 Characterization Techniques

3.3.1 X Ray Diffractrion Studies

The X-ray diffraction (XRD) measurements were performed using a Bruker X-ray diffractometer in the range of 10– 80, 2 ɵ. The crystalline structures of the synthesized product were identified with a powder X-ray diffractometer (BDX3200, operated at 36 kV, 20 mA), employing Cu Kα radiation (λ = 0.15418 nm).

3.3.2. Scanning Electron Microscope (SEM) and Transmission Electron Microscope (TEM)

Scanning Electron Microscope (SEM) and Transmission Electron Microscope (TEM) are powerful tools for the characterization of objects on a very fine scale. The basic steps for imaging a sample comprise formation of an electron beam, interaction between sample and beam, gathering information of the sample and formation of an image. The incident electron beam comes to the surface of the sample and strikes onto it. Various photon and electron signals are generated after the interaction with the sample as shown in the Figure 3.4. The darker areas of the image represent thicker or denser areas of the sample that fewer electrons were transmitted or vice versa.

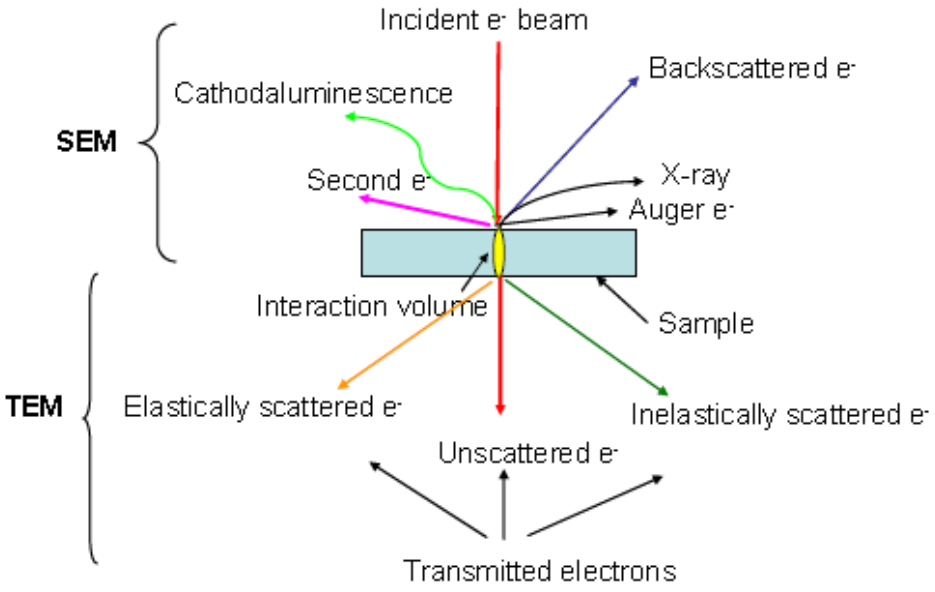

Figure 3.4 Electron-sample interaction and signals emitted from the sample

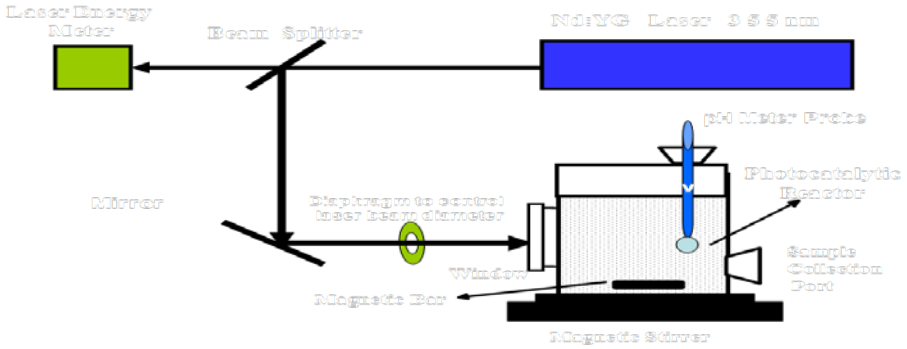

Figure 3.5 Schematic diagram of the experimental set up for removal of toxic pollutants from waste water

3.3.3. UV-Visible Spectrophotometry

UV-Visible spectra measurements were carried out on a Perkin Elmer spectrophotometer in the 200-800 nm wavelength range. The baseline was recorded using a Holmium oxide Reference. The Cintra 303 was also used for UV analysis of the samples. The Cintra 303 is a research grade spectrometer with enhanced sensitivity in the UV range. It has a variable slit width for best sensitivity and resolution, with improved stray light, noise, and drift specifications. The Cintra 303 accepts the full range for its wavelength range of 190 to 900 nm. All spectra were taken under atmospheric conditions.

3.3.4 High Performance Liquid Chromatography

High performance liquid Chromatograph (Waters 2996 Photodiode Array Detector, Waters 1525 Binary HPLC pump and Waters 717 plus Autosampler) was used to analyse the laser irradiated samples. High performance liquid Chromatograph (Waters 2996 Photodiode Array Detector, Waters 1525 Binary HPLC pump and Waters 717 plus Autosampler) was used to analyse the laser irradiated samples. The stationary phase consisted in a Purospher Star RP-18 endcapped column (250mm×4.6mm, 5μm particles) working at room temperature. The mobile phase was a mixture of water and methanol with a isocratic concentration at a flow rate of 1.0 mL min^{-1}.

3.4. Laser Based Photocatalytic Reactor

A laser based photo-catalytic reactor was used for the removal of pollutants. This setup will essentially consist of a Pyrex cell, a laser system. Excimer laser and the third

harmonic from Nd: YAG laser was employed for excitation of aqueous solutions containing the pollutants. Figure 3.5 depicts the schematic of the experimental setup designed locally for the study of removal of dye and phenol from water using laser induced photocatalysis process.

3.5. Photocatalytic Degradation of Dye under UV Laser Irradiation

Stock solutions of the dye containing desired concentrations were prepared in water. For irradiation experiments, 100 mL solution of desired concentration of the dye was taken into the reaction vessel and the required amount of photocatalyst was added and the solution was stirred for at least 15 min in the dark to allow equilibration of the system so that the loss of compound due to adsorption can be taken into account. Irradiations were carried out using a 355 nm wavelength high power laser beam generated from the third harmonic of the Spectra Physics Nd: YAG laser (Model GCR 250), with a pulse width of ~8 ns. In order to avoid the destructive effect of radiation, laser beam diameter was expanded to 1.0 cm. To study the effect of different pH on photocatalytic degradation of the dyes and phenol, the pH of the reaction mixture was adjusted by adding a dilute aqueous solution of HNO_3 or NaOH. Samples (4.0 mL) were collected before and at regular time intervals during the irradiation. The catalyst was removed through filtration (0.2 μm) before the UV analysis. The degradation was monitored by measuring the absorbance at absorption maxima (λ_{max}) of each dye by UV-Vis spectrophotometer. The absorbance Therefore, the degradation of the substrate was estimated at this wavelength as a function of irradiation time. To monitor the removal process of dye form water, the

changes in the absorption spectra of substrate at different laser irradiation times were recorded with a UV–Vis spectrophotometer in the wavelength range from 200 to 800 nm.

3.6. Photocatalytic Degradation of Phenol under UV Laser Irradiation

Photocatalytic activity of the synthesized photocatalysts was evaluated using aqueous solution of phenol under ultraviolet laser (266 nm) irradiation. The experiments were carried out in locally designed photocatalytic reactor with quartz window for illumination of UV laser irradiation. The stock solution of phenol containing 100 mg L^{-1} was prepared in deionized water. The photoreactor was loaded with 120 mL of aqueous suspension of nano ZnO in phenol. The suspensions were irradiated with UV light at constant stirring speed and laser energy. Irradiations were carried out using YAG laser (model no., 266nm). Samples were regularly withdrawn from the reactor and filtered using nano syringe filters prior to analysis for separation of any suspended solid. High performance liquid Chromatograph was used to analyse the laser irradiated samples. The mobile phase was a mixture of water and methanol with an isocratic concentration at a flow rate of 1.0 mL min^{-1}. The concentration remaining after time t was calculated by peak area method.

CHAPTER 4

CHARACTERIZATION OF PHOTOCATALYSTS

This chapter deals with the characterization of the pure and doped nanophotocatalysts synthesized by different methods. The results obtained for the characterization of these nanomaterials using XRD, FESEM and TEM techniques were also described.

4.1. X-Ray Powder Diffraction Studies of Photocatalysts

The nanoparticles of nano WO_3, nano ZnO, nano NiO and doped metal oxides were synthesized using different methods. The x ray diffraction studies of these undoped and doped metal oxides were performed to determine the crystal structure and to calculate the particle size of nanomaterials synthesized.

4.1.1. X Ray Diffraction Pattern of Nano WO_3 and Noble Metal Doped Nano WO_3

Crystal structure and particle size was studied using an X-ray diffractometer. The XRD spectrum for the samples prepared using different concentration of metals is shown in Figure 4.1. XRD spectrum for our synthesized nanocrystalline tungsten oxide and noble metal (Pt, Pd, Ag and Rh) doped tungsten oxides are displayed in Figure 4.2. All the main peaks can be indexed to hexagonal WO_3 (JCPDS card 35-1001) which are consistent with general features of nanomaterials. No characteristic peak of noble metals in XRD was investigated this shows that the metal paticles are bound to the surface of metal oxides.

Table I Particle size of WO_3 doped and undoped estimated using Scherrer equation from XRD analysis

S.No.	Catalyst	2ɵ	d-Val	FWHM	Intensity	Estimated particle size (nm)
1	WO_3	24.3715	3.64930	0.2622	2343	31.0
2	WO_3 calcined at 300 ºC	23.7881	3.73746	1.3463	474	6.0
3	WO_3 calcined at 400 ºC	23.7869	3.73765	1.5088	715	5.4
4	WO_3 calcined at 500 ºC	23.4254	3.79450	0.8530	1151	12.8
5	WO_3 calcined at 550 ºC	24.3184	3.65715	0.3227	1329	25.2
6	WO_3 calcined at 600 ºC	24.3567	3.65148	0.2399	1624	33.9
7	WO_3 calcined at 650 ºC	24.3968	3.64557	0.2366	1735	34.3
8	WO_3 calcined at 700 ºC	23.1011	3.84703	0.2263	1858	35.8
9	1%Pt-WO_3	23.4023	3.79819	0.8489	1284	9.5
10	1%Pd-WO_3	23.6800	3.75428	1.2646	1015	6.4
11	1%Ag-WO_3	24.5004	3.63039	0.2291	1779	35.4
12	1%RhWO_3	23.4424	3.79179	0.9220	1136	8.8
13	2%Pt-WO_3	23.4456	3.79128	0.8578	1313	9.5
14	3%Pt-WO_3	23.6628	3.75697	0.3961	1327	28.0
15	5%Pt-WO_3	24.2748	3.66362	0.3356	938	24.2
16	$ZnWO_4$	30.6195	2.91739	0.5485	2930	15.0
17	$NiWO_4$	24.2754	3.66353	1.2709	573	6.4

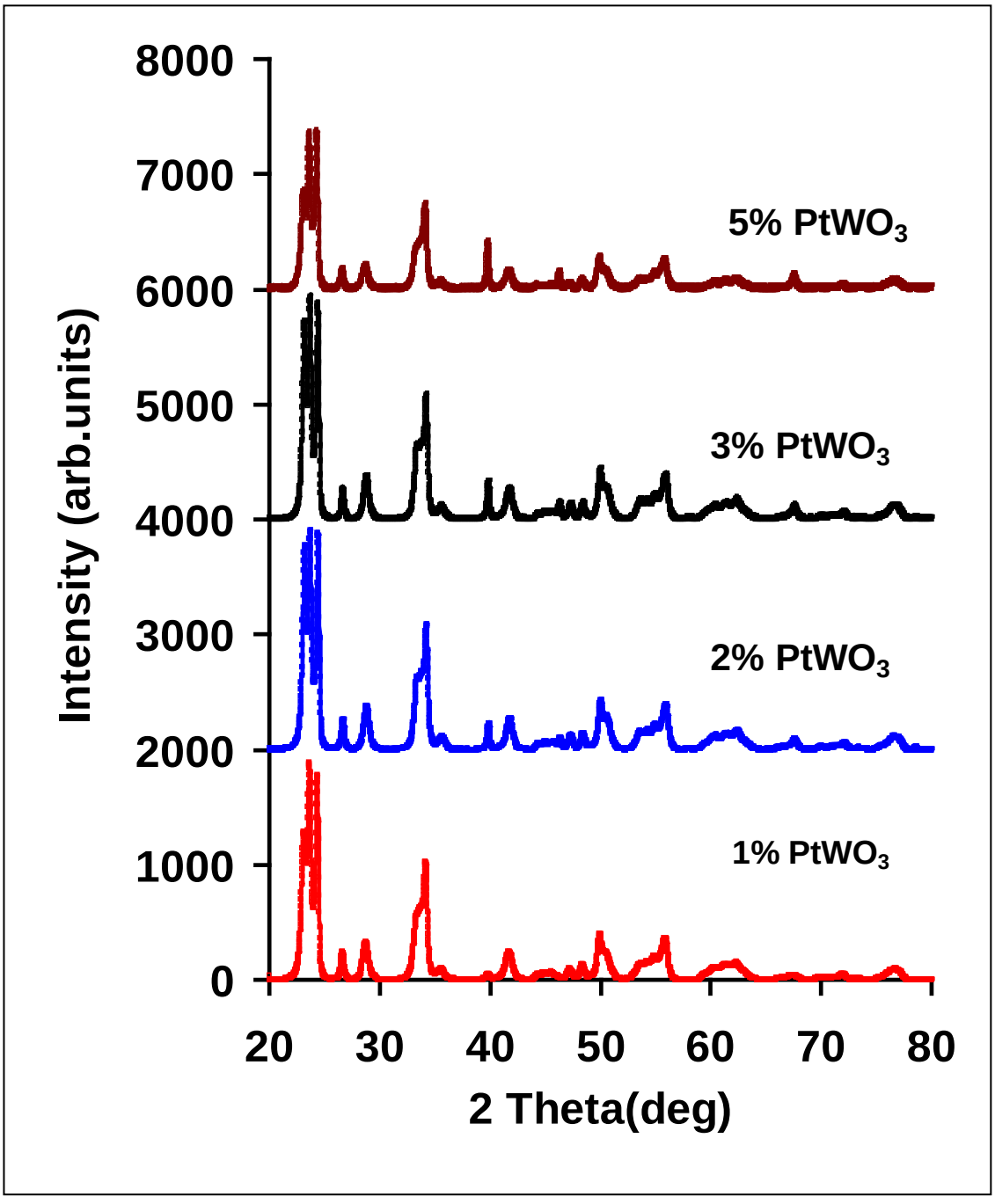

Figure 4.1 X ray diffractogram for WO_3 with different dopant concentrations

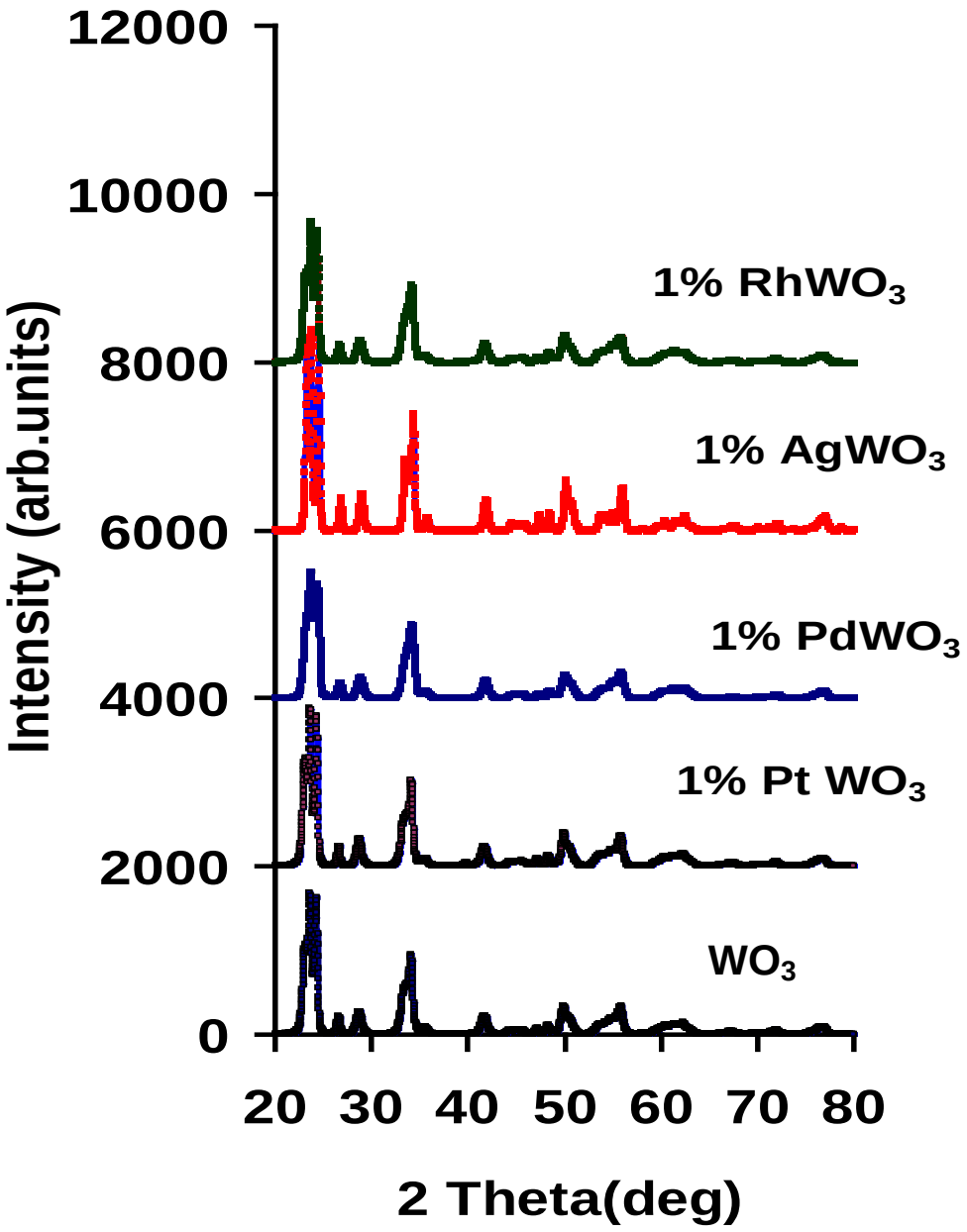

Figure 4.2 XRD pattern of WO_3 and (Pt, Pd, Ag and Rh) doped WO_3

As the dopant concentration increases the intensity of the significant peaks decreases. It was also observed that the peaks became broad. This may be due to the fact that dopant metal particles transform the crystal structure of the nanocrystalline. Particle morphology was also examined using scanning electron microscope. The crystallite size was calculated from peak broadening (in nm) using the Scherrer approximation [175], which is defined as

$$t = [0.9 \lambda / B \cos \theta] \quad (9)$$

where λ is the wavelength of the X-ray (0.15418 nm), B is the full width at half maximum (FWHM, radian) and θ is the Bragg angle (degree). The value of FWHM was obtained by performing profile fitting using an XRD pattern processing software. The crystallite size was 31.0 nm for WO_3 (as-prepared). The average particle size for pure WO_3, WO_3 calcined at different temperatures, noble metals such as (Pt, Pd, Ag and Rh) doped WO_3 and different amuont of Pt varying from (300 °C to 700 °C) was estimated using Scherrer Equation. .The results obtained are depicted in Table I. The diffractogram reveal that the experimental method used in the synthesis of WO_3 yielded crystals with high purity and uniformity.

The average particle size as estimated for doped and undoped nanomaterials is presented in Table I. The XRD diffractogram of all the samples is depicted in Figures 4.1 to 4.4. The surface modification of WO_3 was carried out using noble metals as dopants. XRD pattern for our synthesized pure and doped metal oxides were displayed in Figures 4.1 to 4.4. All the main peaks are consistent with general features of nano metal oxides Figures 4.1 to 4.4 show the XRD patterns of metal oxide semiconductos (before and after the loading of noble metals) and at different calcinination temperatures.

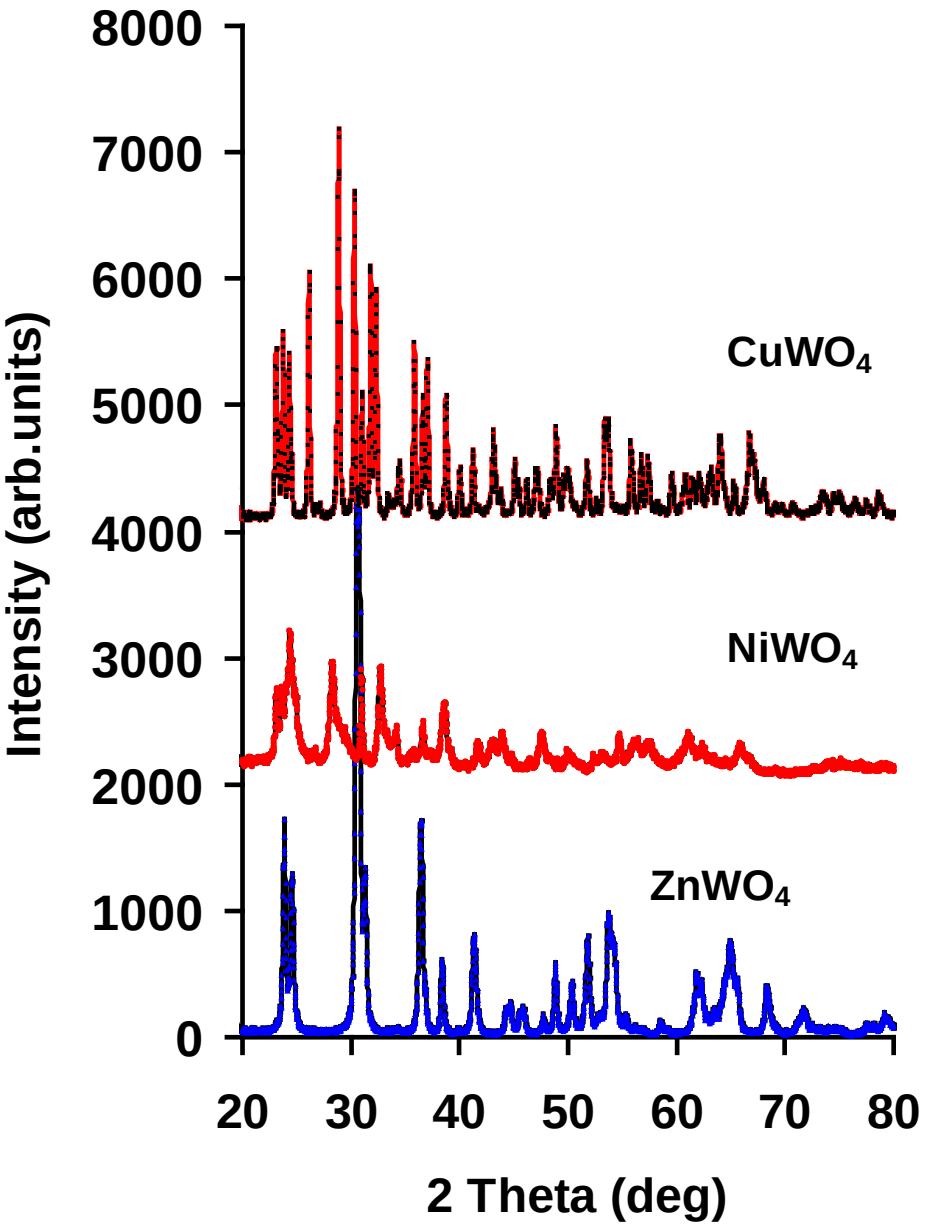

Figure 4.3 X ray diffractogram for as prepared metal tungstates

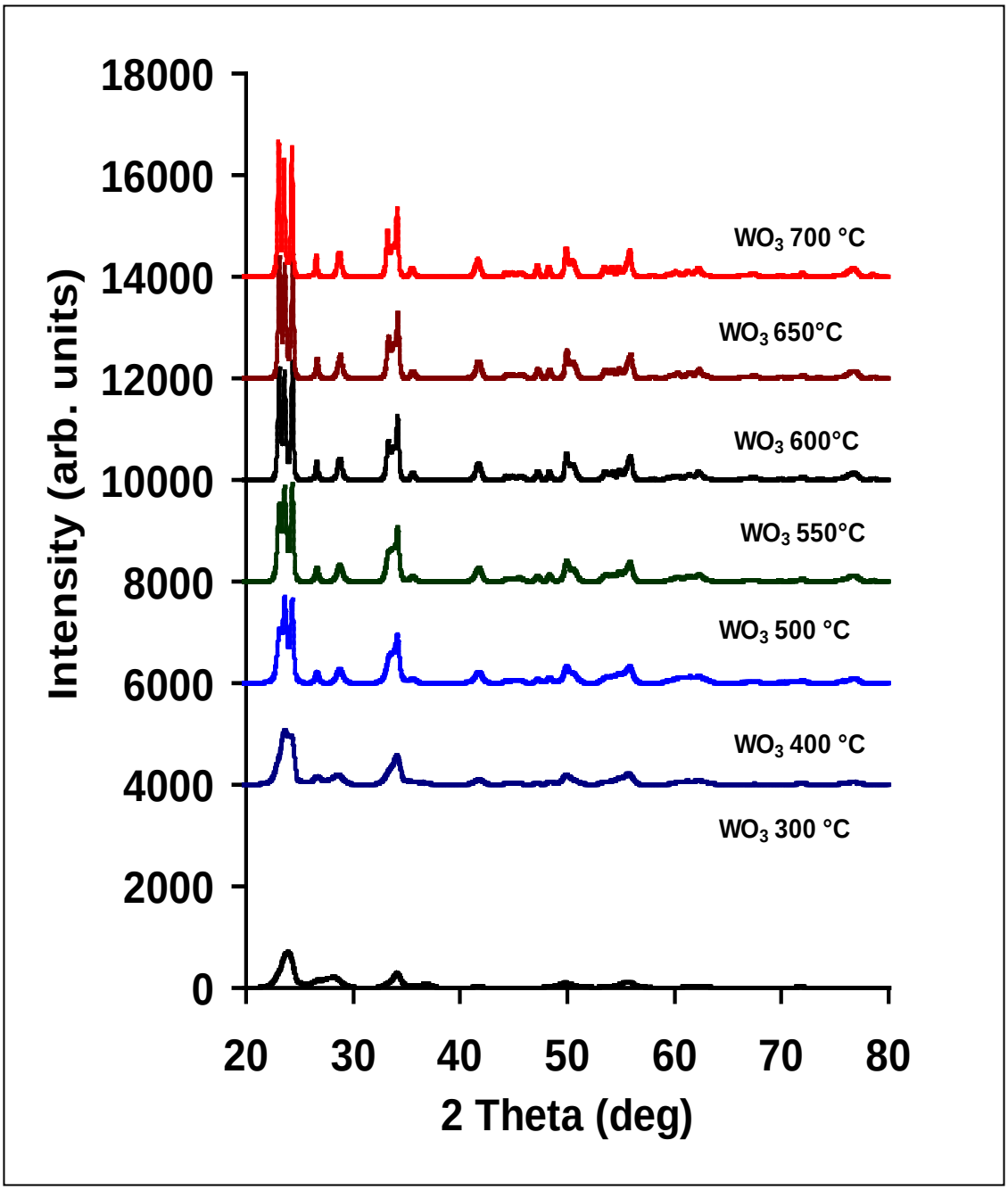

Figure 4.4 XRD pattern of WO_3 at different calcination temperature

It was observed that the incorporation of transition metals into metal oxides may decrease the intensities of the main peak. The XRD reflections are determined to be almost at the same location.One more interesting point is that no peak associated with noble metals could be detected. This indicates that these metal ions are incorporated into the metal oxide structure.

4.1.2 Characterization of Nano ZnO and Noble Metal Doped Nano ZnO

Crystal structure and particle size was studied using an X-ray diffractometer. The particle size estimated for undoped, doped ZnO and nano ZnO calcined at different temperatures are shown in Table II. XRD pattern for our synthesized nano ZnO and noble metal (Pt, Pd, Ag and Rh) doped nano ZnO are displayed in Figure 4.5 and Figure 4.6. All the main peaks can be indexed to nano ZnO (JCPDS card 35-1001) which are consistent with general features of nanomaterials. No characteristic peak of noble metals in XRD was investigated this shows that the metal paticles are bound to the surface of metal oxides. Crystal structure and particle size of modified ZnO was studied using an X-ray diffractometer. The X-ray diffraction patterns of the Nano ZnO without calcination, calcined at 300 ^{0}C and 500 ^{0}C are presented in Figure 4.6.

It shows that ZnO samples have some diffraction peaks of ZnO with 2θ at 31.86^o (100), 34.54 ^{o} (002), 36.32 ^{o} (101), 47.62 ^{o} (102), 56.66 ^{o} (110), 62.96 ^{o} (103), 68.04 ^{o} (112), and 69.18 ^{o} (201). Diffraction peaks in Figure 4.5-4.7 could be readily indexed as hexagonal phase of ZnO, the lattice parameters of which were all consistent with reported values (corresponding to the JCPDS-ICDD 36-1451 card of ZnO). The diffractograms reveal that the nano ZnO yielded crystals with high purity and uniformity.

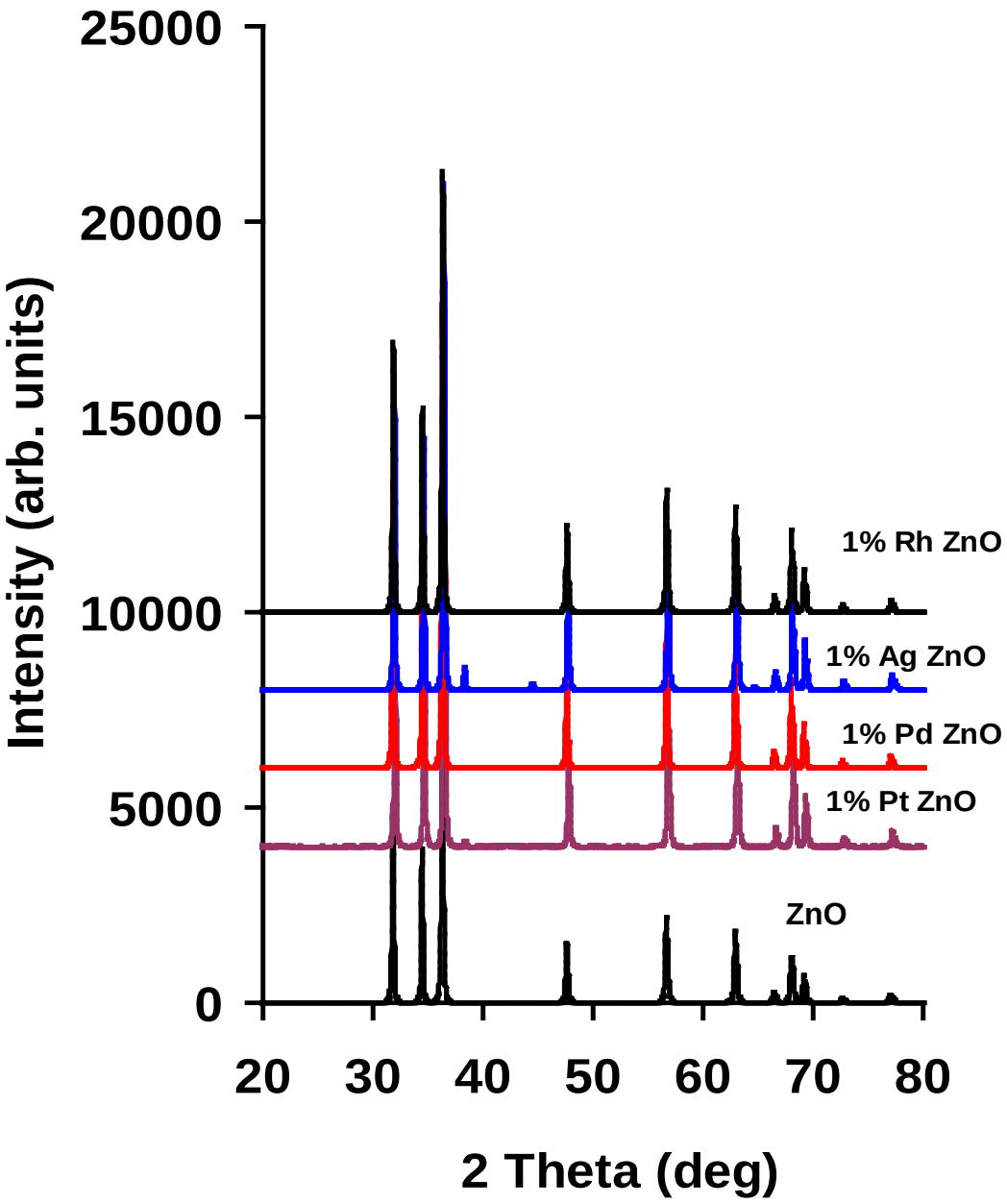

Figure 4.5 X-ray diffractrogram for nano ZnO and doped ZnO

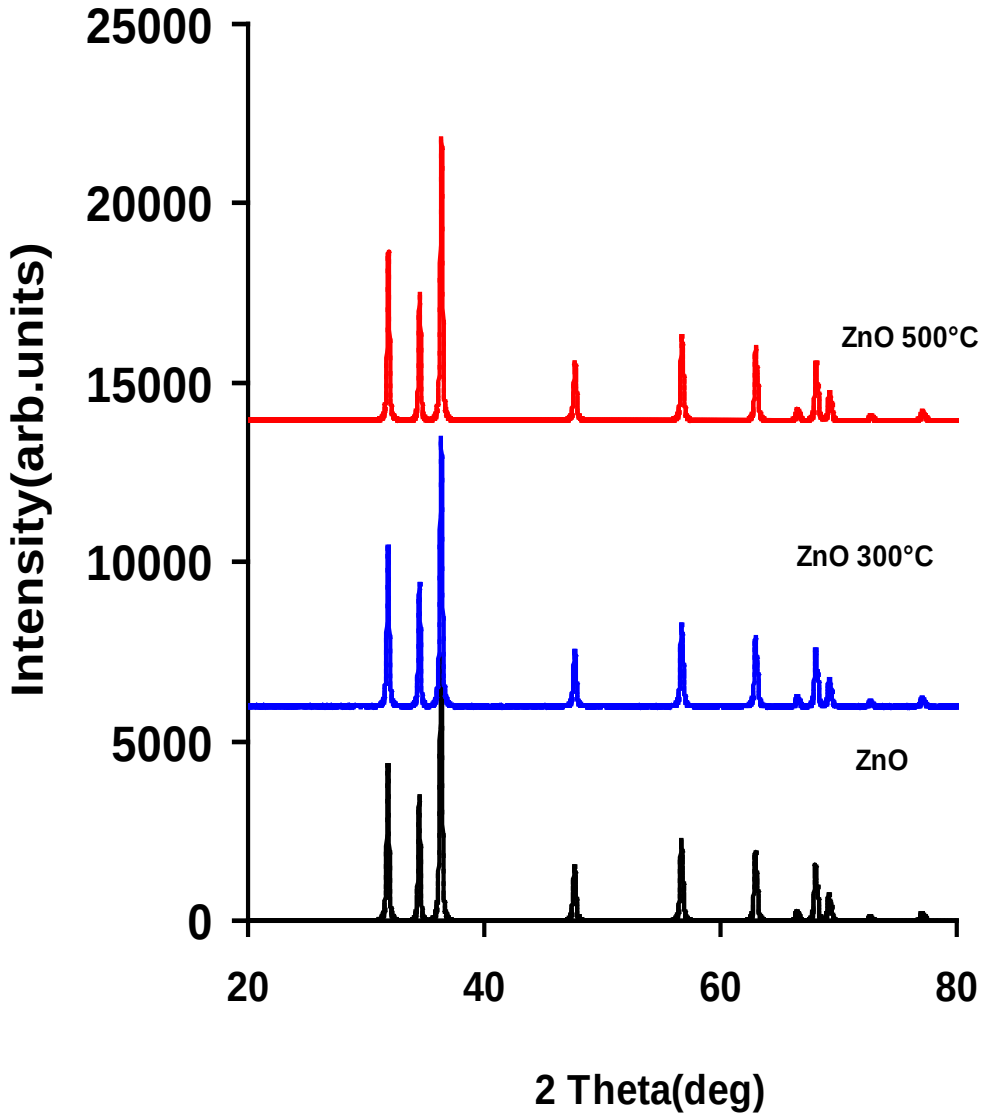

Figure 4.6 X-ray diffractrogram for as received, calcined at 300 ℃ and calcined at 500 ℃ nano ZnO

Table II Particle size of ZnO and ZnO doped and undoped estimated using Scherrer equation from XRD analysis

S.No.	Catalyst	2ɵ	d-Val	FWHM	Intensity	Estimated particle size (nm)
1	ZnO(Com.)	36.3055		0.1932		43.2
2	ZnO(Com.)WH	36.3125	2.47200	0.2097	5539	40.0
3	ZnO(Com.)300DegC	36.3153	2.47182	0.2043	5666	41.0
4	ZnO(Com.)500 degC	36.3085	2.47227	0.1980	5951	43.0
5	Nano ZnO ppt	36.3908	2.46687	0.4698	2606	17.8
6	Nano ZnO 400 ºC	36.2866	2.47371	0.1900	5790	44.0
7	Nano ZnO 500 ºC	36.2841	2.47387	0.1772	6088	47.1
8	Nano ZnO 550 ºC	36.2800	2.47414	0.1725	6431	48.4
9	Nano ZnO 600 ºC	36.3413	2.47011	0.1699	6997	49.2
10	Nano ZnO 700 ºC	36.2834	2.47392	0.1645	7039	50.8
11	1%Pt ZnO	36.4658	2.46196	0.1770	10770	47.2
12	1%Pd ZnO	36.2554	2.47577	0.1631	9559	51.2
13	1%Ag ZnO	36.3777	2.46772	0.1722	10270	48.5
14	1%Rh ZnO	36.2639	2.47521	0.1635	9032	51.1

Scherer's equation leads to an estimated average particle size of 40, 41 and 43 nm for the ZnO without calcination, calcined at 300 ^{0}C and 500 ^{0}C respectively. Although it is evident that the change in crystalline size of nano ZnO is not significant by calcining it at 500 ^{0}C but the particles might be agglomerated after calcination. The commercial nano ZnO is particulated and the mean dimension values are <100nm as reported by Aldrich.Nano ZnO particles were also synthesized by sol gel method and the average particle size was estimated and found to be ranging from 15 nm to 50 nm.

4 .1.3. Characterization of Nano NiO and Noble Metal Doped Nano NiO

The purity and crystallinity of the as-synthesized NiO nanoparticles were examined by using powder X-ray diffraction (XRD). Xray diffractogram of NiO and doped NiO are shown in Figure 4.8.The particle size of doped and undoped NiO using Scherrer equation was presented in Table III. Figure 4.8 shows XRD patterns of the products obtained after the precursors have been calcined. The peaks positions appearing at 2 ɵ = 37.20◦, 43.20◦, 62.87◦, 75.20◦ and 79.38◦ can be readily indexed as (1 1 1), (2 0 0), (2 2 0), (3 1 1), and (2 2 2) crystal planes of the bulk NiO, respectively. The peak positions and lattice parameters of all these diffraction peaks depicted in Figure 4.8 are well consistent with that of the standard JCPDS Card No. 04-0835 for the standard spectrum of pure and cubic NiO. The results indicate that the products are nano-NiO crystal of cubic structure with high purity. The mean particle size of the as-synthesized products is calculated according to this at about 6.5 nm.

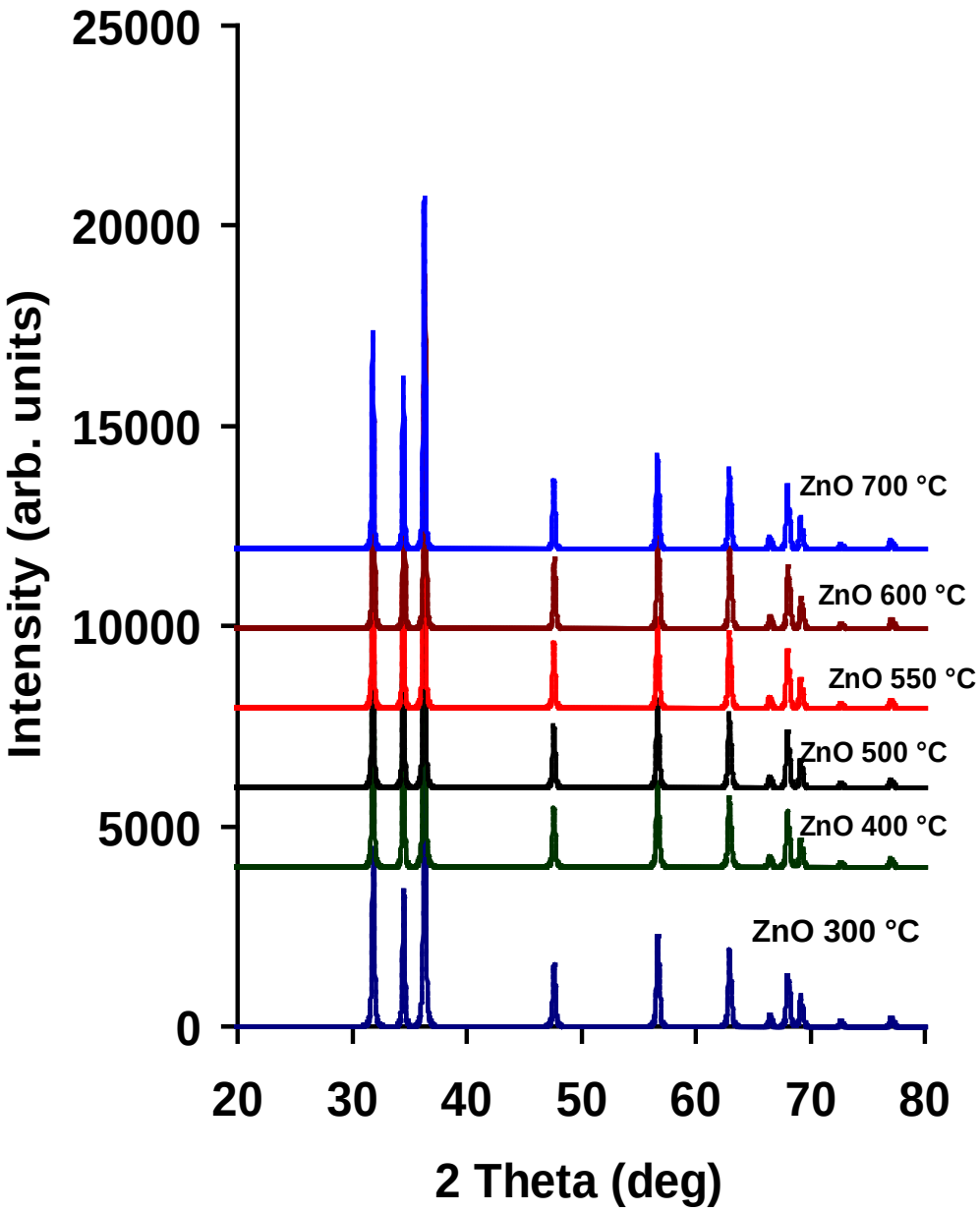

Figure 4.7 X ray diffractogram for nano ZnO at different temperatures

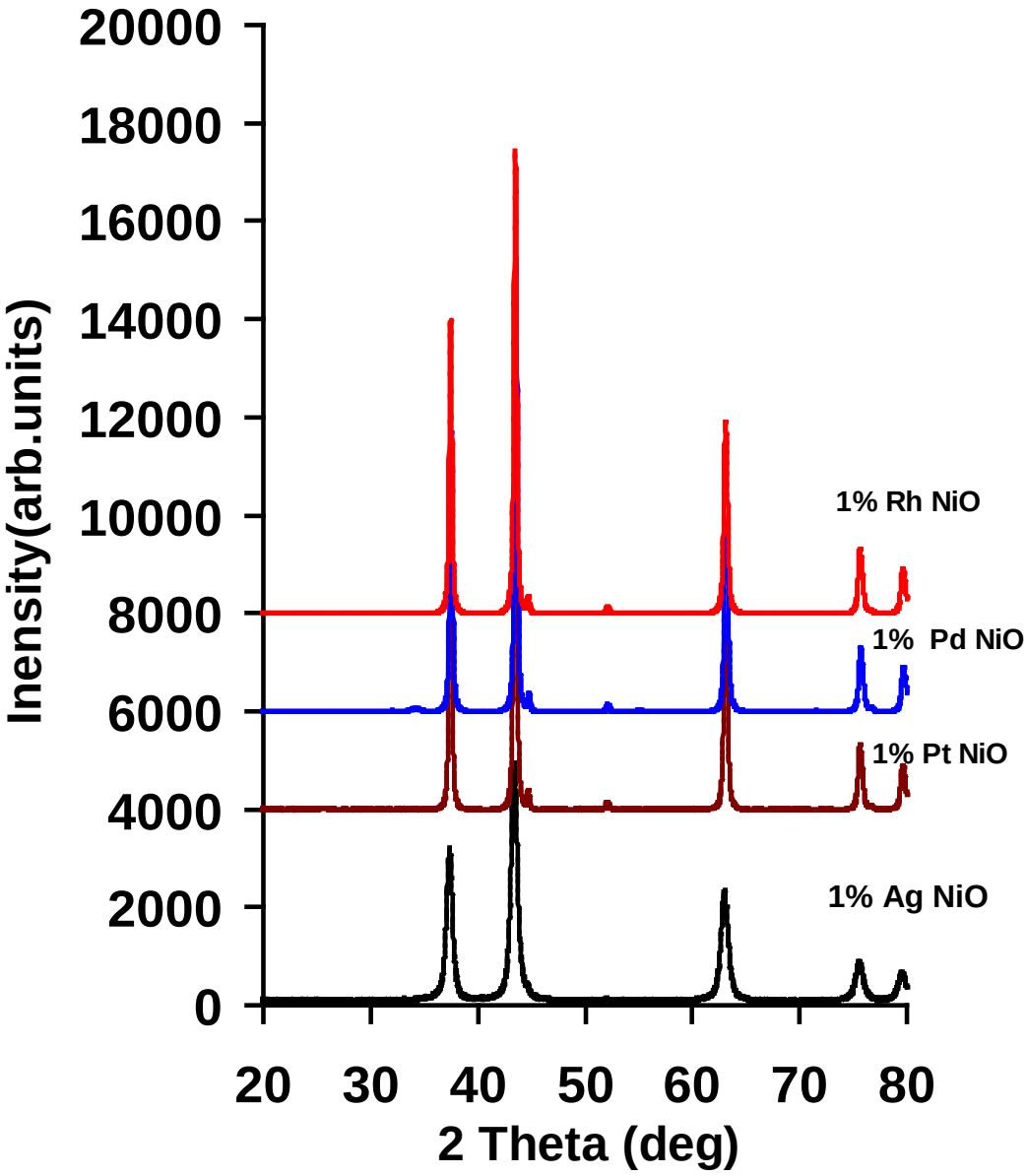

Figure 4.8 X ray diffractogram for nano NiO and doped nano NiO

4.2. Morphology of Nano Metal Oxides

In this study, Nova Nano SEM Ultra-High Resolution was used to study the morphology and composition. The field emission electron source was used. The image types obtained are secondary electron and backscattered electron images. The electrons interact with the atoms that make up the sample producing signals that contain information about the sample's surface topography, composition and other properties such as electrical conductivity. The electron beam, which typically has an energy ranging from 0.5 keV to 40 keV, is focused by one or two condenser lenses to a spot about 0.4 nm to 5 nm in diameter. The beam passes through pairs of scanning coils or pairs of deflector plates in the electron column, typically in the final lens, which deflect the beam in the x and y axes so that it scans in a raster fashion over a rectangular area of the sample surface**.** The energy dispersive X ray spectrometry (EDX) analysis was employed to determine the composition of the semiconductor pure and doped metal oxide.

Transmission electron microscope (Philips EM 301 model) was used in order to study the particle morphology. Transmission electron micrograph gives directly the size and shape distributions. Also, it furnishes details about the crystalline nature of the cluster. The powder samples are examined under the transmission electron microscope. The powders are dispersed in acetone by stirring in an ultrasonic tank for 15 minutes. A drop of the liquid is placed on a carbon film supported on a 3 mm microscope grid. The solvent is allowed to evaporate followed by mounting the grid on the specimen holder of the transmission electron microscope operating at 100 KV.

Table III Particle size of NiO doped and undoped estimated using Scherrer equation from XRD analysis

S.No.	Catalyst	2ɵ	d-Val	FWHM	Intensity	Estimated particle size (nm)
1	Nano NiO-A	44.5573	2.03186	0.2093	5270	41.0
2	Nano NiO SG	43.3604	2.08513	0.7084	3109	12.0
3	1%Pt NiO	43.4559	2.08077	0.2817	7124	30.3
4	1%Pd NiO	43.5125	2.07819	0.2927	6741	29.2
5	1%Rh NiO	43.6399	2.08114	0.2873	6932	29.8

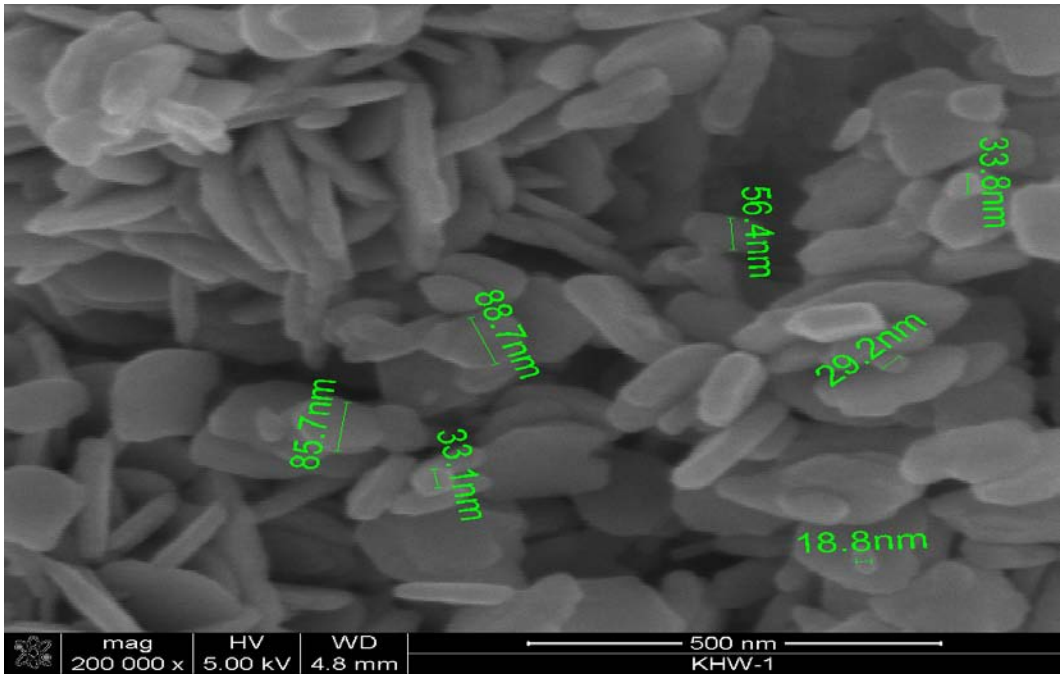

Figure 4.9 SEM micrograph of as prepared WO_3

4.2.1 SEM and TEM Images of Nanocrystalline WO_3 and Doped WO_3

The morphologies of the synthesized nanoparticles were characterized using transmission electron microscopy (TEM, JEM 200CX, 120 kV) and scanning electron microscopy (SEM, Hitachi S-4700 II, 25 kV). SEM images of the synthesized WO_3 nanopowder (doped, undoped and calcined at different temperatures) are depicted in Figure (4.9-4.22). The mean particle size of nano 6.7- 50 nm as investigated by SEM.The energy dispersive spectrometry (EDS) analysis was employed to determine the composition of the doped tungsten oxide and metal tungstates. As is clear from the results given in Figure (4.23-4.30), only oxygen and tungsten elements existed in the nanoparticles of WO_3 with molar ratio of about 3 (O/W). An EDX elemental analysis showed that the WO_3, ZnO and NiO particles calcined at temperatures greater than 500 ºC were composed of mainly W, Zn, Ni and O elements respectively.The elemental composition for doped WO_3 determined using EDX analysis are consistent with the dopant weight % used for synthesis of these samples.

4.2.2 SEM and TEM Images of Nano ZnO and Doped ZnO

The morphology of zinc oxide prepared at different conditions has been analyzed by means of microscopes such as SEM, TEM. Most SEM images show that the as-prepared ZnO consists of mainly individual particles sized around 40 nm in diameter with a narrow size distribution. The results are presented in Figure (4.30-4.43).Various parameters and experimental conditions that could affect the morphology of ZnO are investigated.

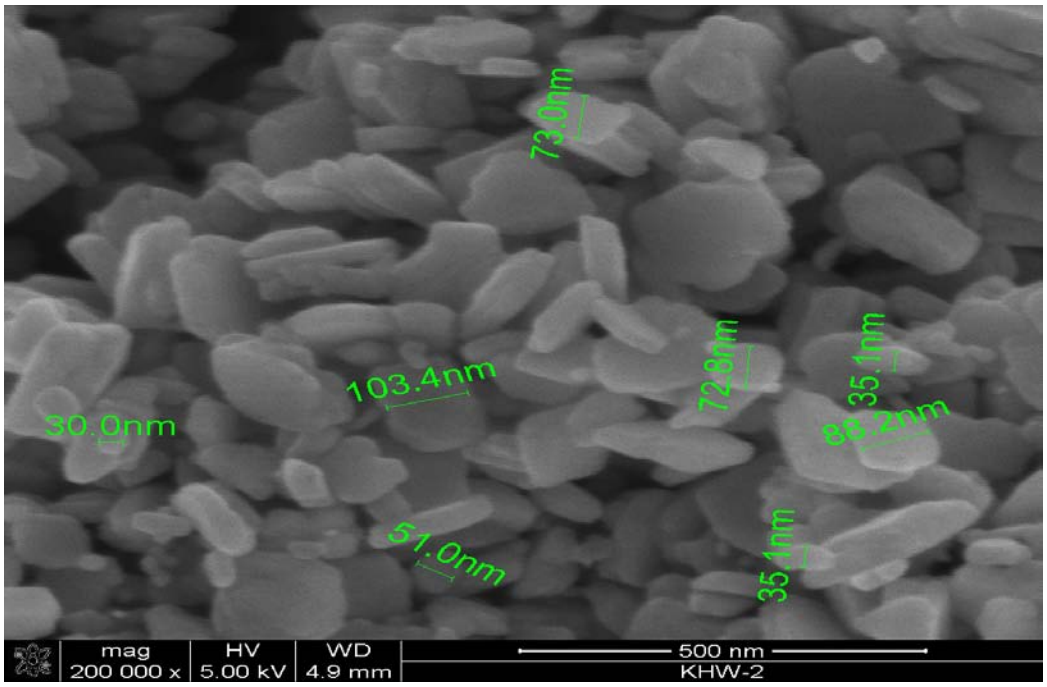

Figure 4.10 SEM micrograph of Pt-doped WO_3

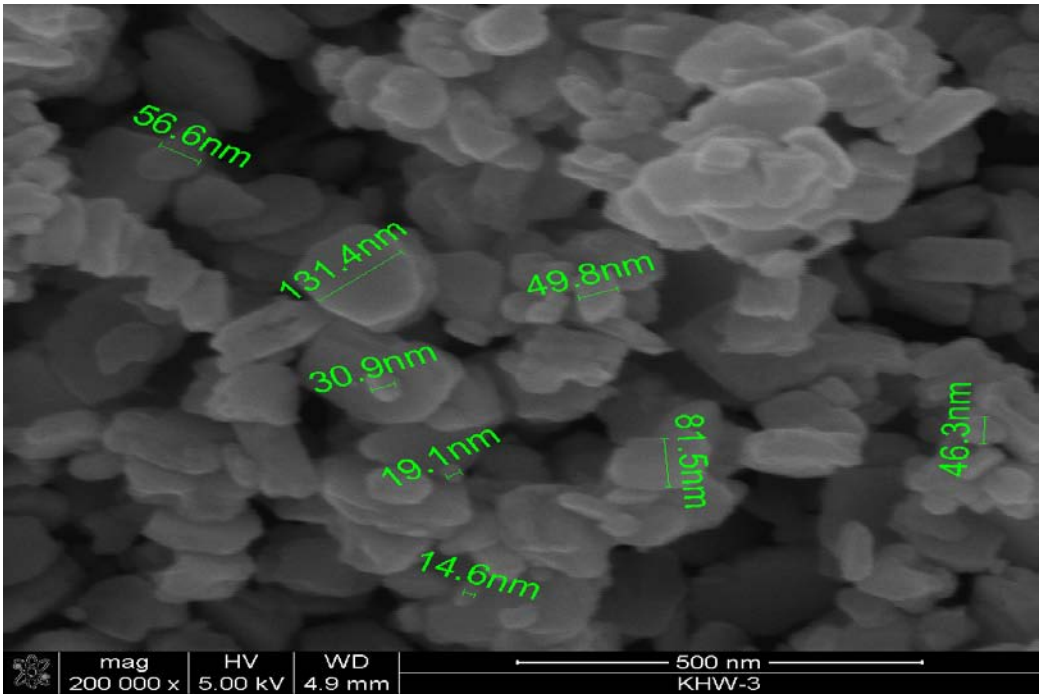

Figure 4.11 SEM micrograph of Pd-doped WO_3

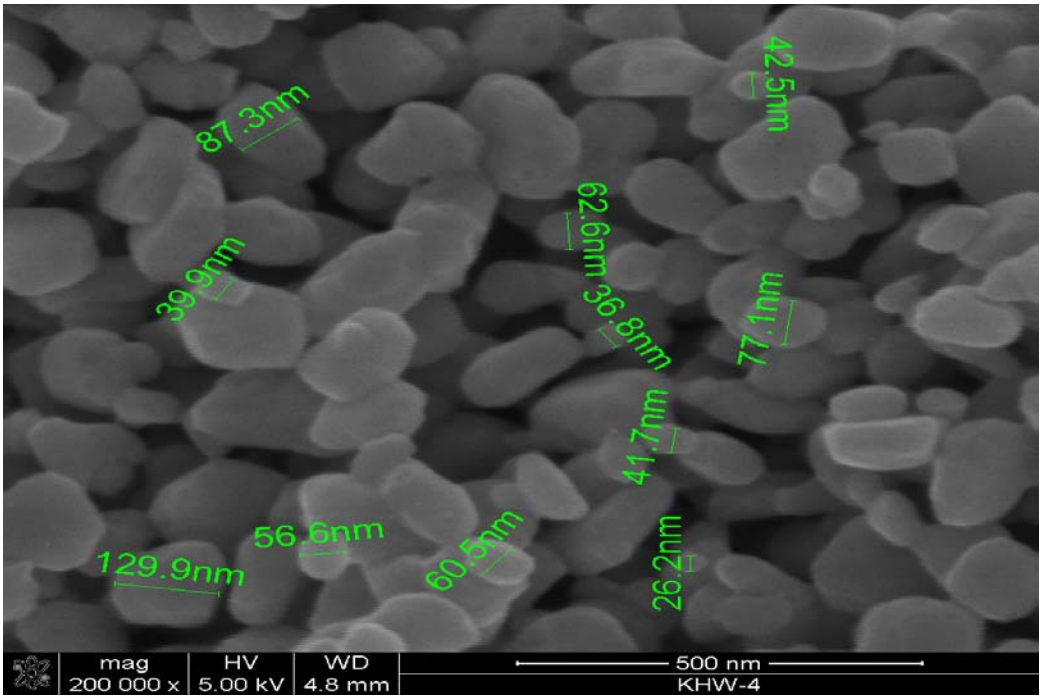

Figure 4.12 SEM micrograph of Ag- doped WO_3

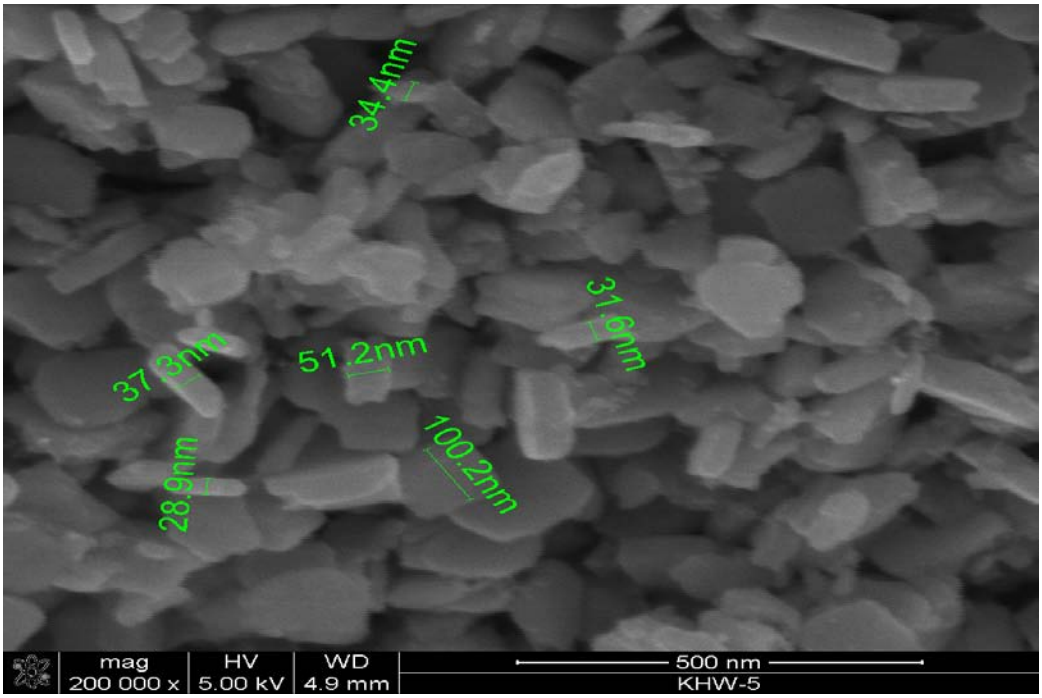

Figure 4.13 SEM micrograph of Rh-doped WO_3

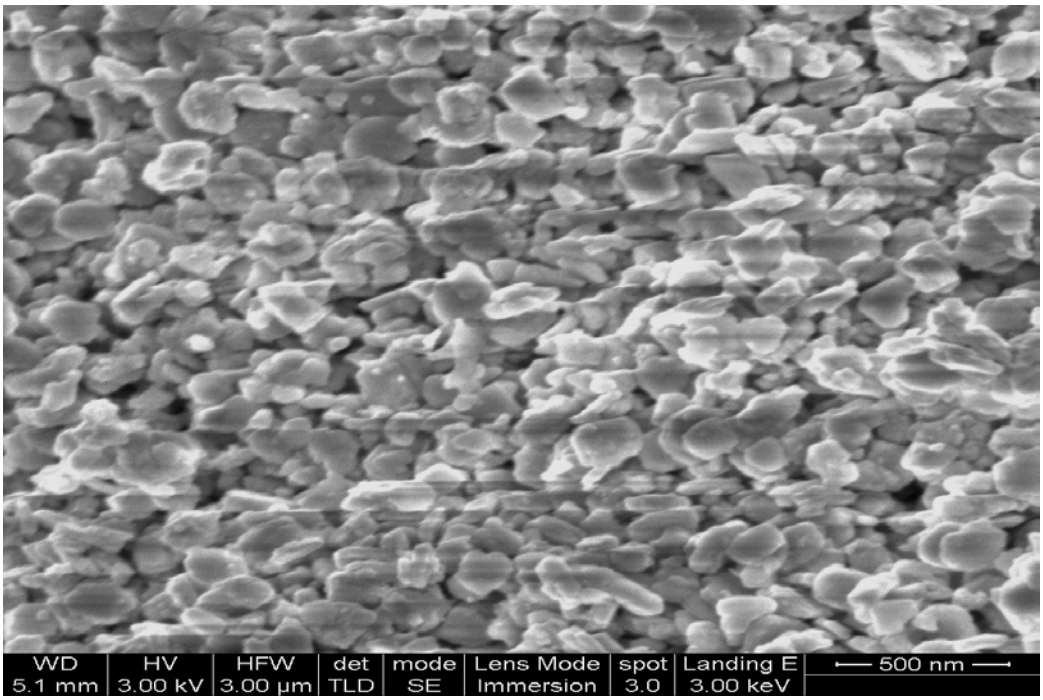

Figure 4.14 SEM micrograph of 5 % Pt-doped WO_3

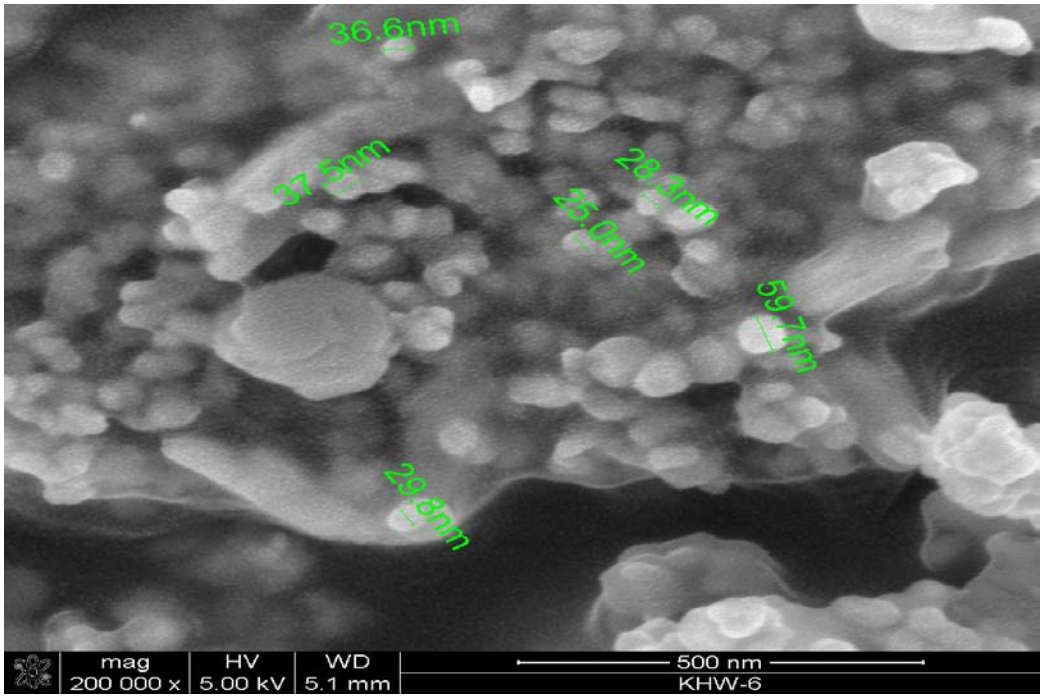

Figure 4.15 SEM micrograph of as prepared $ZnWO_4$

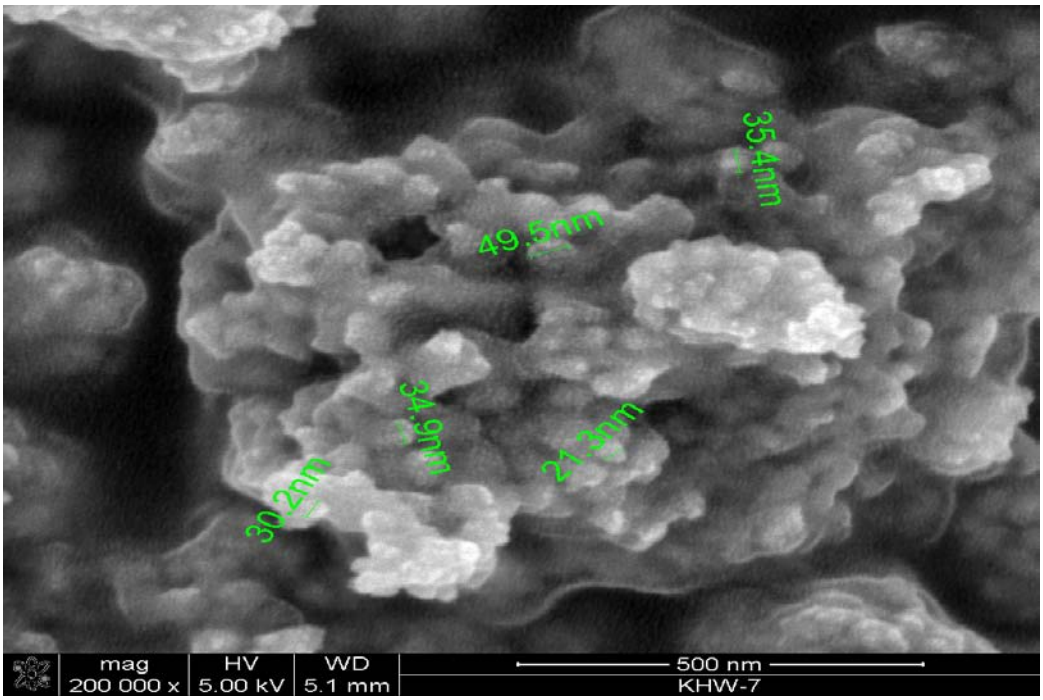

Figure 4.16 SEM micrograph of as prepared $NiWO_4$

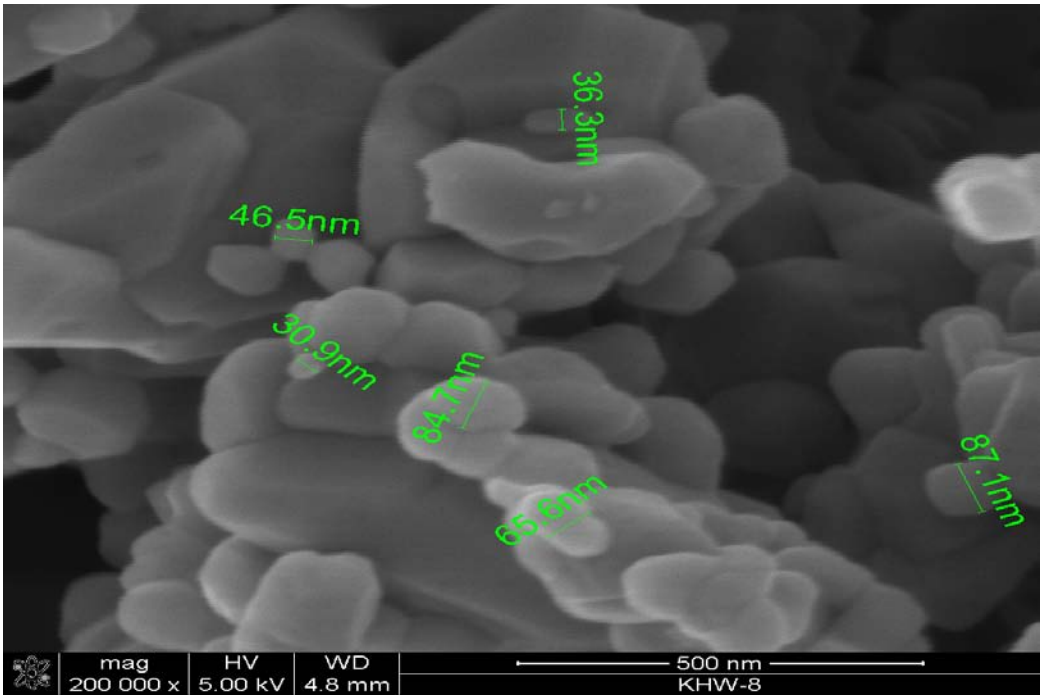

Figure 4.17 SEM micrograph of as prepared $CuWO_4$

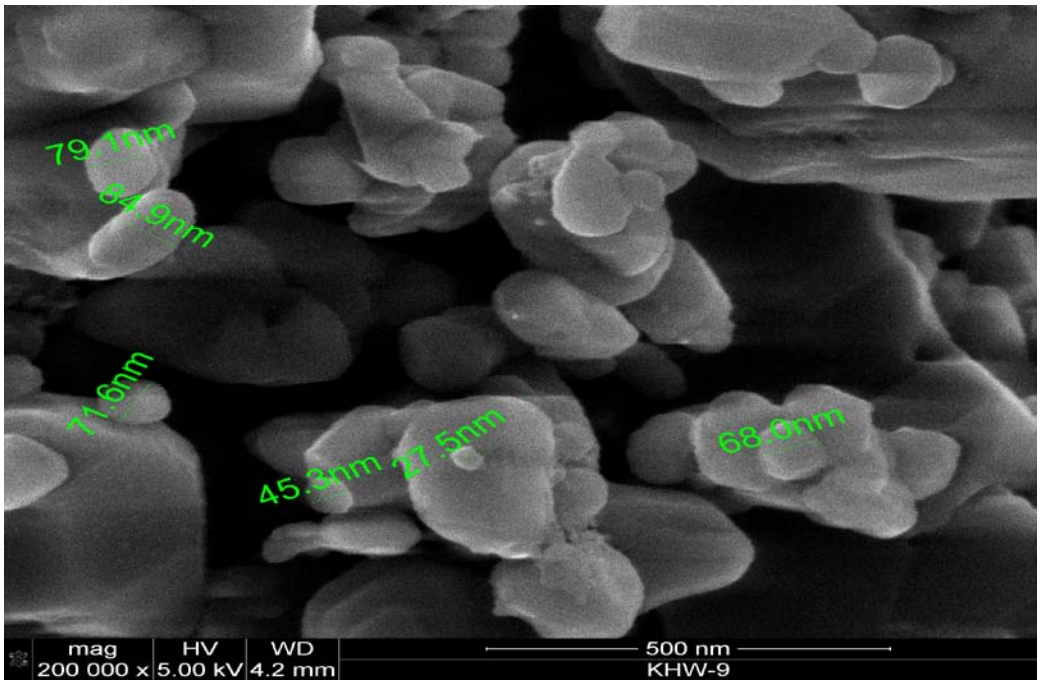

Figure 4.18 SEM micrograph of as prepared Pt- $CuWO_4$

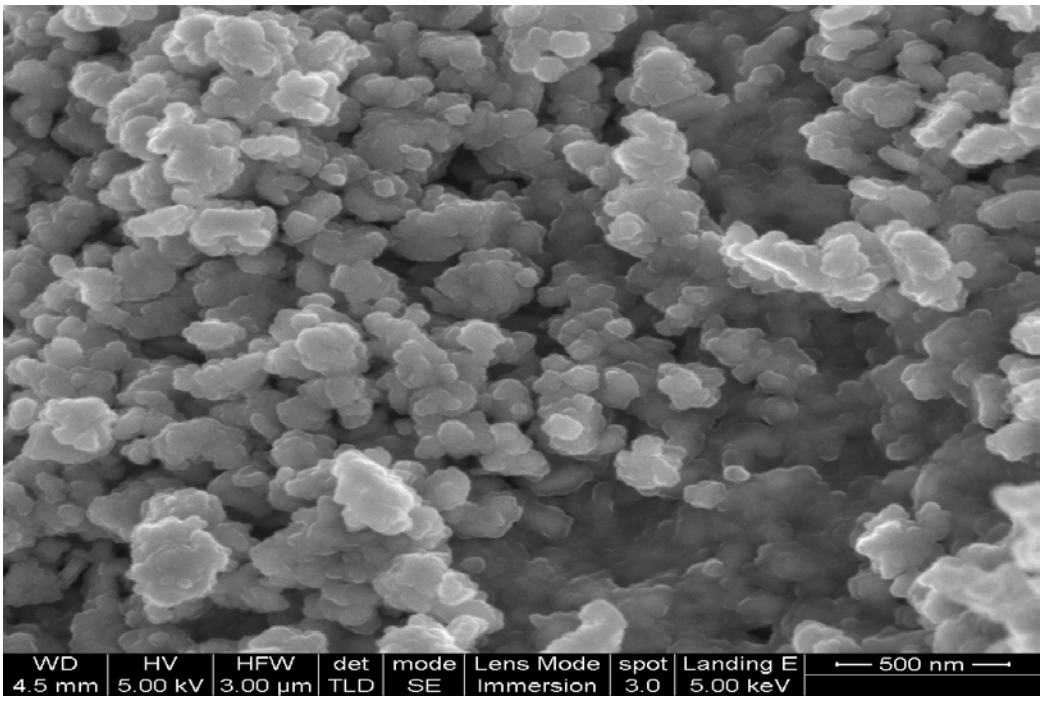

Figure 4.19 SEM micrograph of Nanoccrystalline WO_3 calcined at 300 °C

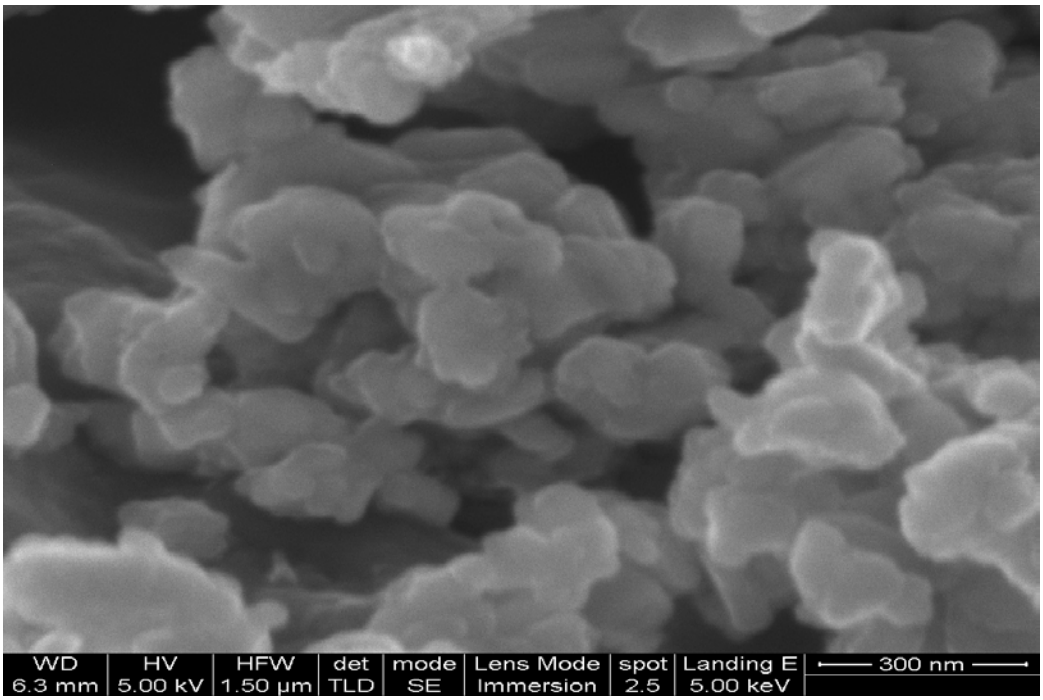

Figure 4.20 SEM micrograph of Nanoccrystalline WO_3 calcined at 400°C

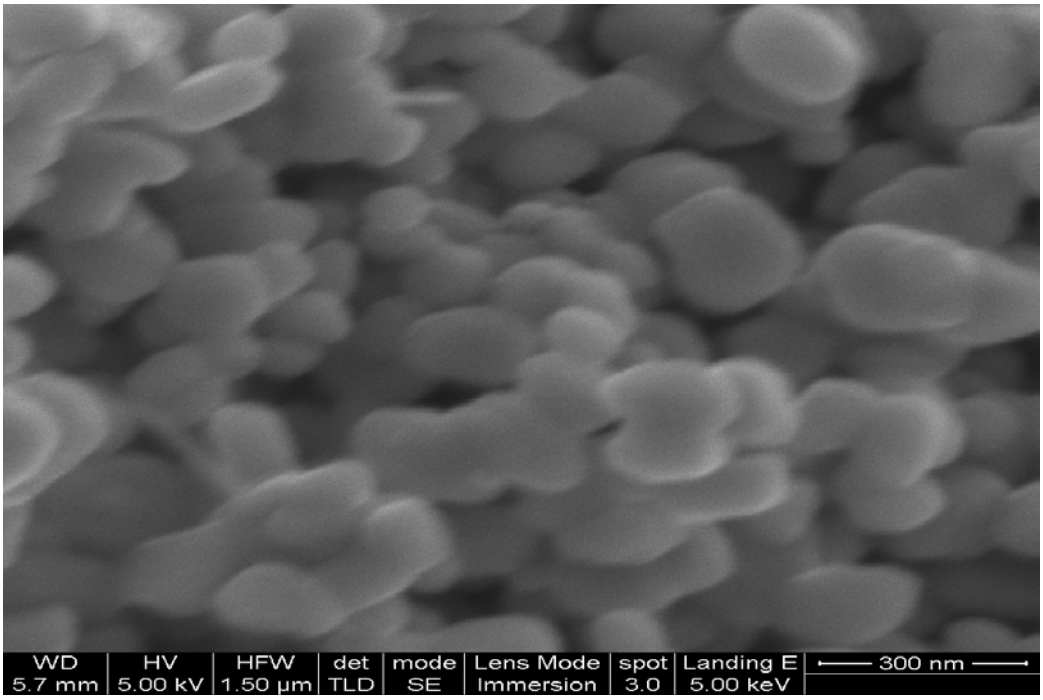

Figure 4.21 SEM micrograph of Nanoccrystalline WO_3 calcined at 600 °C

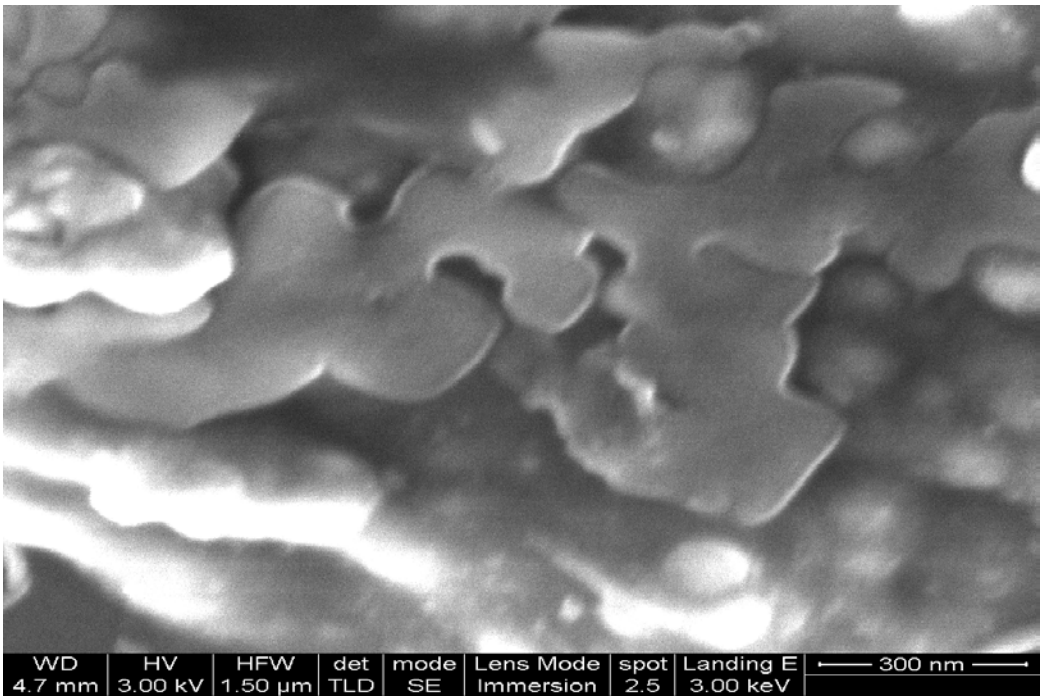

Figure 4.22 SEM micrograph of Nanocrystalline WO_3 calcined at 700 °C

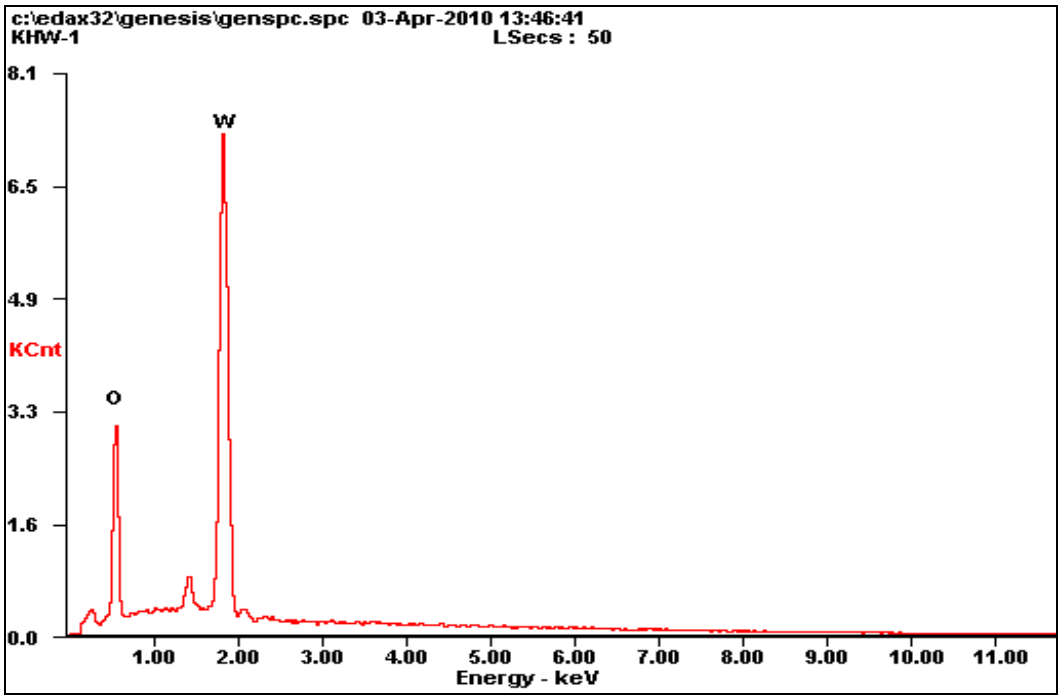

Figure 4.23 EDX spectrum of WO_3

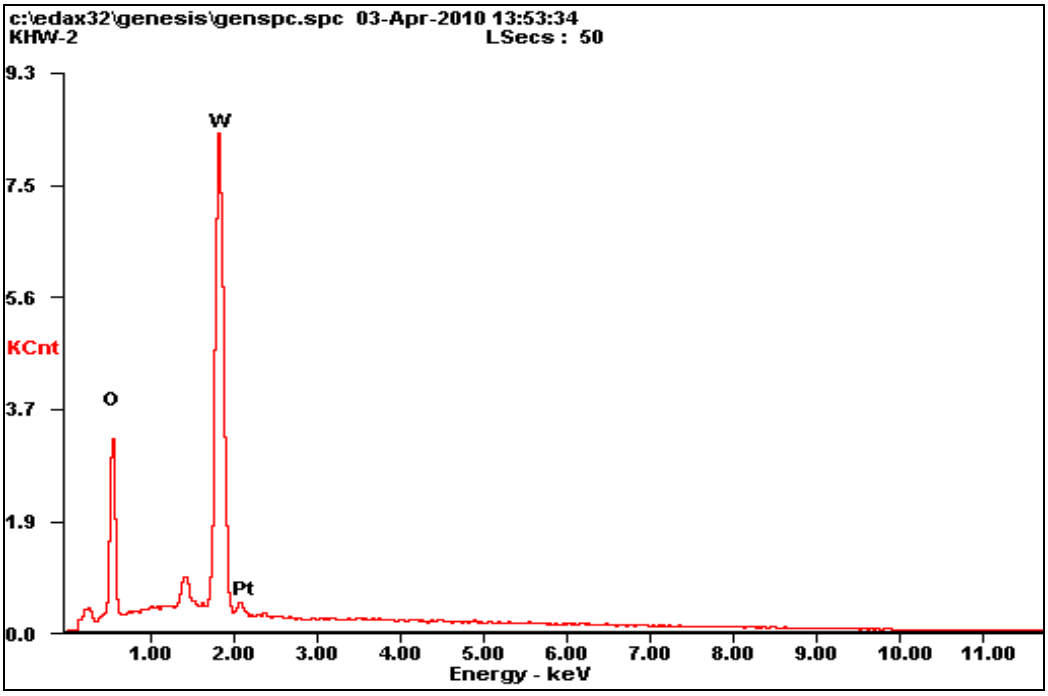

Figure 4.24 EDX spectrum of Pt WO_3

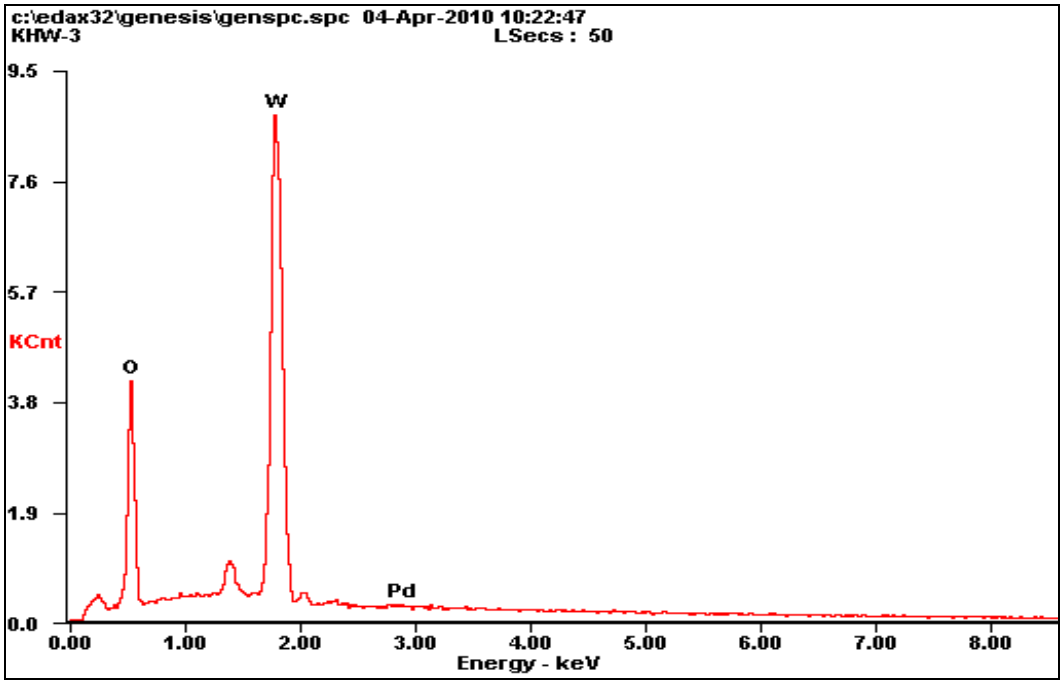

Figure 4.25 EDX spectrum of as prepared $PdWO_3$

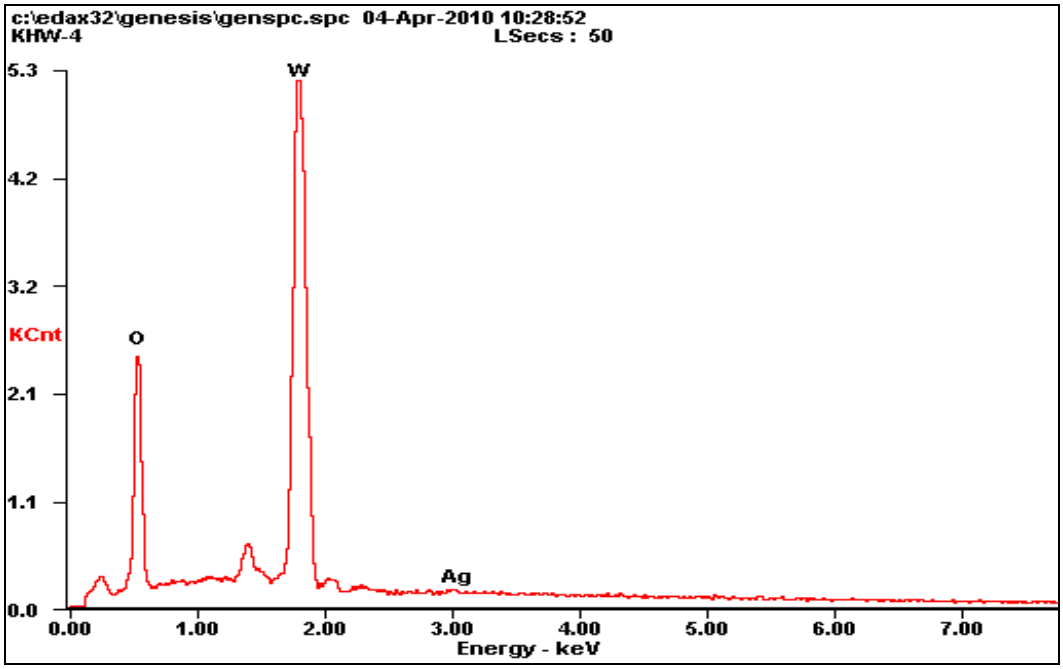

Figure 4.26 EDX spectrum of as prepared $AgWO_3$

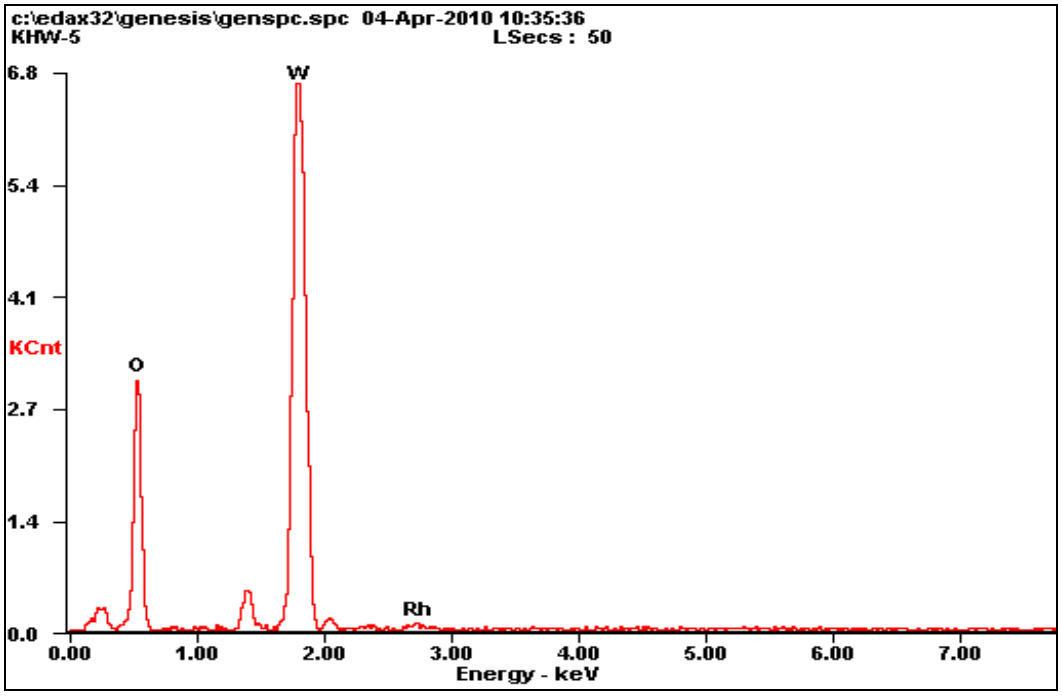

Figure 4.27 EDX spectrum of as prepared $RhWO_3$

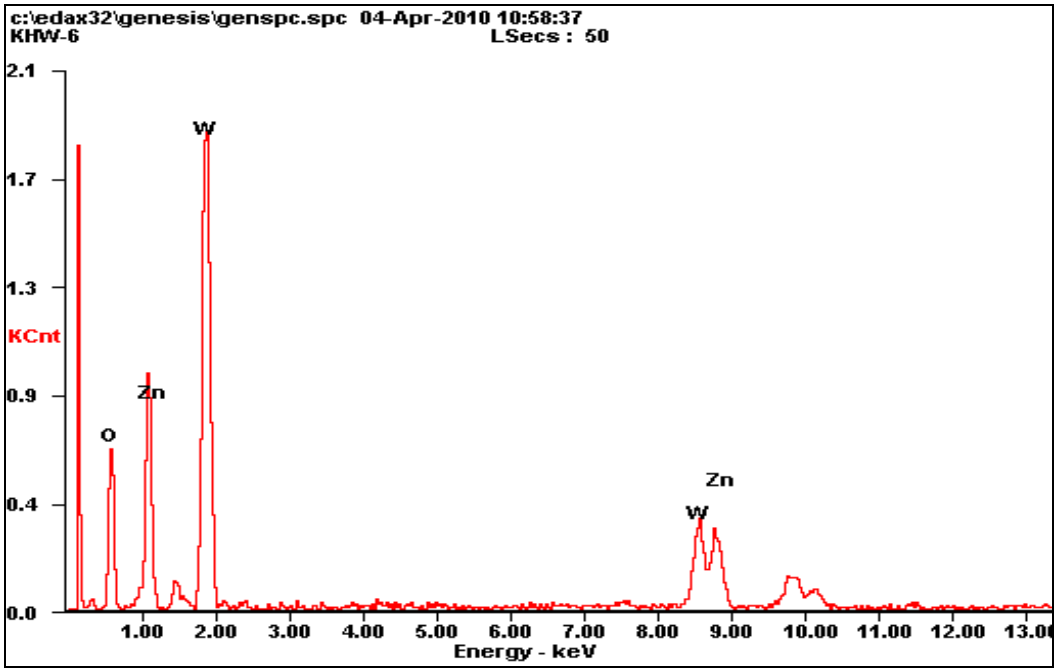

Figure 4.28 EDX spectrum of $ZnWO_4$

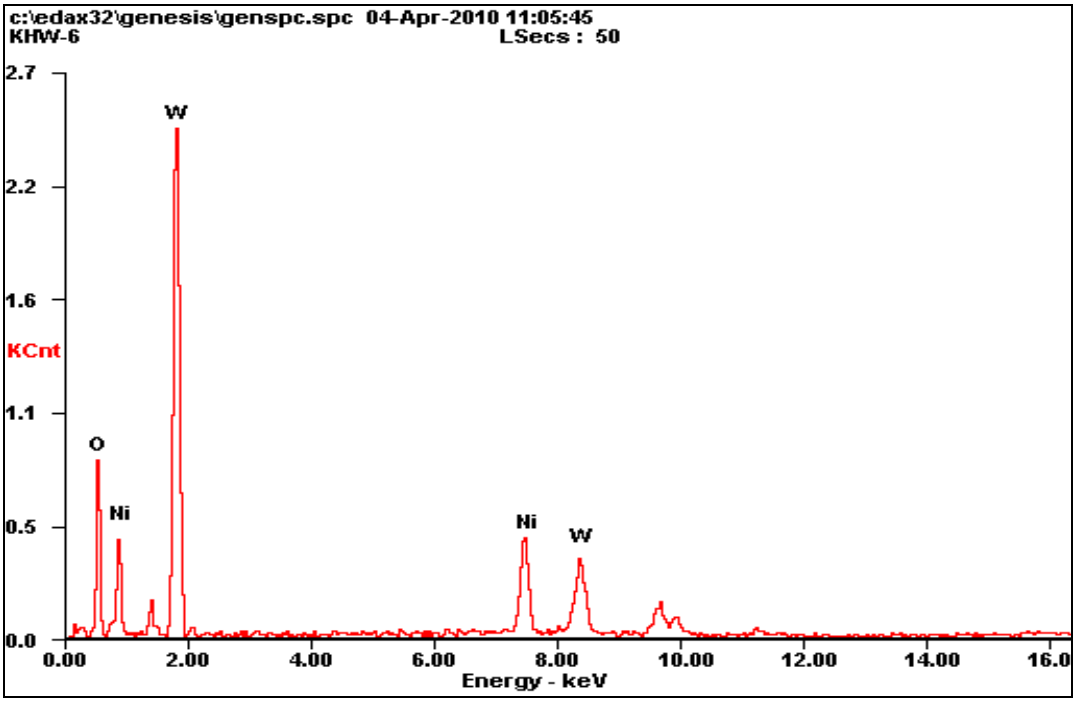

Figure 4.29 EDX spectrum of $NiWO_4$

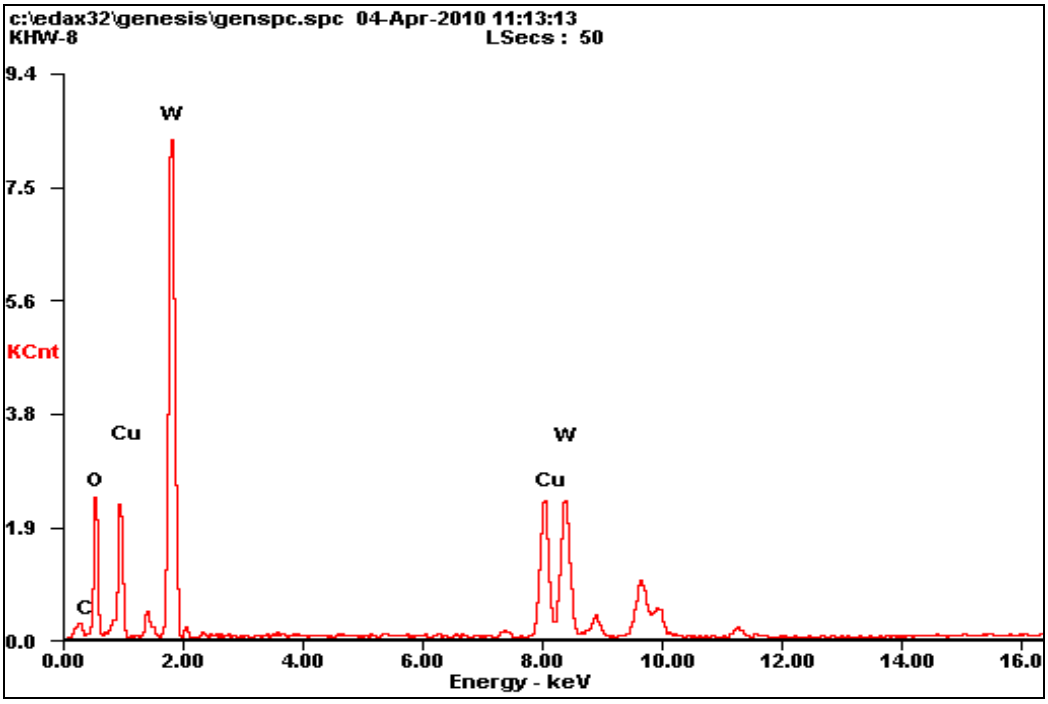

Figure 4.30 EDX spectrum of $CuWO_4$

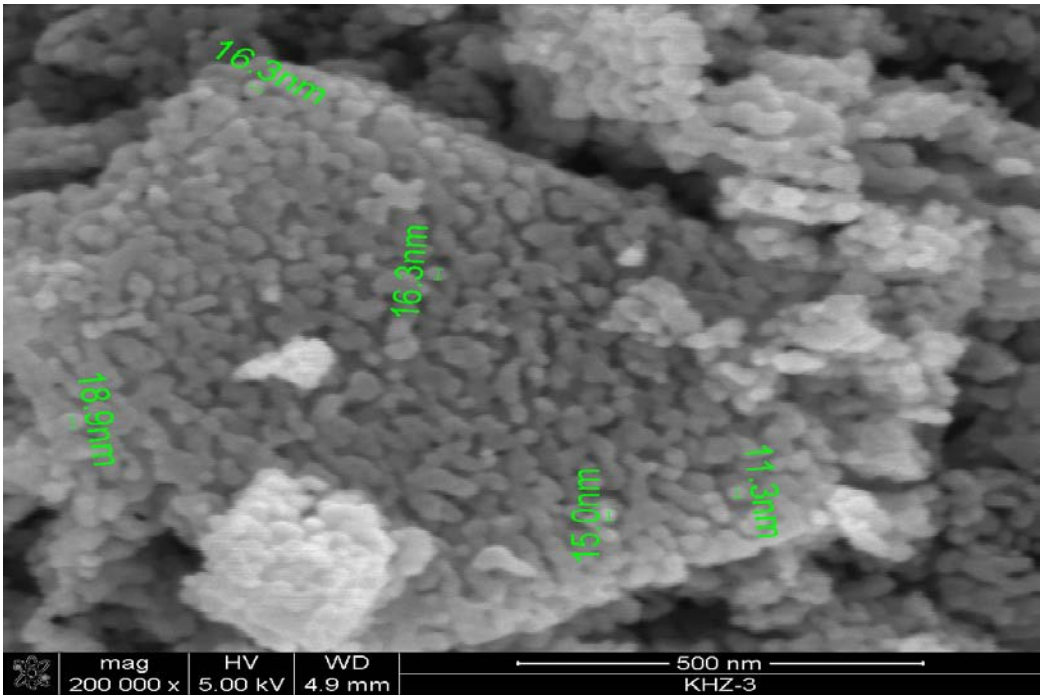

Figure 4.31 SEM micrograph of nano ZnO ppt.

4.3 Effect of Calcination Temperature on Morphology of WO_3 and ZnO

The morphology of zinc oxide prepared at different conditions has been checked by means of FESEM and TEM. The surface morphology and crystallite structure of calcined powders were analyzed using FESEM (model: Nova NanoSEM Ultra-High Resolution, 30 kV). The SEM images validate that ZnO exists in single homogeneous phase with narrow size distribution. The energy dispersive X ray spectrometry (EDXS) analysis was employed to determine the composition of the ZnO. Energy dispersive X-ray spectrum (EDXS) of ZnO -500 shows peaks corresponding to Zn and O, no trace amount of other impurities could be seen in the detection limit of the EDXS.

The results obtained regarding the effect of the calcination temperature on the particle size is depicted in Figure 4.37- Figure 4.40. The decrease in the surface area and the increase in the particle size of the calcined particles are due to the growth and sintering of nanoparticles. The particle size of ZnO increased rapidly when the calcination temperature increased from 600 to 700 °C. The samples were calcined for 7 hour at their respective temperature. The mean particle size was obtained from the images by the statistic method. The results show that the particle size increases with temperature. It is noted that the size determined by Scherer formula are different as compared to the size observed from FESEM except at higher temperatures (600 °C, 700 °C). As calcination temperature increases, crystallites tend to agglomerate originating bigger crystal particles with the subsequent decreasing in the surface area of the solids.

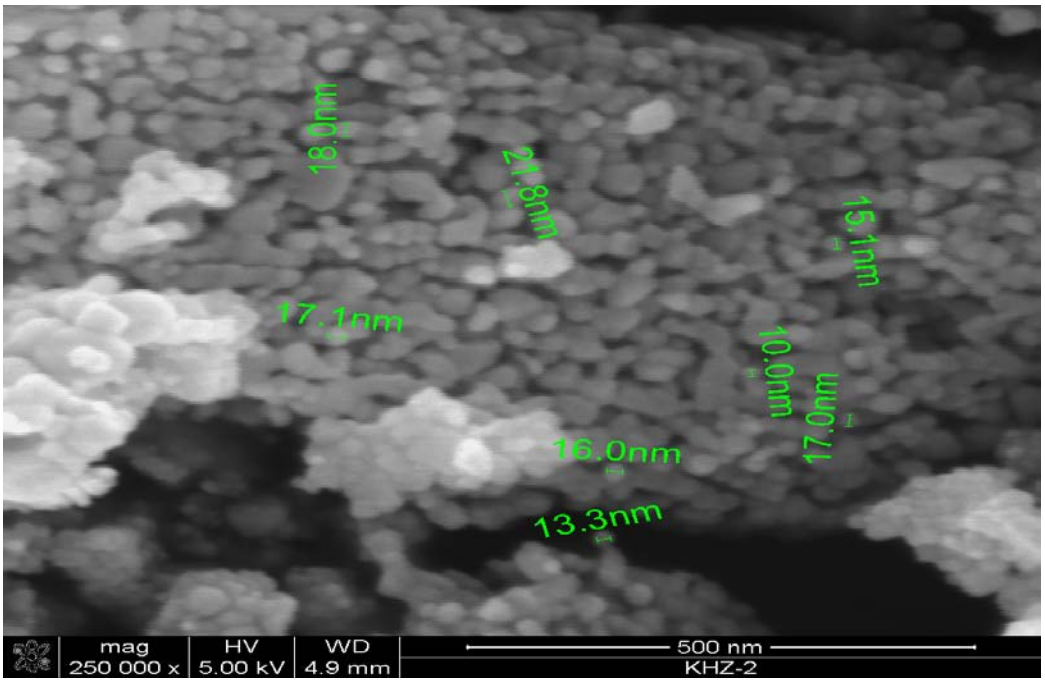

Figure 4.32 SEM micrograph of nano ZnO calcined at 500°C

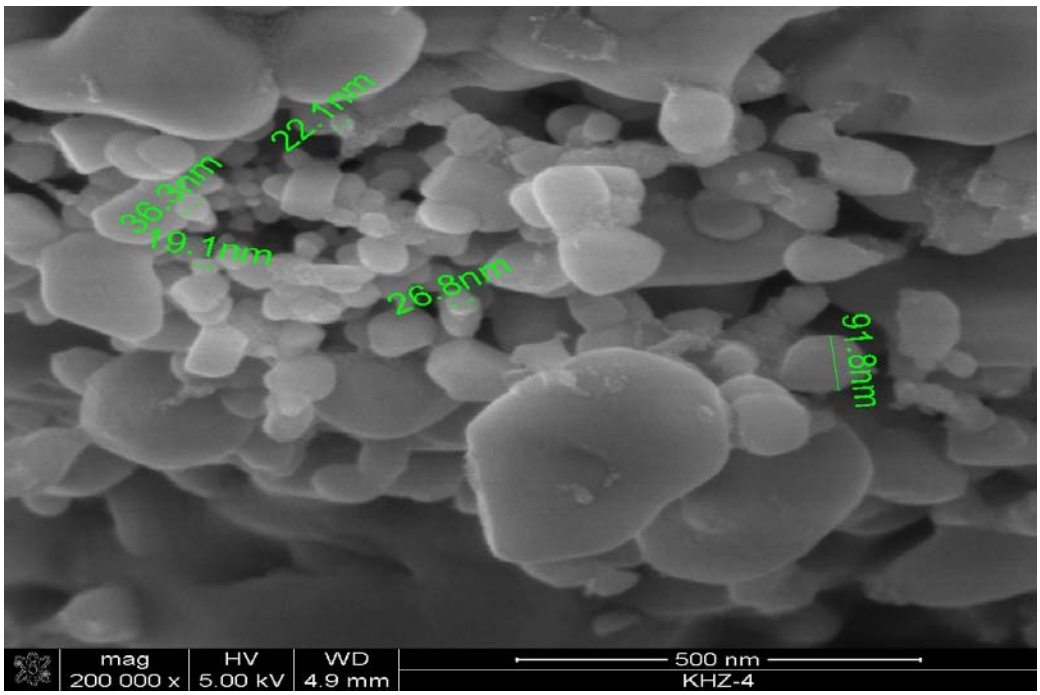

Figure 4.33 SEM micrograph of Pt-doped ZnO

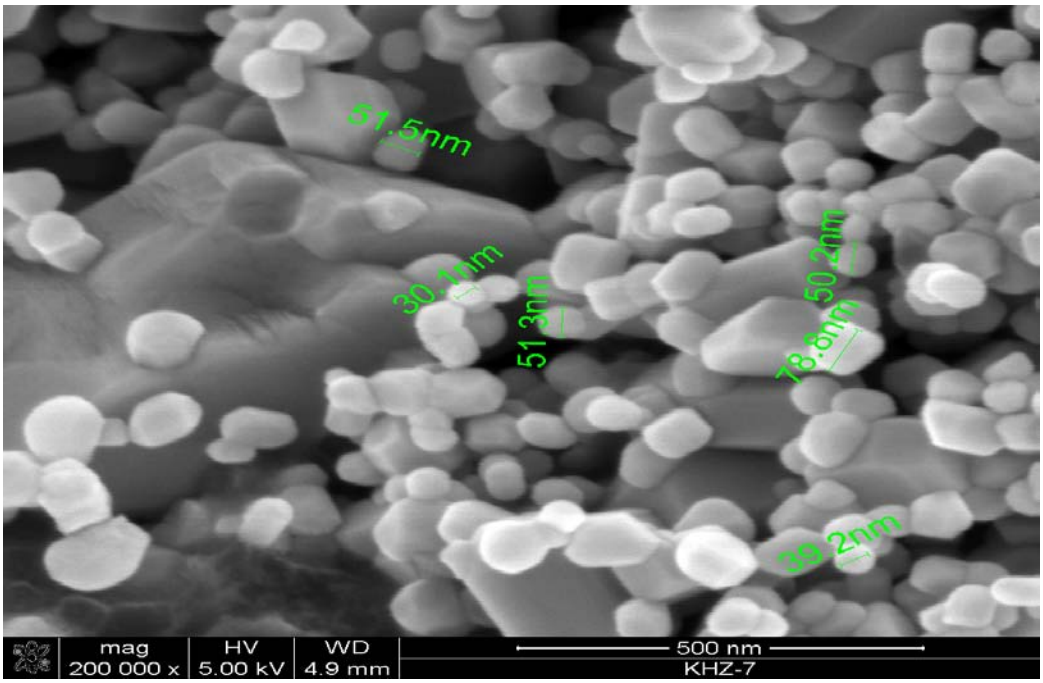

Figure 4.34 SEM micrograph of Pd-doped ZnO

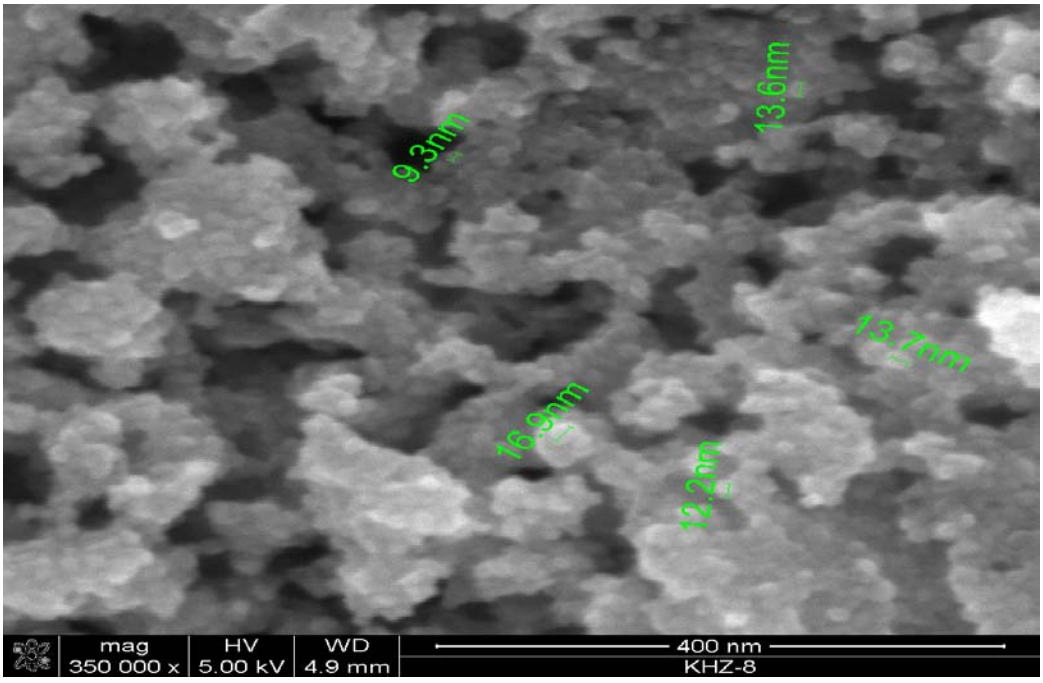

Figure 4.35 SEM micrograph of Ag-doped ZnO

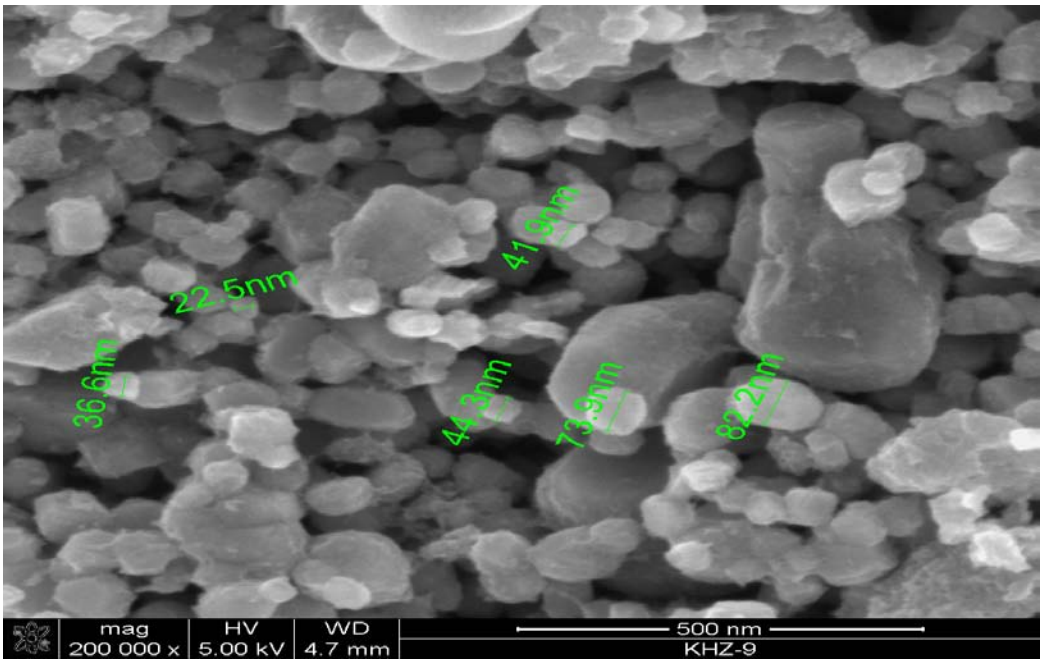

Figure 4.36 SEM micrograph of Rh-doped ZnO

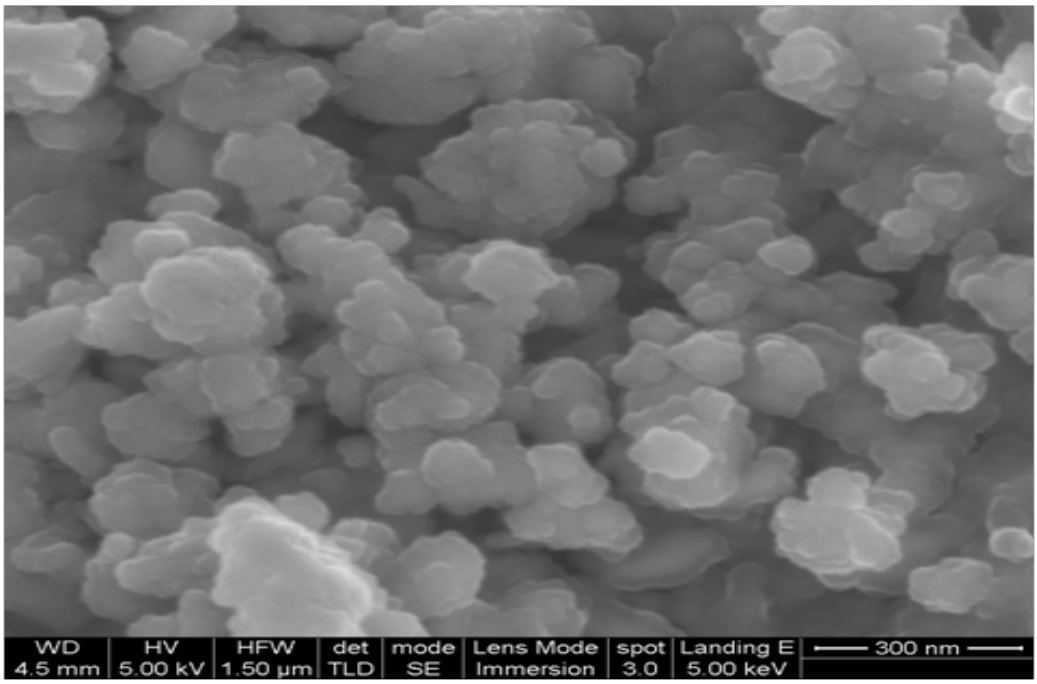

Figure 4.37 SEM micrograph of nano ZnO calcined at 300°C

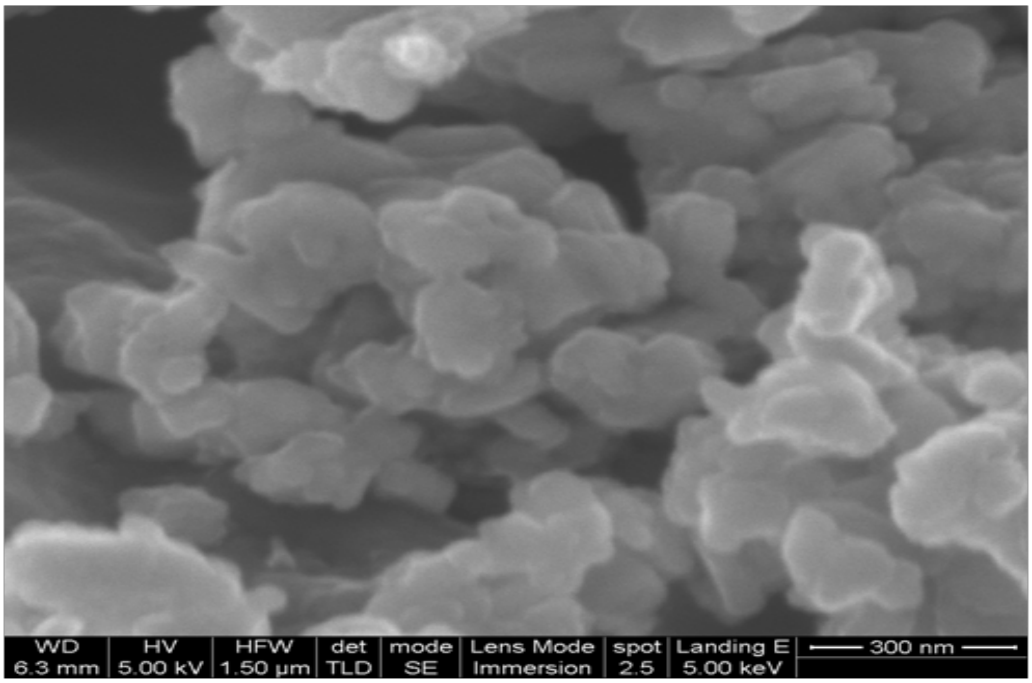

Figure 4.38 SEM micrograph of nano ZnO calcined at 400°C

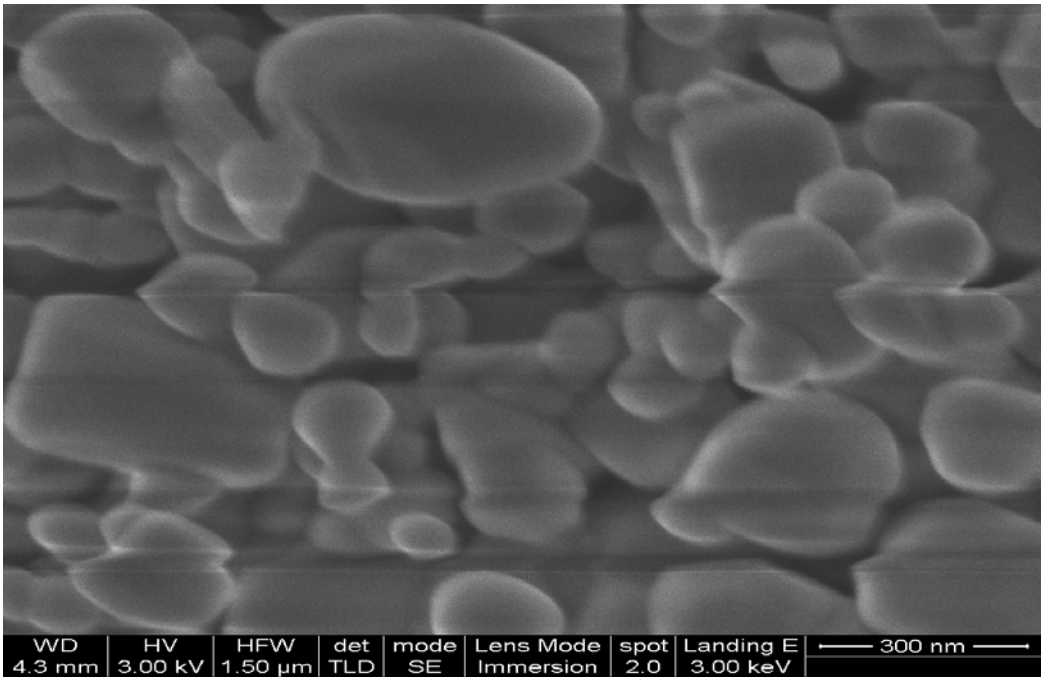

Figure 4.39 SEM micrograph of nano ZnO calcined at 600°C

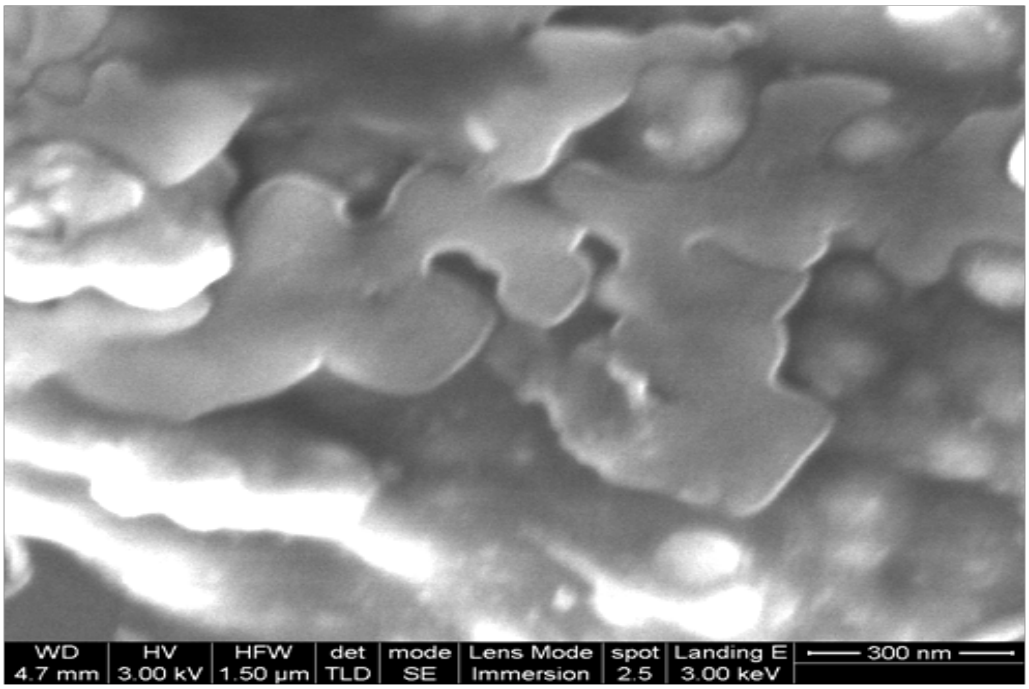

Figure 4.40 SEM micrograph of nano ZnO calcined at 700°C

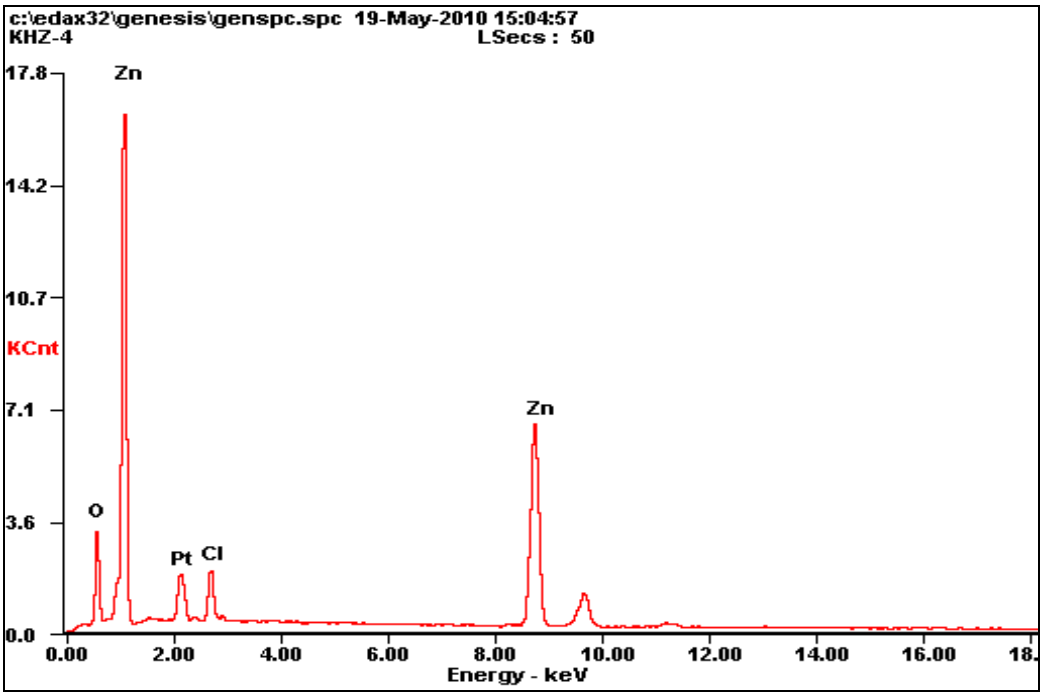

Figure 4.41 EDX spectrum of Pt doped ZnO

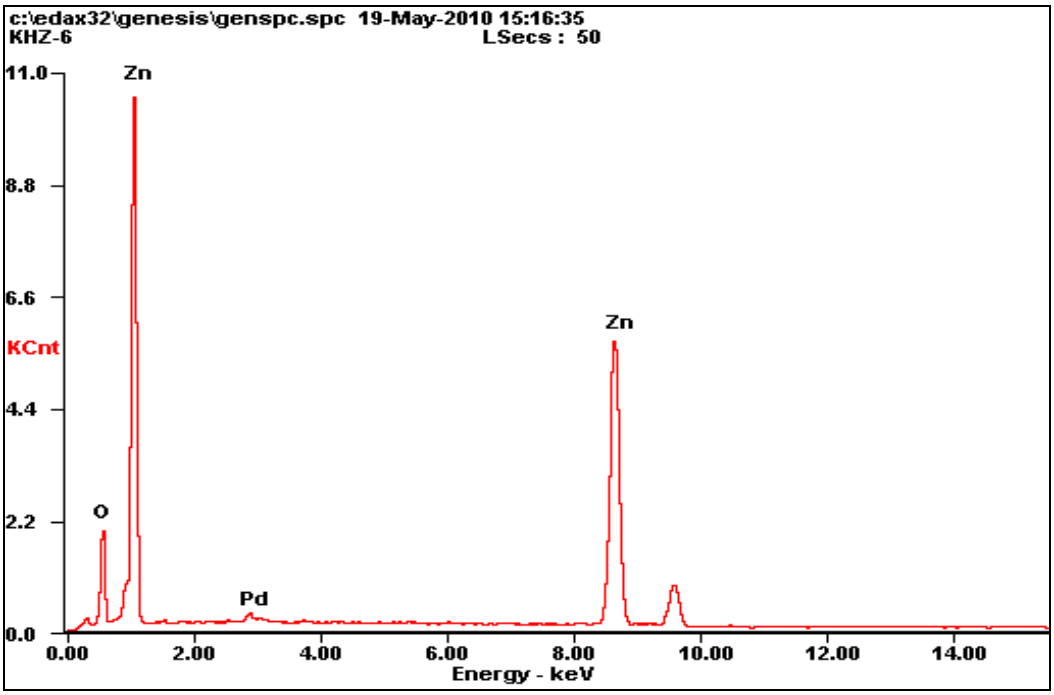

Figure 4.42 EDX spectrum of Pd doped ZnO

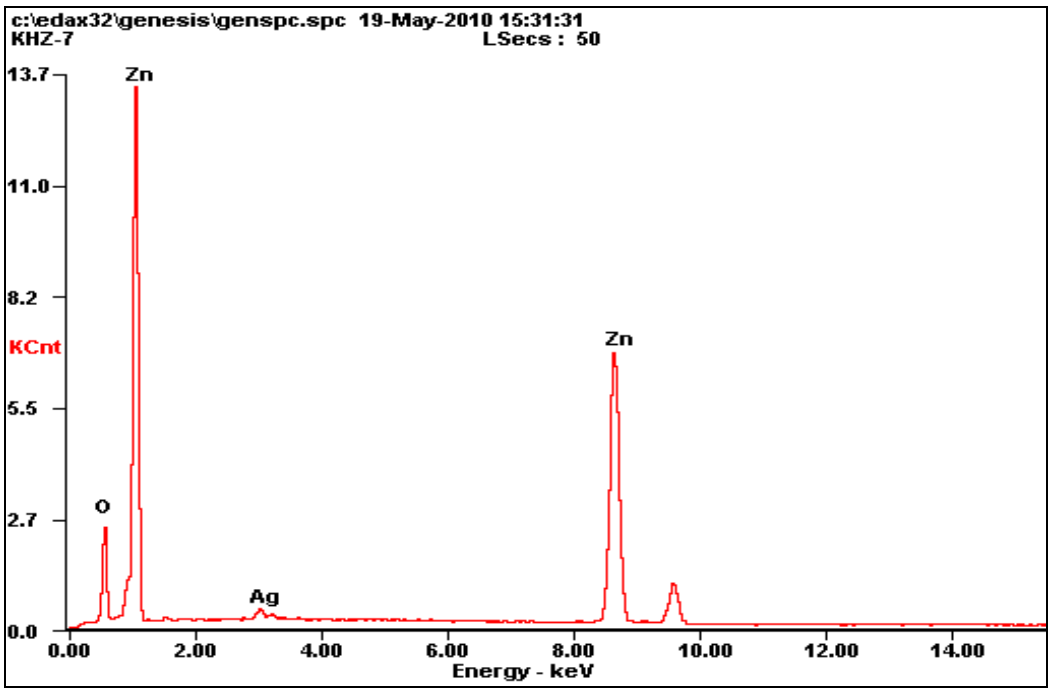

Figure 4.43 EDX spectrum of Ag doped ZnO

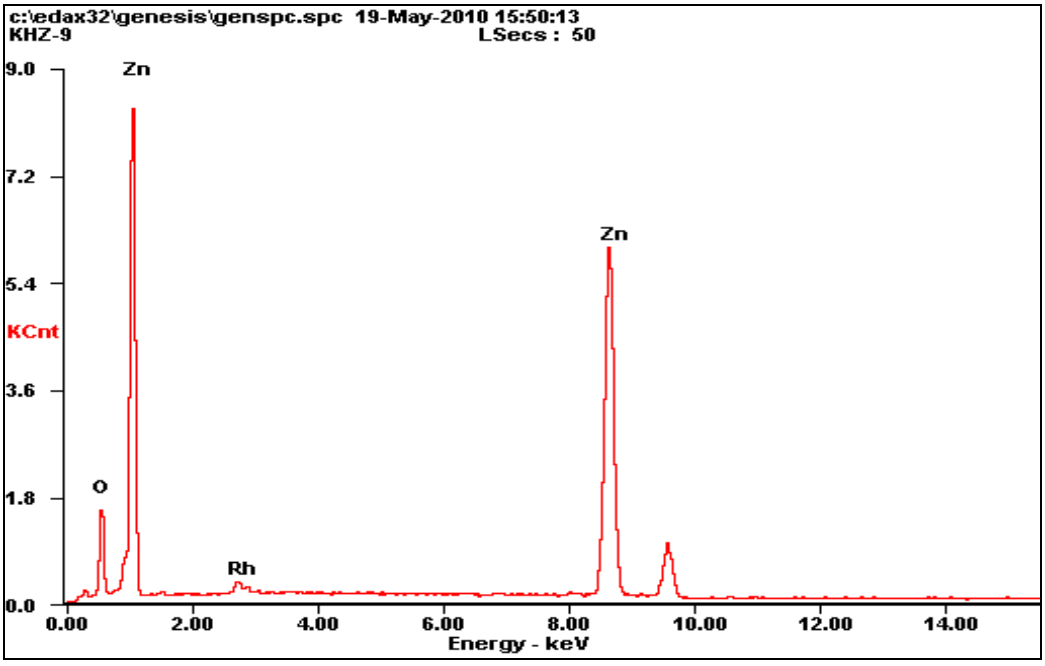

Figure 4.44 EDX spectrum of Rh doped ZnO

4.4 SEM and TEM Images of Nano NiO and Doped NiO

The morphology of NiO prepared at different conditions has been analyzed by means of microscopes such as SEM, TEM. Most SEM images show that the as-prepared NiO consists of mainly individual particles sized around 7.0 nm in diameter with a narrow size distribution. The results are presented in Figure (4.45-4.66). It can be seen from Figure 4.45 that the NiO nanoparticles had spherical shapes and were well dispersed with smooth surface and uniform size. Few small particles aggregate into secondary particles because of their extremely small dimensions and high surface energy. Figure 4.66 shows the representative Transmission Electron Microscopic image of NiO nanoparticles. TEM analysis of the products provided information on the size and morphology of NiO nanoparticles and their state of agglomeration. Figure 4.66 shows a TEM micrograph of the NiO nanoparticles. The results of SEM and TEM observations further confirmed and verified the relevant results obtained by XRD as mentioned above.

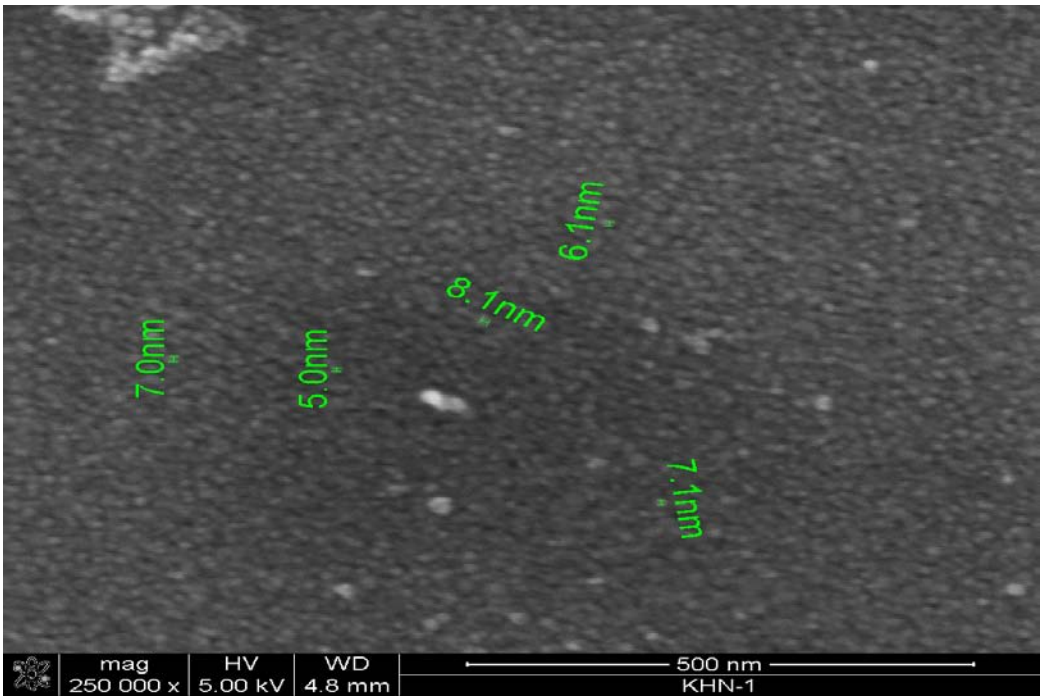

Figure 4.45 SEM micrograph of nano NiO

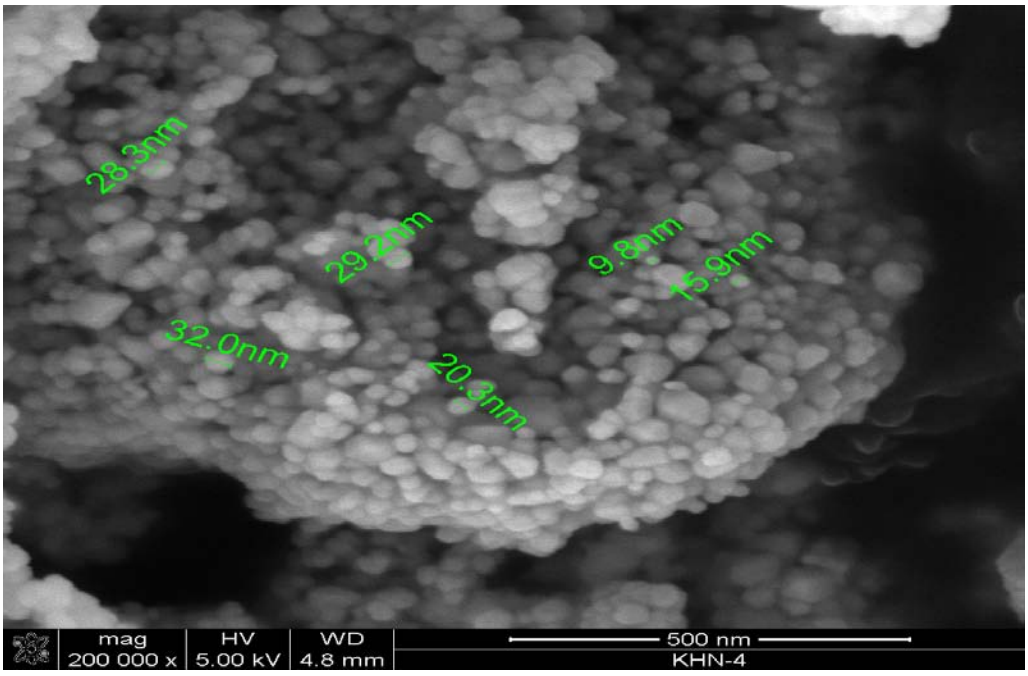

Figure 4.46 SEM micrograph of Pt-doped NiO

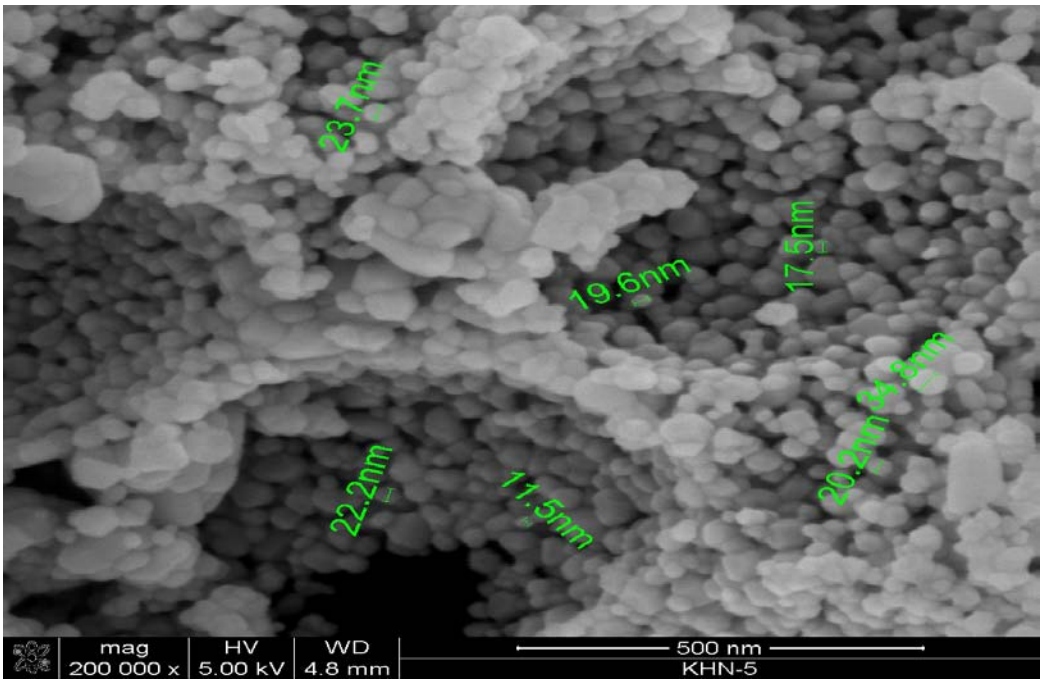

Figure 4.47 SEM micrograph of Pd-doped NiO

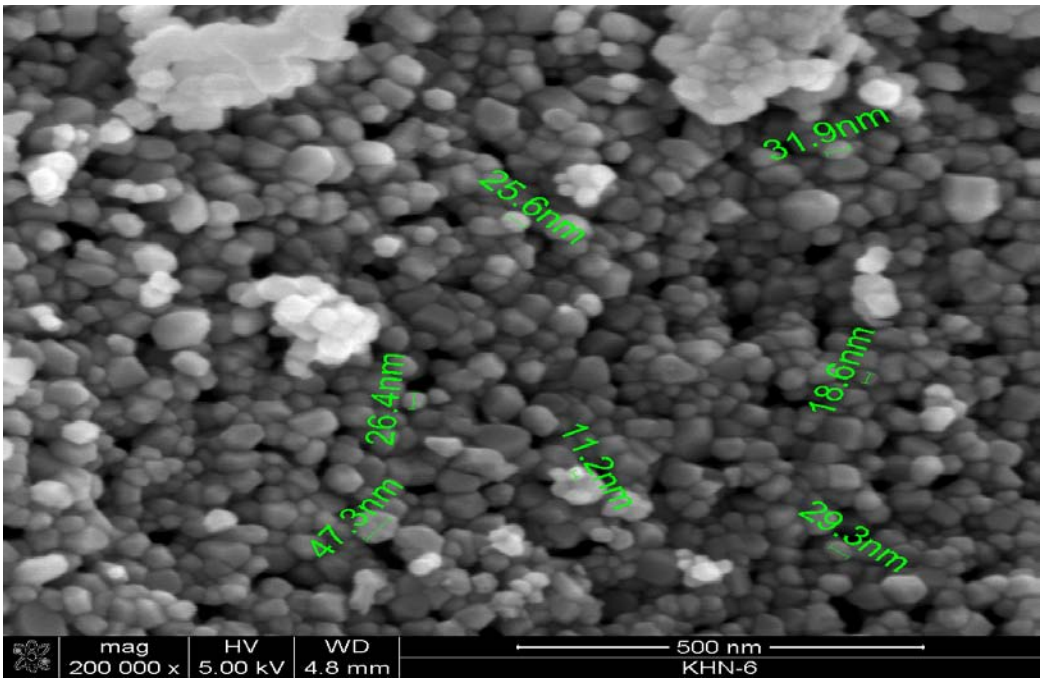

Figure 4.48 SEM micrograph of Ag-doped NiO

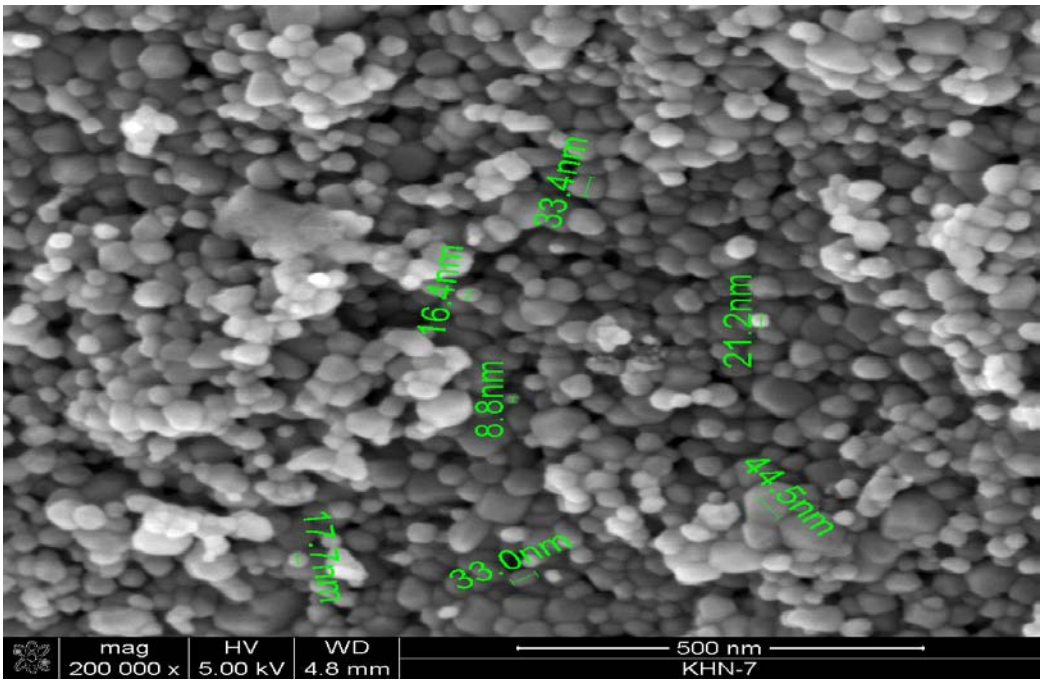

Figure 4.49 SEM micrograph of Rh-doped NiO

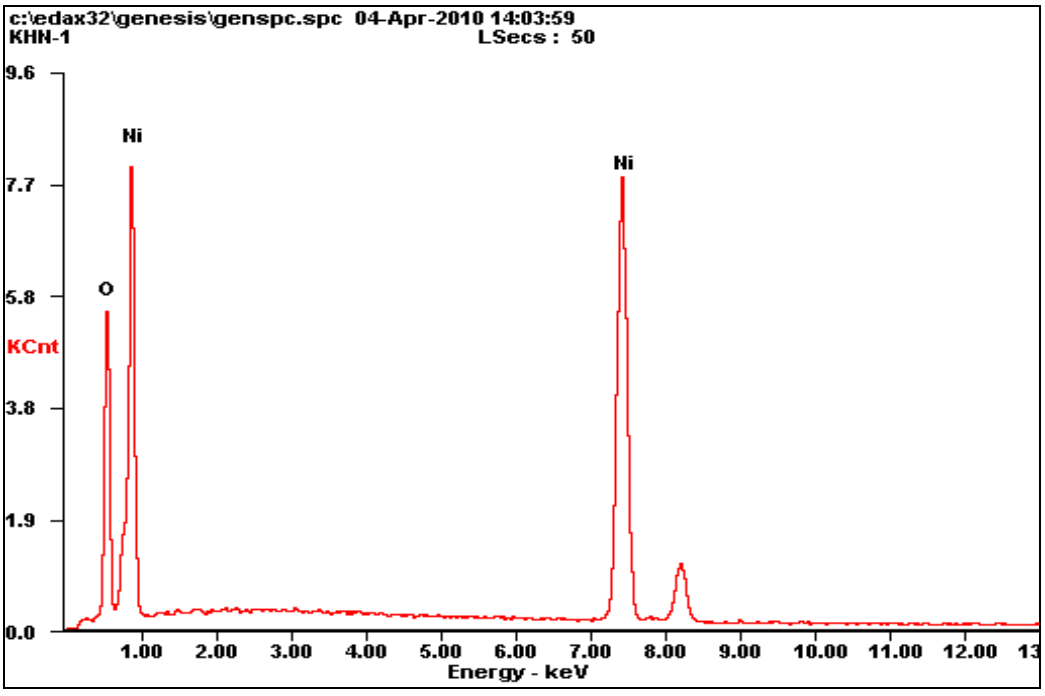

Figure 4.50 EDX spectrum of nano NiO

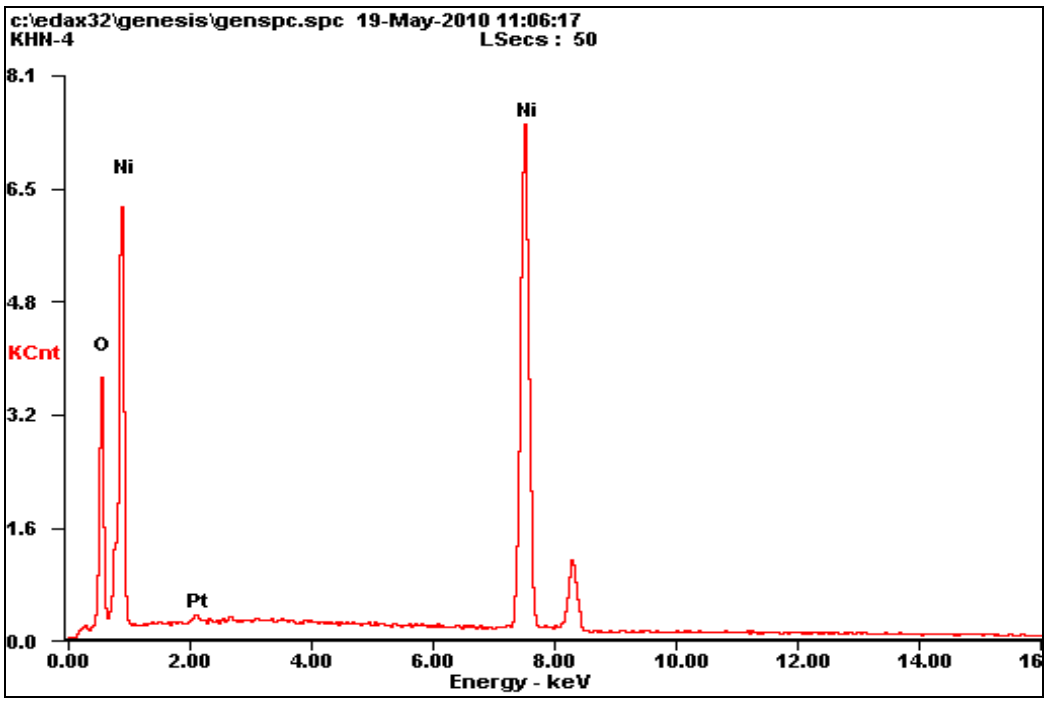

Figure 4.51 EDX spectrum of Pt doped NiO

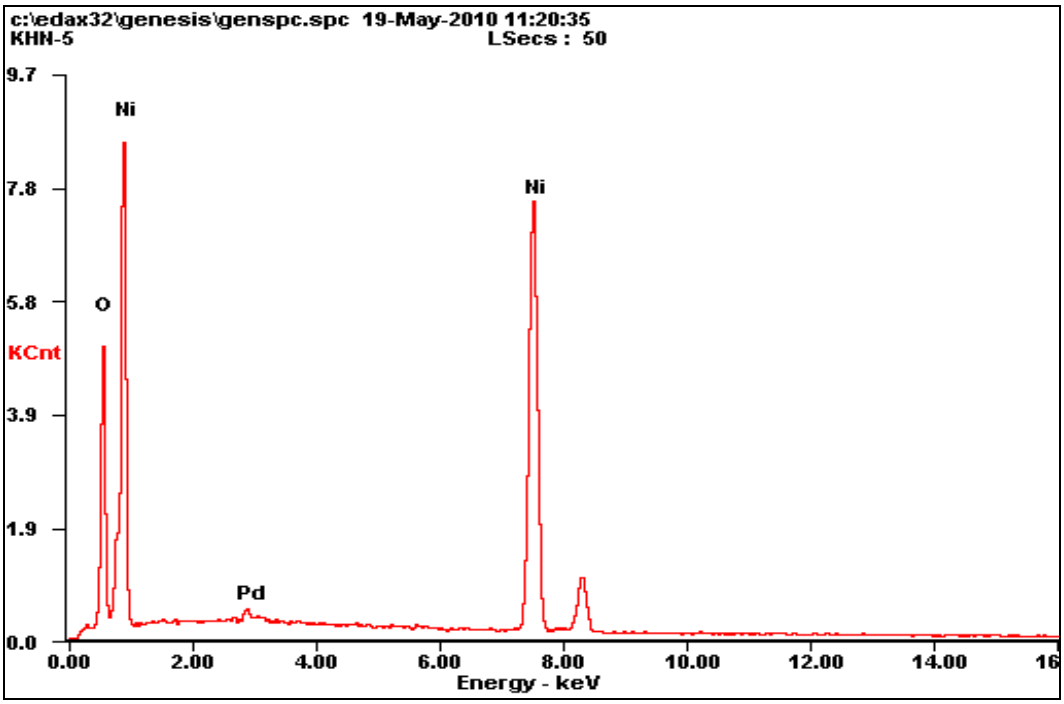

Figure 4.52 EDX spectrum of Pd doped NiO

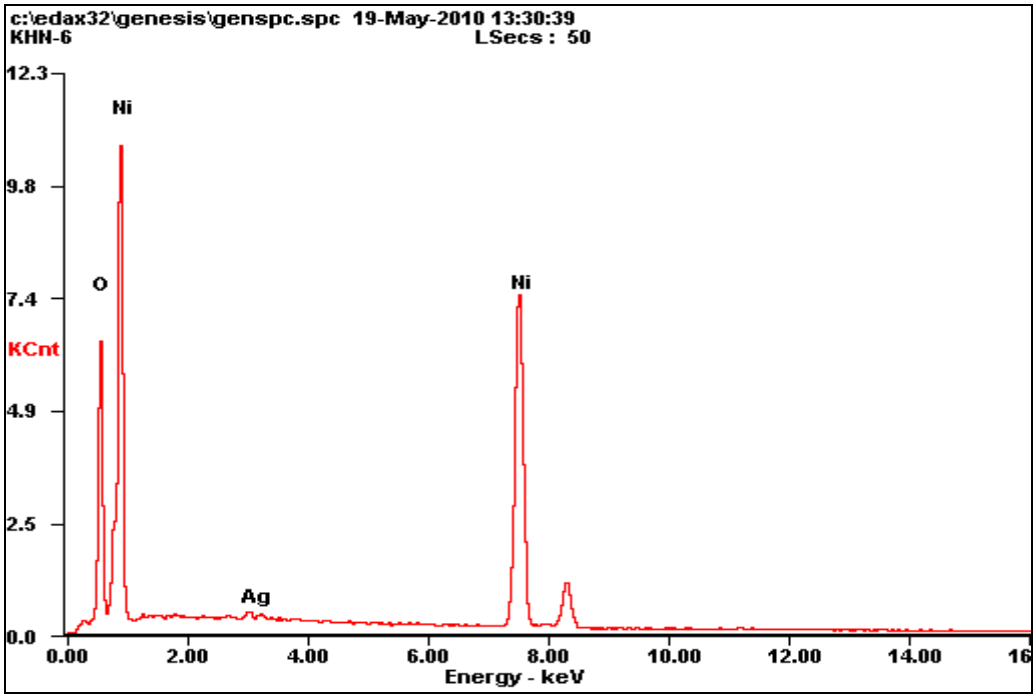

Figure 4.53 EDX spectrum of Ag doped NiO

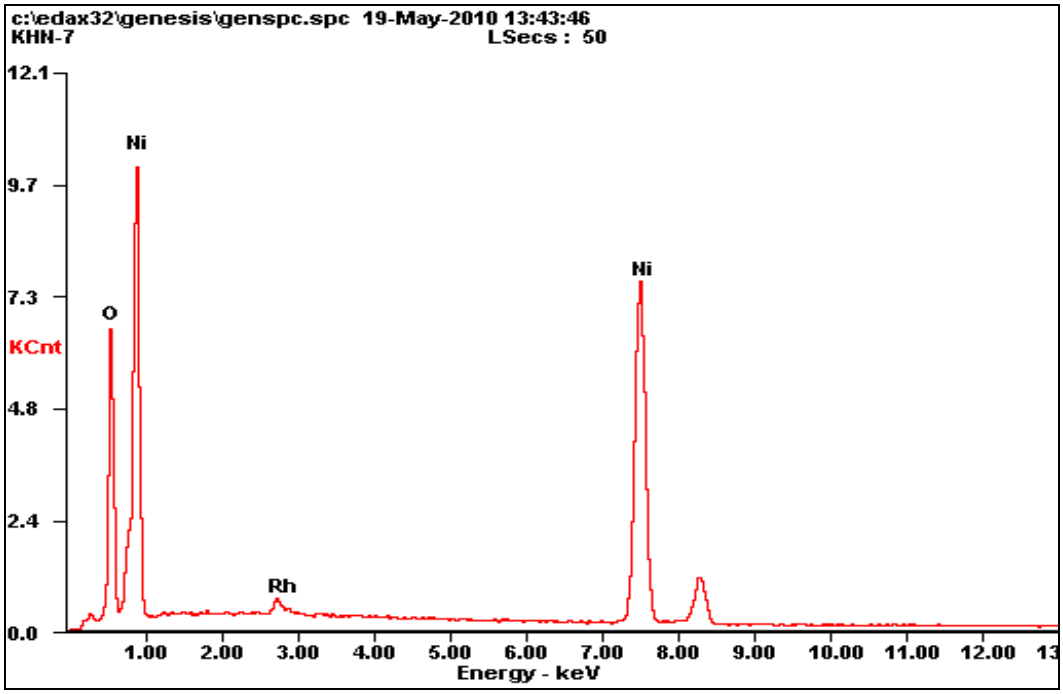

Figure 4.54 EDX spectrum of Rh doped NiO

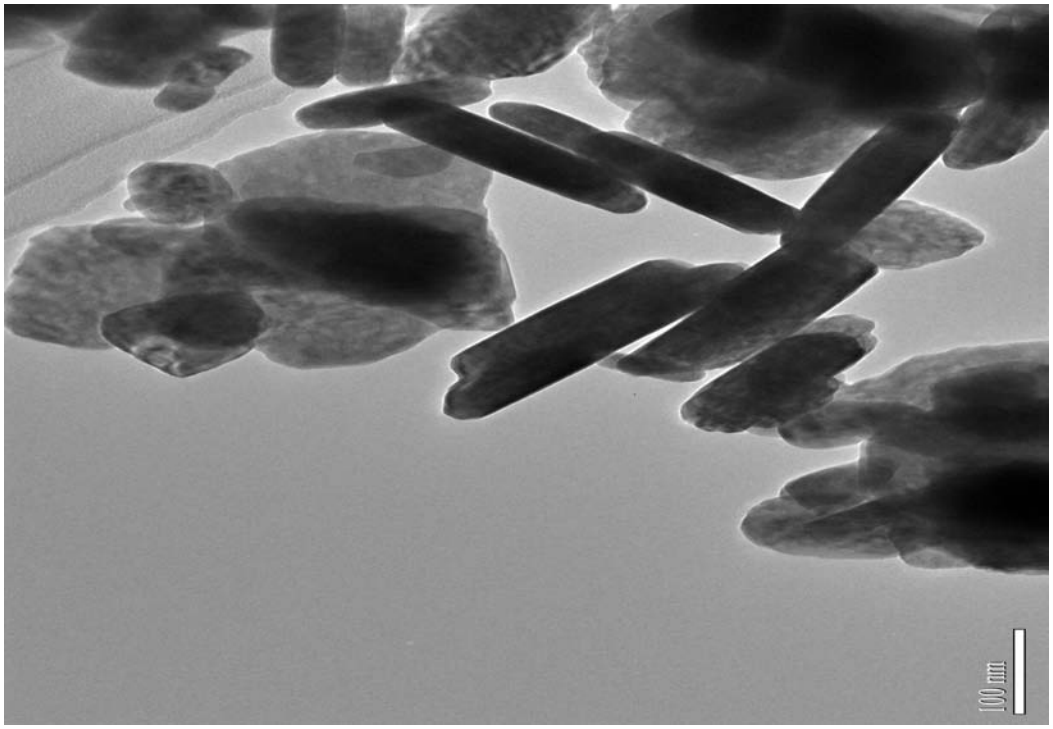

Figure 4.55 TEM micrograph of as prepared WO_3

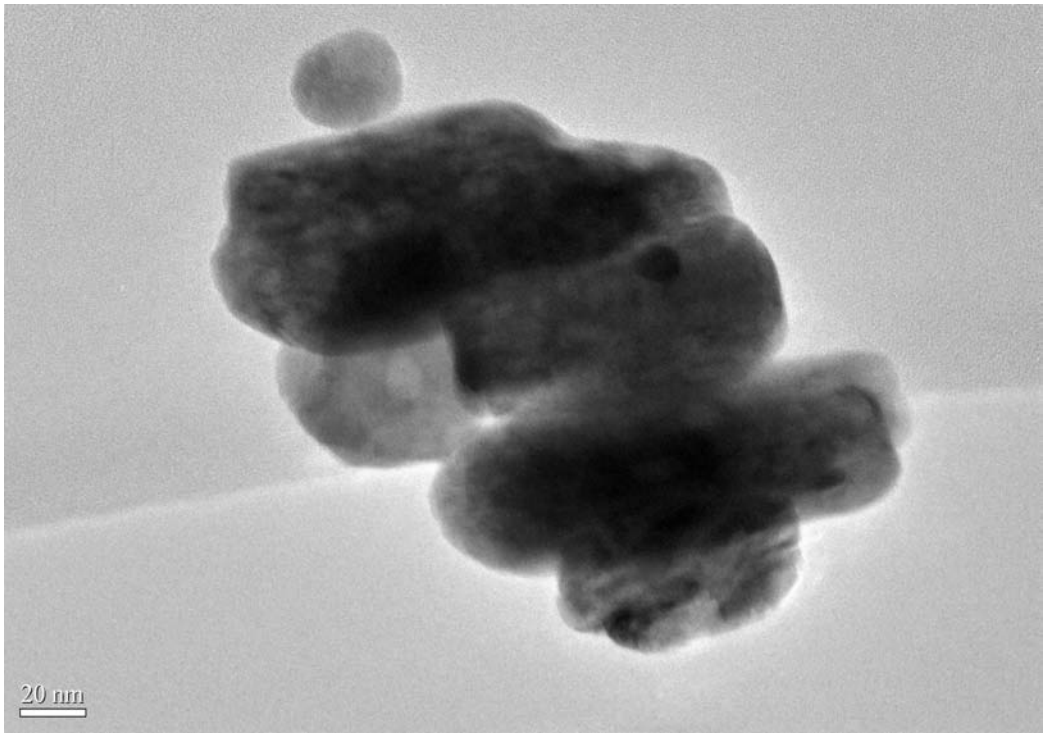

Figure 4.56 TEM micrograph of Pt doped WO_3

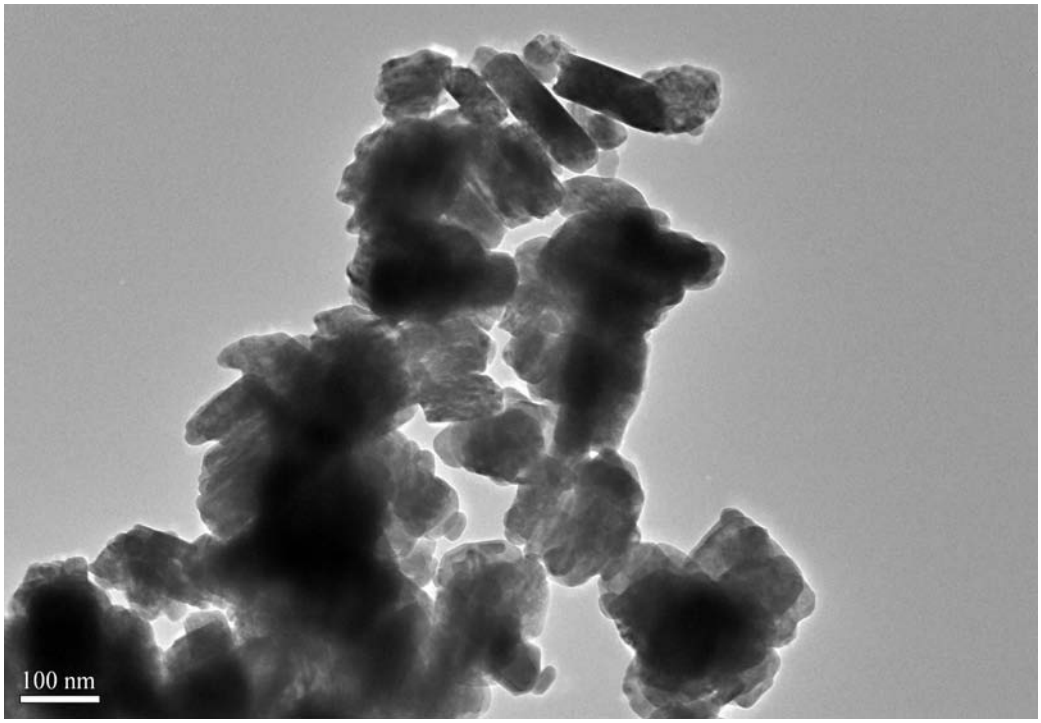

Figure 4.57 TEM micrograph of Pd doped WO_3

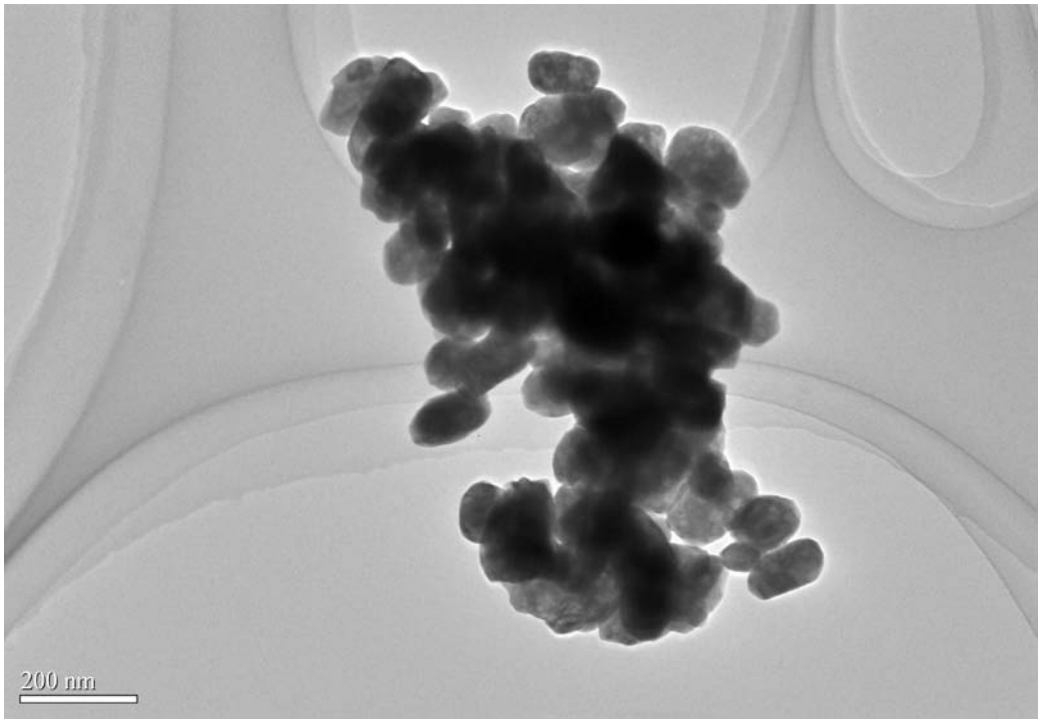

Figure 4.58 TEM micrograph of Ag doped WO_3

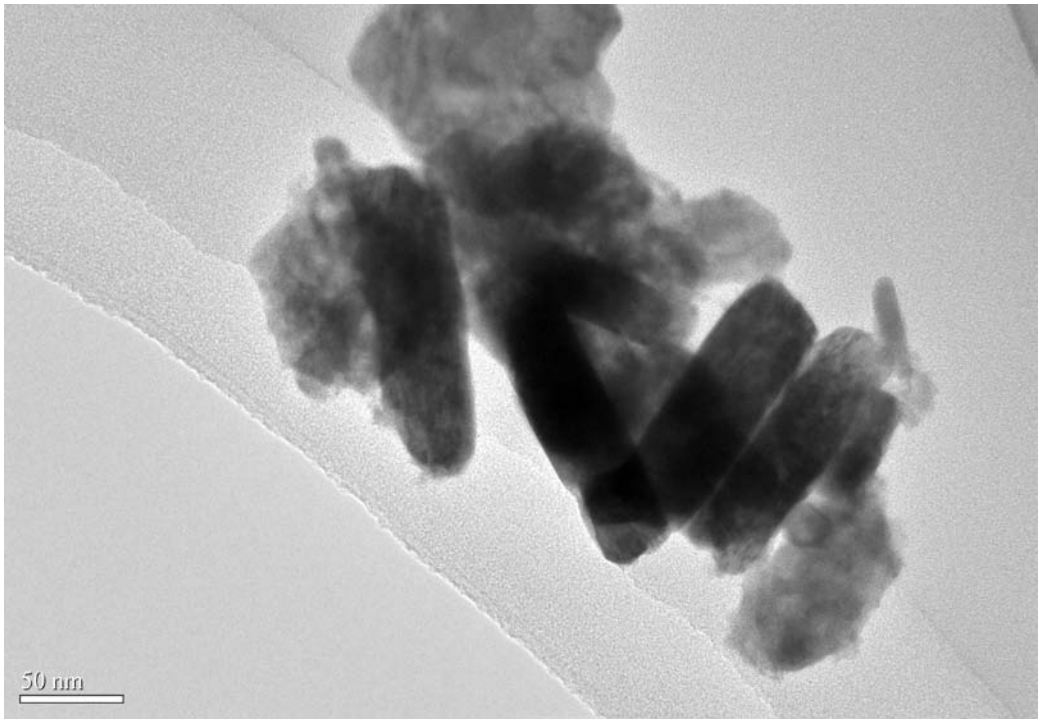

Figure 4.59 TEM micrograph of Rh doped WO_3

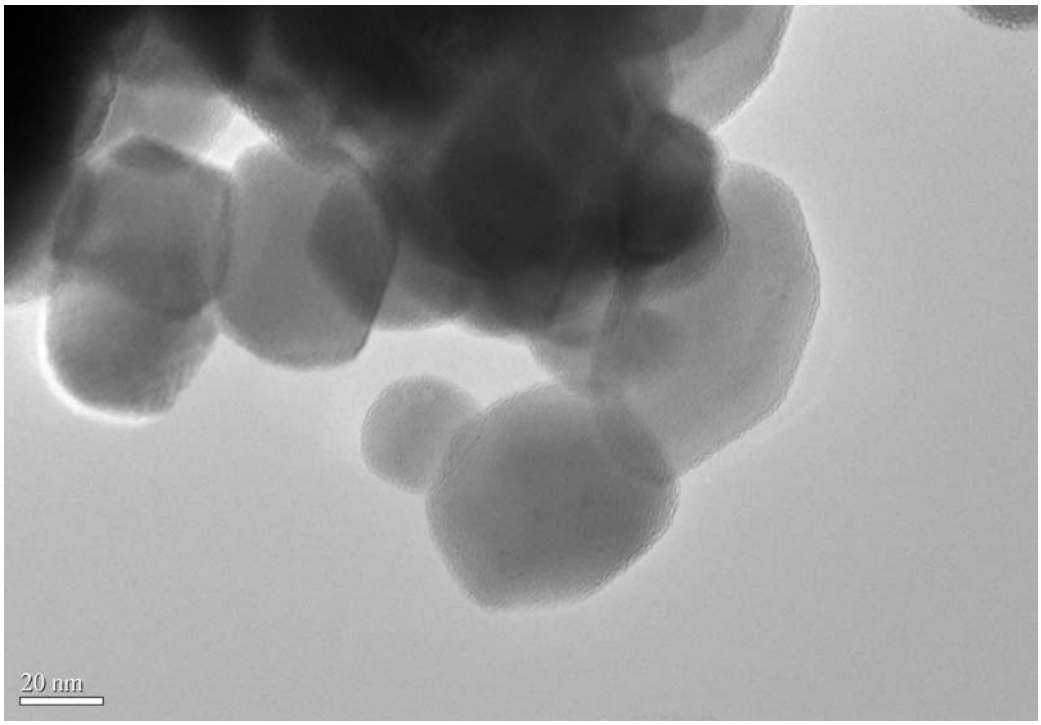

Figure 4.60 TEM micrograph of as prepared $ZnWO_4$

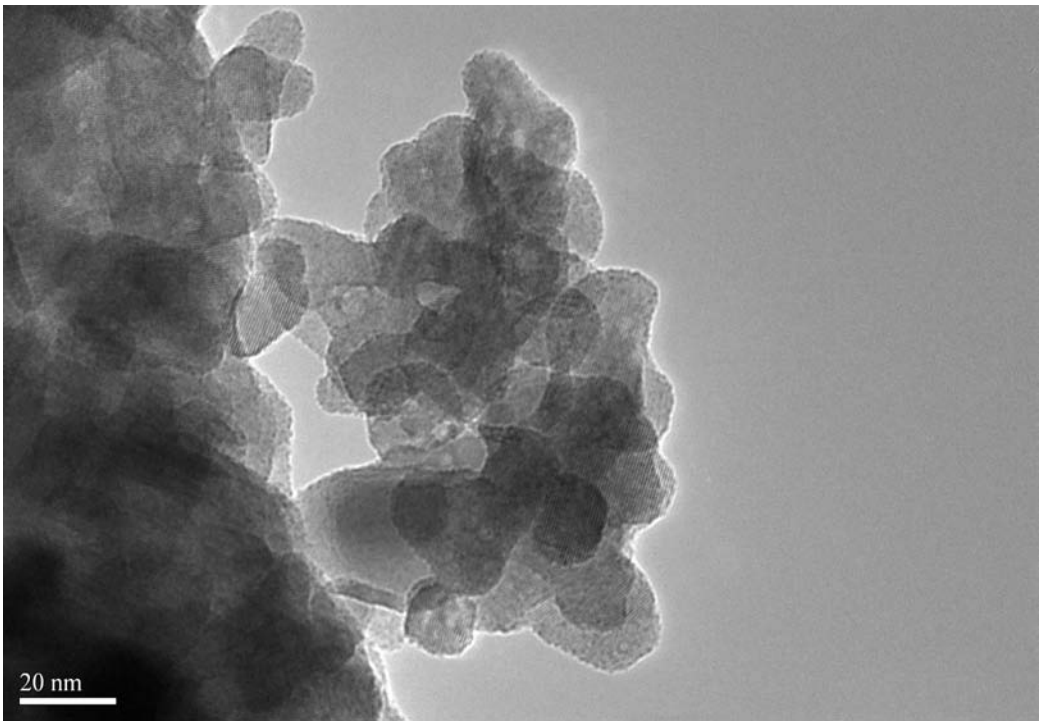

Figure 4.61 TEM micrograph of as prepared $NiWO_4$

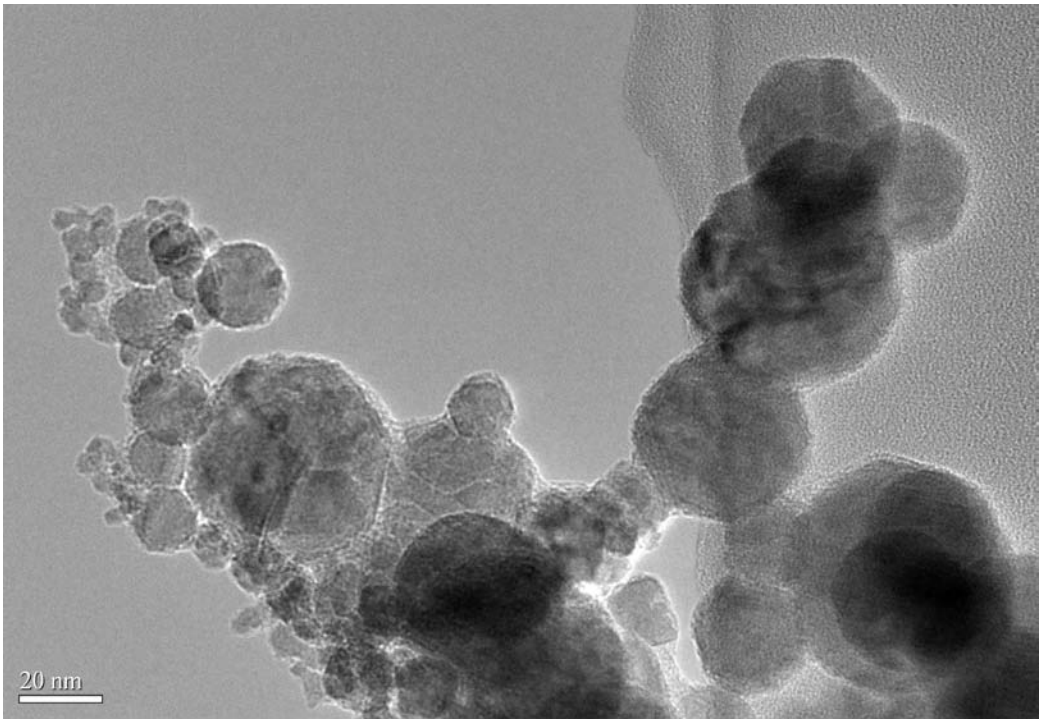

Figure 4.62 TEM micrograph of as prepared $CuWO_4$

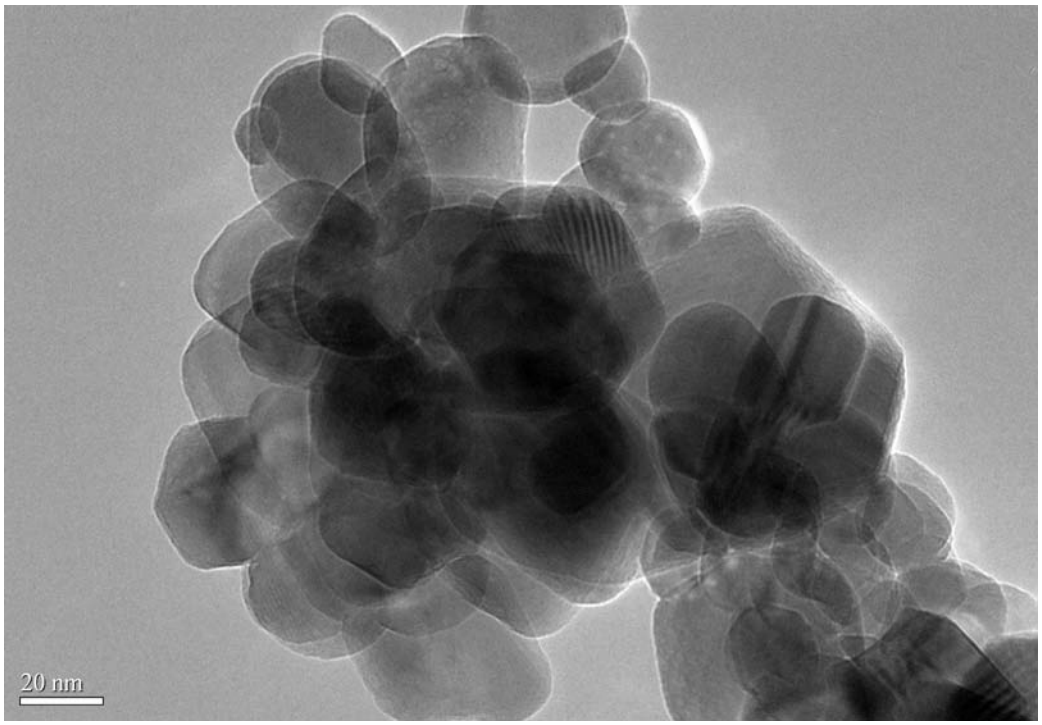

Figure 4.63 TEM micrograph of for nano ZnO

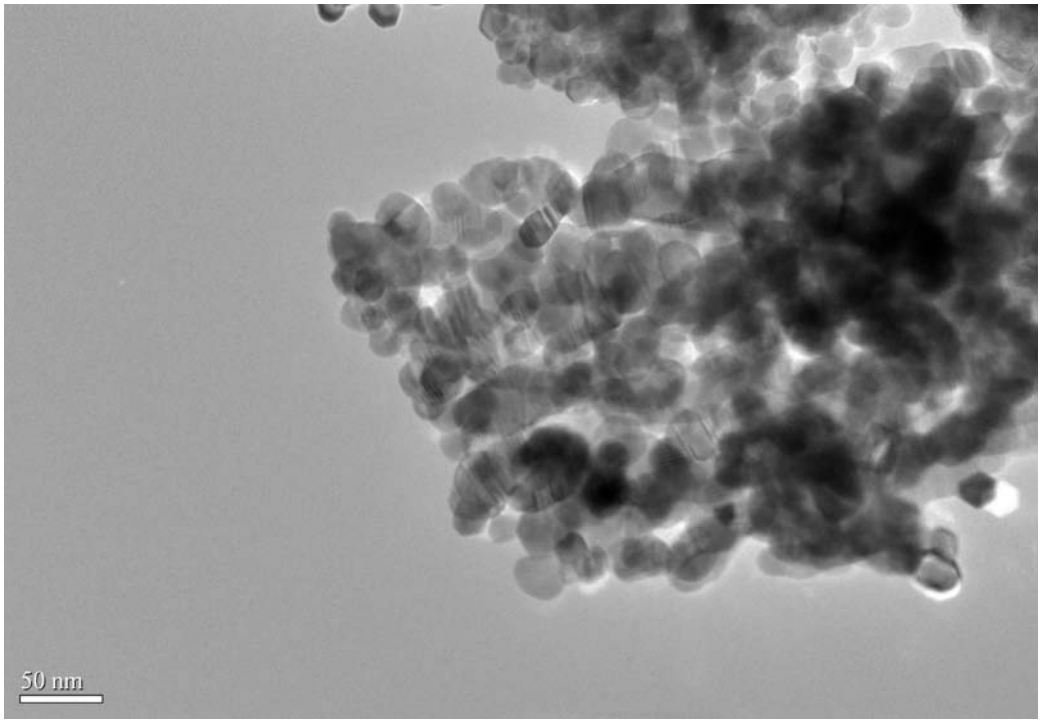

Figure 4.64 TEM micrograph of for nano ZnO calcined at 400 °C

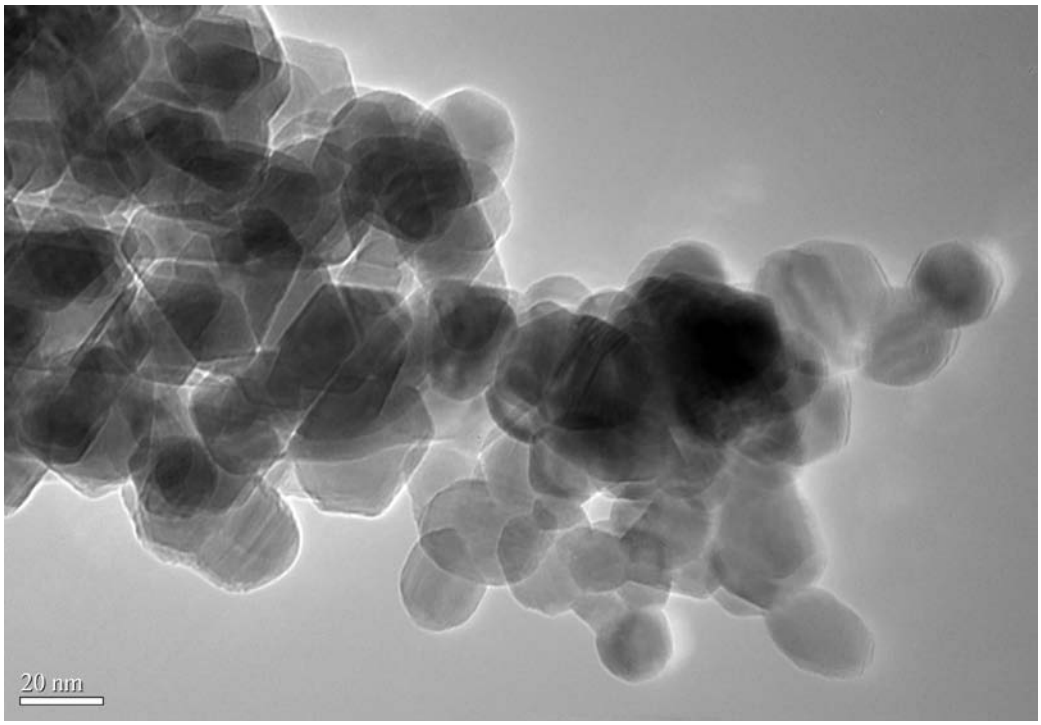

Figure 4.65 TEM micrograph of for nano ZnO synthesized by ppt method

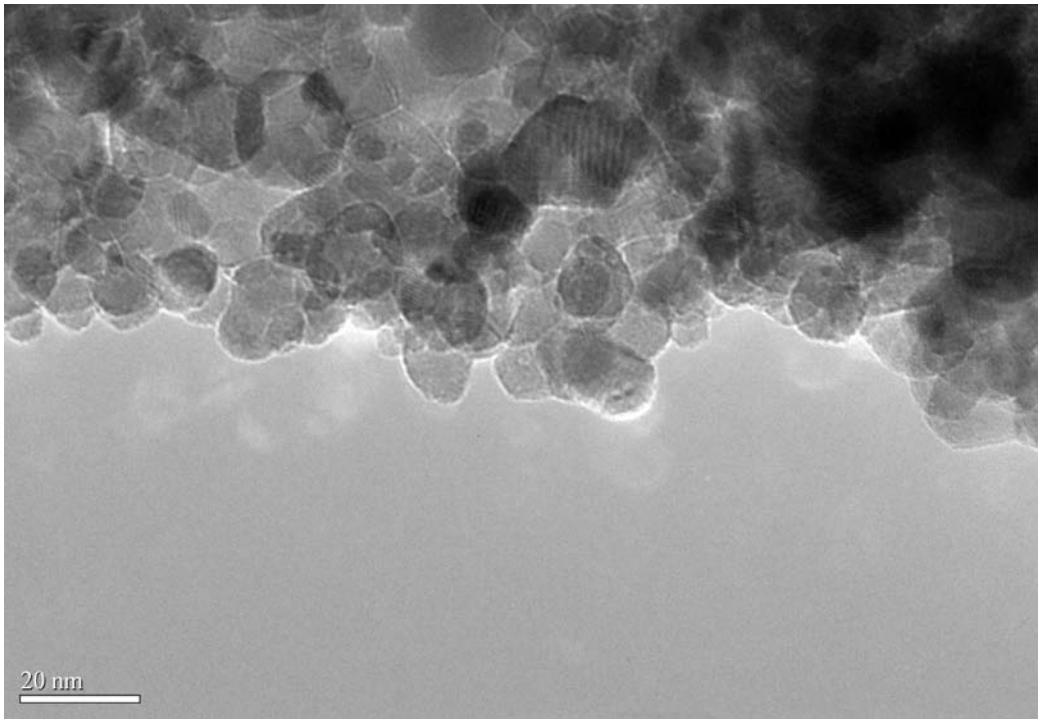

Figure 4.66 TEM micrograph of nano NiO

4.5 UV–Visible Characterization of Pure and Noble Metal Doped Metal Oxides

When a photocatalyst is irradiated with photons with energies greater than that of the semiconductor's band gap, Eg (eV), an electron is transferred to the conduction band, leaving behind a positive hole in the valence band. The pair of photoexcited charges that occurs within a particle is called an electron-hole pair (EHP).The energy of a semiconductor's band gap is equal to the difference in energy between the conduction band edge and the valence band edge.

Knowledge of band-edge positions is useful when creating and analyzing semiconductor photocatalysts because they indicate the thermodynamic limitations for the photoreactions that can be carried out by the charge carriers. For example, if the oxidation of an organic compound is desired by the photocatalyst, then the valence band edge of the semiconductor must be positioned favorably relative to the oxidation potential of the organic compound. On the other hand, if the reduction of a molecule such as O_2 is required, then the conduction band edge of the semiconductor must be positioned favorably relative to the reduction potential of the O_2 molecule. Quantum size (Q-size) effects also must be considered when determining electronic properties of semiconductors such as the energy positions of the valence and conduction band edges. Quantum effects occur when the size of the semiconductor particle is close to or smaller than the Bohr radius of the first excitation state causing the particle to possess properties characteristic of both its bulk and molecular phases.

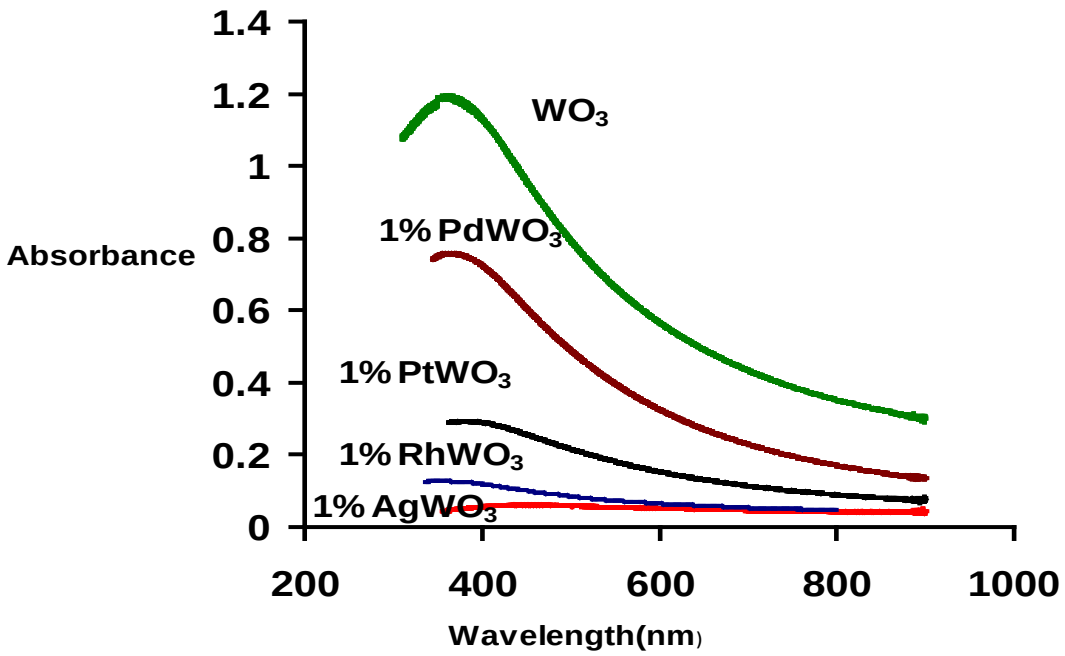

Figure 4.67 Absorption spectra of WO_3 and doped WO_3

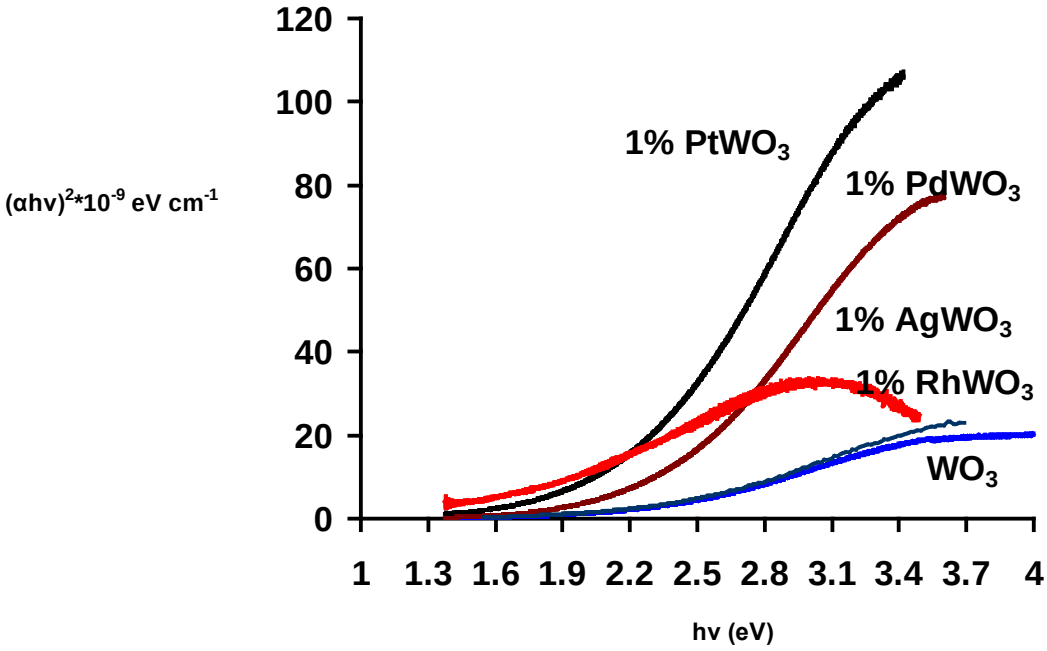

Figure 4.68 Band gap determination of WO_3 and doped WO_3

Quantum effects are common for colloidal solutions and particles with sizes close to or smaller than 10nm. The most dramatic influence of Q-size effects is that it can be used to tailor the band gap and band-edge positions of Q-size semiconductor nanoparticles for sensitive applications. As a nanoparticle size decreases, its band gap increases primarily with an increase in conduction band energy levels and also a slight decrease in valence band energy levels.

A classical semiconductor exhibits minimal optical absorption for photons with energies smaller than the band gap and high absorption for photons with energies greater than the bandgap. As a result, there is a sharp increase in absorption at energies close to the band gap that manifests itself as an absorption edge the UV-Vis absorbance spectrum. Optical absorption spectrum of the pure and doped metal oxides nanoparticles are represented in Figure 4.67- Figure 4.70. From the curves we can calculate the band gap (Eg) energy of the sample by the following equation [176]

$$(\alpha h\nu)^{n} = (h\nu - Eg) \qquad (1)$$

in which hν is photon energy, α is absorption coefficient, and n is either 2 for a direct band gap material or 0.5 for indirect band gap materials. Using equation (1) and taking the value n = 2, the band gap of synthesized photocatalysts are determined. In all cases, a red shift was observed for the noble metal doped nanomaterials.

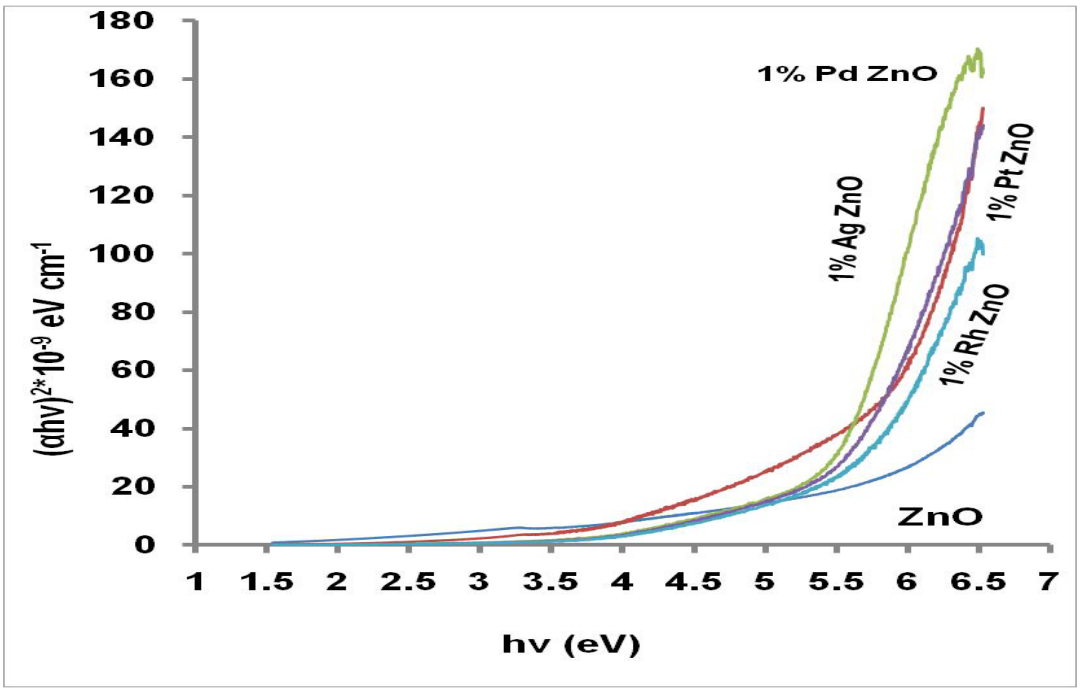

Figure 4.69 Band gap determination of ZnO and doped ZnO

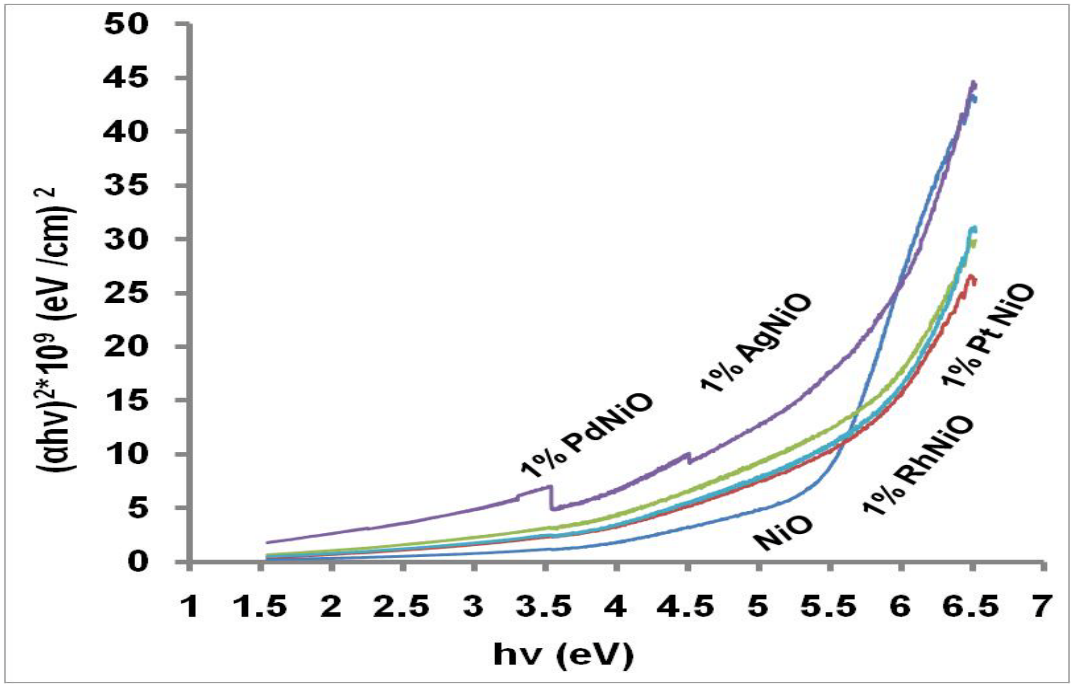

Figure 4.70 Band gap determination of NiO and doped NiO

CHAPTER 5

LASER INDUCED PHOTOCATALYIC DEGRADATION OF SOME SELECTED DYES IN AQUEOUS SUSPENSIONS OF NANOCRYSTALLINE METAL OXIDES

The results related to the photocatalytic degradation of dyes such as Safranin O, Alizarin yellow GG, Acid Red 87 and Cyanosine using nanocrystalline WO_3, nano ZnO and nano NiO synthesized are included in this chapter. The effect of different experimental parameters such as laser energy, catalyst concentration, pH, substrate concentration on photocatalytic degradation of dyes was also studied. The photodegradation rates were found to be strongly influenced by all the above parameters. The results obtained are discussed in this chapter.

The commercial azo dye Safranin O, obtained from Colour Chem, Pondicherry, was used without further purification. The commercial azo dye Alizarin yellow GG, C.I. 14025 was purchased from Fluka and used without further treatment. Acid Red 87 was obtained from BDH Chemicals Ltd. (minimum dye content ~ 88%). Methyl red, Cyanosine and Phenol were purchased from Fluka. The structure of the dyes is shown in Figure 5.1.

A)

B)

(C)

(D)

(E)

Figure 5.1 Structures of organic dyes used in this study: (A) Alizarin Yellow GG, (B) Safranin O (C) Acid Red 87 (D) Methyl Red (E) Cyanosine

5.1. Photocatalyic Degradation of Safranin O by Nanocrystalline WO_3

Since some dyes are photo-degraded by direct UV irradiation. Therefore, the removal of Safranin O was studied under UV laser irradiation without the presence of catalyst. For this purpose, blank experiments were carried out for the dye solution without catalyst. No significant degradation of safranin O (less than 5.0 %) was observed without the catalyst. The results shown in Figure 5.6 indicated that 94.0% degradation was

achieved within very short laser irradiation time (10 minutes) using 355 nm laser and nanocrysralline WO_3. It was observed that both UV light and photo-catalyst are essential for the effective removal of the dye.

5.1.1. Effect of Incident Laser Energy on Photodegradation Process

The influence of laser energy on the rate of dye decolorization was examined at constant initial dye concentration (C_0 = 5.7*10^{-4}M) and catalyst loading (WO_3 = 1.0 g L^{-1}). The effect of incident laser energy on the photodegradation of Safranin O (SO) was investigated and the results are depicted in Figure 5.2. The results indicate that the degradation of the dye was significantly influenced by the laser energy and photodegradation rate of SO was increased almost linearly with the increase in laser energy up to a certain energy level as given in Table IV. When 140 mJ of laser energy was applied, 94.0% degradation was recorded within 10 min of irradiation and a further increase in the laser energy was not found to be more advantageous for the degradation of the dye. This phenomenon may be explained in terms of the fact that when laser energy is increased, incident photon flux increases in the solution exciting more and more catalyst particles which increases the degradation of the dye. The dependency of photocatalytic property on the light intensity observed in this study followed similar trend as explained by Hoffmann et.al. [177] in which, it was concluded that there is a linear relationship between the rate and the light intensity up to a certain level.

5.1.2. Influence of Initial pH on Dye Removal Process

Table IV Laser induced photocatalytic degradation of Safranin O in aqueous suspensions of nanocrystalline WO_3 under different operational parameters.

S.No.	Parameters	Rate constant (min^{-1})	Photodegradation rates ($mM\text{-}min^{-1}$)
1	Initial pH		
	5.0	0.169	0.096
	8.0	0.246	0.140
	10.0	0.314	0.179
	11.6	0.012	0.007
2.	Energy (mJ)		
	40	0.0128	0.0073
	70	0.0515	0.0294
	100	0.173	0.0986
	140	0.256	0.1459
	170	0.405	0.2308
	200	0.701	0.3996

The solution pH appears to play an important role in the photocatalytic process of various pollutants.The effect of pH on the photodegradation of Safranin O was investigated in the pH range 5.0–11.6. The pH of the solution was adjusted before irradiation and it is not controlled during the course of the reaction. It was found that the degradation efficiency increases with increase in pH from 5.0 to 10.0 and then decreases with further increase in pH as shown in Figure 5.3. At acidic pH range the removal efficiency was less and it might be due to the dissolution of WO_3. So the optimum pH for efficient Safranin O removal was found to be 10.0. The values of degradation rates obtained are listed in Table IV. The photocatalytic degradation rate was found to increase with the increase in reaction pH and maximum photocatalytic degradation was achieved at 10.0 pH as shown in Figure 5.3.

The possible reason for the different reaction rates at different pH values may be correlated to the generation of active hydroxyl radicals and occupancy of active sites of catalyst surface for the production of $OH^{\bullet}$ radicals by intermediate products. Values of solution pH can alter the degradation route and lead the formation of different intermediate products [178]. The isoelectric point (pHIEP) corresponds to the zeta potential equal to zero. The surface of photocatalyst was charged positively under pH < pHIEP. The dye used in this study was cationic dye and was positively charged under experimental conditions. Accordingly, electrostatic interactions between the photocatalyst surface and dye cation lead to the formation of little adsorption at low pH range. Some researchers [179] observed the same trend for the photocatalytic degradation of phenol using nanocrystalline TiO_2. This phenomenon might occur because of the cationic nature of the dye. OH radical formation might be suppressed at more alkaline pH and the degradation rate of the dye is decreased.

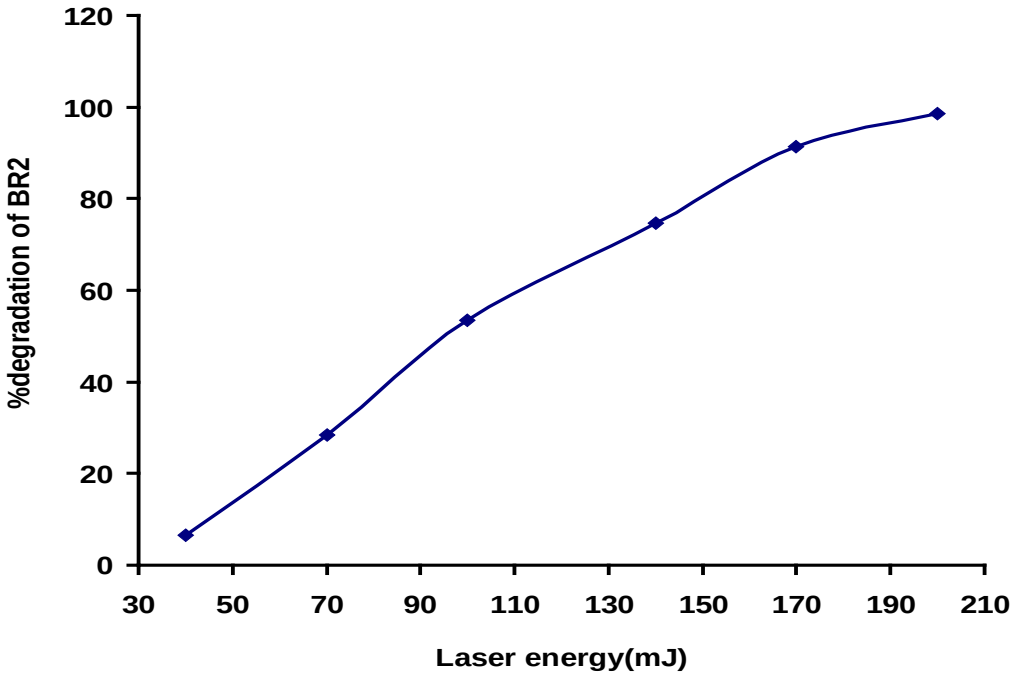

Figure 5.2 Effect of laser energy on photocatalytic degradation of Safranin O (Basic red 2) in presence of nanocrystalline WO_3

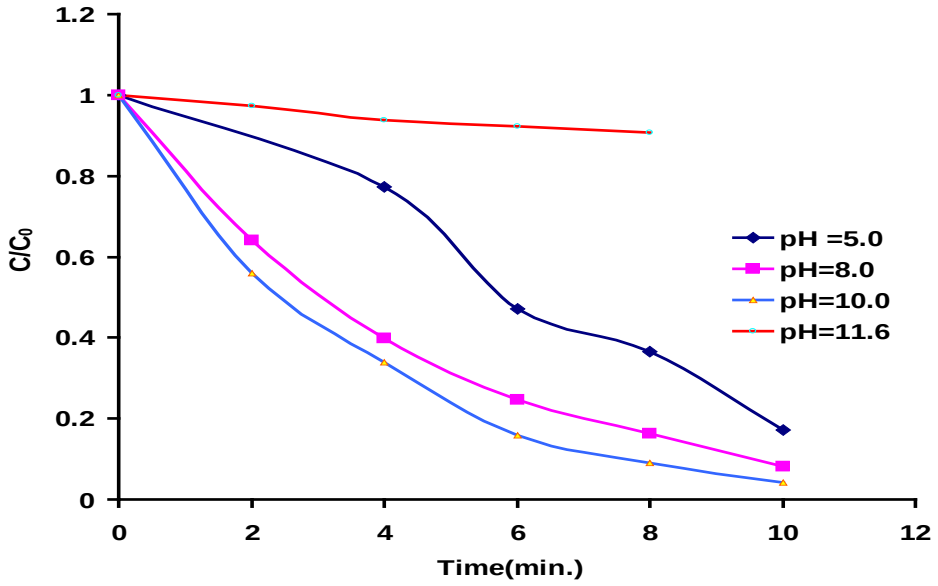

Figure 5.3 Effect of pH on photocatalytic degradation of Safranin O (Basic red 2) as a function of laser irradiation time for nano-structured WO_3

Because several reaction mechanisms can contribute to dye degradation, including OH radical attack, direct oxidation by the positive holes, and direct reduction by the electrons, the effect of pH on degradation efficiency differs from that of photo catalysts and photodegradation of model substrates.

5.1.3. Effect of Catalyst Loading on Dye Removal Process

The effect of photocatalyst concentration was studied by varying catalyst concentration from 1.0 to 8.0 g/L for dye solutions of 0.57mM at natural pH. The degradation efficiency for various catalysts loading for Safranin O has been depicted in agreement with recent reports. when the concentration of the catalyst increases above the optimum value, the degradation rate decreases due to the interception of the light by the suspension. The degradation efficiency for various catalysts loading for Safranin O has been depicted in Figure 5.4. The results reveal that the rate constant increase greatly by increasing catalyst loading from 1.0 to 4.0 g/L for the dye, the rate of photodegradation remains almost constant for the higher catalyst loading. This can be explained on the basis that optimum catalyst loading is found to be dependent on initial solute concentration because with the increase of catalyst dosage, total active surface area increases, hence availability of more active sites on catalyst surface.

The photocatalytic destruction of other organic pollutants has also exhibited the same dependency on catalyst dose [180,181]. At the same time, due to an increase in turbidity of the suspension with high dose of photocatalyst, there will be a decrease in penetration of UV light and hence photo activated volume of suspension decreases [182]. This limit, therefore, depends on the nature and concentration of organic contaminants and the

working conditions of photo reactor. When the catalyst concentration is very high, the efficiency of the catalyst is hindered by the turbidity of suspension which decreases the penetration of light in the reactor. Thus it could be concluded that higher dose of catalyst may not be useful both in view of aggregation as well as reduced irradiation field due to light scattering. Therefore the catalyst dose 1.0 g/L was fixed for further studies.

5.1.4. Effect of Substrate Concentration

It is important both from mechanistic and application points of view to study the dependence of the photocatalytic reaction rate on the substrate concentrations. In order to investigate the influence of initial dyes concentration on the degradation rate, the various initial dye concentrations were used and the correlation between inverse of k and C_0 was also being studied. In all cases, 100 mL of dyes solutions containing 1.0 gL^{-1} of naocrystalline WO_3 were irradiated. The initial concentration of the Safranin O (SO) was varied from $2.85*10^{-4}$ M to $1.425*10^{-3}$ M. In all cases, 100 mL of the dye solutions containing 1.0 gL^{-1} of naocrystalline WO_3 were irradiated. The observed data were plotted as the experimental rate constant versus initial dye concentration as depicted in Figure 5.5. The results presented in Table V are in agreement with recent reports. It was observed that for this range of concentrations the reaction rate gets slower as the initial concentration of the dye in solution increases. As the concentration of SO increases, more reactant and reaction intermediates are adsorbed on the surface of the photocatalyst, therefore, the generation of hydroxyl radicals will be reduced because only a fewer active sites are available for adsorption of hydroxyl anions.

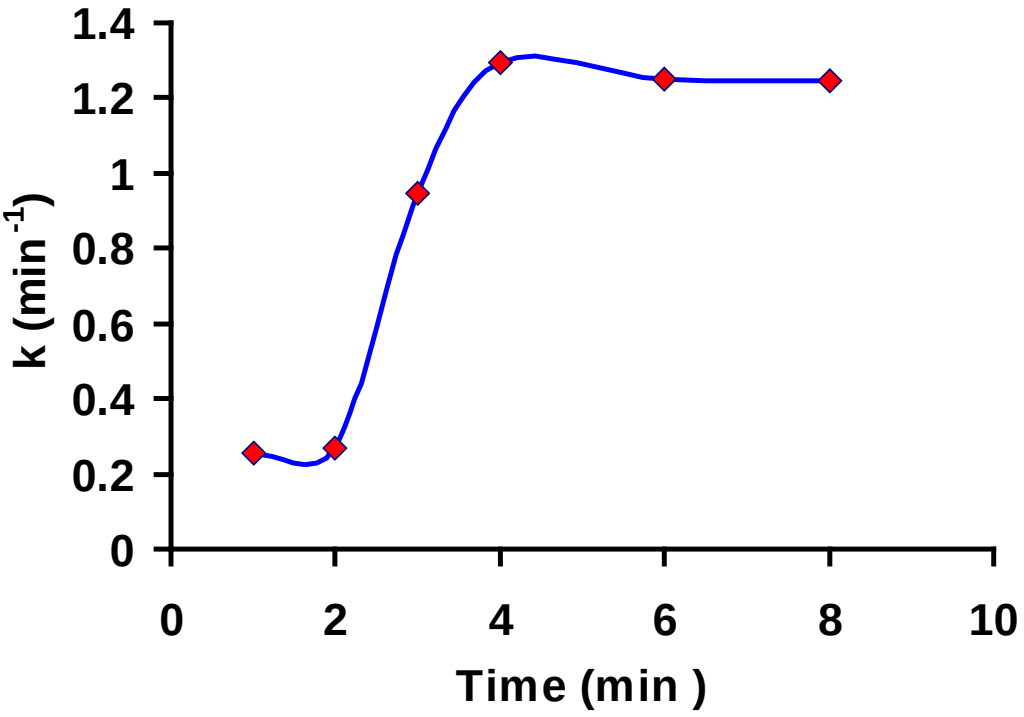

Figure 5.4 Effect of catalyst concentration photocatalytic degradation of Safranin O (Basic red 2) as a function of laser irradiation time for nano-structured WO_3

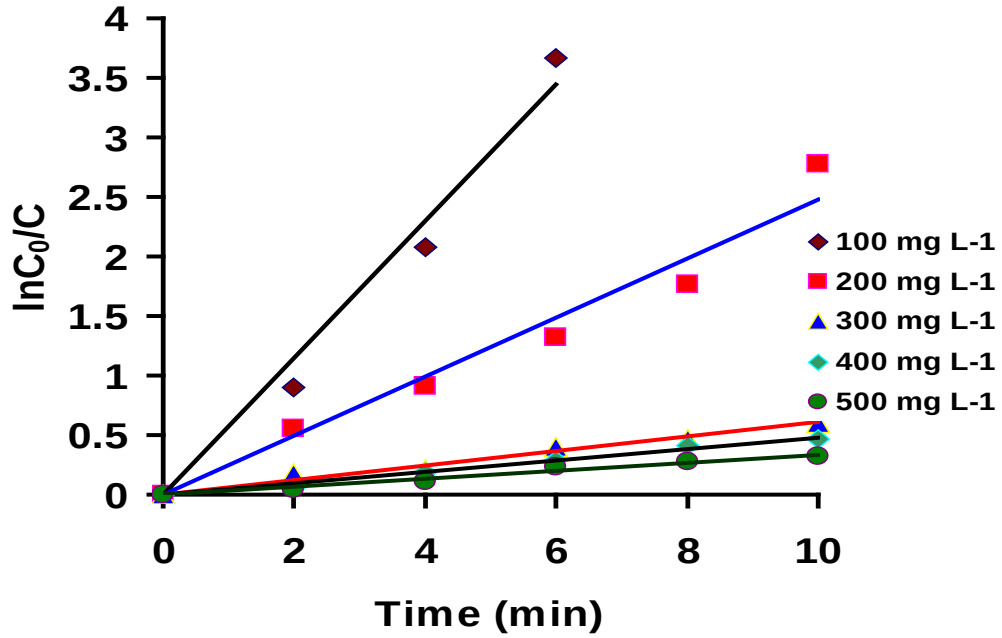

Figure 5.5 Effect of initial dye conc. on photocatalytic degradation of Safranin O (Basic red 2) as a function of laser irradiation time for nano-structured WO_3

The removal rate decreases with the increase in concentration of the dye. Similar results have been reported for the photocatalytic oxidation of other dyes [183]. Increase in the concentration of dye from $2.85*10^{-4}$ M to $1.425*10^{-3}$ M decreases the rate constant from 0.5737 to 0.0355 min^{-1} in 10 min. The linearity of the function with high values of r^2 was observed for all investigated dyes but only in the limited range of their C_0 .The rate constant varies considerably with the increase in the initial dye concencentration. It was found that when the initial concentration of the dye was high, their k were significantly lower as compared to the lower concentration of the dye. The possible explanation for this behavior is that as the initial concentration of the dye increases, the path length of the photons entering the solution decreases and in low concentration the reverse effect is observed, thereby increasing the number of photon absorption by the catalyst in lower concentration. At high concentration of dye, the dye molecules may absorb a significant amount of light rather than the catalyst and this may also reduce the catalytic efficiency [184,185].

5.1.5. Kinetics of Photocatalytic Degradation

The degradation rate for the decomposition of the dye under investigation was calculated [186] using the formula given below,

$$-d[C]/dt = kC^n \qquad (10)$$

where C = concentration of Safranin -O remaining after time t, k = rate constant and n = order of reaction. Figure 5.6 shows the change in absorption intensity as a function of laser irradiation time of an aqueous solution of Safranin O in the presence of nano-structured WO_3. The concentration of safranin O (0.57 mM) was used.

Table V Effect of dye conc. on photocatalytic degradation of Safranin O using nanocrystalline WO_3 prepared by ppt method

Initial dye conc.*10^{-4} mol L^{-1}	k(min^{-1})	r^2	Photodegradation rate*10^{-5} mol L^{-1}
2.85	0.5737	0.9790	16.35
5.70	0.2483	0.9633	14.15
8.55	0.0609	0.9801	5.21
11.4	0.0479	0.9860	5.46
14.25	0.0335	0.9811	4.77

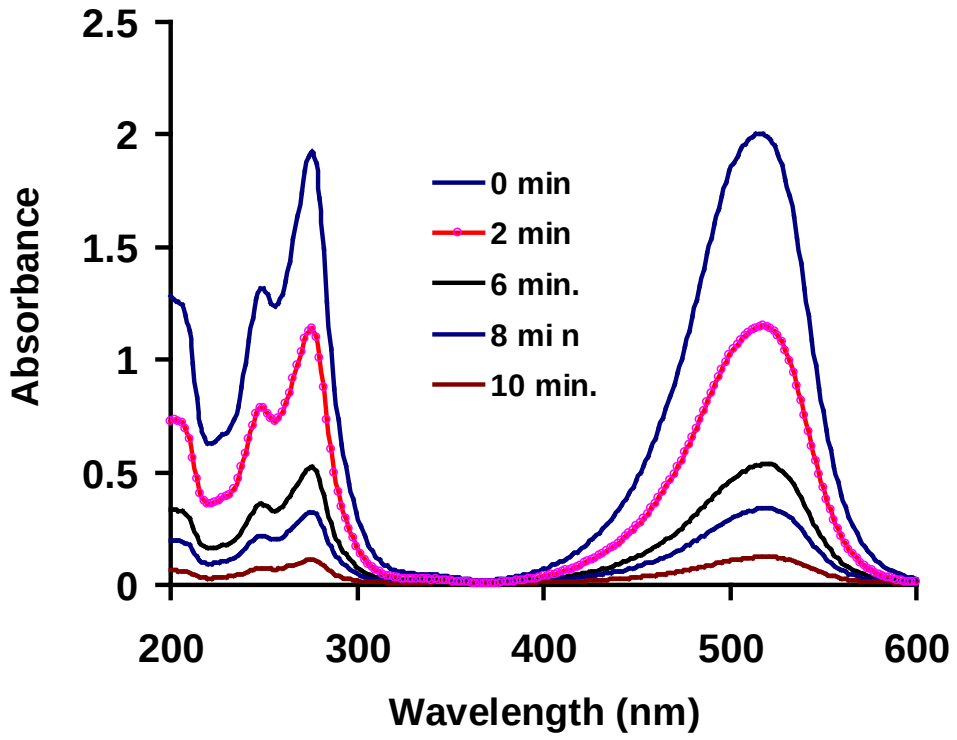

Figure 5.6 Typical UV-Visible spectra showing the change in absorption intensity as a function of laser exposure time for an aqueous solution of Safranin O (Basic red 2) in presence of WO_3.

A plot of ln C_0/C versus laser irradiation time for an aqueous solution of Safranin O in presence of nanocystalline WO_3 and curve fit data for the first order degradation kinetics of Safranin O is depicted Figure 5.7. The least square fit, $r^2 = 0.9649$ and rate constant = 0.2566 min^{-1} was estimated from Figure 5.7. This photodegradation rate could be considered very high as compared with the reported values using conventional setups using broad band spectral sources like lamps. As is clear from the results shown in Table V, almost 94.0 % removal of Safranin O was achieved during only 10 minutes laser irradiation using nanocrystalline WO_3 semiconductor catalyst which is very high in this short span of time. The results indicate that the percentage degradation of Safranin O increases with the increase in laser irradiation time. This increase in degradation of Safranin O with time could be due to the fact that with increase in the laser irradiation time, the number of absorbed laser photons increases, producing more amount of ·OH radicals, thereby facilitating more degradation of the dye.

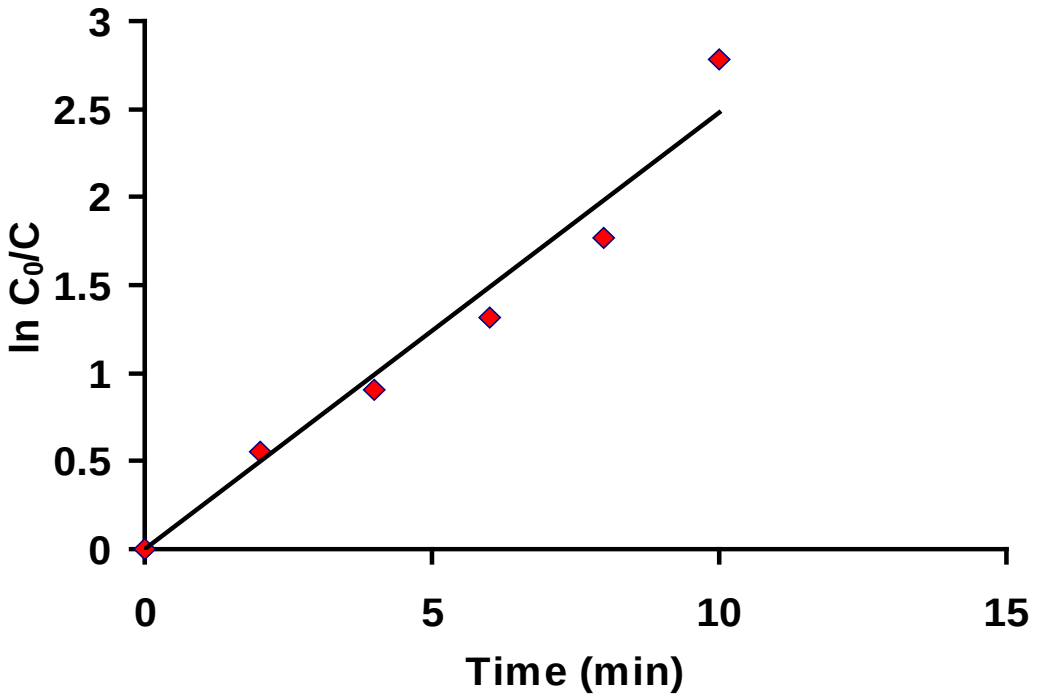

Figure 5.7 Plot of ln C_0/C as a function of laser exposure time for an aqueous solution of Safranin O in presence of WO_3 and curve fit data for the first order degradation kinetics

Table VI Effect of recycling on the photocatalytic activity of WO_3 synthesized by ppt method for the degradation of Safranin O

Number of cycle	k(min^{-1})	r^2	Degradation rates (mM-min^{-1})
0	0.2614	0.9875	0.1489
Ist cycle	0.2473	0.9922	0.1409
2 nd cycle	0.2314	0.9939	0.1319
3 rd cycle	0.2102	0.9875	0.1198
4^{th} cycle	0.1822	0.9752	0.1038
5^{th} cycle	0.1751	0.9867	0.0998

5.1.6. Recycling of Nanocrystalline WO_3 using Safranin O as a Pollutant

Reusability of nanocrystalline WO_3 synthesized by precipitation method was evaluated for the photocatalytic degradation of Safranin O. The photocatalytic degradation studies were carried out under the identical conditions as applied for the evaluation of photocatalytic activity of the catalyst for the degradation of the dye under investigation in order to assess the recyclability of WO_3 prepared by ppt method. The concentration of Safranin O (0.57 mM) was used in this study.The amount of catalyst used for this purpose was 1.0 g L^{-1}. After the completion of the reaction (cycle I), the WO_3 catalyst was collected and utilized for the second and third cycle under the similar conditions. The photocatalytic efficiency of WO_3 was found to decrease after every cycle.

The solutions resulting from the photocatalytic degradation of Safranin O was filtered, washed and the photocatalyst was dried at 200 °C. The dried photocatalyst was used for the degradation of Safranin O, employing similar experimental conditions. The results obtained are presented in Table VI. The percentage reduction in the rates of photocatalysis mediated by WO_3 after five cycles for the degradation of Safranin O was found to be 33%. The decrease in photocatalytic activity was also observed by some othe authors [187]. After completion of the fifth cycle, a decrease of approximately 33 % was observed in the photocatalytic activity of the catalyst.The decrease in photocatalytic activity might be attributed to the loss in amount of catalyst during filtration, washing and other processes involved in the recycling.

5.2 Photocatalytic Degradation of Acid Red 87 by WO_3

Blank experiments were carried out by irradiating the aqueous solution of the dye derivative in the absence of WO_3. Almost 20% degradation of the dye degradation was observed without catalyst. Figure 5.9 depicts typical UV absorption spectrum representing the trend of removal of Acid Red 87 dye for WO_3 at different times (0- 12 minutes) under laser irradiation. It can be seen from the results given in Table VII that ~ 95% degradation was achieved within very short laser exposure time (12 mins.) using 355 nm laser radiations.

5.2.1. Effect of Incident Laser Energy on Degradation Process

The effect of incident laser energy on the degradation of the dye was investigated and the results shown in Table VII. It is obvious from the table that the degradation of the dye was significantly influenced by the laser energy and degradation was found to increase almost linearly with the increase in laser energy upto a certain energy level. When 150 mJ of laser energy was applied, maximum 95% degradation was recorded within 8 mins of irradiation and a further increase in the laser energy was not valuable for the degradation of dye.

This phenomenon may be explained in terms of the fact that when higher laser energy is employed, incident photon flux increases in the solution exciting more and more catalyst particles which, in turn, increases the degradation of the dye derivative. The dependency of photocatalytic property on the light intensity observed in this study

followed similar trend as explained by Ollis et. al. [188], in which, it was concluded that there is a linear relationship between the rate and the light intensity up to a certain level.

5.2.2 Effect of Catalyst Concentration on Dye Removal Process

The effect of photocatalyst concentration on the degradation kinetics of Acid Red 87 was studied employing different concentrations of WO_3 varying from 0.5 gL^{-1} to 7.0 gL^{-1} (Table VII). As expected, the degradation rate for decomposition of the model compound under investigation was found to increase with the increase in catalyst concentration up to a certain catalyst loading (5.0 gL^{-1}) and reaches to saturation limit which is in agreement with a number of studies reported earlier [189,190]. At lower catalyst loading much of light may be transmitted through the solution.

However, higher reaction rates at higher amount of catalyst loading may be explained in terms of complete utilization of incident photons striking on the catalyst surface and/or availability of active sites at the surface i.e., higher adsorption of incident light can lead the formation of high photoactivated volume in suspension thereby increasing the efficiency of the system. It has been found that above a certain concentration, the reaction rate levels off and becomes independent of the catalyst concentration. N. Daneshwar et. al. observed that the optimum catalyst loading for the best degradation is 160 mgL^{-1}. In another study, the optimum catalyst concentration was found to be 1.0 g L^{-1} and moreover, the effect of higher dose was not investigated. Similarly, the nature of the organic molecules under investigation can also affect the optimum catalyst loading.

Table VII Photocatalytic degradation of Acid Red 87 in aqueous suspensions of WO_3 under different conditions.

Parameters		Degradation rates (M min^{-1} * 10^{-3})
Energy (mJ)	40.00	0.0075
	70.00	0.0148
	100.0	0.0378
	130.0	0.0460
	150.0	0.0501
	180.0	0.0523
	200.0	0.0529
Reaction pH	3.10	0.0450
	4.80	0.0378
	7.20	0.0285
	9.20	0.0250
	12.3	0.0196
Substrate concentration (mM)	0.10	0.0114
	0.15	0.0167
	0.25	0.0378
	0.40	0.0293
	0.50	0.0190
Catalyst concentration (gL^{-1})	1.00	0.0378
	2.00	0.0535
	3.00	0.0715
	4.00	0.0790
	5.00	0.0805
	6.00	0.0812
	7.00	0.0809

In a recent study, it has been found that the initial reaction rate increases with increase in catalyst concentration up to 5.0 gL^{-1} for the 1, 2 diphenylhydrazine. In contrast, under identical reaction conditions, the best degradation of benzidine was achieved at 2.0 gL^{-1} catalyst concentration and a further increase in catalyst concentration led a decrease in rate. This limit, therefore, depends on the geometry and working conditions of the photoreactor, concentration and nature of organic contaminants, and a defined amount of catalyst in which all the particles, i.e. the entire surface exposed, are totally illuminated. When the catalyst concentration is very high, after traveling a certain distance on an optical path, turbidity impedes further penetration of light in the reactor lowering the efficiency of the system.

5.2.3 Effect of Solution pH on the Dye Removal

The effect of solution pH of dye derivative was studied in the range of 3 –13 and the results are listed in Table VII. The photocatalytic degradation was found to decrease with the increase in reaction pH and the best result for photocatalytic degradation for acid red 87 was obtained at pH 3.2. Similar results have been reported for the photodegradation of other dyes [191,192].

The decrease of photodegradation rate with increasing reaction pH may be due the surface charge of catalyst and its relation to the adsorption tendency of dye. In this study, it was found that the dye tend to adsorb slightly on the surface of catalyst more in acidic environment as compared to basic i.e., the higher is the adsorption, the higher is the degradation. The result depicts the trend of adsorption versus the solution pH. The adsorption of the dye on the surface of photocatalyst was investigated by stirring the

aqueous solution in the dark at different pH such as 3.2, 4.6, 7.6, 9.7, and 12.1. After removing the catalyst, analysis of the samples with UV spectrophotometer indicates some loss of the compound as shown by the change in absorption intensity as a function of solution pH.

Another possible reason for the different reaction rates at different pH values may be correlated to the generation of active hydroxyl radicals and occupancy of active sites of catalyst surface for the production of $^{\bullet}OH$ radicals by formed intermediate products. Values of solution pH can alter the degradation route and lead the formation of different intermediate products [193]. Based on the photocatalytic mechanism, the active $^{\bullet}OH$ radicals are produced on the surface of catalyst by the reaction of h^{+} and adsorbed OH^{-}. During the course of photocatalytic reactions, formation of some negatively charged species (e.g., intermediate products) can occur and compete with OH^{-} for occupancy of catalyst surface. This competition reduces the possibility of adsorption of OH^{-} on the surface of catalyst which, in turn, affect the generation of active $^{\bullet}OH$ thereby decreasing the efficiency of the process.

5.2.4. Effect of Dye Concentration on Dye Removal Process

The photocatalytic degradation of Acid Red 87 with different concentration svarying from 0.10 to 0.40 mM was investigated.

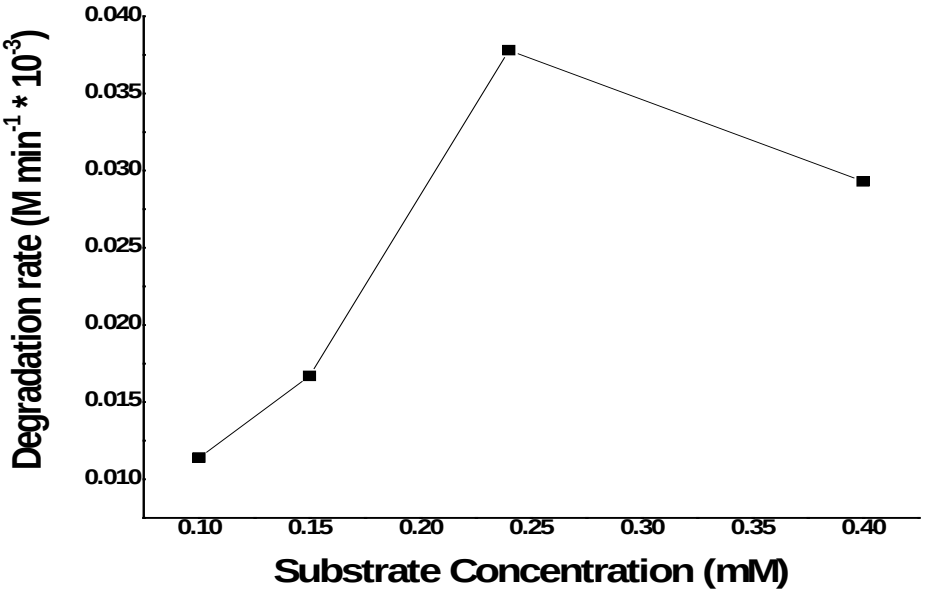

Figure 5.8 Effect of substrate conc on photodegradation rate of Acid red 87 by WO_3

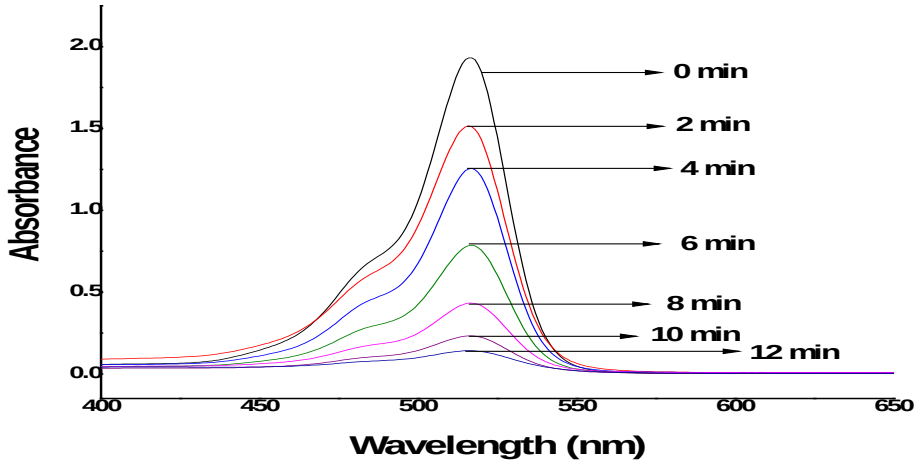

Figure 5.9 Typical UV-Visible spectra showing the change in absorption intensity as a function of laser exposure time for an aqueous solution of Acid red 87 in presence of WO_3.

The results reported in Table VII demonstrate that the degradation rate increased with the increase in substrate concentration from 0.10 to 0.25 mM and a further increase in the concentrations of the substrate led to a decrease in the degradation rate. The decrease in degradation rate at higher concentration of the dye may be rationalized in terms of the fact that as the initial concentrations of the dye increases, the color of the irradiating mixture becomes more and more intense which prevents the penetration of light to the surface of the catalyst. Therefore, the generation of relative amount of reactive species on the surface of the catalyst decreases as the intensity of light, laser irradiation time and concentration of the catalyst are constant. Consequently, the degradation of the dye decreases as the dye concentration exceeds the optimum limit [194-195].

5.2.5. Kinetics of Photocatalytic Degradation of Acid Red 87

The photocatalytic removal of acid red was studied usig different dye concentrations.The photodegradation rates are shown in Table VII. It was observed that initially, the degradation of the dye was very fast and it became slower with the increase in irradiation time. This may be due to the fact that as oxidation proceeds, less and less of the surface of the WO_3 particle is covered as the pollutant is decomposed. In a previous study based on the photocatalytic removal of Acid Red 87 or Eosin Y using a 16 W UV lamp, it has been reported that only ~ 90% degradation of dye was observed even after 2 hr irradiation [196]. Moreover, they removed 50 ppm dye concentration, while in the present study, ~ 95% degradation was achieved using 150 ppm within 12 minutes of laser irradiation using 100 mJ energy. In this study, it is proved experimentally that laser-based heterogeneous photocatalysis could be an efficient and effective method for waste water

treatment for removal of dye derivatives as compared to conventional UV lamp based methods.

5.3. Photocatalyic Degradation of Alizarin Yellow GG by Nanocrystalline Tungsten Oxide

5.3.1. Effect of Laser Irradiation and Photocatalyst on Degradation of the Dye

Blank experiments were performed for the photocatalytic degradation of the dye (AYGG) without laser irradiation and using UV laser irradiation without the presence of catalyst. No appreciable degradation was observed without the catalyst. The results are ddepicted in Figure 5.10. These observations reveal that both UV light and photo-catalyst are essential for the effective removal of the dye (AYGG). The influence of incident laser energy on the degradation efficiency has been examined at constant dye concentration (100 mg L^{-1}) and catalyst loading (3.0 gL^{-1}). It was experimentally demonstrated that the percentage of decolorization and photodegradation increases with the increase in laser energy. As the incident laser energy increases, more and more photons are absorbed by WO_3 catalyst. These more photons excites more electrons to be transferred from the valence band to the conduction band of a semiconductor photocatalyst hence more hydroxyl radicals are produced. As more hydroxyl radicals are generated by more incident laser energy, more degradation of the dye takes place and by this way the rate of degradation process increases.

The catalyst concentration in irradiated suspensions has a significant role on the photocatalytic degradation rate. In order to determinate the optimum nano WO_3

concentration under similar conditions applied in our studies, the degradation rate of AYGG (0.323mM) was determined at different WO_3 concentrations, from 0 to 4.0 g L^{-1} while keeping all the other parameters (laser irradiation time, laser energy, stirring rate etc) constant. With an increased catalyst loading from 1.0g L^{-1} to 3.0 gL^{-1} the percentage degradation increased linearly for 20 min irradiation time. After that the increase in catalyst loading did not affect the degradation rate significantly. Thus, the catalyst loading for maximum degradation of 100 mg L^{-1} of AYGG was 3.0 g L^{-1}under our experimental conditions .

The increase in the amount of catalyst increased the number of active sites on the photocatalyst surface, which in turn increased the number of hydroxyl, and super oxide radicals [197]. When the concentration of WO_3 catalyst was increased above the limiting value, the degradation rate decreased due to an increase in the turbidity of the suspension and a decrease in UV light penetration as a result of increased scattering effect. The plateau, which was observed after addition of a certain amount of WO_3 may be due to the decrease of light penetration into the solutions [198]. Based on these results, the optimum catalyst concentration was estimated as 3.0 g L^{-1}. This concentration was used in further experiments in this study.

5.3.2. Effect of Initial Dye Concentration

It is important both from the mechanistic and application point of view, to study the dependence of the photocatalytic reaction on the substrate concentration. The effect of various initial dye concentrations on the photocatalytic degradation has been investigated from 3.23×10^{-4} to 1.62×10^{-3} mol/L using WO_3.

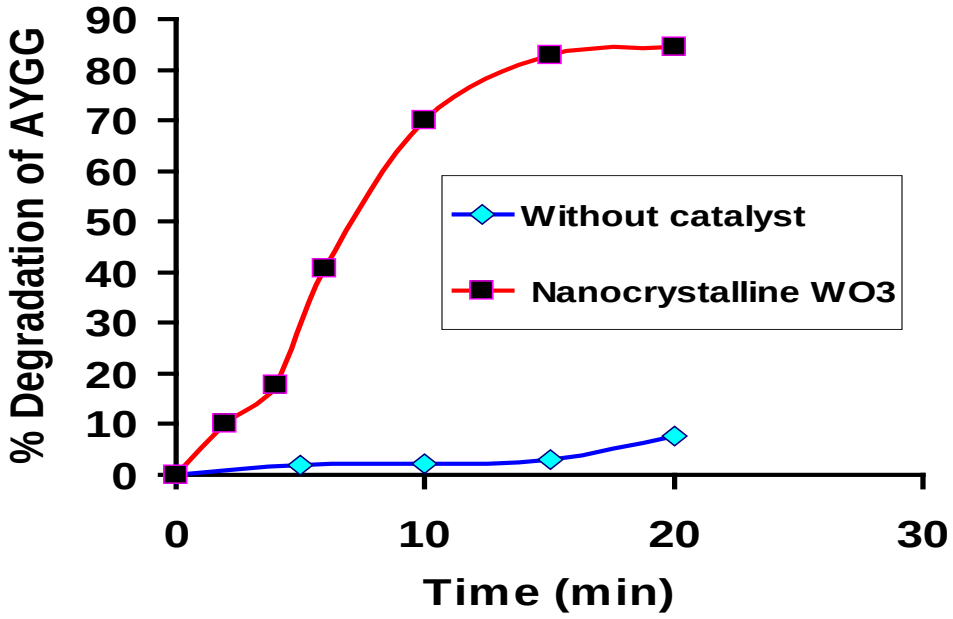

Figure 5.10 Percentage degradation of Alizarin Yellow GG in presence of WO_3

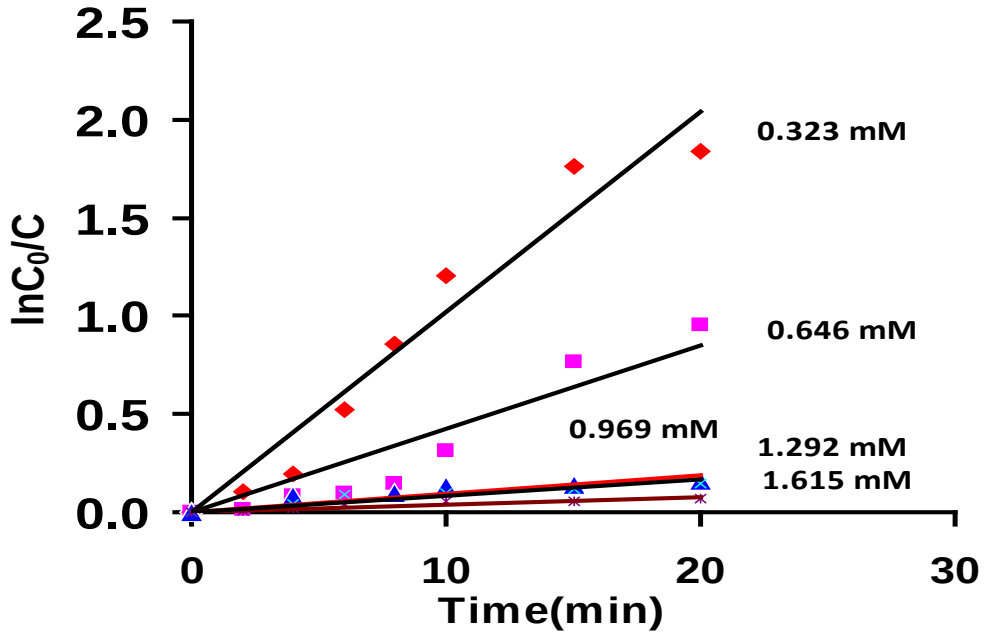

Figure 5.11 Effect of initial dye concentration on photocatalytic degradation of Alizarin Yellow GG as a function of laser irradiation time for nano-structured WO_3

The results obtained are presented in Figure 5.11- Figure 5.13. The results indicate that rate of photocatalytic degradation is decreased as the initial dye concentration is increased.With the increase in the initial dye concentration, more and more dye molecules are adsorbed on the surface of nanocrystalline WO_3 causing the decrease in rate of photodegradation.The large amount of adsorbed dye has an inhibitive effect on the reaction of dye molecules with photogenerated holes or hydroxyl radicals, because of the lack of any direct contact between them. The increase in dye concentration also causes the dye molecules to absorb light and the photons never reach the photocatalyst surface, thus the photocatalytic degradation efficiency decreases. The study of the effect of initial concentration of the dye is indicate that the data obey the the Langmuir-Hinshelwood model.

When the dye concentration increases the amount of dye adsorbed on the catalytic surface increases. This affects the catalytic activity of WO_3. The increase in dye concentration also decreases the path length of photon entering into the dye solution.

At high concentration of dye, the dye molecules may absorb a significant amount of light rather than the catalyst and this may also reduce the catalytic efficiency [199]. The photocatalytic degradation of AY dye containing WO_3 obeys pseudo-first-order kinetics**.** In all cases, 100mL dyes solutions containing 3.0 gL^{-1} of WO_3 were irradiated.

5.3.3. Kinetics of Photocatalytic Degradation Process of Alizarin Yellow GG

It was found from the results depicted in Figue 5.14 that the photocatalytic removal of Alizarin Yellow GG follows the pseudo first order rate constants.

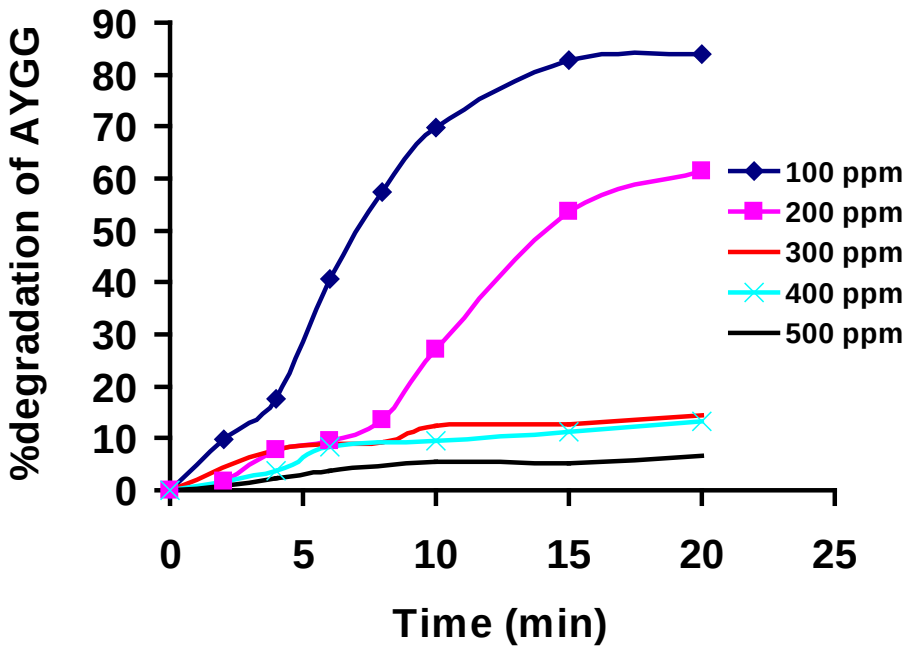

Figure 5.12 Percentage degradation showing the effect of initial dye concentration on photocatalytic degradation of Alizarin Yellow GG as a function of laser irradiation time for nano-structured WO_3

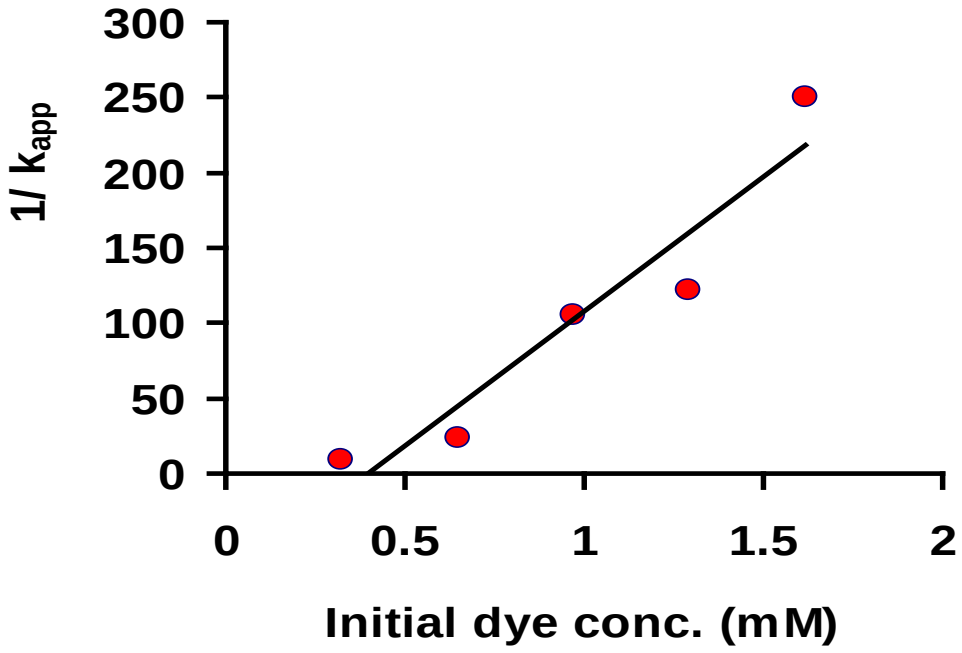

Figure 5.13 Effect of initial dye concentration on photocatalytic degradation of Alizarin Yellow GG as a function of rate constant for nano-structured WO_3

It can be seen from the Figure that ~ 85 % degradation was achieved within very short laser irradiation time (~20 minutes) using 355 nm laser a coherent UV irradiation source. A typical plot of $\ln C_0/C$ versus time is depicted in Figure 5.15 for dye degradation. The least square fit, $R^2 = 0.8798$ and rate constant was estimated from Figure 5.15.The pseudo first order rate constant for WO_3 calculated was 0.1077 min^{-1}.

$$\text{AYGG Degradation (\%)} = \left\{ \frac{C_0 - C_t}{C_0} \times 100 \right\} \qquad (11)$$

Where C_0 = initial concentration of AYYG, C_t = concentration of AYYG at any time't'

As is clear from Figure 5.14, almost 83 % removal of alizarin yellow GG was achieved during first 15 minute laser irradiation using nanostructured WO_3 semiconductor catalyst which is reasonably high in this short span of time. It was observed that with the increase in laser irradiation time, the percentage of alizarin yellow GG degradation increases. This increase in alizarin yellow GG degradation with time could be due to the fact that with increase in the irradiation time, the number of absorbed laser photons increases, producing more amount of $OH^{\bullet}$ radicals, thereby facilitating more degradation of alizarin yellow GG.

5.4. Photocatalyic Degradation of Methyl Red by Nanocrystalline WO_3

The photocatalytic activity of WO_3 was checked using Methyl red as a model pollutant.

5.4.1. Effect of Laser Irradiation and Photocatalyst on Degradation of Methyl Red

The degradation of Methyl red under UV laser irradiation without the presence of the catalyst was studied.

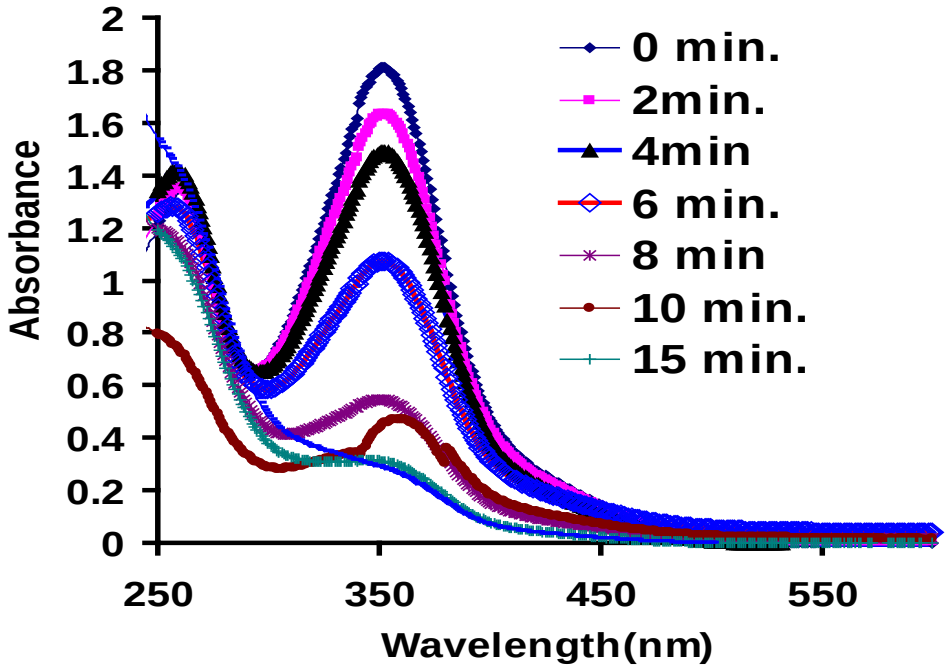

Figure 5.14 Typical UV-Visible spectra showing the change in absorption intensity as a function of laser exposure time for an aqueous solution of Alizarin yellow GG in presence of WO_3

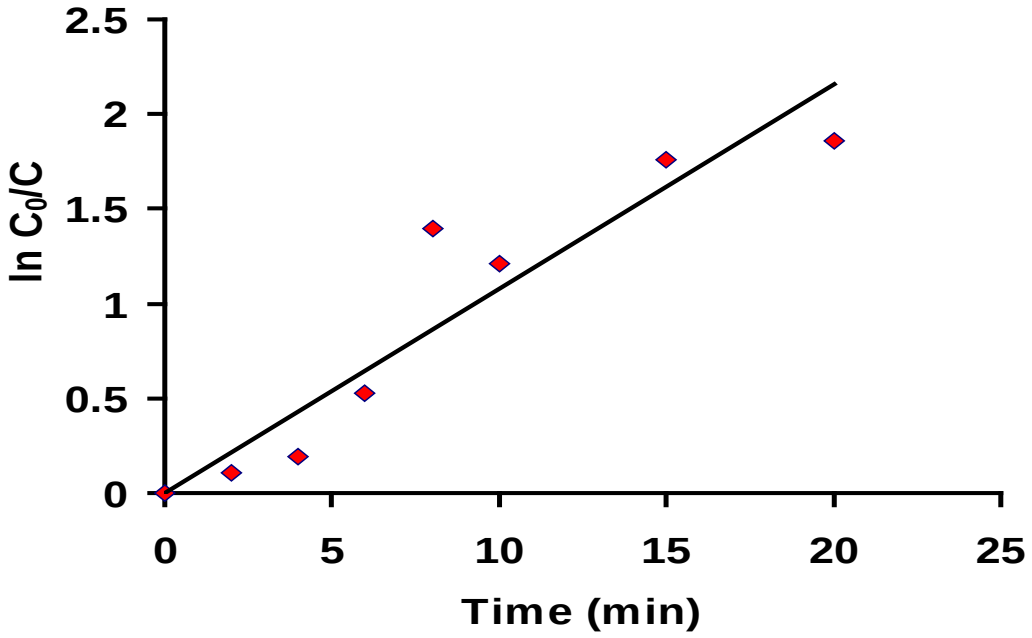

Figure 5.15 A plot of ln C_0/C as a function of laser exposure time for an aqueous solution of Alizarin yellow GG in presence of WO_3 and curve fit data for the first order degradation kinetics

For this purpose, blank experiments were carried out for the dye solution. No significant degradation of Methyl red was observed without the catalyst. Figure 5.14 shows the change in absorption intensity as a function of laser irradiation time of an aqueous solution of Methyl red in the presence of nano-structured WO_3.The results depicted in Figure 5.15 demonstrate that 90.0% degradation was achieved within very short laser irradiation time using 355 nm laser. It is clear from the results that both UV light and photo-catalyst are essential for the effective removal of the dye.

5.4.2. Kinetics of Photocatalytic Degradation Process

The results of photocatalytic degradation of Methyl red under laser UV irradiation over nanocystalline WO_3 are shown in Figure 5.16. The degradation rate for the decomposition of the dye under investigation was calculated using the formula given below,

$$-d[C]/dt = kC^{n} \qquad (12)$$

where C = Concentration of Methyl red remaining after time t, k = rate constant and n = order of reaction.

A typical plot of $\ln C_0/C$ versus laser irradiation time is depicted in Figure 5.17 for dye degradation. The least square fit, $r^2 = 0.9649$ and rate constant = 0.2566 min^{-1} was estimated from Fig 6.2. This photodegradation rate could be considered very high as compared with the reported values using conventional setups using broad band spectral sources like lamps. The results indicate that the percentage degradation of Methyl red increases with the increase in laser irradiation time.

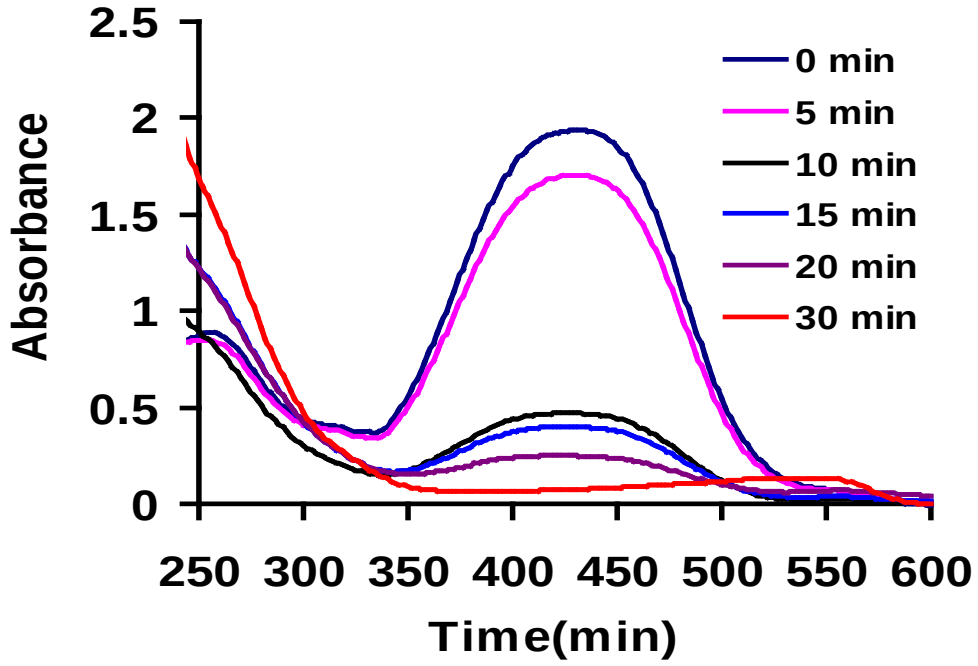

Figure 5.16 Typical UV-Visible spectra showing the change in absorption intensity as a function of laser exposure time for an aqueous solution of Methyl red in presence of WO_3.

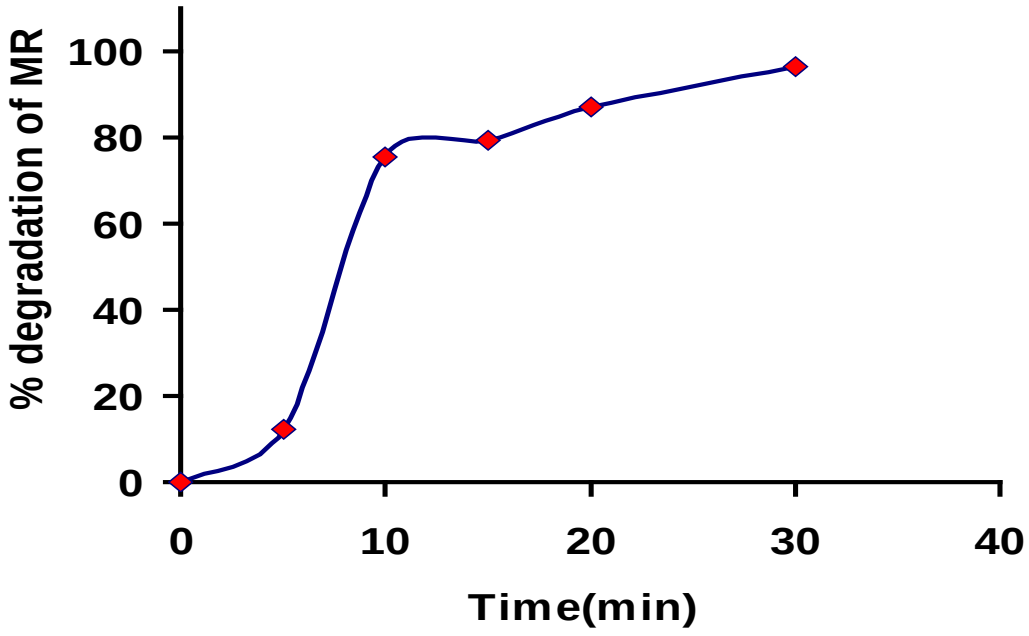

Figure 5.17 Percent degradation of an aqueous solution of Methyl red in presence of WO_3

This increase in degradation of the dye with time could be due to the fact that with increase in the laser irradiation time, the number of absorbed laser photons increases, producing more amount of OH. radicals, thereby facilitating more degradation of the dye.

5.4.3. Influence of Calcination Temperature on Photocatalytic Activity of Nanocrystalline WO_3

The effect of calcination temperature on the grain size and photocatalytic activity of WO_3 was investigated in this study. The results obtained are depicted in Figure 5.19. Depending on the method of the preparation and the end usage of the metal oxide semiconductor or doped photocatalysts, calcination temperatures have prominent influence on the activity of the prepared photocatalysts. The nanocrystalline WO_3 samples were subjected to various calcination temperatures ranging from 300 to 700 $^{\circ}$C.

The results of their investigations revealed that the photocatalytic activity of the prepared photocatalysts increased with increase in temperature from300 to 500 $^{\circ}$C. At 500 $^{\circ}$C, it reached the maximum. However, the catalytic activity of the WO_3 decreased with further increase of calcination temperature from500 to 700 $^{\circ}$C.

This was also found to be consistent with their SEM analysis and XRD data which showed that at 600 $^{\circ}$C and above, particle size has been increased because of agglomeration of the sample. Yu et al. [200] prepared nitrogen-doped TiO_2 nanoparticle catalyst and analyzed its catalytic activity under visible light.He also observed the similar effect of calcination temperature.

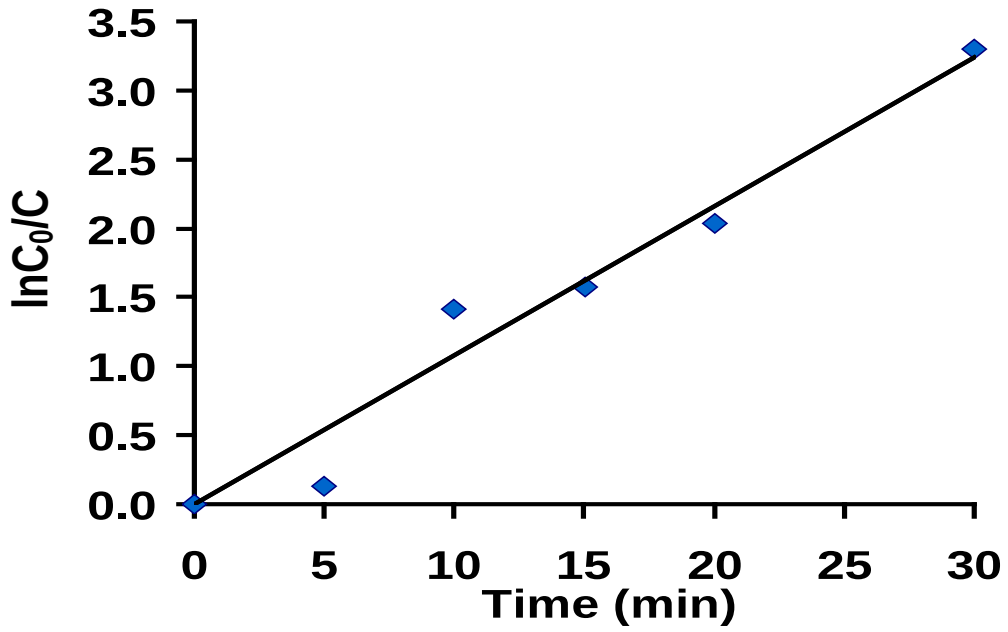

Figure 5.18 A plot of ln C_0/C as a function of laser exposure time for an aqueous solution of methyl red in presence of WO_3 and curve fit data for the first order degradation kinetics

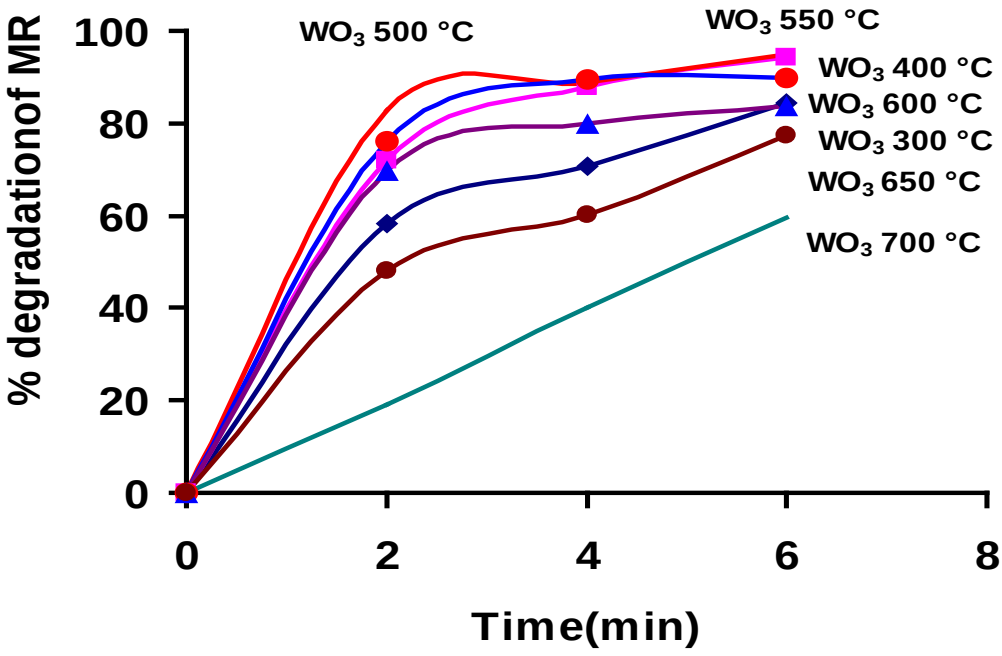

Figure 5.19 Percent degradation as a function of laser exposure time for an aqueous solution of methyl red in presence of WO_3 calcined at different temperatures

5.5. Comparison of Photocatalytic Activity of Nanocrystalline WO_3 for Degradation of Four Dyes

The photocatalytic degradation of four dyes with different structure and containing different substitutent groups have been investigated using nanocrystalline WO_3 as photocatalyst in aqueous suspension under UV laser irradiation. The photodegradation rate of the dye was detected. The results are given in figure 5.20. The photodegradation rate for the photocatalytic degradation of the dyes such as Safranin O, Acid Red 87, Alizarin Yellow GG and Methyl Red using WO_3 are as follows:

Safranin O > Acid Red 87 > Alizarin Yellow GG > Methyl Red

It was observed that different experimental parameters effect the degradation of the dyes significantly. The results obtained demonstrate that the rate of degradation also depends upon the nature of the dyes.It was observed that the photodegradation rate was increased with the increase in laser energy and increase in laser exposure time.It was also found that as the amount of photocatalyst increases, the rate increases until certain limit, then starts decreasing with further increase of the amount of the catalyst. This is the characteristic behaviour of heterogeneous photocatalysis. The rate of photocatalytic degradation of these four dyes under investigation decreases as the initial concentration of the dye increased. The degradation of the catioinic dyes increase significantly in basic pH while acidic pH facilitates the degradation of the other dyes used in this study.The interpretation of pH effects on the efficiency of dye photodegradation process is a very difficult assignment because of its multiple roles.

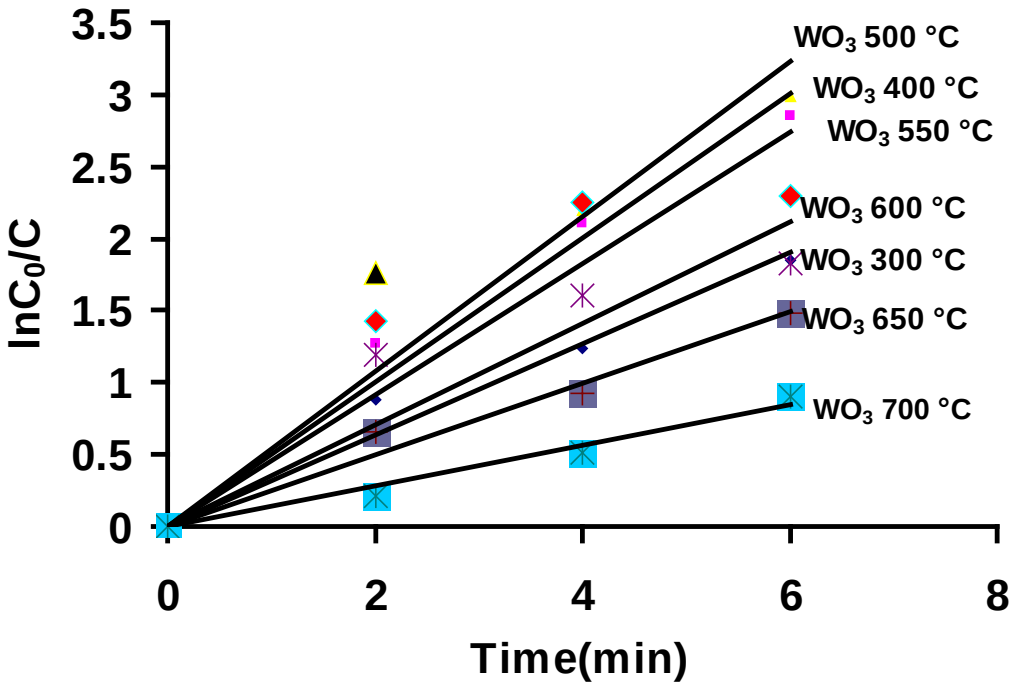

Figure 5.20 Plot of ln C_0/C as a function of laser exposure time for an aqueous solution of methyl red in presence of WO_3 calcined at different temperatures

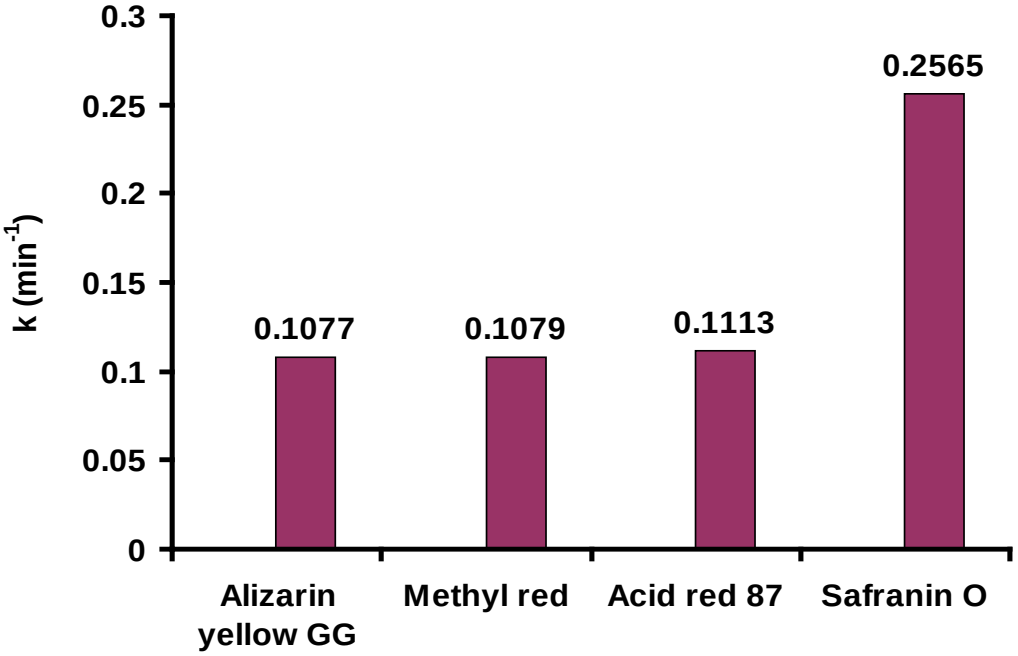

Figure 5.21 Comparative degradation of the dyes using aqueous suspension of WO_3

First, it is related to the ionization state of the surface according to the following reactions,

$$MOH + H^{+} = MOH_2^{+}$$

$$MOH + OH^{-} = MO^{-} + H_2O$$

pH changes can thus influence the adsorption of dye molecules onto the photocatalyst surfaces, an important step for the photocatalytic oxidation to take place. Second, hydroxyl radicals can be formed by the reaction between hydroxide ions and positive holes. The positive holes are considered as the major oxidation species at low pH, whereas hydroxyl radicals are considered as the predominant species at neutral or high pH levels. It was stated that in alkaline solution, •OH are easier to be generated by oxidizing more hydroxide ions available on metal oxides surface, thus the efficiency of the process is logically enhanced.

Similar results are reported in the photocatalyzed degradation of acidic azo dyes and triazine containing azo dyes [201]. Although it should be noted that in alkaline solution there is a coulombic repulsion between the negative charged surface of photocatalyst and the hydroxide anions. This fact could prevent the formation of $^{\bullet}OH$ and thus decrease the photoxidation. Third, it must also be noted that metal oxide particles tend to agglomerate under acidic condition and the surface area available for dye adsorption and photon absorption would be reduced. The degradation rate of some azo dyes increases with decrease in pH.

The mechanism of the photocatalytic reaction in the presence of metal oxide consists of a free radical reaction initiated by UV light. The mechanism may depend on the ability of the degraded compound to be adsorbed on the surface of the catalyst. The extent of such adsorption depends on many factors, and one of it is the charge of the

degraded compound. It was found that in photocatalytic degradation, the adsorption level on unmodified TiO_2 is higher for dyes with a positive charge (cationic) than for those with a negative charge (anionic) [202]. As the charge depends on the pH of a given solution, it follows that both pH and the nature of a particular dye influence the photocatalyst activity. The experimental results indicate that four dyes could be degradated effciently at different levels.

5.6. Photocatalytic Degradation of Alizarin Yellow GG by Nano ZnO

The photocatalytic removal of Alizarin Yellow GG using nano ZnO was investigated. The effect of different parameters was also studied.

5.6.1. Effect of Laser Irradiation and Photoatalyst on Degradation of the Dye

Since some dyes are photo bleached or degraded by direct UV irradiation without catalyst. Therefore, prior to study the photocatalytical removal, it is required to examine to what extent the dye (AYGG) is degraded under UV laser irradiation without the presence of catalyst. Blank experiments were carried out for the dye solution without catalyst. No significant degradation (almost 9.0 %) was observed without the catalyst. Laser induced photocatalytic degradation of AYGG using nano ZnO was studied. The change in absorption intensity as a function of laser irradiation time of an aqueous solution of AYGG in the presence of nano-structured ZnO is shown in Figure 5.22. It was observed that almost 90% degradation was achieved within very short laser irradiation time using 355 nm laser, a coherent UV irradiation source. These results indicate that both UV light and photo-catalyst are essential for the effective removal of the dye (AYGG).

5.6.2. Effect of Catalyst Loading

It is known that catalyst concentration in irradiated suspensions has a significant role in the studies concerning the photocatalytic degradation rate [203]. In order to determine the optimum nano ZnO concentration under conditions used in our studies, the degradation rate of AYGG (0.323 mM) was investigated at different ZnO concentrations, from 0 to 4.0 g L^{-1}. The volume of irradiated samples was 100mL.The results obtained are presented in Figure 5.23 It is also interesting to determine the minimum amount of catalyst required to degrade the maximum amount of dye at a particular experimental condition. It was found that the increase in amount of ZnO enhances the initial degradation rate of dye achieving the maximum rate at the nano ZnO concentration equal 3.0g L^{-1}. It was also observed that an increased catalyst loading from 1.0g L^{-1} to 3.0 g L^{-1} increases the rate of degradation. After that the increase in catalyst loading decreases the degradation rate. Thus, the catalyst loading for maximum degradation of 100 mg L^{-1} of AYGG was 3.0g L^{-1} under the experimental conditions specified. The increase in the amount of catalyst increased the number of active sites on the photocatalyst surface, which in turn increased the number of hydroxyl, and super oxide radicals [204].

When the concentration of ZnO catalyst was increased above the limiting value, the degradation rate decreased due to an increase in the turbidity of the suspension and a decrease in UV light penetration as a result of increased scattering effect [205]. Based on these results, the optimum catalyst concentration was estimated as 3.0 g $L^{-1.}$ This concentration was used in further experiments in this study to see the effect of other parameters like laser energy, laser irradiation time and pH.

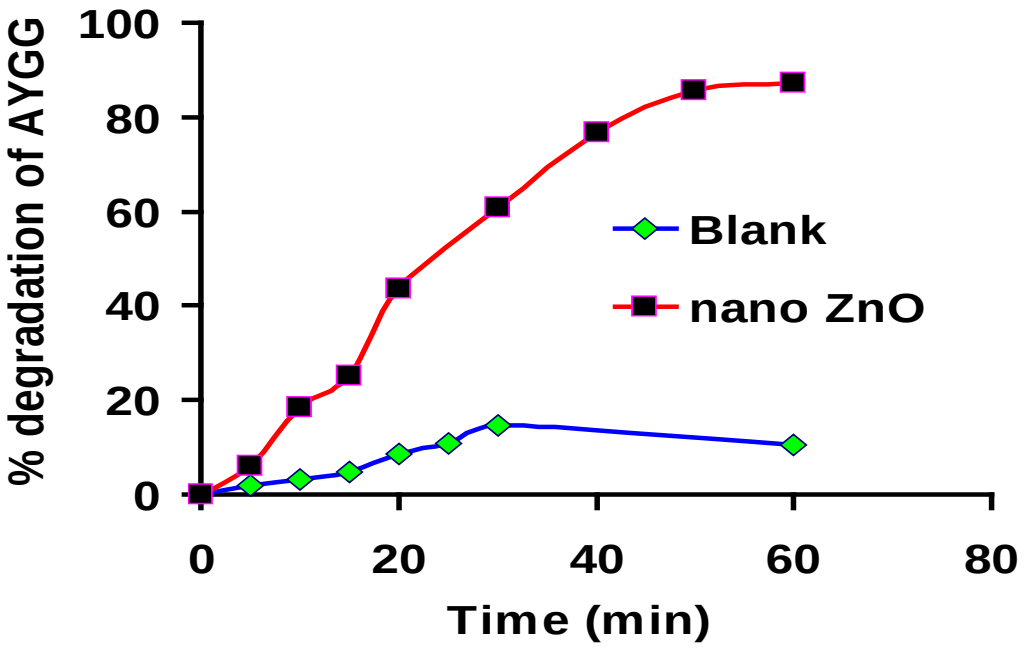

Figure 5.22 Percentage degradation showing photocatalytic degradation of Alizarin Yellow GG as a function of laser irradiation time using nano- ZnO and without ZnO

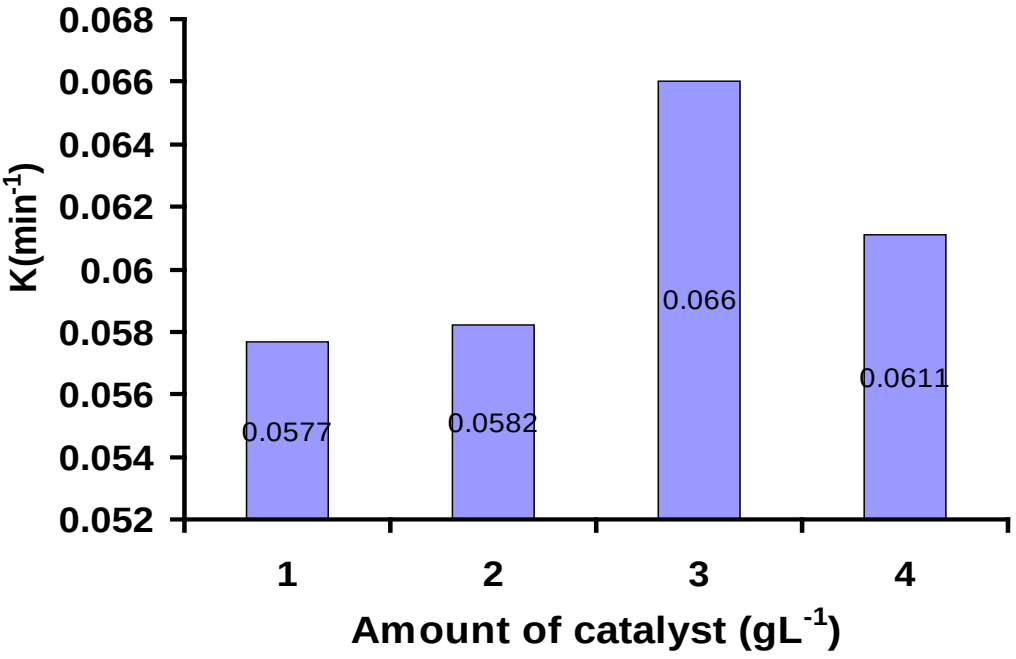

Figure 5.23 Effect of catalyst concentration on photocatalytic degradation of Alizarin Yellow GG as a function of laser irradiation time for nano ZnO

5.6.3. Effect of Laser Energy

The influence of laser energy on the degradation efficiency has been investigated at constant dye concentration (100 mg L^{-1}) and catalyst loading (3.0 g L^{-1}). The intensity of laser was varied in the range (2.2 -6.0)*10^{6} w/cm^2. The laser energy was measured with a calibrated energy meter manufactured by Ophir, USA. It is evident that the percentage decolorization and photodegradation of the dye increases with the increase in laser energy as depicted in Figure 5.24. Because the laser UV irradiation generates the photons required for the electron transfer from the valence band to the conduction band of a semiconductor photocatalyst and the energy of a photon is related to its wavelength and the overall energy input to a photocatalytic process is dependent on light intensity. The rate of degradation increases when more radiations (more photons) fall on the catalyst surface and hence more hydroxyl radicals are produced [206,207]. It was found experimentally that the percentage of decolorization and photodegradation increases with the increase in laser energy. As the incident laser energy increases, more and more photons are absorbed by ZnO catalyst. These more photons excites more electrons to be transferred from the valence band to the conduction band of a semiconductor photocatalyst hence more hydroxyl radicals are produced. As more hydroxyl radicals are generated by more incident laser energy, more degradation of the dye takes place and by this way the rate of degradation process increases.

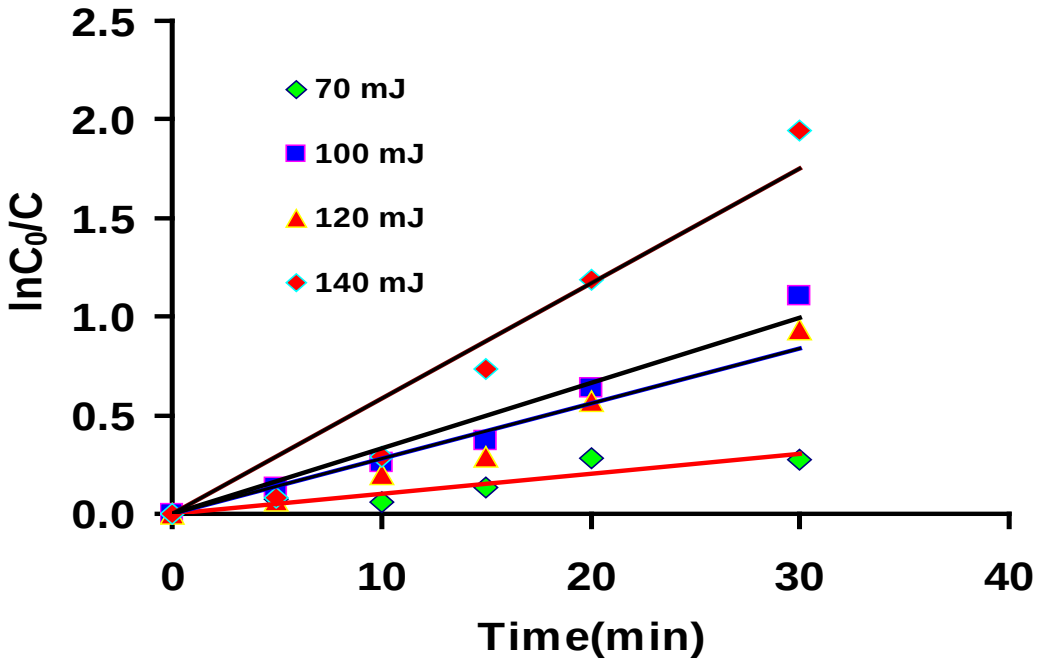

Figure 5.24 Effect of laser energy for ZnO and AYGG

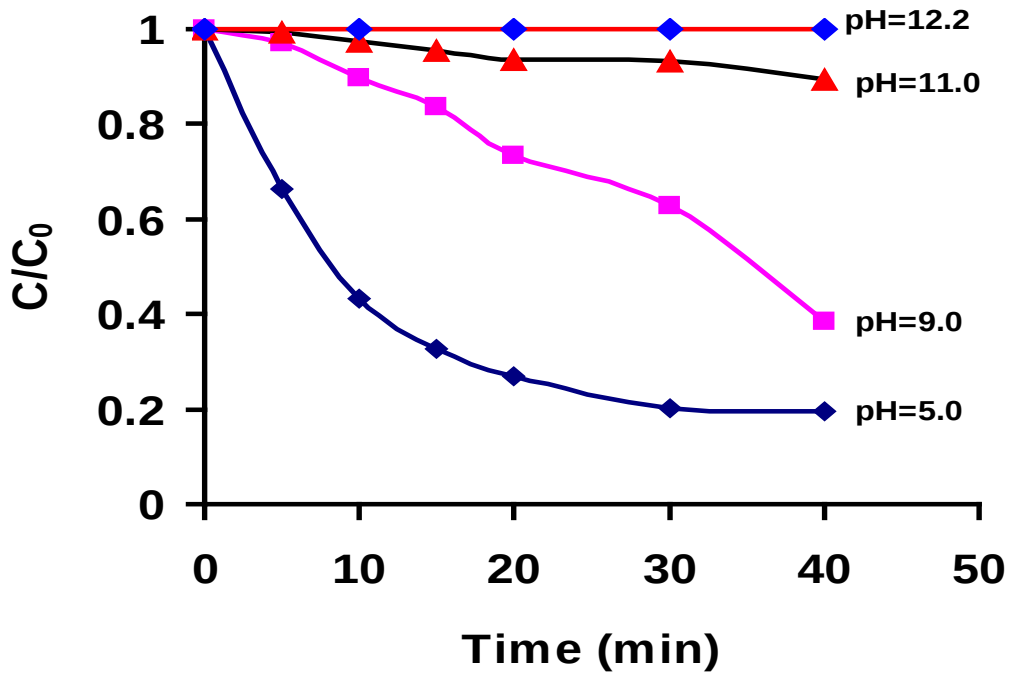

Figure 5.25 Effect of pH on photocatalytic degradation of Alizarin Yellow GG as a function of laser irradiation time for nano ZnO

5.6.4. Effect of pH

The photocatalytic removal of Alizarin yellow GG by nano ZnO in aqueous solutions of different pH levels is depicted in Figure 5.25. The effect of pH on photocatalytic degradation was observed for the range (5.0 -12.2) in this study. As is clear from the results given in Figure 5.25 that the photodegradation rate decreases with the increase in pH. The kinetic behavior of photocatalytic decomposition can be explained by Langmuir–Hinshelwood rate equation described in Equation 6. Because of the amphoteric behaviour of most of the semiconductor oxides, an important parameter in the reaction taking place on the semiconductor particle surface is the pH of dispersions, since it influences the surface charge properties of photo-catalyst. The zero point charge (zpc) is 8.9 for ZnO [208]. The results shown in Figure 5.25 that the degradation of the AYGG decreases with the rise of pH. Because the anionic dye molecule is negatively charged, so low pH favors adsorption on the catalyst surface. The photocatalytic decomposition of AYGG using ZnO was favored to occur in acidic conditions and exhibited a minimum decomposition rate in more alkaline solutions (at pH= 12.2). The results indicate that the adsorption of AY GG on catalyst surface is preferred at lower pH, and thus promotes the photocatalytic reaction.

5.6.5. Effect of Initial Dye Concentration

The study of the effect of initial concentration of the dye is also important for the Langmuir-Hinshelwood model. The effect of initial AYGG concentration on photocatalytic degradation efficiency is depicted in Figure 5.26. The results given in table 1 also indicate that rate of photocatalytic degradation is decreased as the initial dye concentration is increased. With the increase in the initial dye concentration, more and

more dye molecules are adsorbed on the surface of ZnO nanopowder causing the decrease in rate of photodegradation [209]. The large amount of adsorbed dye has an inhibitive effect on the reaction of dye molecules with photogenerated holes or hydroxyl radicals, because of the lack of any direct contact between them. The increase in dye concentration also causes the dye molecules to absorb light and the photons never reach the photocatalyst surface, thus the photocatalytic degradation efficiency decreases.

5.6.6. Kinetics of Photocatalytic Degradation Process

The initial Alizarin Yellow GG concentration was varied from 50 to 250 mgL^{-1}. Results showed that for this range of concentrations the reaction rate gets slower as the initial concentration of the dye in solution increases. As AYGG concentration increases, more reactant and reaction intermediates are adsorbed on the surface of the photocatalyst, therefore, the generation of hydroxyl radicals will be reduced since are only a fewer active sites for adsorption of hydroxyl anions.

The kinetic behavior of photocatalytic decomposition of Alizarin Yellow GG can be described by Langmuir–Hinshelwood's rate equation which is further simplified to a pseudo-first order rate equation with respect to the low dye concentrations studied in this research.

$$\text{rate} = -dC/dt = kKC/1 + KC = k_{app}C \qquad (13)$$

$$1/k_{app} = 1/kcK + C_0/kc \qquad (14)$$

Where C_0 = initial concentration of AYYG

C_t = concentration of AYYG at any time't'

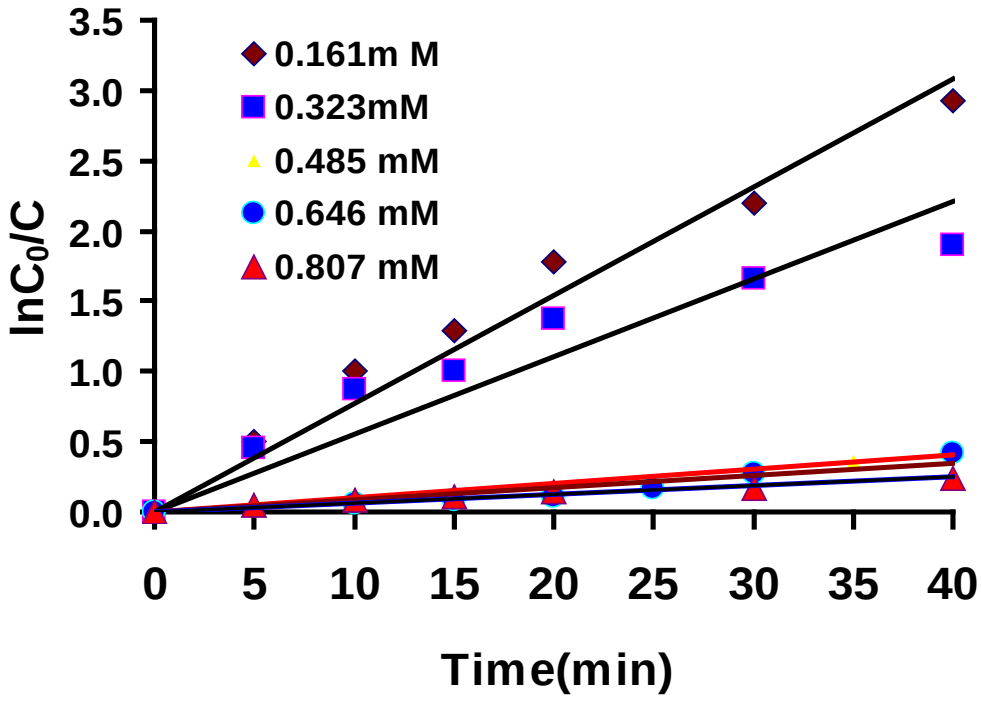

Figure 5.26 Effect of initial dye concentration on photocatalytic degradation of Alizarin Yellow GG as a function of laser irradiation time for nano ZnO

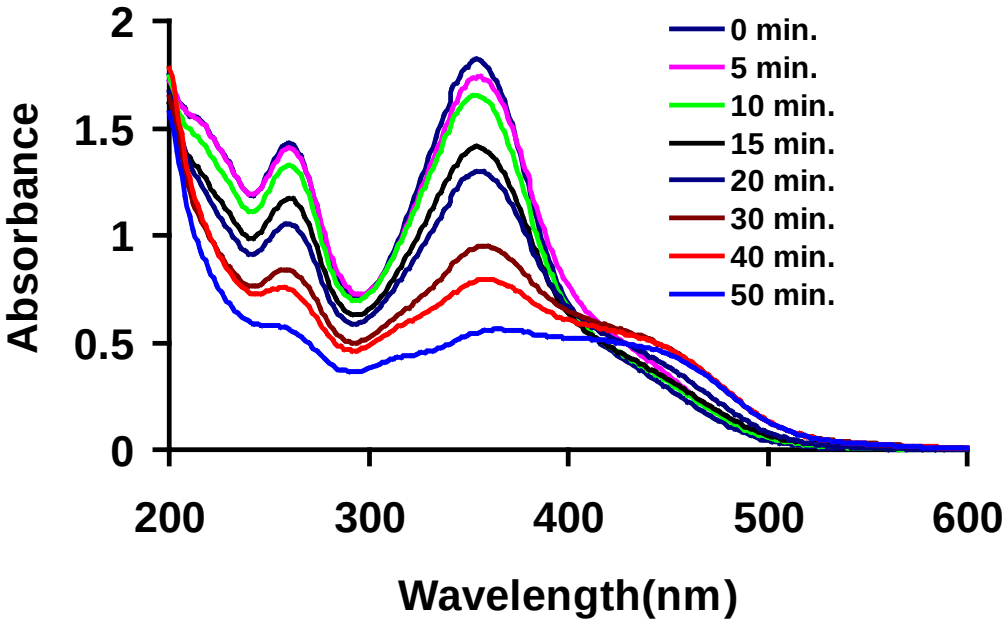

Figure 5.27 Typical UV-Visible spectra showing the change in absorption intensity as a function of laser exposure time for an aqueous solution of Alizarin Yellow GG in presence of nano ZnO

k, K, kc and kapp are the rate constant, the equilibrium adsorption constant, the kinetic rate constant of surface reaction and the apparent pseudo-first order rate constant respectively. The author used micro ZnO for photocatalytic degradation of phenol and observed that 70 % degradation of phenol was achieved within one hour of irradiation.

Dutta and Chakrabarti [210] proposed a rate equation based on Langmuir–Hinshelwood model for photocatalytic degradation of two textile dyes in wastewater using ZnO as catalyst. The reported values of Langmuir–Hinshelwood equation constants of Methylene Blue and Eosin Y are 0.0345 and 0.0859 (mg $L^{-1})^{-1}$, respectively. A plot of 1/kapp versus initial dye concentration is presented in Figure 10. The adsorption equilibrium constant, K = 0.0214 (mg L−1) $^{-1}$ and kinetic rate constant of surface reaction kc = 1.27 mgL^{-1} min^{-1} were determined. Photocatalytic activity of nano ZnO and ZnO were studied. The results are shown in Figure 5.27 and Figure 5.28 .These results provides a comparison between commercial micro sized ZnO oxide and modified nano-ZnO procured for this study. The observed rate constant of photocatalytic degradation of the dye by nano ZnO was 0.062 min^{-1} which is four times higher than values using microstructure ZnO. The results indicate that the data obey the Langmuir-Hinshelwood model.

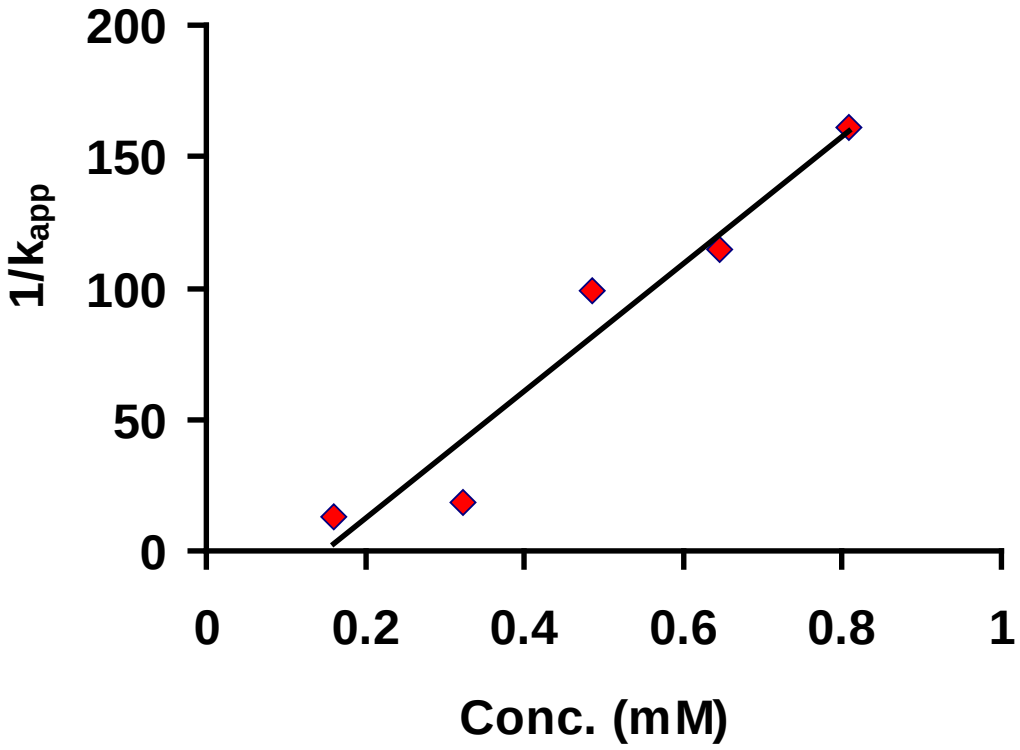

Figure 5.28 Determination of the adsorption equilibrium constant, K and the second order rate constant, kc for the Langmuir–Hinshelwood kinetic model.

5.7. Photocatalytic Degradation of Cyanosine by Nano ZnO

Preliminary photocatalytic studies were carried out by the nano ZnO containing solution in the dark. Decrease in absorbance of dye in absence of laser UV light was very slow. Presence of nano ZnO only does not catalyze the degradation of the dye. It was found that only a minor loss of the dye adsorption was observed in the absence of both NiO and laser, while better results were observed when small amount of ZnO is added to the solution in the presence of UV light.The photocatalytic degradation of cyanosine was monitored by change in absorption intensity as a function of laser irradiation time of an aqueous solution of the dye in the presence of nano-structured ZnO .It was observed that almost 94 % degradation was achieved within very short laser irradiation time using 266 nm laser irradiation. A plot of ln C_0/C vs laser exposure time was shown in Figure 5.29. The rate constant calculated from the graph was 0.124 min^{-1} which is very high as compared to bulk or conventional setup.

5.7.1. Effect of Amount of Photocatalyst

The rate of photocatalytic reaction is affected by concentration of the photocatalyst. The optimum catalyst concentration was determined to avoid excess catalyst and ensure total absorption of efficient photons. The effect of photocatalyst concentration on the photodegradation rate of the Cyanosine was studied by employing different concentrations of ZnO ranging from 1.0 g L^{-1} to 6.0 g L^{-1}.

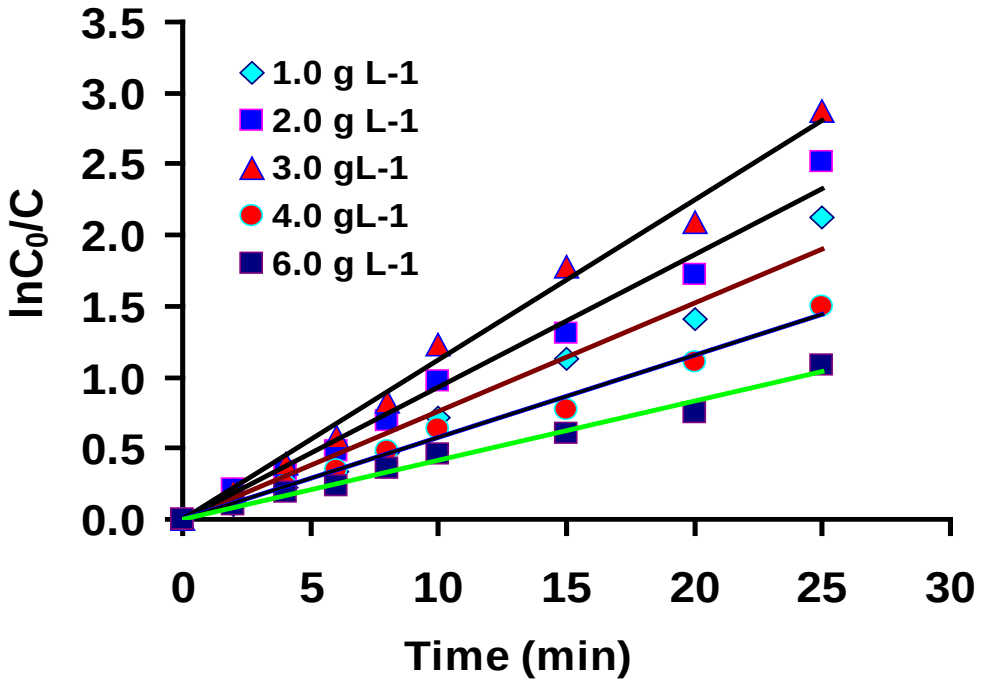

Figure 5.29 Effect of catalyst concentration on photocatalytic degradation of Cyanosine as a function of laser irradiation time for nano ZnO

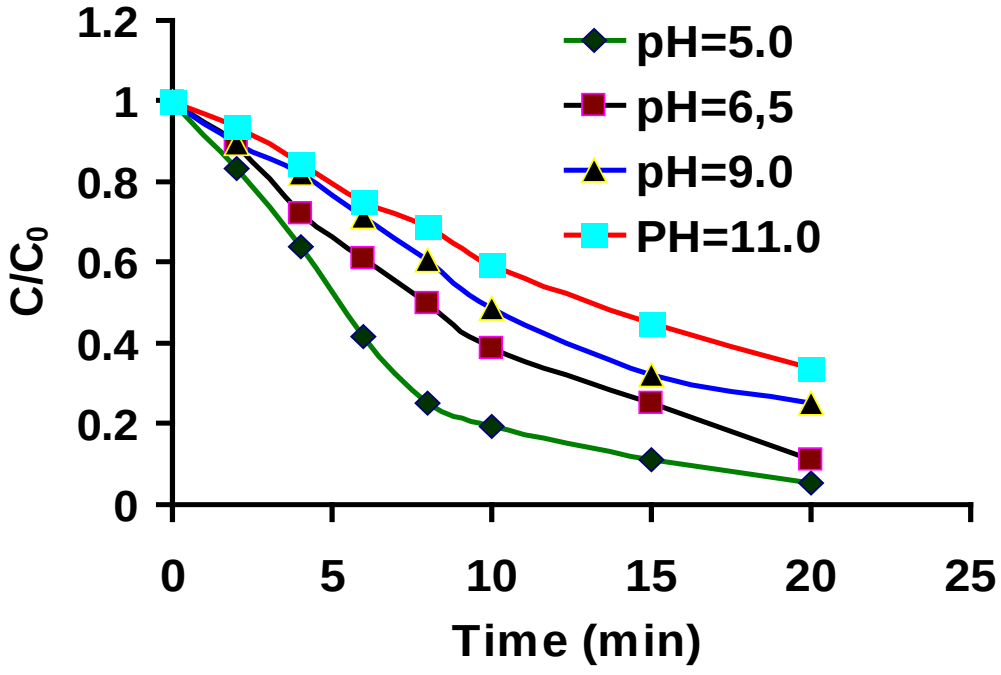

Figure 5.30 Effect of pH on photocatalytic degradation of Cyanosine as a function of laser irradiation time for nano ZnO

Figure 5.29 represents the amount of ZnO vs. rate constant graph for the photocatalytic degradation of 1.2×10^{-4} M cyanosine. A small but significant increase in the rate of the degradation observed with an increase in the catalyst weight up to an optimum loading. The optimum amount of catalyst loading was found to be in the range of 1.0–3.0 g L^{-1}. Further increase in the catalyst amount resulted in the decrease of the reaction rate. But at the catalyst weight above optimum loading there is a decrease in UV light penetration due to screening effect of excess catalyst particle in the solution.

The increase in the amount of catalyst increases the number of active sites on the NiO surface which in turn increases the number of $^{\bullet}OH$ and $O_2^{\cdot-}$ radicals. Although the rate constant increases with increasing the amount of catalyst from 1.0 to 3.0 1.0 gL^{-1} but the reasonable rate of photocatalytic degradation of the dye was achieved with 1.0 gL^{-1}. Due to this reason, 1.0 $gL^{-1}$was used for further studies.

5.7.2. Effect of Solution pH

The role of pH on the rate of photocatalytic degradation of cyanosine was studied in the pH range 5.0–11.0 at the dye conc. (1.2×10^{-4}M) was studied. The photocatalytic degradation of Cyanosine was studied at different pH values as it is an important parameter for reaction taking place on the particulate surface. The role of pH on the rate of photocatalytic degradation of cyanosine was studied in the pH range 5.0–11.0 at the dye conc (1.2×10^{-4}M) was studied. The results are represented in Figure 5.30.

The zero point charge (zpc) is 8.9 for ZnO. Because the anionic dye molecule is negatively charged, so low pH favors adsorption on the catalyst surface [211]. The degradation of the dye increases with the increase in adsorption.

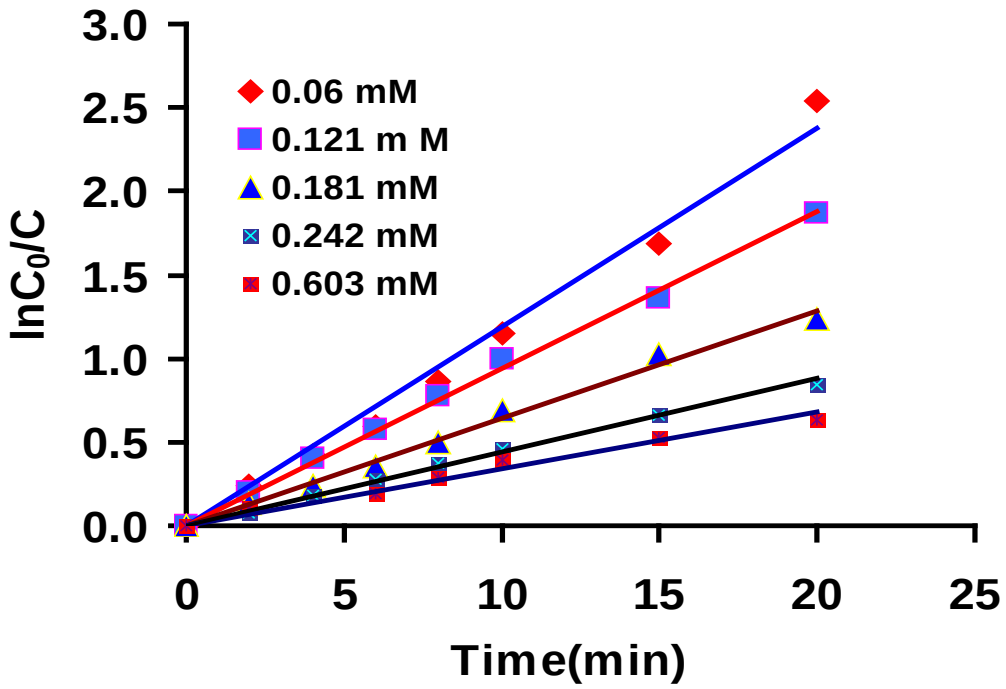

Figure 5.31 Effect of initial dye conc. on photocatalytic degradation of Cyanosine as a function of laser irradiation time for nano ZnO

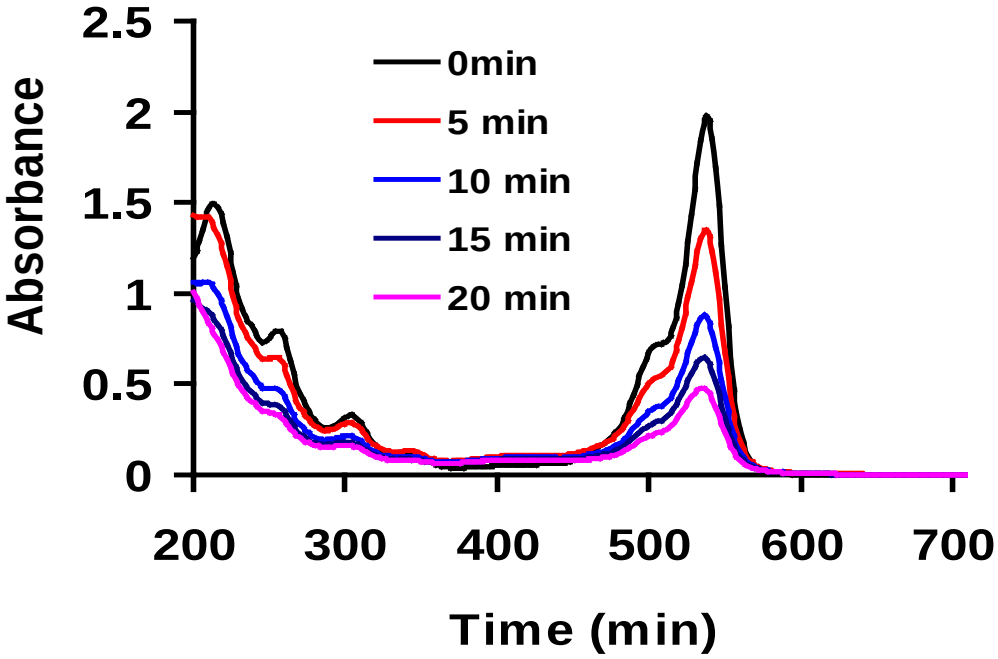

Figure 5.32 Typical UV-Visible spectra showing the change in absorption intensity as a function of laser exposure time for an aqueous solution of Cyanosine in presence of nano ZnO

The photocatalytic decomposition of the dye using NiO was favored to occur in acidic conditions and exhibited a minimum decomposition rate in more alkaline solutions (at pH= 11.0). The results indicate that the adsorption of the on catalyst surface is preferred at lower pH, and thus promotes the photocatalytic reaction.

5.7.3. Effect of Initial Dye Concentration

The photocatalytic degradation of different concentrations of cyanosine has been investigated in aqueous suspension of ZnO as a function of irradiation time. The results obtained are depicted in Figure 5.31. The rate of photodegradation of cyanosine dye was studied by varying the substrate concentrations from 6.0×10^{-5} M to 3.0×10^{-3} M. The experiment was carried out at initial pH=7.5 and catalyst concentration = 3.0 g L^{-1}. It was found that the photocatalytic degradation of cyanosine over ZnO obey apparently the first-order kinetics model, when the initial dye concentration was less than 1.2×10^{-4} M.

5.7.4. Kinetics of Photocatalytic Degradation Process

The photocatalytic degradation of different concentrations of cyanosine has been investigated in aqueous suspension of ZnO as a function of irradiation time Figure 5.32. The rate of photodegradation of cyanosine dye was studied by varying the substrate concentrations from 6.0×10^{-5} M to 3.0×10^{-3} M. The experiment was carried out at initial pH=7.5 and catalyst concentration =1.0 g L^{-1}. The influence of initial dye concentration on the photocatalytic rate and apparent rate constant was also investigated, as shown in Figure 5.31. It is known that the Langmuir–Hinshelwood model is usually used to express the degradation rate descriptions in terms of the removal of compounds or the formation

of CO_2. It was found that the photocatalytic degradation of cyanosine over ZnO was apparently the first-order kinetics model, when the initial dye concentration was less than 1.2×10^{-4} M.

It was noted that when the initial dye concentration was $>1.2\times10^{-4}$ M, the first order kinetics relationship was not pronounced.This can be explained by the fact that higher initial dye concentrations increase the percentage of UV photons absorbed by the dye molecules rather than by photocatalyst particles resulting in lower catalyst efficiency.

According to the Langmuir–Hinshelwood model, which ignores the effect of the intermediate product, the photocatalytic reaction rate (r) can be expressed briefly as:

$$\text{rate} = -dC/dt = K_r K_a C_0 /(1 + K_a C_0) \qquad (15)$$

where K_r refers to the apparent rate constant, K_a is the adsorption equilibrium constant and C_0 is the initial concentration. If $K_a C_0 \leq 1$, this expression can be further simplified to:

$$\text{rate} = K_r K_a C_0 \qquad (16)$$

This simplified expression suggests that the first-order kinetics will become not important when the initial concentration was high. On the other hand, apparent rate constant (k) was determined to be 0.16 min^{-1}, 0.124 min^{-1}, 0.098 min^{-1}, 0.06 min^{-1} and 0.046 min^{-1} for initial concentrations of dye concentration of 6.0×10^{-5} M, 1.2×10^{-4} , 1.8×10^{-4}, 2.4×10^{-4} and 3.0×10^{-3} M respectively. Therefore, the k value increases with the decreasing concentration. The adsorption performance and the intermediates are also parameters which will influence the kinetic performance.

Thus, the initial concentration was important to the k value of the photocatalytic n reaction. The k value can be increased through decreasing the initial dye concentration. Other authors have reported similar results [212] by using different catalysts. It is considered that if the concentration of the organic compound is relative low, the reaction

between the photo-generated hole (or hydroxyl radical $^{\bullet}OH$) and the compounds determine the whole photocatalytic process. It was found that photocatalytic degradation rate decreases from 6.0×10^{-5} M to 3.0×10^{-3} M, because for a fixed catalyst concentration active sites remaining the same, the number of substrate ions accommodated in the inter layer space increases so that the degradation decreases.

This may be due to the fact that with increase in initial concentration of the dye, more dye molecules are adsorbed on the surface of ZnO. Thus, increase in the number of substrate ions accommodating in inter layer spacing inhibit the action of catalyst, which thereby decreases the reactive $OH^{\bullet}$ and$O_2^{\bullet-}$ free radicals attacking the dye molecules and photodegradation efficiency [213].

Figure 5.33shows a typical UV-visible spectrum representing the change in absorption intensity as a function of laser exposure time for an aqueous solution of Cyanosine in the presence of ZnO. This increase in Cyanosine degradation with time could be due to the fact that with increase in the irradiation time, the number of absorbed laser photons increases, producing more amount of $OH^{\bullet}$ radicals. Hence, it facilitaties more degradation of alizarin yellow GG.The results indicate that the data obey the first order rate law kinetics.

5.8. Photocatalyic Degradation of Cyanosine by Nano NiO

NiO has better photocatalytic activity for photodegradation of Cyanosine than nano ZnO.It was also observed that NiO performance is better for the removal of phenol. Preliminary photocatalytic studies were carried out by the NiO containing solution in the dark. Decrease in absorbance of dye in absence of laser UV light was very slow. Presence

of NiO only does not catalyze the degradation of the dye. It was found that only a minor loss of the dye adsorption was observed in the absence of both NiO and laser, while better results were observed when small amount of NiO is added to the solution in the presence of UV light.

5.8.1. Effect of Catalyst Concentration

The effect of photocatalyst concentration on the degradation kinetics of cyanosine was investigated employing different concentrations of the nano NiO varying from 1.0 to 6.0 g L^{-1} Figure 5.33. Photodegradation of cyanosine increases rapidly with increasing the amount of NiO from 1.0 g L-1 to 3.0 g L-1 for dye concentration 1.2×10^{-4}M. The increase in the amount of catalyst increases the number of active sites on the NiO surface which in turn increases the number of •OH and O_2^- radicals. It was observed that 3.0 g L-1 of NiO is the optimum dose for efficient degradation of cyanosine dye. Figure 5.5 represents the amount of NiO vs. rate constant graph for the photocatalytic degradation of 1.2×10^{-4} M cyanosine (pH 8.0).

5.8.2. Effect of pH

The photocatalytic degradation of Cyanosine was studied at different pH values as it is an important parameter for reaction taking place on the particulate surface. The role of pH on the rate of photocatalytic degradation of cyanosine was studied in the pH range 5.0–11.0 at dye conc was studied. The results are shown in Figure 5.34. It was observed that the degradation rate increased with an increase in pH. Similar results were reported earlier for the acid blue 40 dye degradation [245].

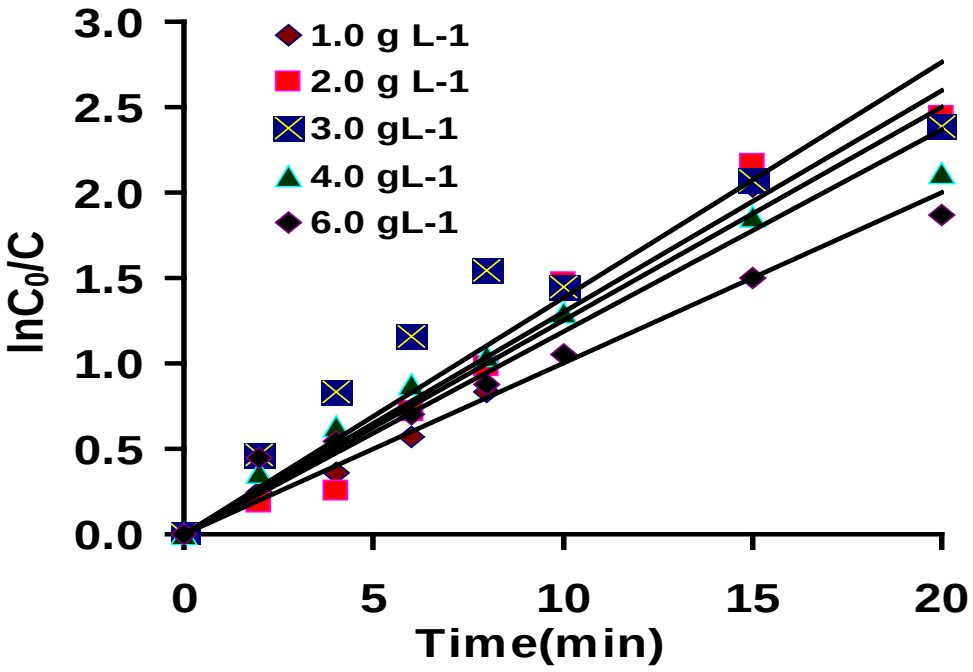

Figure 5.33 Effect of catalyst concentration on photocatalytic degradation of Cyanosine as a function of laser irradiation time for nano NiO

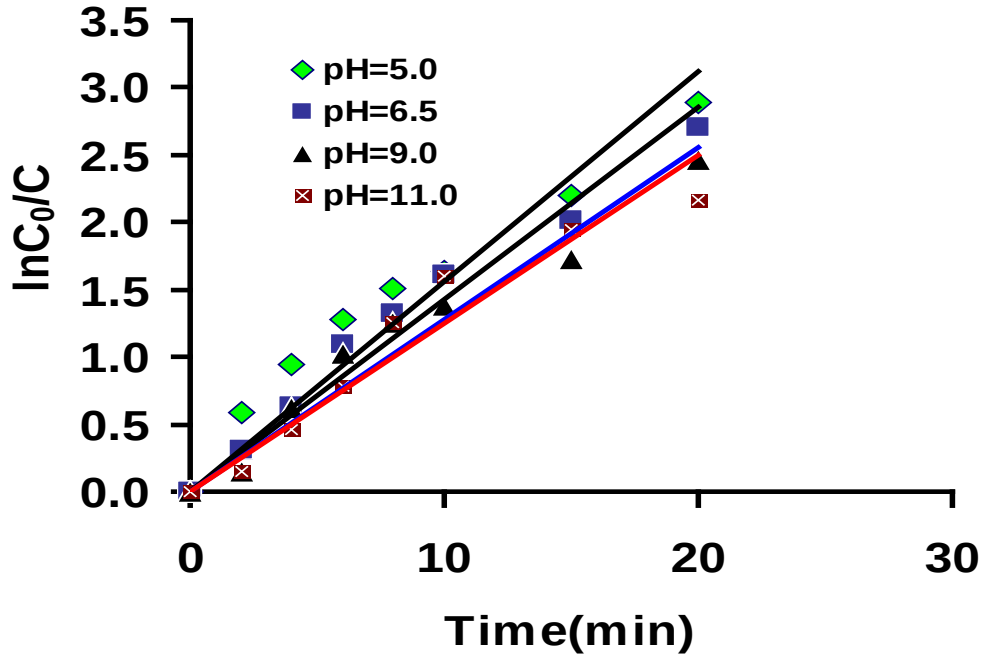

Figure 5.34 Effect of pH on photocatalytic degradation of Cyanosine as a function of laser irradiation time for nano NiO

This effect may be attributed to more efficient generation of hydroxyl radicals by NiO with an increasing concentration of hydroxide ion.It is apparent that the rate of degradation of cyanosine with increase in the pH values upto 11.0 and beyond this the rate of photodegradation becomes constant. This may be due to the fact that as the pH increases onwards 11.0 the repulsion of the dye anion by negatively charged NiO surface would result in reduction in efficiency of photodegradation of cyanosine dye.

5.8.3. Effect of Substrate Concentration

The photocatalytic degradation of different concentrations of cyanosine has been investigated in aqueous suspension of NiO as a function of irradiation time Figure 5.35. The rate of photodegradation of cyanosine dye was studied by varying the substrate concentrations from 6.0×10^{-5} M to 3.0×10^{-3} M. The experiment was carried out at fixed pH 8 and catalyst concentration 3.0 g L^{-1}. It was found that photocatalytic degradation decreases from 6.0×10^{-5} M to 3.0×10^{-3} M.

5.8.4. Kinetics of Photocatalytic Degradation of Cyanosine using Nano NiO

The photocatalytic degradation of different concentrations of cyanosine has been investigated in aqueous suspension of NiO as a function of irradiation time Figure 5.35. The rate of photodegradation of cyanosine dye was studied by varying the substrate concentrations from 6.0×10^{-5} M to 3.0×10^{-3} M. It was found that the photocatalytic degradation of cyanosine over NiO was apparently the first-order kinetics. According to the Langmuir–Hinshelwood model, the photocatalytic reaction rate (r) can be expressed briefly as:

$$\text{rate} = -dC/dt = K_r K_a C_0 /(1 + K_a C_0) = K_r K_a C_0 \qquad (17)$$

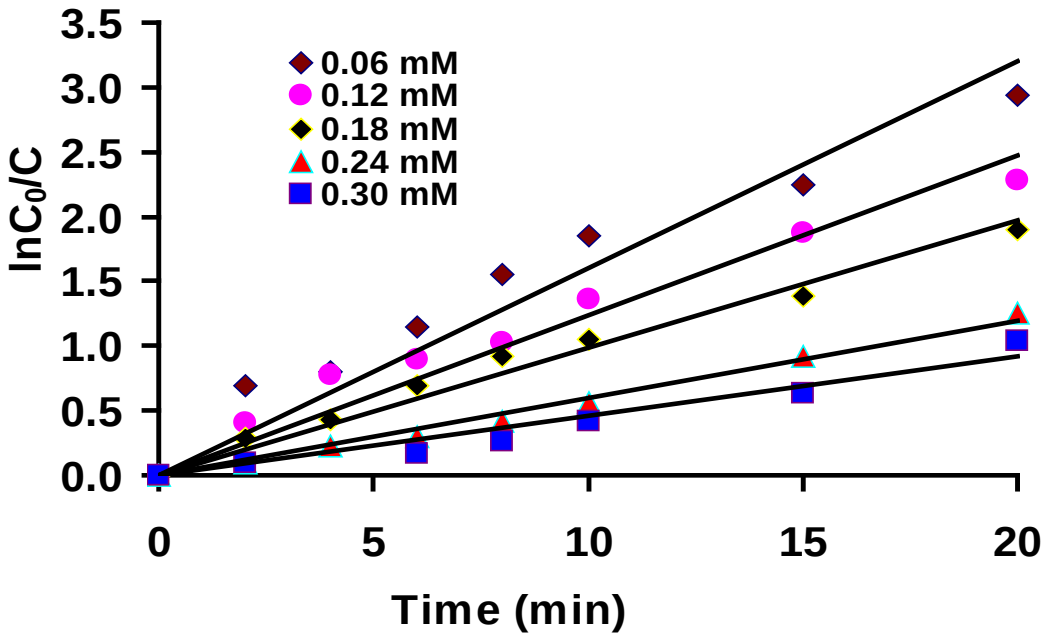

Figure 5.35 Effect of initial dye conc. on photocatalytic degradation of Cyanosine as a function of laser irradiation time for nano NiO

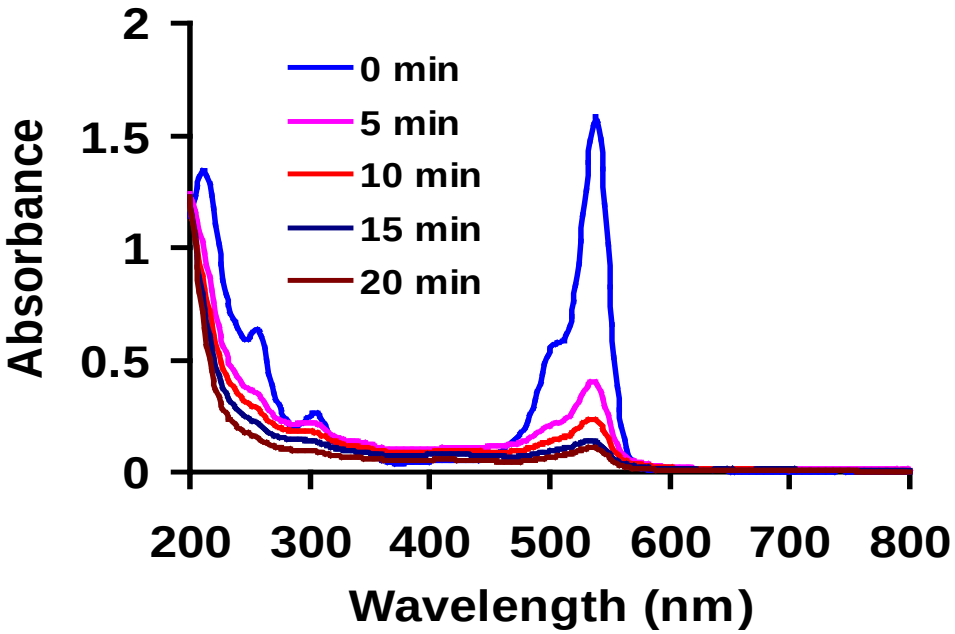

Figure 5.36 Change in absorption intensity as a function of laser exposure time for an aqueous solution of Cyanosine in presence of nano NiO

The apparent rate constant (k) was determined to be 0.16 min^{-1}, 0.124 min^{-1}, 0.098 min^{-1}, 0.06 min^{-1} and 0.046 min^{-1} for initial concentrations of dye concentration of 6.0×10^{-5} M, 1.2×10^{-4} , 1.8×10^{-4}, 2.4×10^{-4} and 3.0×10^{-3} M respectively. Therefore, the k value increases with the decreasing concentration. It was found that photocatalytic degradation rate decreases from 6.0×10^{-5} M to 3.0×10^{-3} M, because for a fixed catalyst concentration active sites remaining the same, the number of substrate ions accommodated in the inter layer space increases so that the degradation decreases. This may be due to the fact that with increase in initial concentration of the dye, more dye molecules are adsorbed on the surface of NiO. Thus, increase in the number of substrate ions accommodating in inter layer spacing inhibit the action of catalyst, which thereby decreases the reactive $OH^{\bullet}$ and $O_2^{\bullet-}$ free radicals attacking the dye molecules and photodegradation efficiency.

CHAPTER 6

LASER INDUCED PHOTOCATALYTIC DEGRADATION OF PHENOL IN AQUEOUS SUSPENSIONS OF PURE ZnO AND NiO

In industry and daily life, phenolic compounds are widely used. The use of phenol and phenolic compounds in industrial processes and their presence in the resulting wastewaters is an issue of environmental concern. Their high toxicity, even at low concentrations, has motivated the search and improvement of many treatment techniques. In this sense, photocatalysis can yield feasible, convenient methods for the treatment of phenolic wastewaters. As they have high stability, high toxicity and a carcinogenic character, they have caused considerable damage and threat to the ecosystem in water bodies and human health. To eliminate phenolics in wastewater effectively is an urgent demand. The phenolic compounds are usually used as the basic industrial, commercial and medical raw materials and thus are common pollutants found in industrial wastewaters. Since phenolic compounds contain the OH group, they are more soluble in water than other organic pollutants that do not contain the OH group. Hence, phenolic compounds are more capable of moving and transforming in the environment to cause added serious environmental problems and adverse impact.

The results related to photocatalytic degradation of phenol using different photocatalysts synthesized in our own laboratotory are presented in this chapter.

6.1. Photocatalytic Degradation of Phenol by Nano ZnO

The photocatalytic degradation of phenol was studied using nano ZnO synthesized by sol gel method.The aqueous suspension of ZnO containing phenol was irradiated at 266 nm.The concentration of the pollutant remaining after time t was calculated using the peak area method after analyzing on HPLC.It was observed that almost 90% degradation was achieved within one hour. Photocatalytic studies are carried out by the nano ZnO containing solution in the dark. Decrease in concentration of phenol in absence of laser UV light was not significant. Presence of nano ZnO only does not catalyze the degradation of the dye. It was found that only a minor loss of phenol adsorption was observed in the absence of both ZnO and laser, while almost 86 % degradation was achieved within very short time when small amount of ZnO is added to the solution in the presence of UV light.

6.1.1. Effect of Calcination Temperature on Photocatalytic Activity of Nano ZnO

Photocatalytic efficiency of ZnO depends upon morphology and particle size. The photocatalytic activity of ZnO catalysts obtained by modified sol–gel method at different calcination temperature was evaluated for the photo degradation of phenol under UV laser irradiation.

The effect of calcination temperature on the photocatalytic degradation of phenol is also investigated. Plot of ln C_0/C vs laser exposure time for the catalysts is depicted in Figure

6.1 (Experimental conditions: laser energy=50 mJ (266nm), laser exposure time= 60 min., amount of catalyst=2.5 g-L^{-1} and phenol conc.=1.064 mM). The observed rate constants are found to be 0.028 min^{-1}, 0.0391 min^{-1}, 0.0308 min^{-1}, 0.0224 $min^{-1}$and 0.0195 min^{-1} corresponding to the photocatalysts nano ZnO-400, nano ZnO-500, nano ZnO-550, nano ZnO-600 and nano ZnO-700.The results reveal that the photocatalytic efficiency decreases with increasing calcination temperature from 400 °C to 500 °C and then the degradation rate decreases with further increase in calcination temperature as is clear from the Figure 6.1. Nano ZnO-500 is found to be the most active catalyst for the photodecomposition of phenol under UV laser light. The deterioration of photocatalysis efficiency is attributed to particle segregation after calcination at higher temperature [215,216]. Thus, nano ZnO-500 was used as catalyst in order to optimize key parameters of the photodegradation of phenol under UV light.

6.1.2. Effect of Catalyst Concentration on Photocatalytic Degrdation of Phenol using Nano ZnO

In order to avoid an ineffective excess of catalyst and to ensure a total absorption of efficient photons, the optimum mass of catalyst needs to be found.The effect of photocatalyst concentration on the photodegradation rate of the Phenol was studied by employing different concentrations of ZnO ranging from 0.8 g L^{-1} to 5.0 g L^{-1}. The photocatalytic degradation rate of the phenol was found to increase and then decrease with the increase in the catalyst concentration. The results are shown in Figure 6.2.

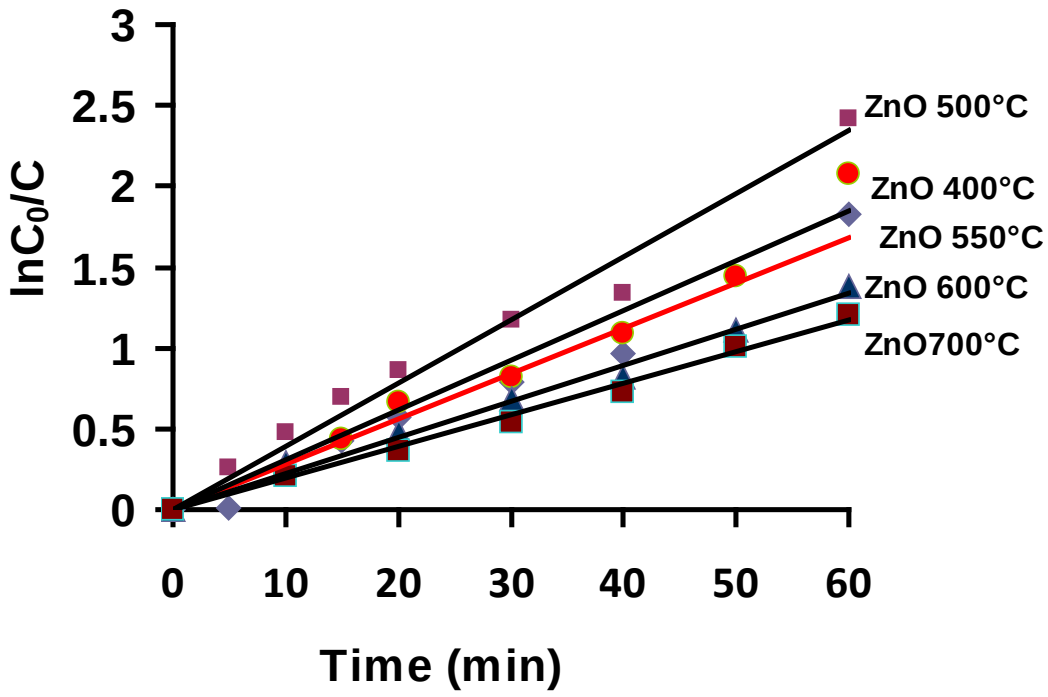

Figure 6.1 Effect of calcination temperature on photocatalytic degradation of phenol as a function of laser irradiation time for nano ZnO

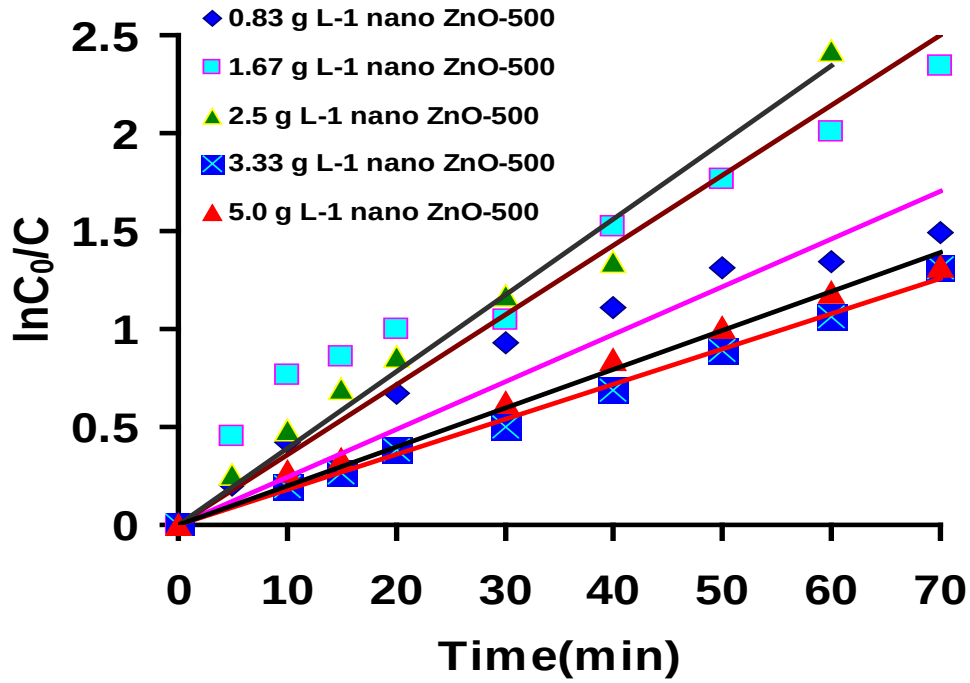

Figure 6.2 Effect of catalyst concentration on photocatalytic degradation of phenol as a function of laser irradiation time for nano ZnO

This is a general characteristic of heterogeneous photocatalysts and our results are in agreement with earlier reports [217]. It was observed that the initial rate of phenol degradation is not affected further by a progressive increase in ZnO concentration above 0.5 g L^{-1} of ZnO. This phenomenon may be due to the aggregation of ZnO particles at high concentrations, causing a decrease in the number of surface active sites. However, it is known that there exists a practical limit of the scattering light above which the degradation rate will decrease due to the reduction of the photonic flux within the irradiated solution.The photodegradation rate was found to increase with the increase in mass of catalyst up to an amount of 3.0 g L^{-1}, as shown in Table VIII .This behavior could be associated to an increment of the active sites available for phenol adsorption and degradation.

However, an increase on the catalyst loading to 6.0 g L^{-1} resulted in a decrease in the rate constant, which can be attributed to a screening effect due to the redundant dispersion of UV radiation caused by the substantial amount of suspended photocatalyst.Furthermore, in these conditions, particles tend to agglomerate, making a significant fraction of the catalyst to be inaccessible to either adsorbing the molecules or absorbing the radiation, with consequent decrease in the active sites available to the catalytic reaction. Following these observations, it was decided to keep the amount of nano ZnO at the optimum value of 3.0 g L^{-1} in subsequent photocatalytic degradation experiments.

Table VIII Effect of experimental parameters on photodegradation rate of phenol using nano ZnO-500

Parameters.	k(min^{-1})	r^2	Photodegradation rate(μM-min^{-1})
Amount of catalyst(g L^{-1})	—	—	—
0.83	0.0224	0.9124	23.83
1.67	0.0357	0.8994	37.98
2.5	0.0391	0.9789	41.60
3.33	0.018	0.9957	19.15
5.0	0.0198	0.9900	21.07
Solution pH	—	—	—
5.0	0.0697	0.9817	74.16
6.5	0.0398	0.9743	42.35
9.0	0.0286	0.9845	30.43
11.0	0.0079	0.9573	8.41

[a] Nano ZnO (C) represents the commercial nano ZnO
[b] Nano ZnO(ppt) designate the sample synthesized by precipitation method
[c] Nano ZnO-400, Nano ZnO-500, Nano ZnO-550, Nano ZnO-600 and Nano ZnO-700 represents the photocatalysts synthesized at calcination temperatures ranging from 400-700°C

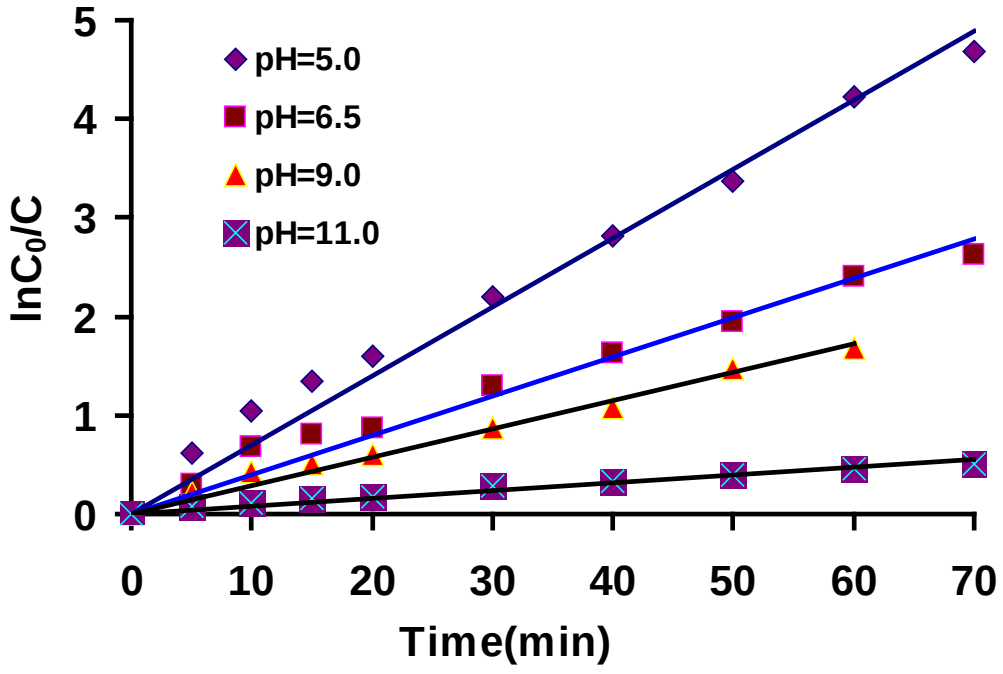

Figure 6.3 Effect of pH on photocatalytic degradation of phenol as a function of laser irradiation time for nano ZnO

6.1.3. Effect of pH on Photocatalytic Degrdation of Phenol using Nano ZnO

The pH of the suspensions was varied in order to study its effect in the photocatalytic degradation of phenol. Reactions were performed at different pH values using ZnO as a photocatalyst. The role of pH in the photodegradation of phenol was studied in the pH range of 5.0–11.0 at a 1.064 mM of phenol concentration and 3.0 g L^{-1} catalyst loading. First order kinetic rate constants were found to be of 3.98 $\times 10^{-2}$ min^{-1} and 6.97$\times 10^{-2}$ min^{-1} at pH =7.0 and pH= 5.0 respectively.

The photocatalytic degradation of phenol depended on the initial pH of the solution used in the reaction as shown in Figure 6.3. Nano ZnO showed amphoteric behavior in aqueous media. The zero point charge for ZnO is 8.9, and above this value, the ZnO surface is predominantly negatively charged when the pH is higher than the ZnO isoelectric point. Thus, the electrical property of the ZnO surface varies with the pH of the dispersion [218]. At pH higher than pHpzc nano ZnO surface is negatively charged and ZnO^- appears to be the predominant form. For lower pH values, nano ZnO surface is in the protonated form ($ZnOH^{2+}$). Electric charge properties of both, catalyst and substrate, are found to play an important role on adsorption process. Under aqueous media, phenol shows a pKa of 9.9 (at 25 ◦C), which means that for pH<pKa, it is in the molecular form (C_6H_5OH) and at pH> pKa the molecule undergoes deprotonation becoming negatively charged ($C_6H_5O^-$).

However, at pH 11.0 the photoefficiency of the process decreases and phenol removal becomes very slow, with a k of 7.90$\times 10^{-3}$ min^{-1}. Under these conditions, both catalyst and substrate are negatively charged, developing repulsive forces between them, thus decreasing substrate adsorption.

6.1.4. Comparison of Photocatalytic Efficiency of Different ZnO Catalysts for Phenol Degradation

Comparative study of photocatalytic activity of Micro ZnO, nano ZnO (Commercial), nano ZnO (ppt) and nano ZnO-500 was investigated .The results obtained are depicted in Figure 6.4. It is evident from photodegradation rates shown in table1 that the nano ZnO prepared by modified sol gel method calcined at 500 ºC showed the best efficiency for phenol degradation as compared to the photocatalytic efficiency of nano ZnO synthesized by precipitation method and other photocatalysts used in this study. Both of the catalysts synthesized in our laboratory has almost 4 to 5 fold photocatalytic activity than either nano ZnO (commercial) or micron size ZnO.

The results depicted in Table IX could be correlated with the particle size and homogeneity of the ZnO. Studies performed with different ZnO powders that presented different morphologies indicated that particle size as well as the crystallinity played the key role. It was reported that complete disappearance of phenol (more than 95% of conversion) was observed in about 6 h of UV irradiation for neat TiO_2. Similar results are obtained by using commercially available TiO_2 P25 under the same reaction condition [219]

The ZnO powder having smaller size and more uniform particles has better activity than the bigger, non uniform counterpart. The photodegradation efficiency was enhanced because the amount of the dispersion particles per volume in the solution increases with the decrease in the size of ZnO particles.

Table IX Comparison of photocatalytic activity of different catalysts for degradation of phenol

S.No.	Photocatalyst	k(min^{-1})	r^2	Photodegradation rate(μM-min^{-1})
1	—	0.0018	0.6740	1.915
2	Micro ZnO	0.0063	0.9141	6.703
3	Nano ZnO(C)[a]	0.0098	0.9666	10.43
4	Nano ZnO(ppt)[b]	0.0240	0.9859	25.54
5	Nano ZnO-500[c]	0.0391	0.9789	41.60
6	Nano ZnO-400 [c]	0.028	0.9742	29.79
7	Nano ZnO-550 [c]	0.0308	0.9691	32.77
8	Nano ZnO-600 [c]	0.0224	0.9905	23.84
9	Nano ZnO-70 0 [c]	0.0195	0.9933	20.75

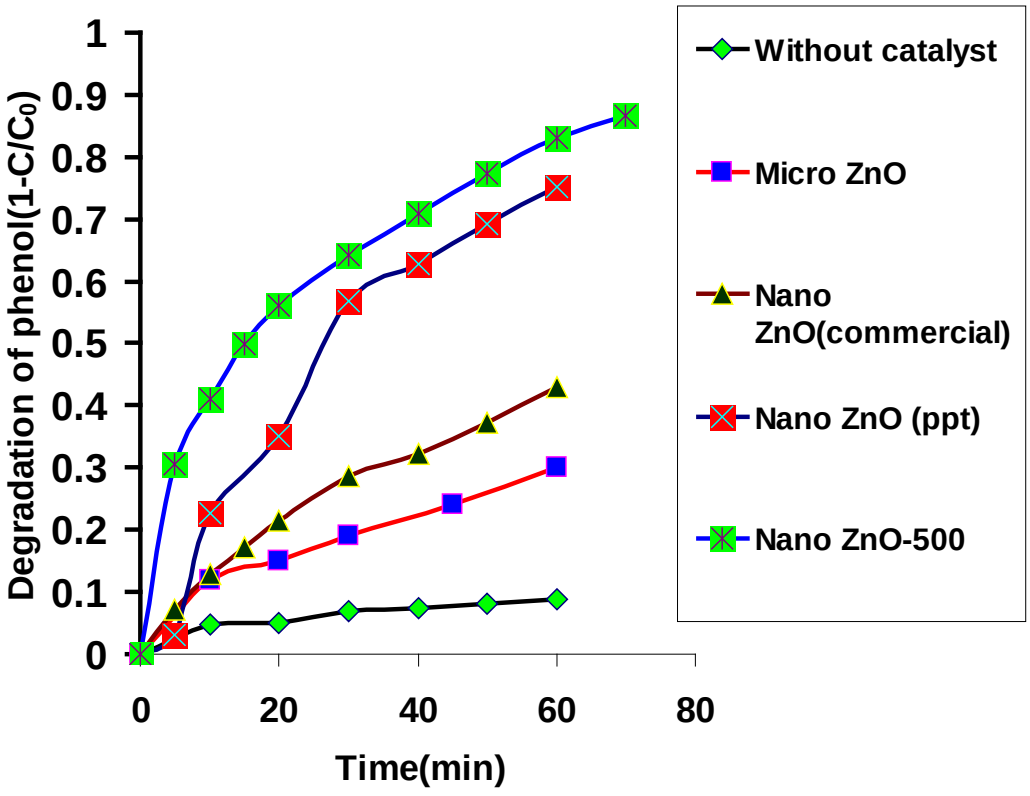

Figure 6.4 Photodegradation of phenol using different ZnO catalysts

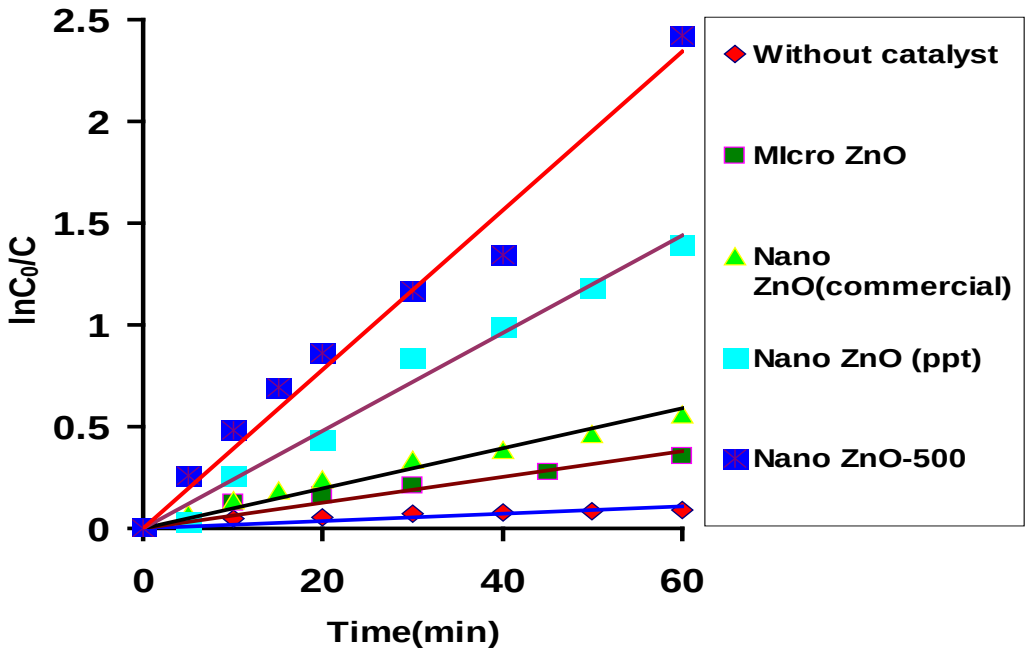

Figure 6.5 Comparison of photocatalytic activity of ZnO catalysts for degradation of phenol

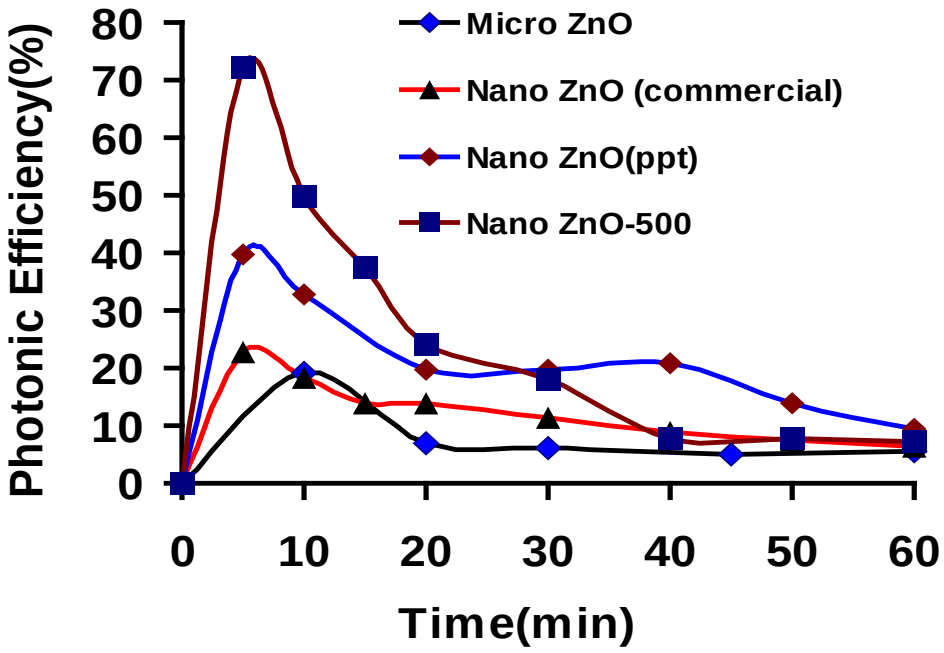

Figure 6.6 Photonic efficiency of different ZnO Photocatalysts

The electron-hole recombination was also suppressed. Furthermore, the surface area of ZnO photocatalyst was increased which increased the adsorption of more dye molecules on the surface.

In this study, we estimated the photonic efficiency (PE) for the photo-degradation of phenol using four catalysts. The plots of PE as a function of laser exposure time for phenol removal for all four catalyst are depicted in Figure 6.6 For all the catalysts, the photonic efficiency initially increases and then decreases. This is due to the fact that initially more OH radicals are produced but with the rise in laser irradiation time recombination process increases [220,221] due to which the absorbed photons are not able to generate desired products and triggers the decrease in photonic efficiency.

Maximum photonic efficiency was recorded for WO_3 catalyst. This is due to the suitability of band-gap of WO_3 with the applied laser wavelength (355 nm) which initially supports to enhance the degradation process and with the rise in laser irradiation time the recombination process decreases the photonic efficiency.

6.1.5. Effect of Concentration on Photocatalytic Degradation of Phenol using Nano ZnO

The initial phenol concentration was varied from 50 mg L^{-1} to 250 mg L^{-1} . Results showed that for this range of concentrations the reaction rate gets slower as the initial concentration of phenol in solution increases Figure 6.7. The first-order apparent rate constant obtained for the reaction with the 100 mgL^{-1} phenol solution was of 9.32×10^{-2} min^{-1} while for the higher initial concentration 250 mgL^{-1} a k_{app} of 2.04×10^{-2} min^{-1} was obtained. As phenol concentration increases, more reactant and reaction

intermediates are adsorbed on the surface of the photocatalyst, therefore, the generation of hydroxyl radicals will be reduced since are only a fewer active sites for adsorption of hydroxyl anions. The dependency of the photocatalytic reaction rate on the concentration of the organic substrate has been generally well described by a Langmuir–Hinshelwood kinetic model.

6.1.6. Kinetics of Phenol Degradation using Nano ZnO

The reaction mechanism usually considered for heterogeneous photocatalyzed reactions consist in two main steps: fast adsorption of the reactants on the catalyst surface and a slow step of reaction in the adsorbed phase of the organic compound and a photogenerated hydroxyl radical. It has been recognized that kLH and KLH are light intensity-dependent [222]. The Langmuir–Hinshelwood model is commonly used to describe the kinetics of photocatalytic reactions of organic compounds in aqueous solutions. It relates the degradation rate r and the concentration of organic compound C, and is expressed as follows:

$$\text{rate} = -dC/dt = krKadC/1 + KadC = k_{app}C \qquad (18)$$

where k_r is the intrinsic rate constant and K_{ad} is the adsorption equilibrium constant. When the adsorption is relatively weak and the concentration of organic compounds is low, the factor KadC is insignificant, and the equation can be simplified to the first-order kinetics with an apparent rate constant ($Kapp = k_rK_{ad}$), which gives

$$\ln C_0/C = K_{app}\, t \qquad (19)$$

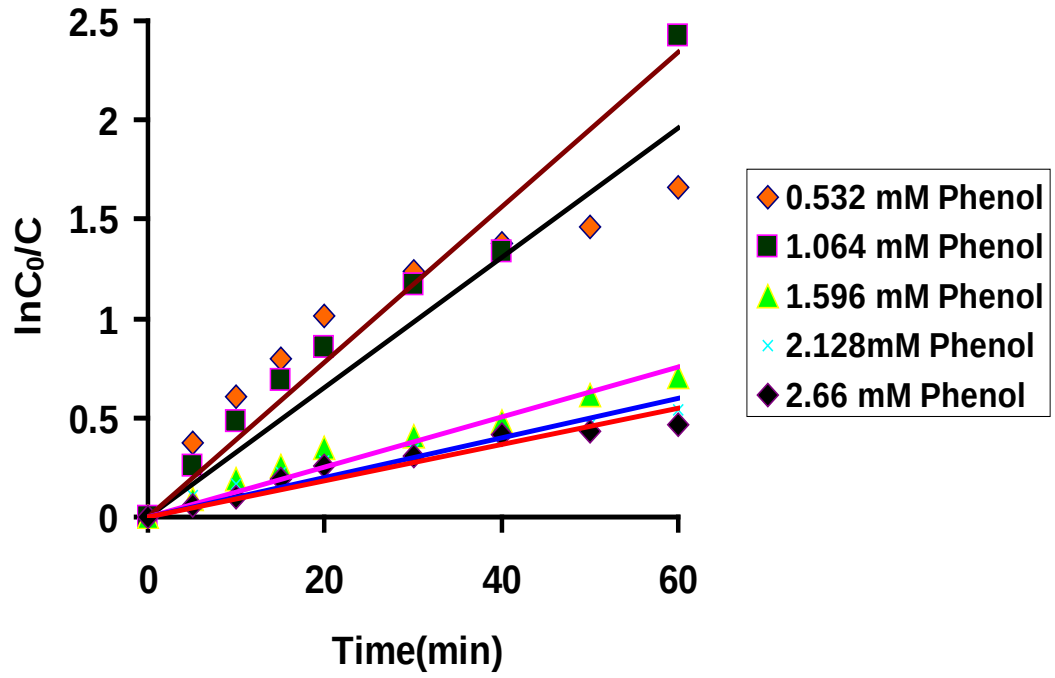

Figure 6.7 Effect of phenol concentration on photocatalytic degradation of phenol as a function of laser irradiation time for nano ZnO

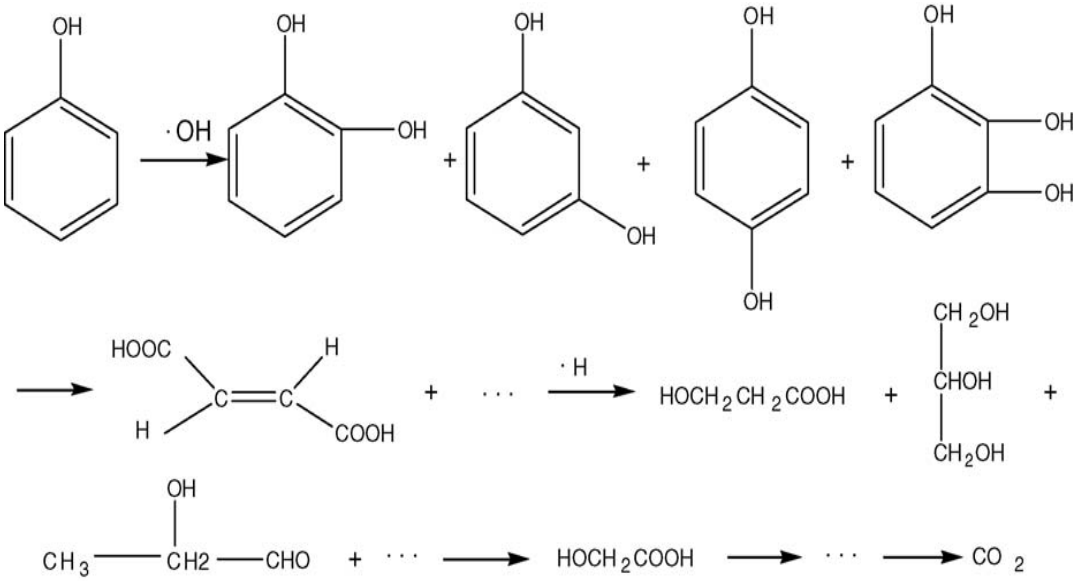

Figure 6.8 Proposed mechanism for degradation of phenol

Plotting of ln (C_0/C) versus reaction time t yields a straight line, where the slope is the apparent rate constant. Figure shows the lineal plot of phenol photodegradation, which adjusts well to a pseudo-first-order kinetic behavior.

As photon flow increases, the number of photogenerated $HO^{\bullet}$ radicals rise up accelerating the oxidation of the substrate molecules. Simultaneously, the increase of surface active species such as electrons, holes and $HO^{\bullet}$ radicals lead to a decrease in the available sites for adsorption of the primary molecule and therefore a decrease in KLH. The results revealed that photocatalytic oxidation of phenol follow a pseudo-first order kinetic model.

6.1.7. Identification of Intermediates

An attempt has been made to identify the intermediates of the phenol degradation and to confirm the analyte identities. The sample drawn from the reactor during the degradation experiment has been fed into the HPLC and gas chromatograph/mass spectrometer (GC/MS). Initially the phenol photodegradation proceeds with the formation of reaction intermediates that are subsequently converted to CO_2, H_2O and HCI. Four significant intermediate compounds such as benzoquinone, hydroquinone, catechol and (E)-2-butenedioic acid have been identified through HPLC and GC /MS analysis from the reaction medium sampled at the beginning of the degradation experiment. As the laser irradiation time increases, a decrease in the concentration of these intermediate products was observed. The amount of intermediates remainining after time‘t’ are depicted in Table X. After 70 min of laser irradiation, they might be converted to gaseous products like CO_2, water and inorganic acids. The results are shown in Figure 6.12- Figure 6.20.

Sobezynski et al. [223] proposed a reaction mechanism to illustrate the photocatalytic procedure of decomposing phenolic compounds. Iliev, V. et. al also observed that the main intermediates of phenol degradation under ultraviolet illumination are 2-hydroxy-propaldehyde, hydroxy-acetic acid, 3-hydroxy-propyl acid, glycerol, catechol, (E)-2-butenedioic acid, resorcinol, hydroquinone and 1, 2, 3-benzenetriol. The formation of glycerol, hydroxyaldehyde and hydroxyacid showed that besides $^{\bullet}OH$, $^{\bullet}H$ is also an important active free radical in the degradation. [224]. The photocatalytic degradation of phenol is the hydroxylation of the phenyl ring the hydroxyl radicals are generated either through the combination of water molecule and valence band holes or that of adsorbed oxygen and conduction band electrons. In aqueous solutions, the holes are scavenged by surface hydroxyl groups to generate the strong oxidizing hydroxyl radical ($^{\bullet}OH$) which can promote the oxidation of organic compounds as decribed in Figure 6.8.

6.1.8. Calibration Curves of Intermediates of Phenol

The samples containing suspension of nano ZnO and phenol were irradiated by 266 nm laser.The aliquot of sample was taken after regular interval and were analyzed for the qualitative and quantitative determination of the significant intermediate products.It was observed that the main by products are benzoquinone,Hydroquinone and Catechol. The calibration curves for these intermediates were shown in Figure 6.9- Figure 6.11. A linear relation was observed by plotting a graph between peak area versus concentration. For quantitative analysis of the intermediate products, peak area method was used using the calibration curves depicted in Figure 6. 9 - Figure 6.11. . The results obtained are presented in Table X.

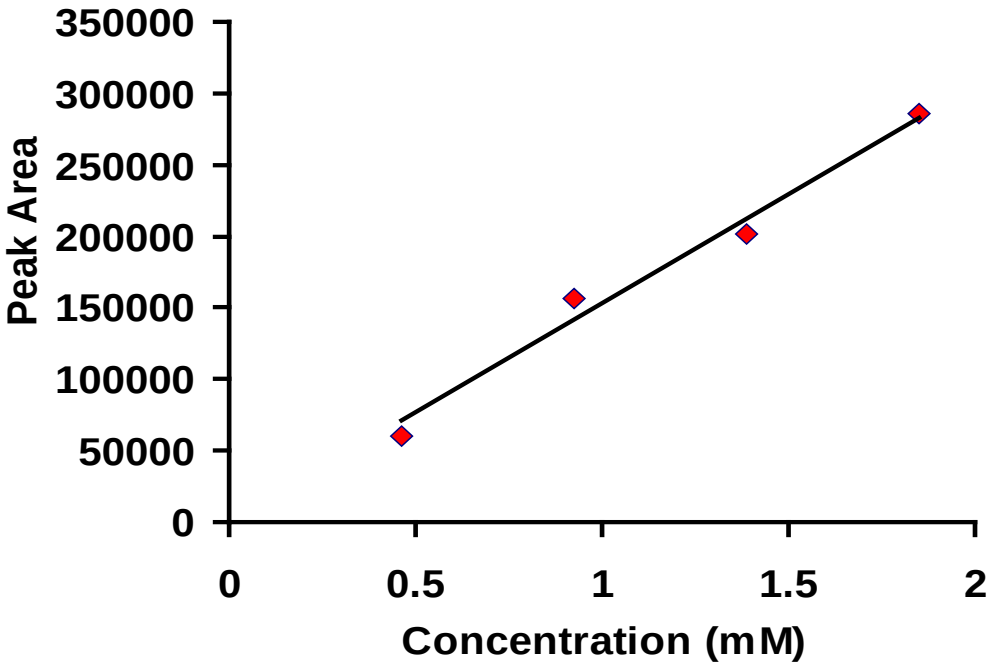

Figure 6.9 Calibration curve showing the change in peak area vs Concentration for Benzoquinone

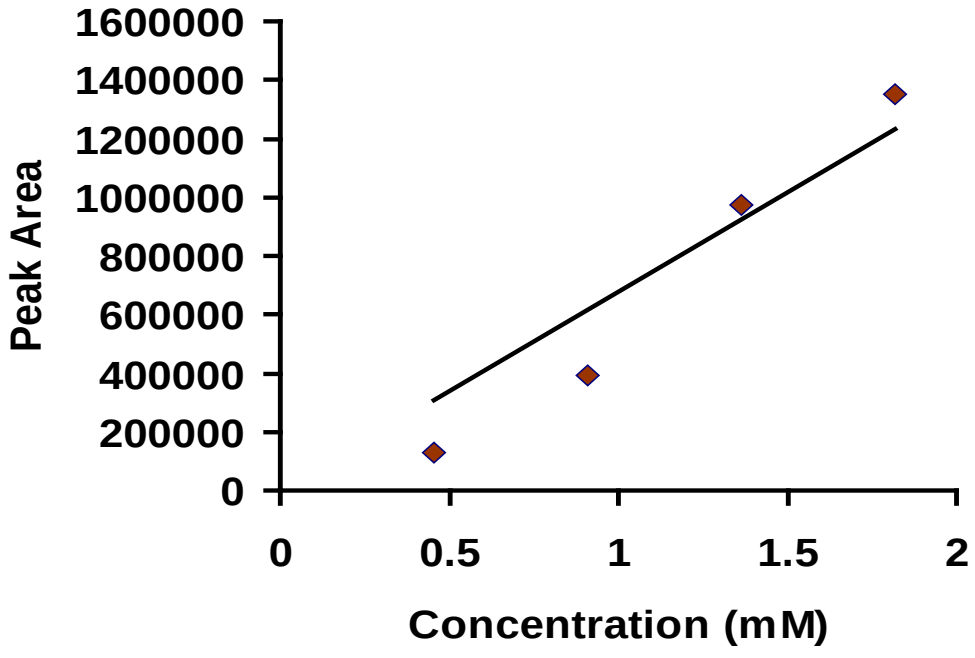

Figure 6.10 Calibration curve showing the change in peak area vs Concentration for Catechol

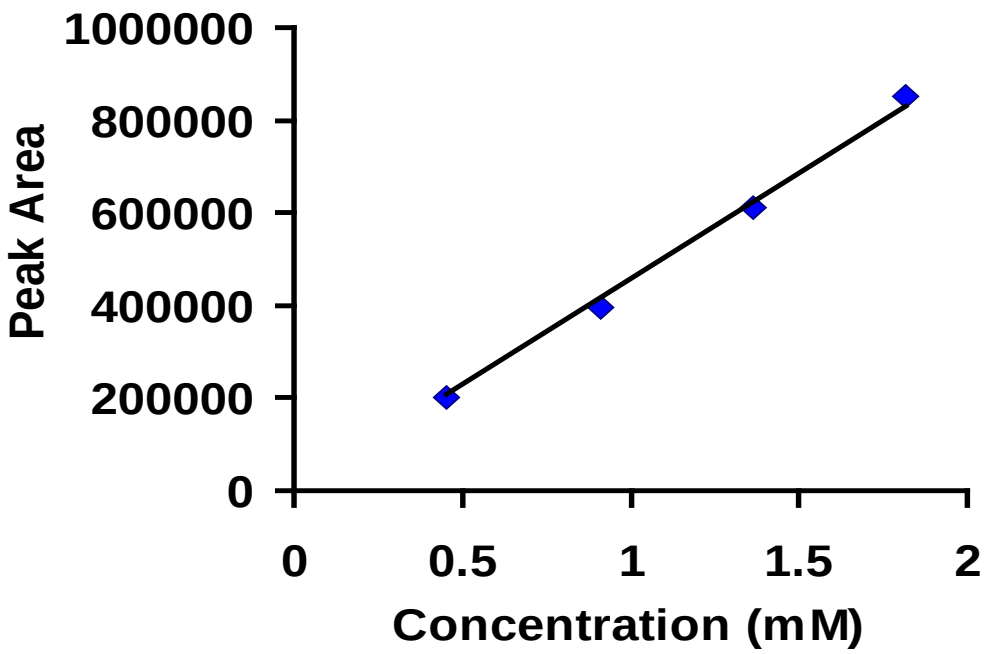

Figure 6.11 Calibration curve showing the change in peak area vs Concentration for Hydroquinone

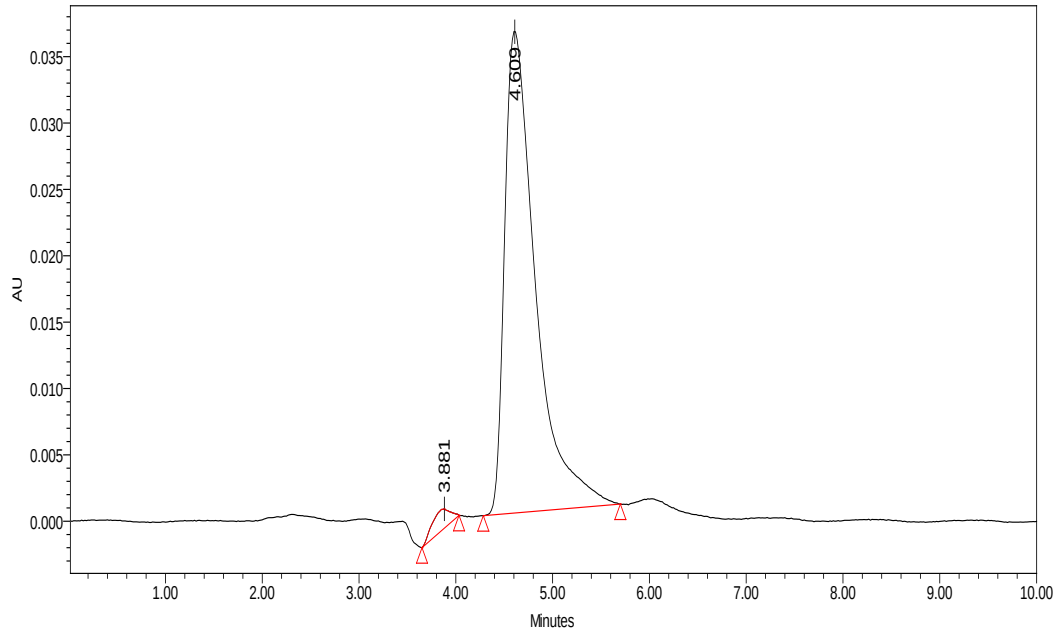

Figure 6.12 HPLC chromatogram of Phenol without laser irradiation

Table X The concentration of by-products remaining after laser irradiation

Laser irradiation time (min)	Product Name	Peak Area	Concentration(mM)
0 min	Phenol	718791	2.66
10 min	Benzoquinone	43423	0.284
	Hydroquinone	27934	0.061
	Phenol	521559	1.93
20 min	Benzoquinone	113536	0.742
	Hydroquinone	38876	0.085
	Catechol	13803	0.020
	Phenol	440583	1.63
25 min	Benzoquinone	130941	0.856
	Hydroquinone	73174	0.160
	Catechol	31754	0.047
	Phenol	422970	1.565
30 min	Benzoquinone	209894	1.373
	Hydroquinone	63813	0.139
	Catechol	35478	0.052
	Phenol	329494	1.219
40 min	Benzoquinone	135034	0.883
	Hydroquinone	46305	0.101
	Catechol	22376	0.033
	Phenol	242802	0.898
50 min	Hydroquinone	42938	0.093
	Catechol	20068	0.0296
	Phenol	154638	0.572
60 min	Benzoquinone	44978	0.294
	Phenol	86102	0.318
70 min	Benzoquinone	25221	0.165
	Phenol	65745	0.243

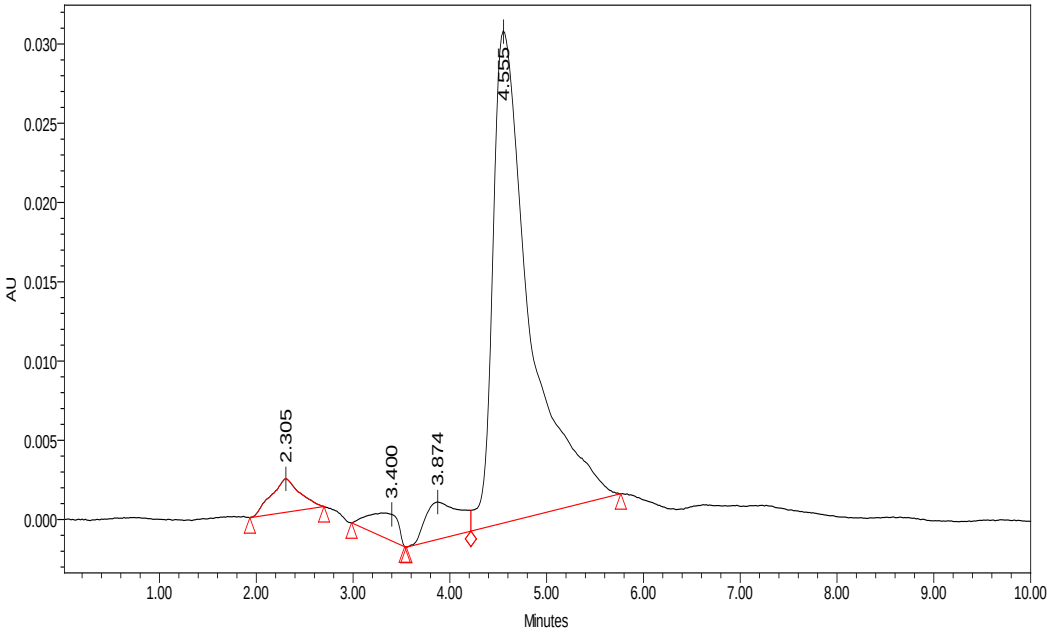

Figure 6.13 HPLC chromatogram of Phenol after 10 minutes laser irradiation

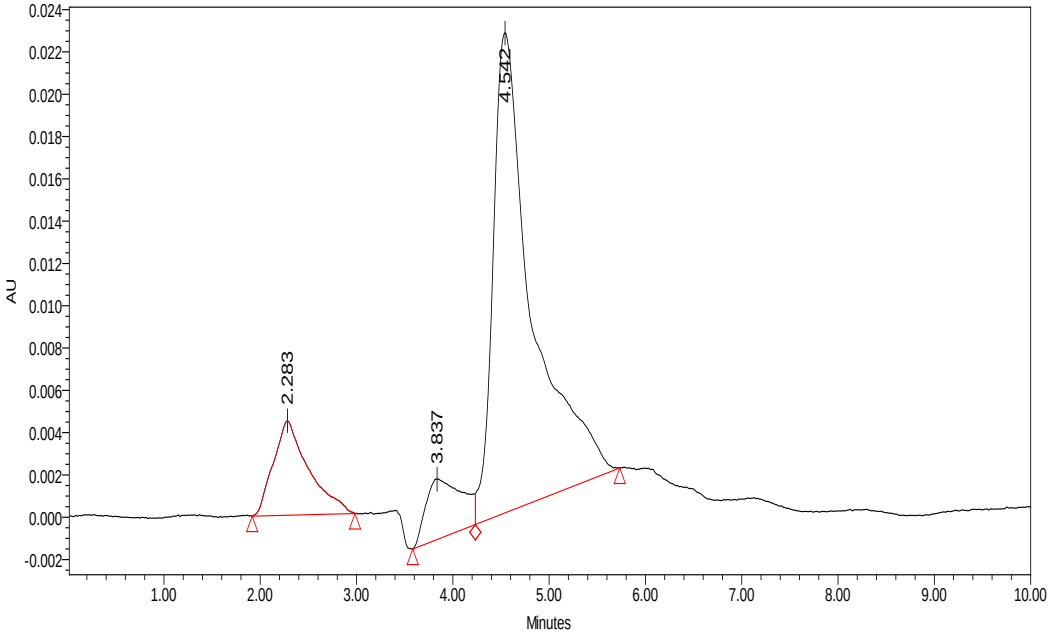

Figure 6.14 HPLC chromatogram of Phenol after 20 minutes laser irradiation

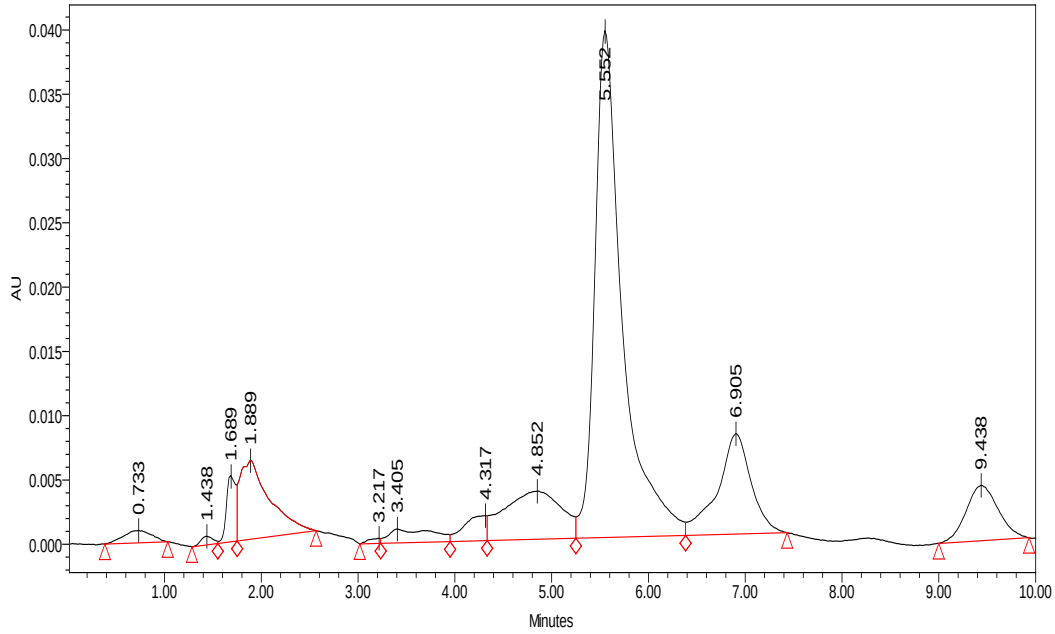

Figure 6.15 HPLC chromatogram of Phenol after 25 minutes laser irradiation

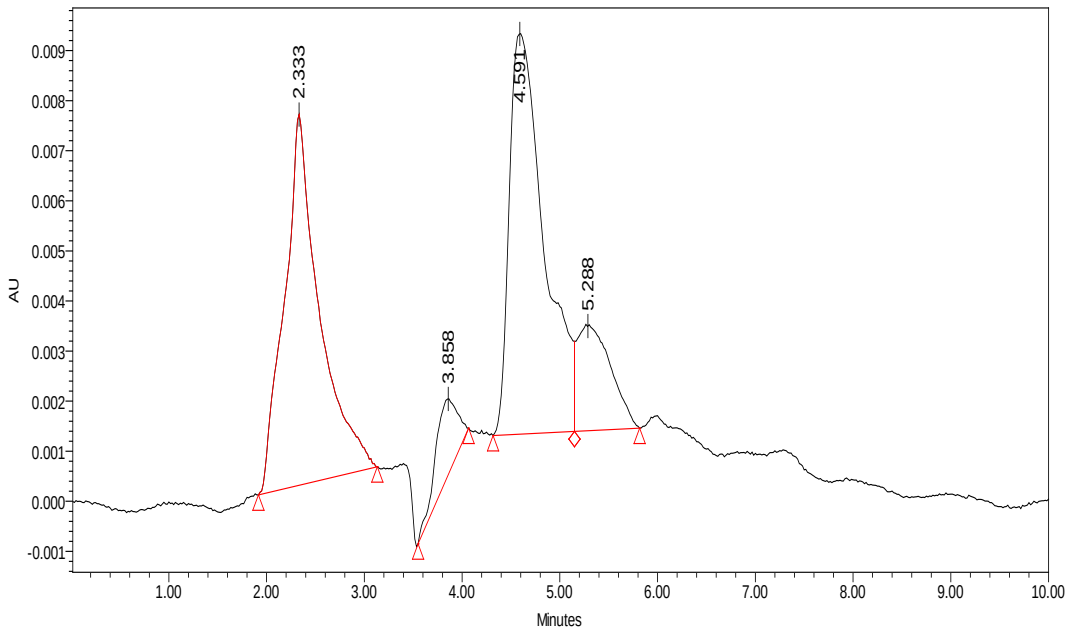

Figure 6.16 HPLC chromatogram of Phenol after 30 minutes laser irradiation

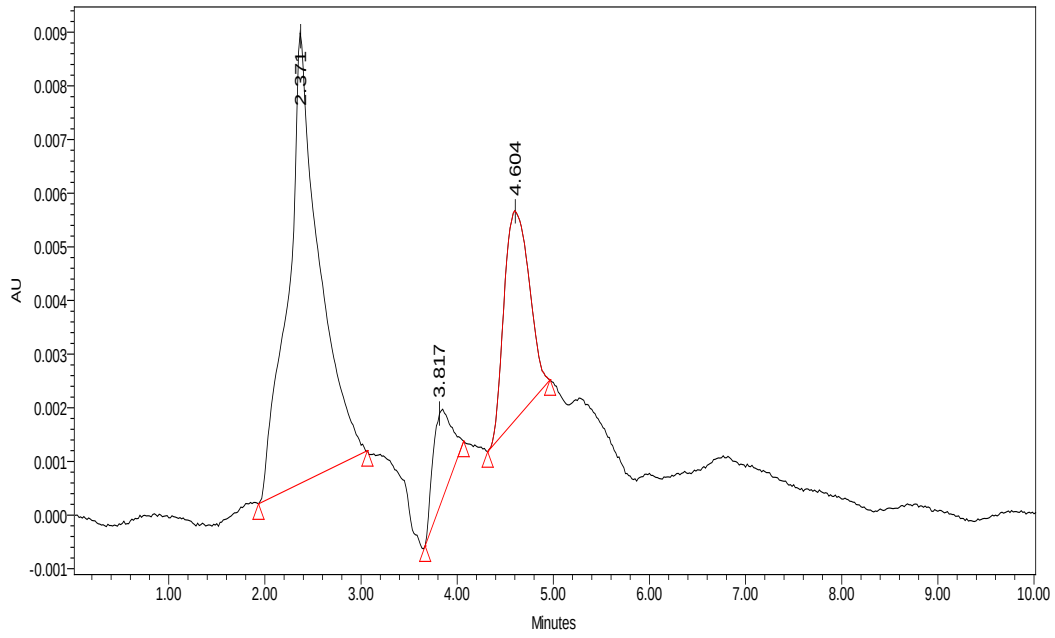

Figure 6.17 HPLC chromatogram of Phenol after 40 minutes laser irradiation

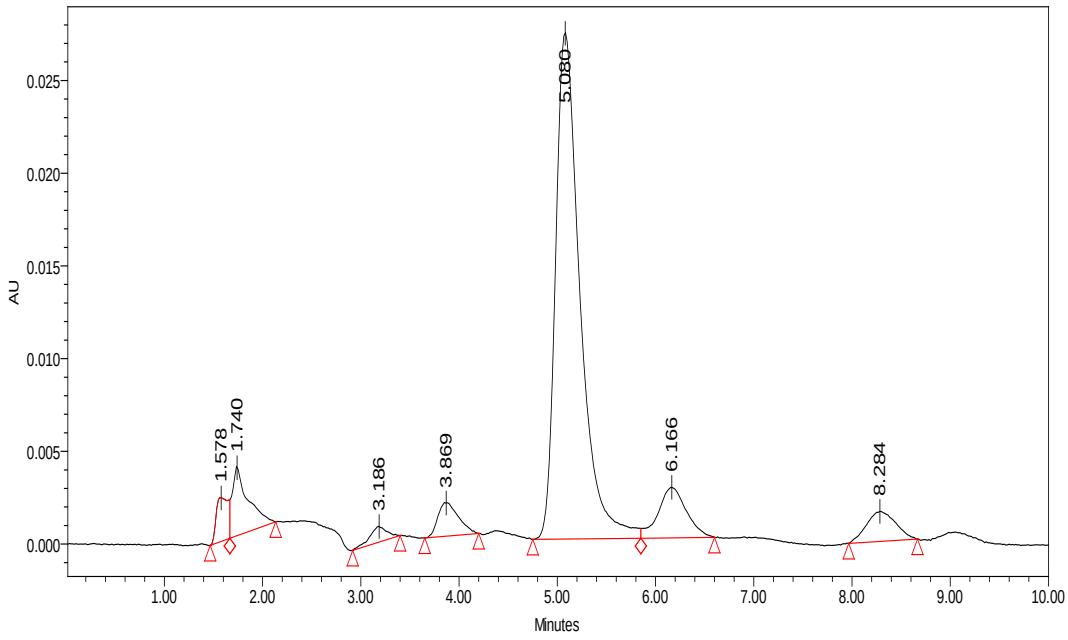

Figure 6.18 HPLC chromatogram of Phenol after 50 minutes laser irradiation

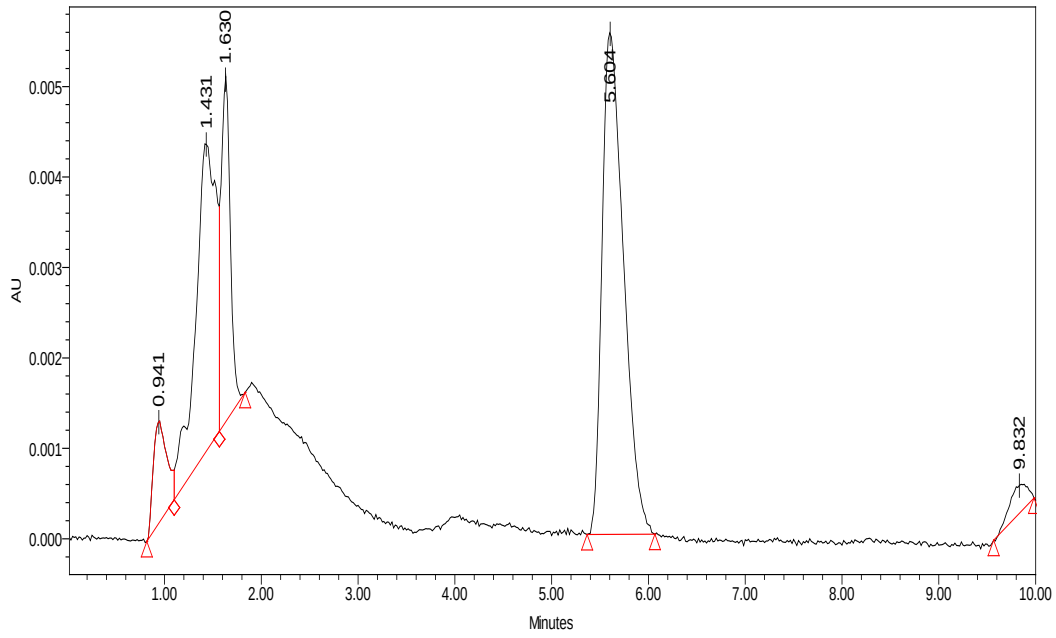

Figure 6.19 HPLC chromatogram of Phenol after 60 minutes laser irradiation

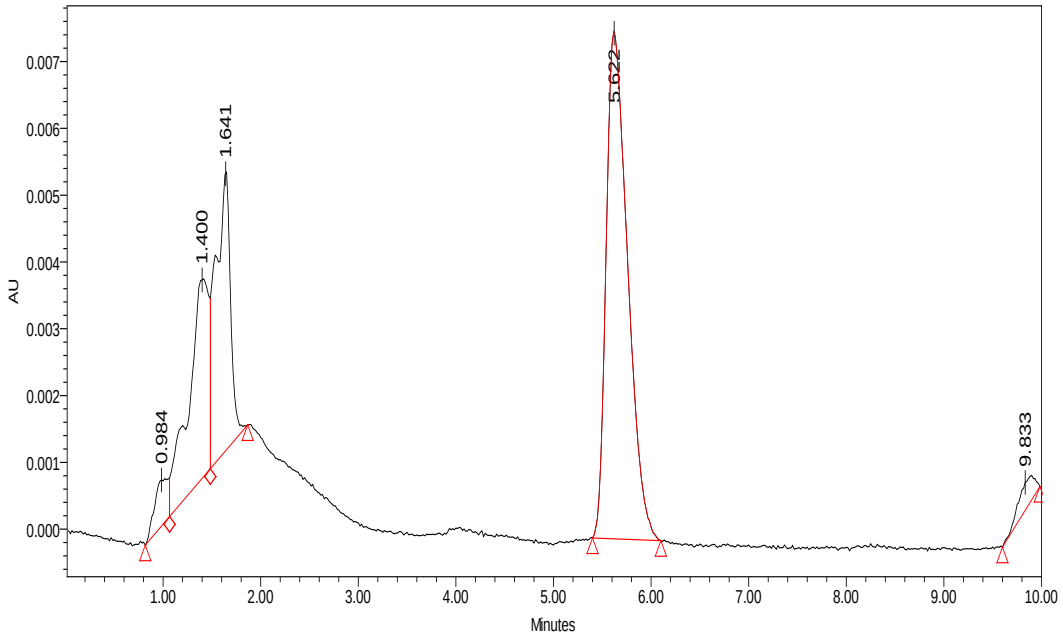

Figure 6.20 HPLC chromatogram of Phenol after 70 minutes laser irradiation

6.2. Photocatalytic Degradation of Phenol by Nano NiO

Photocatalytic degradation of phenol was investigated without NiO catalyst as well as in the absence of laser UV light. Only nano NiO without UV laser irradiation could not catalyze the degradation of the phenol. It was observed that phenol degradation was not significant in the absence of laser or nano NiO. The results indicate that both the catalyst and light are essential for efficient phenol degradation.

Photocatalytic degradation of phenol was investigated without NiO catalyst as well as in the absence of laser UV light. Only nano NiO without UV laser irradiation could not catalyze the degradation of the phenol. It was observed that phenol degradation was not significant in the absence of laser or nano NiO. The results indicate that both the catalyst and light are essential for efficient phenol degradation.

The results demonstrate that almost 97% of phenol was degraded within 60 minutes using laser irradiation by nano NiO catalyst. The results obtained demonstrate that the percentage of phenol degradation increases with the increase in laser irradiation exposure time, This increase in phenol degradation might be due to increase in the amount of $^{\bullet}OH$ radicals with time.

6.2.1. Effect of Catalyst Amount on Photocatalytic Degradation of Phenol using Nano NiO

The optimum amount of catalyst needs to be found in order to avoid ineffective excess of catalyst and to ensure a total absorption of efficient photons.

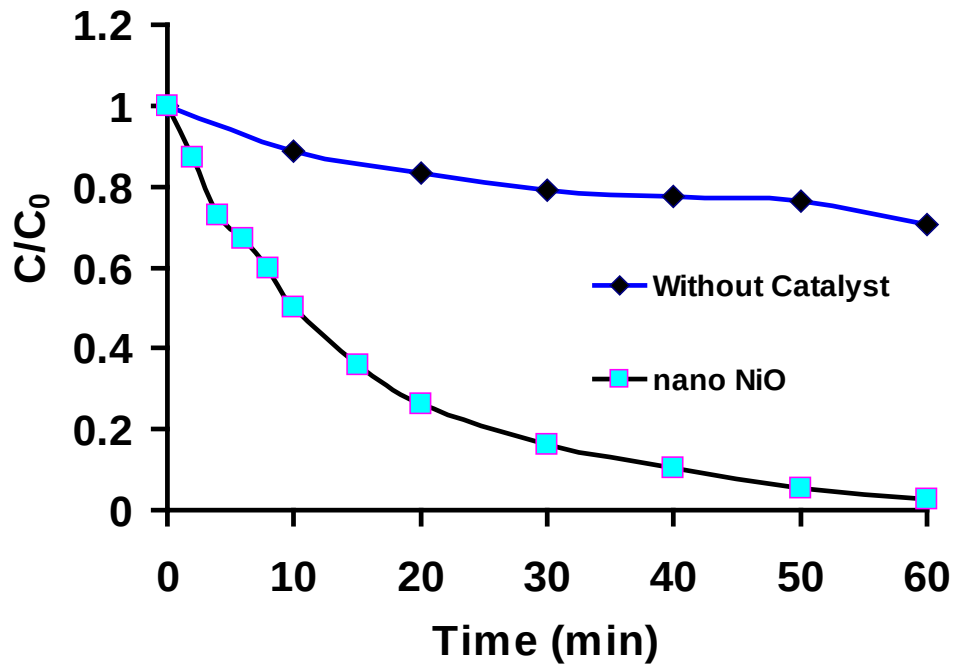

Figure 6.21 Photodegradation of phenol as a function of laser irradiation time by NiO

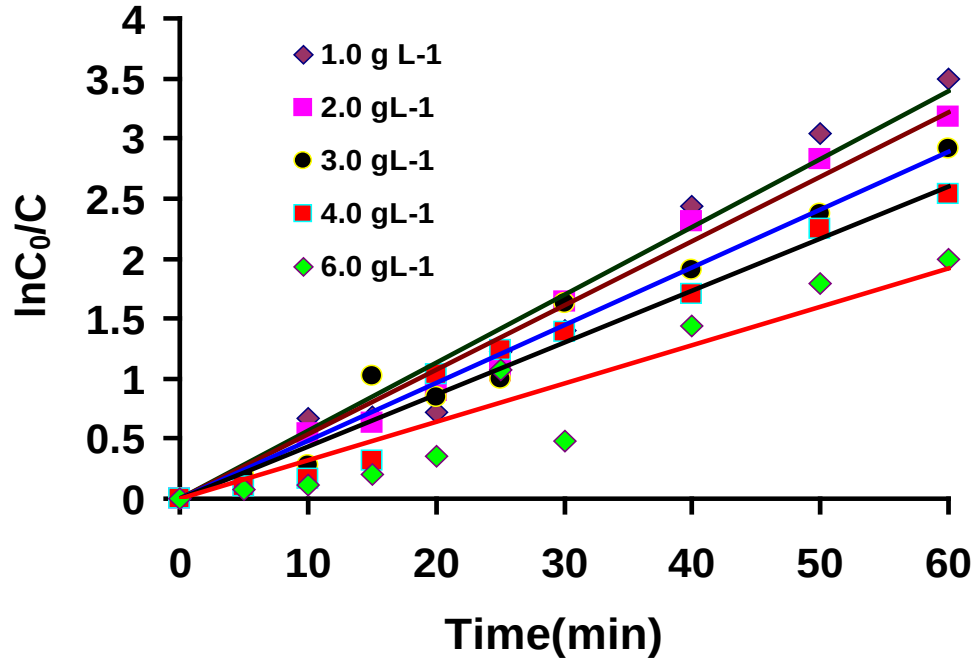

Figure 6.22 Effect of catalyst concentration on photocatalytic degradation of phenol as a function of laser irradiation time for nano NiO

In this study, the weight of nano NiO in the suspension was varied from 1.0 to 6.0 g L^{-1}. An increase in the catalyst loading up to an amount of 6.0 g L^{-1} resulted in a decrease in the rate constant as shown in Figure 6.22 which can be attributed to a screening effect due to the redundant dispersion of UV radiation caused by the ample amount of suspended photocatalyst. In addition, particles tend to agglomerate, making a significant fraction of the catalyst to be inaccessible to either adsorbing the molecules or absorbing the radiation, with consequent decrease in the active sites available to the catalytic reaction [225].The results given in Table 1 indicate that the photodegradation rate decreases as the amount of catalyst increases from 1.0 to 6.0 g L^{-1}. Following these observations, it was decided to keep the amount of nano NiO at the optimum value of 1.0 g L^{-1} in subsequent photocatalytic degradation experiments.

6.2.2. Effect of pH on Photocatalytic Degradation of Phenol using Nano NiO

The pH of the suspension was varied in the range (5.0-11.0) to study its effect on the photocatalytic degradation of phenol. The plot of pH vs ln C_0/C is depicted in Figure 6.23. It is evident from the results that the rate photocatalytic degradation was increased when pH was decreased from natural to pH to 5. It is clear from the results that the photoefficiency of the process decreases and phenol removal becomes slow with a k of 1.15×10^{-3} min^{-1} at pH 11. Similar behavi0ur of photocatalysts was also observed by some researchers during their studies [226].

Nano NiO shows amphoteric behavior in aqueous media. Electric charge properties of both, catalyst and substrate, are found to play an important role on adsorption process.

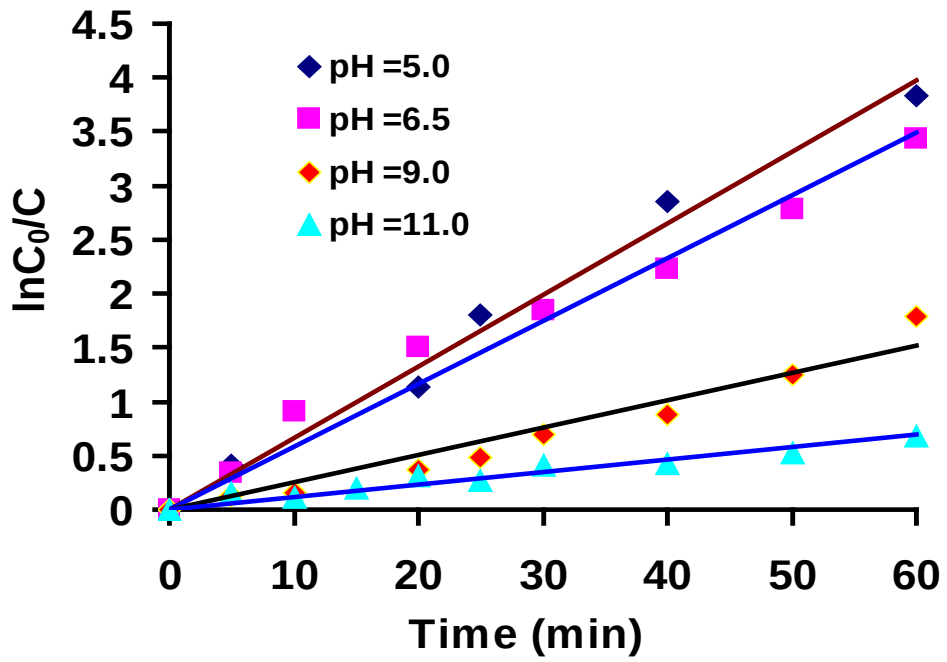

Figure 6.23 Effect of initial pH on photodegradation of aqueous solution of phenol in presence of NiO

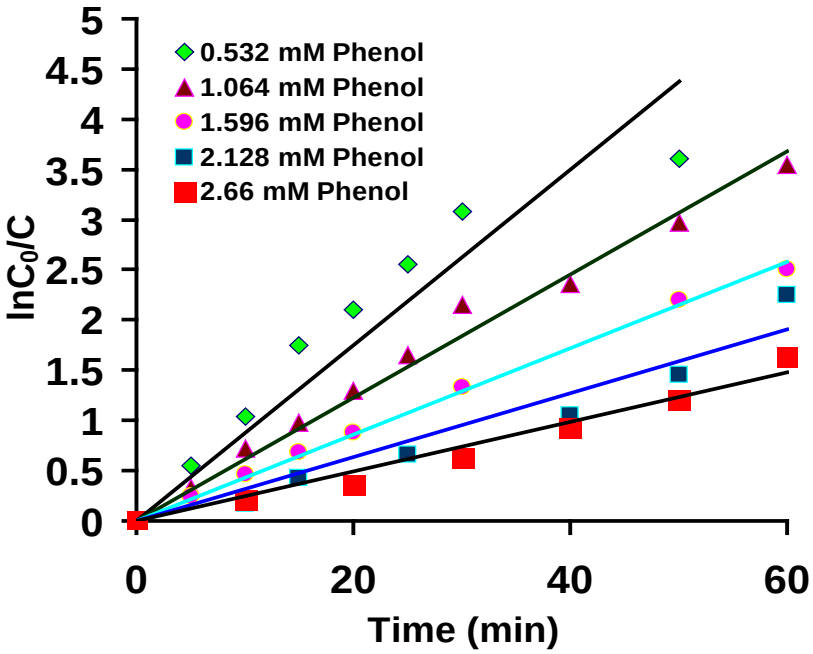

Figure 6.24 The diagram showing the effect of initial dye concentration on photocatalytic degradation rate of phenol by nano NiO

The point of zero charge (pzc) of nano NiO i.e. the point at which the surface charge density is zero, determined by Lewis and was found to be of 10.5 [227]. At pH higher than pHpzc nano NiO surface is negatively charged and NiO^- appears to be the predominant form. For lower pH values, nano NiO surface is in the protonated form ($NiOH^{2+}$). Phenol shows a pKa of 9.9 (at 25 °C) under aqueous media. If pH<pKa, phenol is in the molecular form (C_6H_5OH) and at pH> pKa the molecule undergoes deprotonation becoming negatively charged ($C_6H_5O^-$). Under these conditions, both catalyst and substrate are negatively charged, developing repulsive forces between them. Consequently, the phenol adsorption is decreased and hence decreasing the degradation of it.

6.2.3. Effect of Concentration on Photocatalytic Degradation of Phenol using Nano NiO

The effect of initial phenol concentration was investigated varying the concentration from 0.532 mM to 2.66 mM . Results showed that for this range of concentrations the reaction rate gets slower as the initial concentration of phenol in solution increases as depicted in Figure 6.24. The reason for this behavior is attributed to, as the initial concentration increases, more and more organic substances are adsorbed on the surface of NiO, therefore, the generation of hydroxyl radicals will be reduced since there are only a fewer active sites for adsorption of hydroxyl ions and the generation of hydroxyl radicals. Further, as the concentration of a substrate increases, the photons get intercepted before they can reach the catalyst surface, hence the absorption of photons by the catalyst decreases, and consequently the degradation percent is reduced [228].

As phenol concentration increases, more reactant and reaction intermediates are adsorbed on the surface of the photocatalyst, therefore, the generation of hydroxyl radicals will be reduced since are only a fewer active sites for adsorption of hydroxyl anions. The photodgradation rate decreases with the increase in phenol concentration. The dependency of the photocatalytic reaction rate on the concentration of the organic substrate has been generally well described by a Langmuir–Hinshelwood kinetic model.

6.2.4. Kinetics of Photocatalytic Degradation of Phenol

The kinetic behavior of photocatalytic degradation of phenol can be described by Langmuir– Hinshelwood equation, which was developed and can be expressed as Eq.

$$\text{rate} = -dC/dt = kKC/1 + KC = k_{app}C \quad (9)$$

$$1/kapp = 1/kcK + C_0/k_c \quad (10)$$

where C_0 = initial concentration of phenol

C = concentration of phenol at any time‘t’

k, K, kc and k_{app} are the rate constant, the equilibrium adsorption constant, the kinetic rate constant of surface reaction and the apparent pseudo-first order rate constant respectively. The reaction mechanism usually considered for heterogeneous photocatalyzed reactions consist of two main steps: fast adsorption of the reactants on the catalyst surface and a slow step of reaction in the adsorbed phase of the organic compound and a photogenerated hydroxyl radical .The results reported in the literature show that k_c and K are light intensity-dependent .

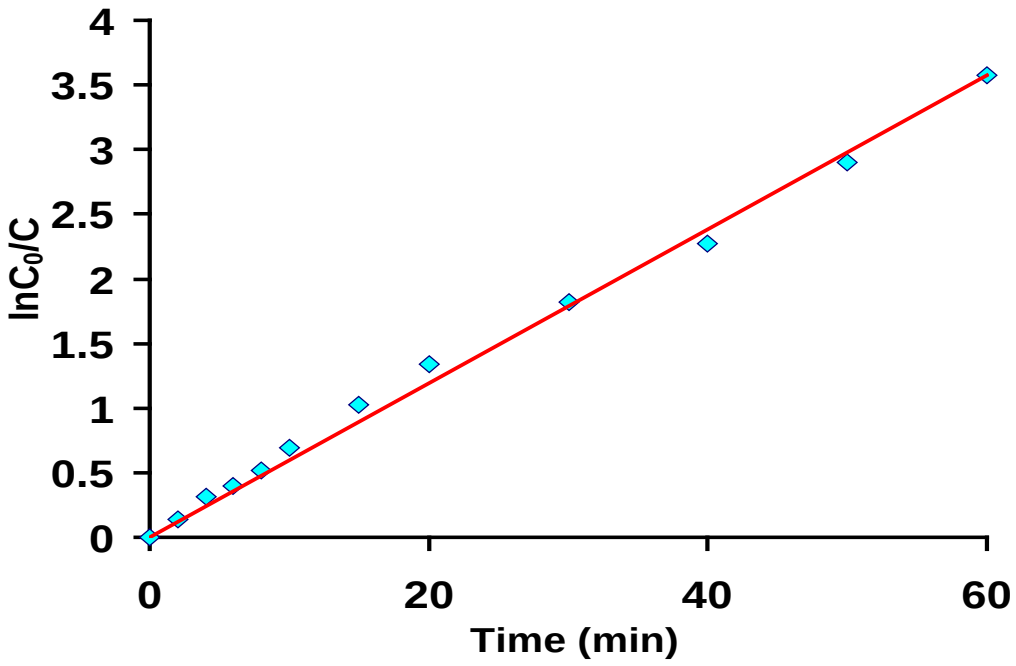

Figure 6.25 A plot of ln C_0/C as a function of laser irradiation time for an aqueous solution of phenol in presence of NiO.

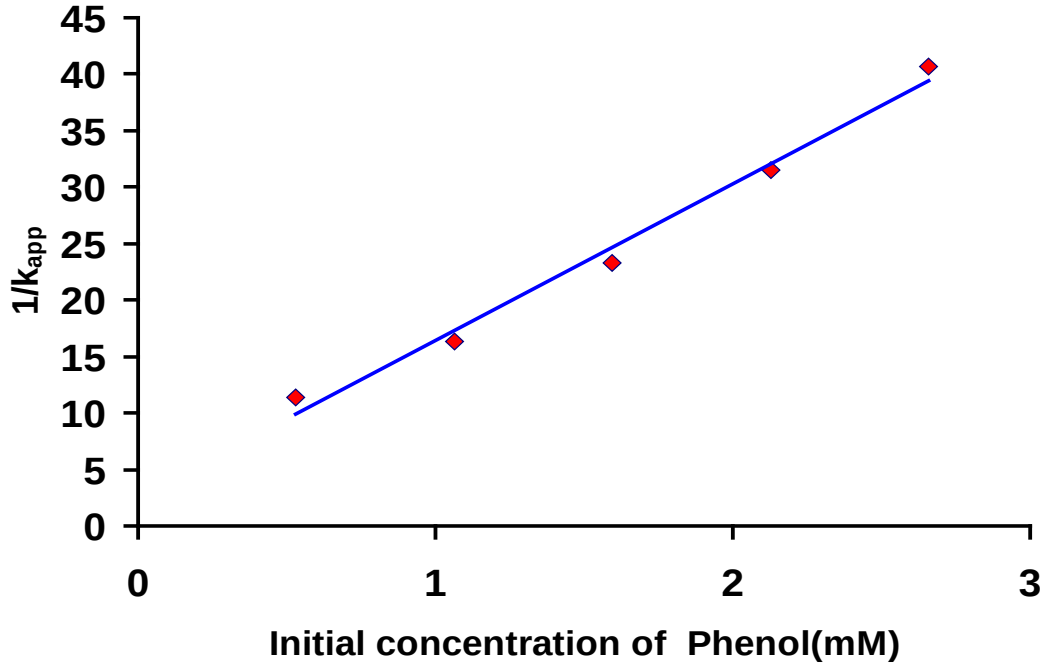

Figure 6.26 A plot of $1/k_{app}$ against initial phenol concentration

The photodegradation of phenol in aqueous solution as a function of laser irradiation time in the presence of nano-structured NiO is shown in Figure 6.25. The percentage degradation of phenol was calculated using the following relation:

$$\text{Phenol degradation (\%)} = [C_0\text{-}C_t/C_0]*100 \qquad (8)$$

A plot of $1/k_{app}$ versus initial dye concentration is presented in Figure 6.26. The adsorption equilibrium constant, K = 0.0722 $(mM)^{-1}$ and kinetic rate constant of surface reaction k_c = 0.18 mM min^{-1} were determined. Dutta and Chakrabarti reported similar results using Langmuir–Hinshelwood model for photocatalytic degradation of two textile dyes in wastewater using ZnO as catalyst.

In photo-induced reactions, the number of active catalyst sites is much fewer than the total surface adsorption sites. The results demonstrate that photocatalytic oxidation of phenol follow a pseudo-first order kinetic model. As photon flow increases, the number of photogenerated $HO^{\bullet}$ radicals rise up accelerating the oxidation of the substrate molecules. Simultaneously, the increase of surface active species such as electrons, holes and $HO^{\bullet}$ radicals lead to a decrease in the available sites for adsorption of the primary molecule and therefore a decrease in K.

CHAPTER 7

PHOTOCATALYIC DEGRADATION OF DYES AND PHENOL IN AQUEOUS SUSPENSION OF DOPED METAL OXIDES

The photocatalytic efficiency of noble metal doped WO_3, ZnO and NiO for degradation of dyes and phenol was investigated. The results obtained are discussed in this chapter.The basic mechanism for the decomposition of organic compounds is the same, although variations exist in the photocatalyst characteristics that are critical to the reaction such as the number and strength of surface acid sites and the redox potentials of the photocatalyst relative to that of the organic and inorganic reaction species.

The following reactions describe the formation of hydroxyl radicals and organic peroxides, which are significant species for the oxidation of organic molecules.

$$MO + h\nu \longrightarrow h_{vb}^{+} + e_{cb}^{-} \quad (20)$$

$$O^2 + e^{cb} \longrightarrow O_2^{\cdot -} \quad (21)$$

$$O_2^{\cdot -} + H^{+} \longrightarrow HO_2^{\cdot} \quad (22)$$

$$HO_2^{\cdot} + HO_2^{\cdot} \longrightarrow H_2O_2 + O_2 \quad (23)$$

$$O_2^{\cdot -} + HO_2^{\cdot} \longrightarrow HO_2^{-} + O_2 \quad (24)$$

$$HO_2^{-} + H^{+} \longrightarrow H_2O_2 \quad (25)$$

$$H2O2 + h\nu \longrightarrow 2\ {}^{\bullet}OH \quad (26)$$

$$O_2^{\cdot -} + \text{dye} \longrightarrow \text{dye}^{-}OO^{\cdot} \quad (27)$$

$$^{\cdot}OH + dye \longrightarrow \text{degradation of dye} \quad (28)$$

$$M^{x+} + 2\,e^-_{(cb)} \longrightarrow M^{y+} \quad (29)$$

In this work, the photocatalytic oxidation of dyes and phenol catalyzed by WO_3, ZnO, NiO was studied.The photocatalytic activity of corresponding noble metals (Pt,Pd,Ag and Rh) modified materials, Pt/WO_3, Pd/WO_3 ,Ag/WO_3 and Rh/WO_3 was compared with pure metal oxide semiconductor under UV laser irradiation. The metal oxides photocatalysts (WO_3, ZnO, and NiO) were synthesized by precipitation and sol gel methods. The surface modification was carried out by noble metals such as Pt, Pd, and Ag and Rh for the preparation of the doped nanomaterials using wet incipient impregnation method.The Photocatalytic activity of the doped WO_3 catalysts was tested using methyl red solution as a model pollutant.The effect of noble metals on the photocatalytic activity of nanostructured metal oxides was elucidated. The influence of the amount of dopant on the photocatalytic efficiency of doped material for the degradation of the dye was also investigated.

Blank experiments were perfomed to study the degradation of methyl red under UV laser irradiation without the presence of catalyst. It was found that the degradation of Methyl red without the catalyst was not significant. It was also observed that the adsorption of the dye in the dark using only photocatalyst was negligible.Hence; both the photocatlyst and UV laser are required for the removal of the pollutant.

7.1 Effect of Noble Metal Doping on Photocatalytic Activity of WO_3

The main purpose of doping WO_3 with transition metals or other dopants is to shift light absorption into the visible and to enhance the photocatalytic efficiency of the catalyst. The Photocatalytic degradation of Methyl red was investigated using the doped (Pt, Pd, Ag and Rh) WO_3 and the effect of different concentration of the doped materials were also studied. Red shift was observed in case of doped WO_3 studied. The shift in wavelength towards the visible region increased with the concentration of the dopant. The presence of dopant ion results (Figure 7.1) in a large red shift of the absorption onset. This spectral behavior is indicative of the preservation of the semiconductive nature of the noble metal doped material.The spectral red shift originates from excitation of 3d electrons from metal ions into the conduction band of the semiconductor .It was observed that the optimum dopant either mol% or wt% vary from catalyst to catalyst. The contents of different dopants at various ratios also exerted different effects on the photocatalytic activity of the prepared photocatalyst.

A decrease in the degradation of the dye was observed as the dopant content increased from 1.0 to 5.0 wt % Pt. The results indicate that the maximum photocatalytic degradation of methyl red was obtained with 1.0 wt% doping content. The decrease in photodegradation rate could be rationalized as follows:

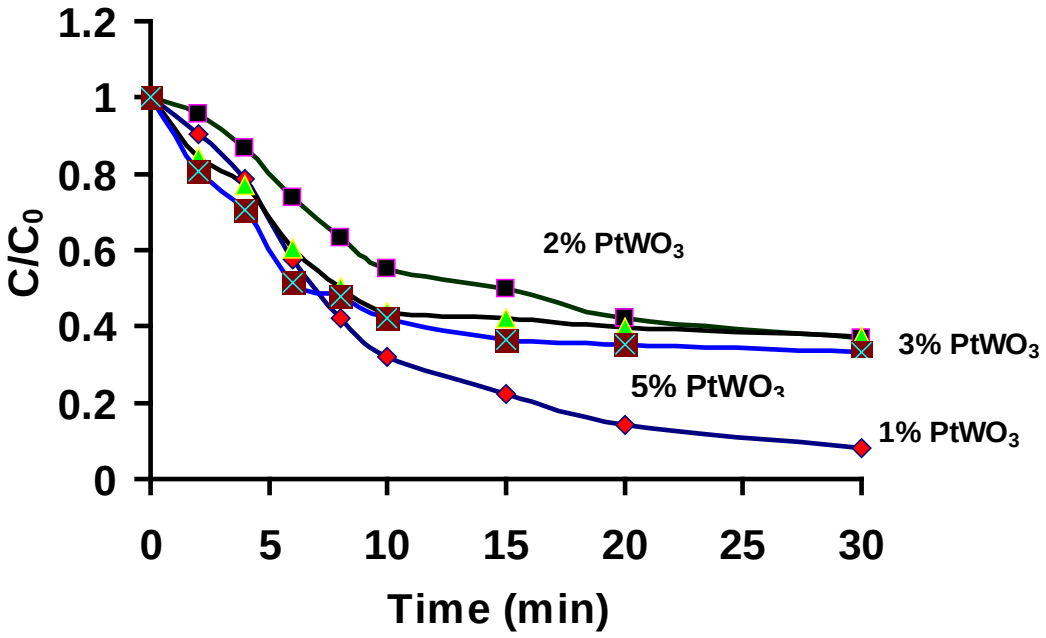

Figure 7.1 Effect of dopant concentration on degradation of methyl red by doped WO_3

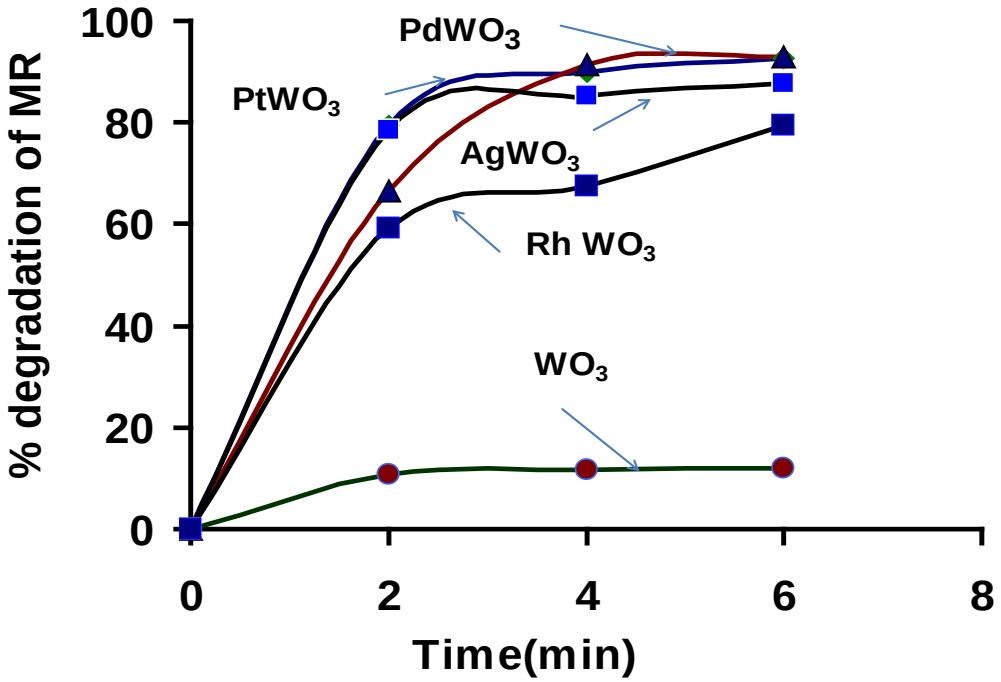

Figure 7.2 Effect of dopant on photocatalytic activity of WO_3

a) As the concentration of dopants increases, the surface barrier becomes higher and the electron–hole pairs within the region are efficiently separated by the large electric field. Due to the difference in electron negativity between W and M, the W–O–M formed via metal cation could promote the charges to transfer, resulting in an increase of photocatalytic activity.

b) The noble metal ion doping might cause a lattice deformation and produce defects in the crystal. The defects could inhibit the recombination of electron–hole pairs and ultimately, enhance the activityof the photocatalyst.

The dopant content was increased from 1.0 to 5.0 wt %. The excess dopant decreases the specific area of metal oxide inhibits the photocatalytic activity. Excess amount of dopant also could notably screen the UV light and inhibit the interfacial electron and hole to transfer which would result in a low photo-activity.

The photocatalytic activity of 1% Pt/WO_3, 1% Pd/ WO_3, 1% Ag/ WO_3 and 1% Rh/ WO_3 was tested using methyl red under UV laser irradiation. The results obtained are depicted in Figure 7.2- Figure 7.2. They reveal that the photocatalytic degradation of Methyl red under UV light was more favored in the presence of 1% Pt doped WO_3 than the presence of other three noble metal doped materials. The increase in the photocatalytic activity could be attributed to decrease in the e^- / h^+ recombination rate.

Some researchers [229, 230] offered explanation for the continuous increase in activity of photocatalyst with increase in dopant content until it reaches the optimum. Some researchers support the idea that cationic dopants of higher valence than Ti^{4+} increase photocatalytic efficiency while cationic dopants of lower valence (like the present ones) have adverse effects on photocatalysis [231].

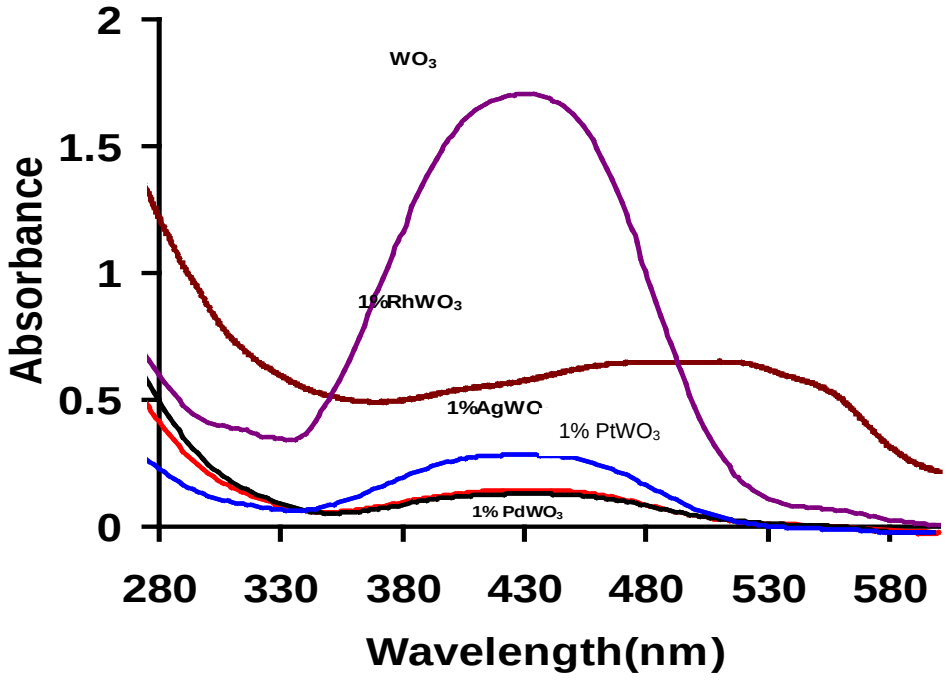

Figure 7.3 Overlay graph showing the degradation of methyl red after 6 minutes irradiation time for doped WO_3

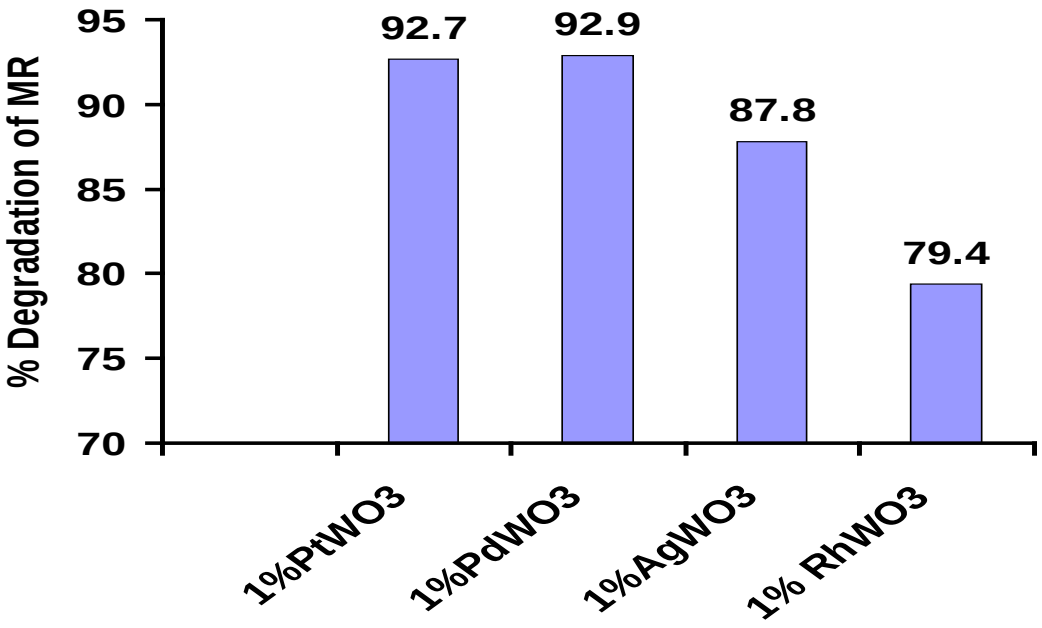

Figure 7.4 Percent degradation of methyl red by doped WO_3

On the other hand, It was found that the decrease of photodegradation efficiency in the presence of dopants may be due to the following reasons: (1) electron–hole recombination at dopant sites; (2) loss of crystallinity in the presence of dopants other possible reasons such as population of lower lying dopant energy states and decrease of electron reductive capacity.

7.2. Effect of Noble Metal Doping on Photocatalytic Activity of ZnO using Cyanosine

The photocatalytic activity of ZnO and surface modified ZnO photocatalysts was investigated using Cyanosine (toxic dye) as a model pollutant. The photodegradation of Cyanosine in aqueous solution as a function of laser irradiation time in the presence of nano-structured ZnO is shown in Figure 7.5. The degradation of the dye increases with the increase in laser irradiation time. The results indicate that the percentage degradation of Methyl red increases with the increase in laser irradiation time. This increase in degradation of the dye with time could be due to the fact that with increase in the laser irradiation time, the number of absorbed laser photons increases, producing more amount of $OH^{\cdot}$ radicals, thereby facilitating more degradation of the dye.

A plot of ln C_0/C as a function of laser irradiation time for an aqueous solution of Cyanosine in presence of doped ZnO is shown in Figure 7.5. The rate constants as obtained from the results given in Table XI for the photocatalytic degradation of phenol are 0.0909, 0.1445, 0.1291, 0.1538, and 0.1759 min^{-1} for ZnO and (Pt, Pd, Ag and Rh) doped ZnO respectively. The photocatalytic efficiency follows the order:

RhZnO> AgZnO > PtZnO >Pd ZnO > ZnO

Table XI Effect of dopant on photocatalytic activity of ZnO for cyanosine degradation

Cyanosine ZnO					
Time(min)	A	C	$\ln(C_0/C)$	k	r^2
0	2.18	0.1205	0	0.0909	0.9759
2	1.987	0.109832	0.092699		
4	1.541	0.085179	0.346893		
6	1.171	0.064727	0.621467		
8	0.984	0.054391	0.795454		
10	0.739	0.040848	1.081782		
15	0.623	0.034436	1.252534		
20	0.369	0.020397	1.776284		
Pt- doped ZnO					
0	2.2	0.1205	0	0.1445	0.9388
2	1.59	0.087089	0.324723		
4	1.087	0.059538	0.705036		
6	0.762	0.041737	1.060266		
8	0.541	0.029632	1.402793		
10	0.414	0.022676	1.670347		
15	0.22	0.01205	2.302585		
20	0.182	0.009969	2.492206		
Pd- doped ZnO					
0	2.268	0.1205	0	0.1291	0.8408
2	1.425	0.075711	0.464727		
4	0.963	0.051165	0.8566		
6	0.698	0.037085	1.178435		
8	0.612	0.032516	1.309921		
10	0.53	0.028159	1.453777		
15	0.327	0.017374	1.936693		
20	0.256	0.013601	2.181476		

Table (cont…)

Time(min)	A	C	$\ln(C_0/C)$	k	r^2
Ag- doped ZnO					
0	2.469	0.1205	0	0.1538	0.8987
2	1.348	0.065789	0.605191		
4	0.988	0.04822	0.915886		
6	0.724	0.035335	1.226777		
8	0.553	0.776023	1.49621		
10	0.393	0.840826	1.837759		
15	0.3	0.878493	2.107786		
20	0.152	0.938437	2.787688		
Rh- doped ZnO					
0	2.538	0.1205	0	0.1759	0.8592
2	1.519	0.07212	0.513324		
4	0.737	0.034992	1.236544		
6	0.56	0.026588	1.511195		
8	0.478	0.022695	1.669521		
10	0.287	0.013626	2.179649		
15	0.21	0.00997	2.492024		
20	0.12	0.005697	3.05164		

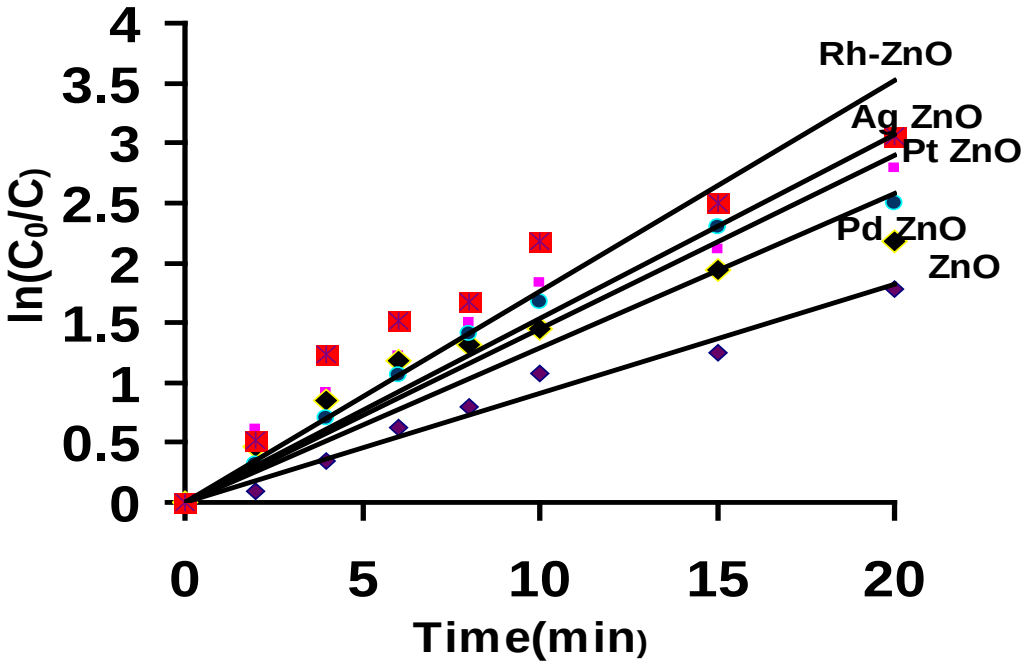

Figure 7.5 Effect of dopants on photocatalytic activity of ZnO

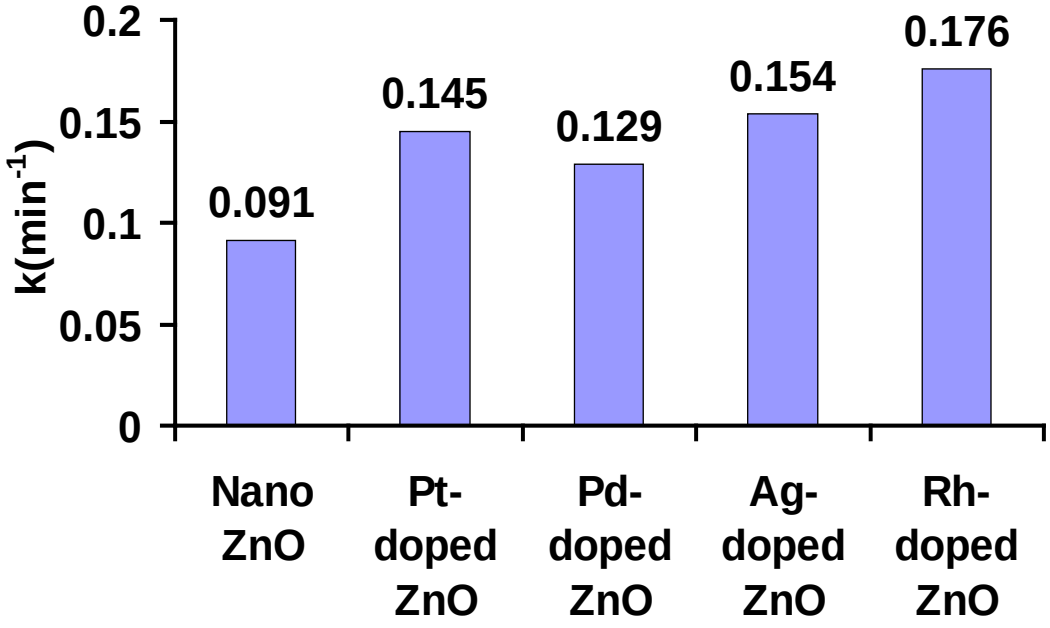

Figure 7.6 Aplot showing the comparison of rate constants for degradation of Cyanosine using doped ZnO

The enhancement in the rate of photodegradation for doped ZnO of cyanosine was found to be higher as compared to undoped ZnO.This could be attributed to the band gap suitability of the doped metal oxides. Molecular oxygen, adsorbed on the surface of the Ag doped ZnO photocatalyst, prevents the hole-electron pair recombination process. Recombination of hole-electron pairs decreases the rate of photocatalytic degradation. It was observed that superoxide may be the source of hydroxyl radicals.

Although charge transfer to adsorbate species is the desired fate of electron-hole pairs (EHPs), the vast majorities recombine, creating a loss in photocatalytic efficiency often greater than 90%. This recombination process between the photoexcited electron and hole can occur either in the volume of the semiconductor particle or on the surface of the particle with a byproduct of heat release [232]. The EHP recombination process itself results when the electron-hole recombination time is shorter than the time it takes for the carrier to diffuse to the surface.

7.3. Effect of Noble Metal Doping on Photocatalytic Activity of ZnO using Phenol

The photocatalytic activity of surface modified ZnO photocatalysts was studied using phenol as a model pollutant. As metal ions are incorporated into the catalyst lattice impurity energy levels in the band gap of catalyst are formed. In addition to that the electron (hole) transfer between metal ions and the catalyst can alter electron hole recombination. Carrier transferring is as important as carrier trapping for photocatalytic reactions. Photocatalytic reactions can occur only if the trapped electron and hole are transferred to the surface.

A qualitative analysis in investigating the effects of doping noble metal ions (Pt, Pd, Ag, and Rh) on photocatalytic activity of ZnO was carried out. Photocatalytic oxidation of phenol was employed to evaluate the effects of different metal ion doping. Enhanced photocatalytic activities and red shift of photo-response were observed at certain doping content. Plantinum as dopant ions were found to be most effective in enhancing the photocatalytic activity due to its highest ability to transfer charge carriers to the interface. The results are shown in Figure 7.6 and Table XII. The rate constants for the photocatalytic degradation of phenol were found to be 0.0391, 0.054, 0.0447, 0.0416, and 0.0473. The photocatalytic efficiency could be shown in decreasing order:

RhZnO > PtZnO >Pd ZnO > AgZnO >ZnO

Metal–semiconductor modifications are used primarily to inhibit charge recombination and increase the selectivity of a particular product. The addition of metals to a semiconductor surface changes the efficiency of photocatalytic processes by changing the surface properties of the semiconductor. The contact between a semiconductor and metal generally involves a re-distribution of charges and the formation of double layers at metal–semiconductor interfaces.

The improvement in the rate of photodegradation of phenol for doped ZnO was found to be higher as compared to simple metal oxides.This could be attributed to the band gap suitability of nano ZnO and doped ZnO photocatalysts. As the size of the particle decreases approaching approximately 10-15 nm, EHP recombination decreases since the diffusing charge carriers can quickly reach the surface of the particle. If the particle size decreases below this optimal particle size leading to quantum sizes, however, EHP recombination again increases due to the close proximity of the charges [233].

Table XII Effect of dopants on photocatalytic activity of ZnO for phenol degradation

Nano ZnO SG Time(min)	Area	C(mM)	lnC_0/C	$k(min^{-1})$	r^2
0	727347	1.064	0	0.0391	0.9789
5	562742	0.82321	0.25658		
10	448879	0.65664	0.48265		
15	363969	0.53243	0.69233		
20	308021	0.45059	0.85924		
30	225494	0.32986	1.17111		
Pt-doped ZnO					
0	38774	1.064	0	0.0447	0.7814
5	25168	0.69064	0.43218		
10	19665	0.53963	0.67891		
15	17070	0.46842	0.82043		
20	14904	0.40898	0.95612		
30	12752	0.34993	1.11206		
Pd- doped ZnO					
0	727347	1.064	0	0.0416	0.9901
5	602742	0.881722	0.187914		
10	498879	0.729785	0.37704		
15	403969	0.590946	0.588066		
20	308021	0.450589	0.859236		
30	205494	0.300607	1.263987		

Ag- doped ZnO Time	Height	C	lnC_0/C	k	r^2
0	40068	1.064	0	0.0473	0.8854
5	26396	0.700942	0.417366		
10	21017	0.558103	0.645246		
15	17332	0.460249	0.838024		
20	15075	0.400314	0.97754		
30	11547	0.306629	1.244152		
Rh- doped ZnO					
0	38159	1.064	0	0.054	0.8803
5	24396	0.68024	0.44734		
10	17357	0.48397	0.78777		
15	15172	0.42305	0.92231		
20	12195	0.34004	1.14074		
30	9289	0.25901	1.41293		

7.4. Effect of Noble Metal Doping on Photocatalytic Activity of NiO for Degradation of Cyanosine

The photocatalytic degradation of Cyanosine using NiO and surface modified NiO photocatalysts was studied.The results are presented in Figure 7.7. Peng et al. [234] investigated that doping the metal ions near the surface was beneficial for charge carrier transferring, while deep doping led to poor performance.For a semiconductor to have high quantum efficiency, its photoinduced charges must freely migrate to the surface of the particle so that they can participate in reactions with adsorbed species. The migration of electrons to the surface is not only in competition with EHP recombination but also with trapping by coordination defects at the surface and by lattice defects in the particles bulk. The photogenerated electrons that are able to migrate to the surface are primarily used in the reduction of O_2, other reactive species such as the superoxide radical $O_2^{\bullet -}$ or the singlet oxygen, which can in turn stimulate other radical chain reactions involving H_2O_2 or O_3. The positively charged photogenerated holes that are able to migrate to the surface can either directly oxidize organic species with lower oxidation potentials.

The results depicted in Table XIII which shows that the photodegradation rates for removal of phenol by doped NiO photocatalysts are 0.1771, 0.1648, 0.1693, 0.135 and 0.1199. The trend observed in photocatalytic efficiency was given below:

Rh NiO > Pt NiO > Pd NiO > Ag NiO

The trend observed could be correlated with the band gaps of these doped materials.

Table XIII Effect of dopants on photocatalytic activity of NiO for removal of Cyanosine

nano NiO					
Time	A	C	lnC_0/C	k (min^{-1})	r^2
0	1.7	0.121	0	0.1199	0.992
2	1.336	0.095092	0.240948		
4	1.064	0.075732	0.468593		
6	0.792	0.056372	0.763822		
8	0.639	0.045482	0.978479		
10	0.469	0.033382	1.287781		
15	0.306	0.02178	1.714798		
Pt doped NiO					
0	1.86	0.121	0	0.1648	0.9736
2	1.204	0.078325	0.434927		
4	0.869	0.056532	0.760989		
6	0.592	0.038512	1.144825		
8	0.469	0.03051	1.377729		
10	0.327	0.021273	1.738372		
15	0.191	0.012425	2.276058		
Pd doped NiO					
0	1.76	0.121	0	0.1693	0.9764
2	1.258	0.086488	0.335791		
4	0.809	0.055619	0.77727		
6	0.604	0.041525	1.069495		
8	0.408	0.02805	1.461802		
10	0.275	0.018906	1.856298		
15	0.172	0.011825	2.325575		

Ag doped NiO Time	A	C	$\ln C_0/C$	k (min^{-1})	r^2
0	1.75	0.121	0	0.135	0.9865
2	1.284	0.088779	0.309636		
4	0.954	0.065962	0.606707		
6	0.753	0.052065	0.843306		
8	0.536	0.037061	1.183237		
10	0.433	0.029939	1.396633		
15	0.261	0.018046	1.902851		
Rh doped NiO					
0	1.98	0.121	0	0.1771	0.9322
2	1.094	0.066856	0.593256		
4	0.779	0.047606	0.932841		
6	0.584	0.035689	1.220951		
8	0.411	0.025117	1.572259		
10	0.306	0.0187	1.867267		
15	0.188	0.011489	2.35441		

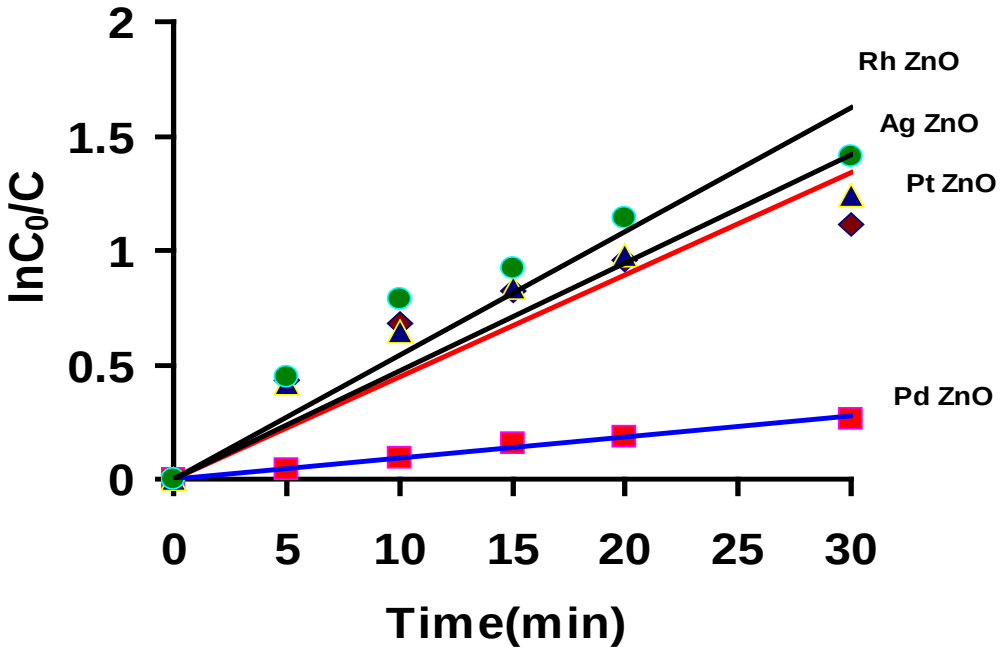

Figure 7.7 Effect of doped ZnO on degradation of phenol

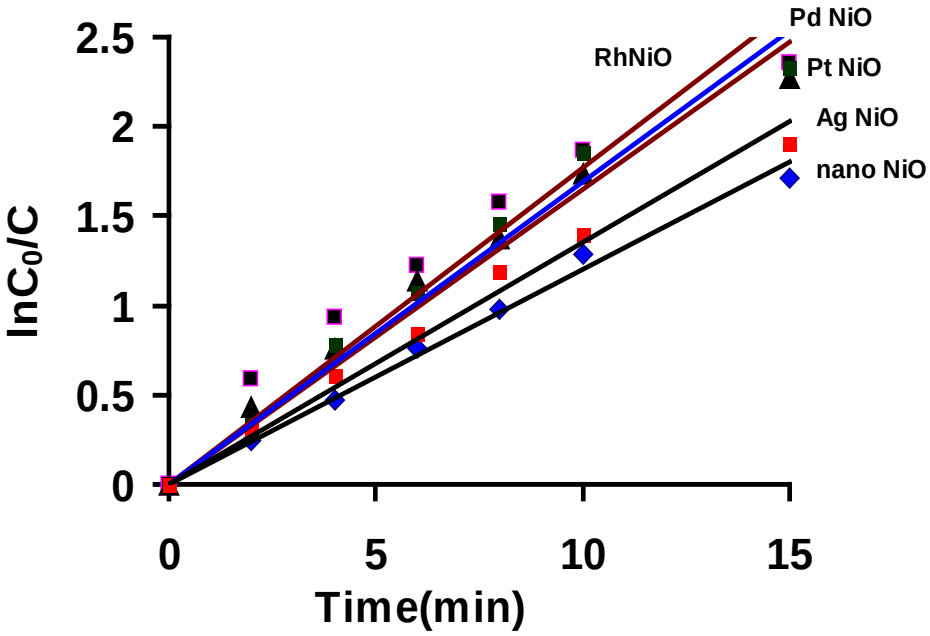

Figure 7.8 Effect of doped NiO on degradation of Cyanosine

Table XIV Effect of dopant on photocatalytic activity of NiO for degradation of phenol

Time	Retention time	Area	C(mM)	lnC_0/C	k(min^{-1})	r^2
Nano NiO						
0	4.609	806053	1.064	0	0.0565	0.9662
10	4.603	625338	0.825454	0.253857		
15	4.607	456789	0.602967	0.567928		
20	4.579	312993	0.413155	0.945969		
25	4.588	236633	0.312359	1.225639		
30	4.591	198072	0.261458	1.403519		
40	4.604	70652	0.093262	2.434383		
50	4.577	38643	0.051009	3.037784		
60	4.569	24450	0.032274	3.495519		
Pt NiO						
0	4.609	806143	1.064	0	0.0621	0.9897
10	4.603	505338	0.666978	0.467034		
15	4.607	356789	0.470913	0.815117		
20	4.579	262893	0.346983	1.120514		
25	4.588	176633	0.233132	1.518187		
30	4.591	96072	0.126802	2.127163		
40	4.604	65652	0.086652	2.507893		
50	4.577	35643	0.047044	3.118708		
60	4.569	20450	0.026991	3.674278		
Pd NiO						
0	4.609	806343	1.064	0	0.0595	0.9842
10	4.603	482438	0.636595	0.513657		
15	4.607	346789	0.457601	0.843793		
20	4.579	282876	0.373266	1.047501		
25	4.588	186733	0.246401	1.462829		
30	4.591	98072	0.12941	2.106807		
40	4.604	65652	0.08663	2.508141		
50	4.577	47643	0.062867	2.828773		

60	4.569	23675	0.03124	3.52809		
	Ag NiO					
Time		Retention time	Area	C(mM)	lnC0/C	k(min^{-1})
0	4.609	814678	1.064	0	0.0655	0.9722
10	4.603	452438	0.590901	0.588142		
15	4.607	306780	0.400666	0.976662		
20	4.579	191875	0.250596	1.445949		
25	4.588	106433	0.139005	2.035277		
30	4.591	87072	0.113719	2.236058		
40	4.604	58652	0.076602	2.631171		
50	4.577	38623	0.050443	3.048945		
60	4.569	18673	0.024388	3.775714		
	Rh NiO					
0	4.609	824658	1.064	0	0.0846	0.9695
10	4.603	412438	0.532141	0.692883		
15	4.607	255780	0.330015	1.170651		
20	4.579	121875	0.157247	1.911973		
25	4.588	76433	0.098616	2.378554		
30	4.591	47052	0.060708	2.863715		
40	4.604	20652	0.026646	3.687157		
50	4.577	11623	0.014996	4.261983		
60	4.569	8673	0.01119	4.554754		

7.5 Effect of Noble Metal Doping on Photocatalytic Activity of NiO for Degradation of Phenol

The photocatalytic activity of surface modified NiO photocatalysts was studied using phenol as a model pollutant. A plot of ln C_0/C as a function of laser irradiation time for an aqueous solution of phenol in presence of doped NiO is shown in Figure 7.9.
The rate constants for the photocatalytic degradation of phenol using NiO and noble metal doped NiO were observed and shown in Table XIV.These k have the values 0.0846, 0.0655, 0.0621, 0.0595 and 0.0565. The photocatalytic efficiency obeys the order as shown below:

Rh NiO > Ag NiO >Pt NiO > Pd NiO > NiO

The photocatalytic activity was in coincidence with the band gaps of doped NiO. Phenol adsorbed by the photocatalysts could be decomposed mainly by the valence band holes and radicals induced by holes. Therefore, the mechanism involved in transferring these photogenerated holes to the interface is of vital importance in the photocatalytic efficiency.

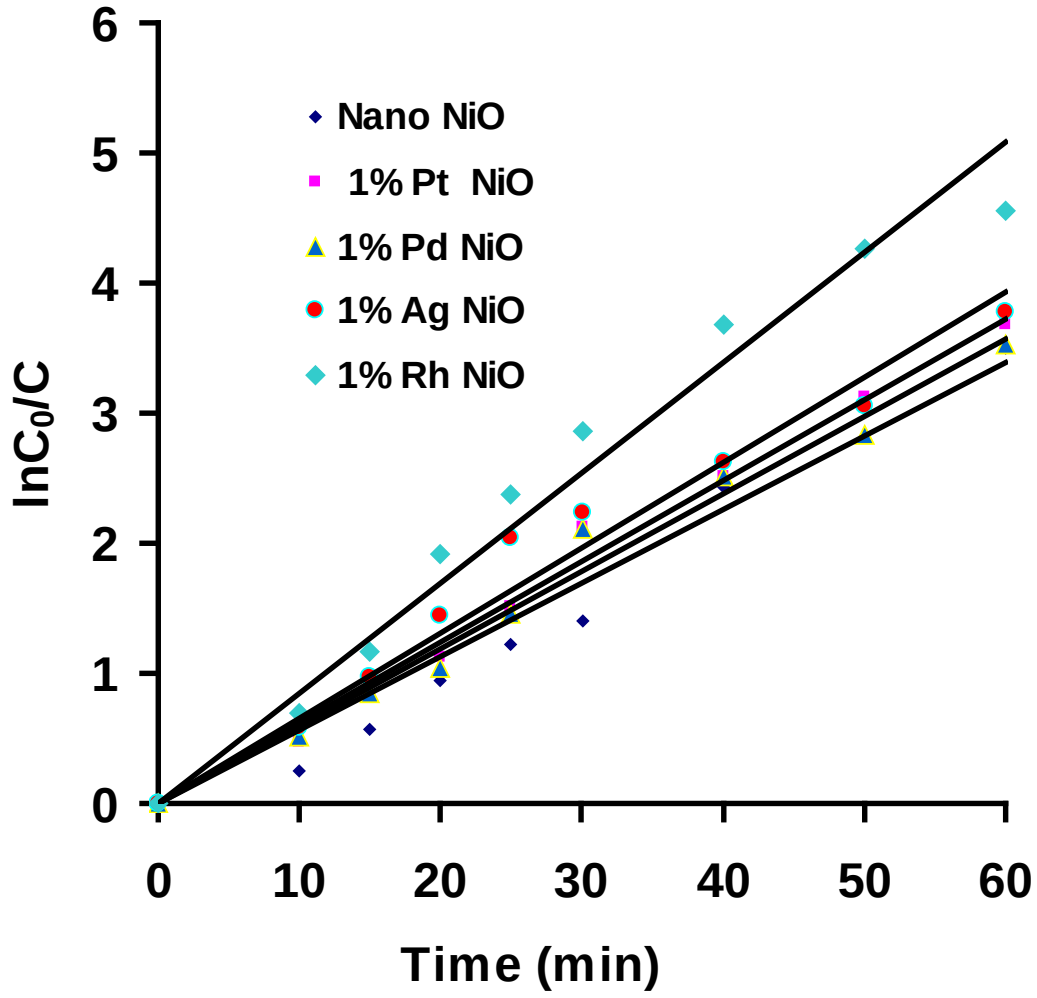

Figure 7.9 Effect of doped NiO on photodegradation of Phenol

CHAPTER 8

CONCLUSIONS AND FUTURE PROSPECTS

8.1 Conclusions

- Nanometer sized metal oxide catalysts were synthesized successfully by sol-gel and precipitation methods.
- Impregnation of nansized metal oxides was carried out using noble metals (Pt, Pd, Ag and Rh) as dopants.
- The morphology of the synthesized nanoparticles was studied using XRD, FESEM and HRTEM.
- Metal oxide (WO_3, ZnO and NiO) and noble metal (Pt, Pd, Ag and Rh) doped nanoparticles having high purity, well-dispersed and narrow size distribution ranging from 7 to 50 nm were obtained.
- The particle size as estimated from XRD using Scherrer Equation was compared with the particle size obtained by FESEM.
- The morphology was verified by HRTEM and percentage composition of doped materials was copmared by the EDX.
- Band gap of doped and undoped nanoparticles was measured using UV-Visible spectrophotometry and a red shift was observed in almost all of our doped nanomaterials.

- The effect of calcination temperature on particle morphology ranging from 300 °C to 700 °C was studied. The particle size increases because of agglomeration of particles.
- The photocatalytic activity was found to increase with the increase in calcination temperature till 500 °C and then decreases.
- The rate of the laser induced removal of the pollutants by nanocrystalline WO_3 and other nanomaterials is very high as compared to the conventional UV lamps.
- Experimental results demonstrate that the maximum degradation of the dye was achieved at pH=10.0 for Safranin O. The removal of the dye was achieved with a degradation rate = $1.46 * 10^{-4}$ M min^{-1} .
- The various operational parameters were optimized to achieve the maximum degradation efficiency. It was observed that the photodegradation rate of the pollutant increased as catalyst concentration increased. After an optimum concentration, the rate was found to decrease.
- The degradation rate was decreased with the increase of pollutant concentration.
- Alkaline pH favours degradation of dyes investigated except the degradation of acid red 87.
- The rate constants of photocatalytic degradation of the dyes such as Safranin O, Acid Red 87, Alizarin Yellow GG and Methyl Red using WO_3 are as follows:

SO > AR87 >AYGG > MR

- The photocatalytic activity of Pt/WO_3 catalyst with respect to the amount of dopant was in the following order :

1% Pt/WO_3> 2% Pt/WO_3 > 3% Pt/WO_3 > 5% Pt/WO_3

- The photocatalytic activity of WO_3 and doped WO_3 was evaluated for the degradation of methyl red and the rate constant was in the following order:

$$Pt/WO_3 > Pd/WO_3 > Ag/WO_3 > Rh/WO_3 > WO_3$$

- The rate constants for photocatalytic degradation of cyanosine using ZnO, Pt/ZnO, Pd/ZnO, Ag/ZnO and Rh/ZnO are 0.0909 min^{-1}, 0.1445 min^{-1}, 0.1291 min^{-1}, 0.1538 min^{-1} and0.1759 min^{-1}.
- The Rh doped ZnO showed better photocatalytic activity for the degradation of dyes and phenol as compared to metal oxides.
- Similar trend as mentioned above was observed for NiO and noble metal doped NiO for the degeadation of dyes and phenol.

8.2 Future Prospects

Photocatalysis is still in the developing stage and big challenges in this process are:

- One of the major challenges for the scientific community involved in photocatalytic research is to increase the spectral sensitivity of photocatalysts to visible light, which composes the largest part of solar radiation.
- It is desirable to have a semiconductor that could meet the requirements of band gap, chemical stability and photocatalytic activity together for environmental applications.
- Utilization of semiconductors, which can absorb visible light, to capture solar energy for production of hydrogen from water splitting.
- The mixed semiconductor photocatalysts (nanocomposites) should continue to be explored to obtain inexpensive and visible light absorbing alternatives.

- Physical properties such as charge transfer mechanisms, the critical nature of catalyst particle size, and the role of crystal structure of photocatalyst might also be thoroughly investigated.
- Effort is needed to to enhance the photocatalytic activities under visible light of anion-doped photocatalysts.
- Many interesting composite materials could be obtained using the soft chemical approach for photocatalytic applications in future.

REFERENCES

[1] L.K .Wang, Y.T. Hung, H.H. Lo, C.Yapijakis, Marcel Dekker, Inc., 2004.

[2] V.J. Inglezakis, S.G. Poulopoulos, Elsevier Science, 2006.

[3] R.B. Pojasek, Toxic and Hazardous Waste Proposal Vols. I-III, Ann Arbor Science, 1979.

[4] H. Morales-Rojas, R.A. Moss, Chem. Rev. 102 (2002) 2497.

[5] I. Casero, D. Sicilia, S. Rubio, D. Perez-Bendito, Water Res. 31 (1997) 1985.

[6] O. Legrini, E. Oliveros, A.M. Braun, Chem. Rev. 93 (1993) 671.

[7] W.H. Glaze, J.W. Kang, Ind. Eng. Chem. Res. 28 (1989) 1573.

[8] W.R. Haag, C.C.D. Yao, Environ. Sci. Technol. 26 (1992) 1005.

[9] G.R. Peyton, F.R. Huang, J.L. Burleson, W.H. Glaze, Environ. Sci. Technol. 16 (1982) 454.

[10] C.C. Chen, A.J. Chaudhary, S.M. Grimes, J. Hazard. Mater. 117 (2005) 171.

[11] K. Byrappa, A.K. Subramani, S. Ananda, K.M. Lokanatha Rai, R. Dinesh, M. Yoshimura, Bull. Mater. Sci. 29 (2006) 433.

[12] A. Mittal, J. Mittal, L. Kurup, J. Hazard. Mater. 136 (2006) 567.

[13] U. Kolb, S. A. Quaiser, M. Winter, and M. T. Reetz. Chem. Mater. 8 (1996) 1889.

[14] Kari Pirkanniemi , Mika Sillanp, Chemosphere 48 (2002) 1047.

[15] E. Gaffet, M. Tachikart, O. El Kedim, and R. Rahouadj. Mater. Charact. 36 (1996)

[16] Y. Yang, H. Chen, B. Zhao, X. Bao, J. Cryst. Growth 263 (2004) 447.

[17] Z.M. Dang, L.Z. Fan, S.J. Zhao, C.W.Nan, Mater. Sci. Eng. B 99 (2003) 386.

[18] Z.-L. Lu, E. Lindner, H.A. Mayer, Chem. Rev. 102 (2002) 3543.

[19] M. Toba, F. Mizukami, S. Niwa, K. Maeda, J. Chem. Soc., Chem. Commun. (1990)1211.

[20] J.B. Miller, E.I. Ko, J. Catal. 159 (1996) 58.

[21] B. L Cushing, V. L. Kolesnichenko, C. J. O'Connor, Chem. Rev. 2004 104 3893.

[22] L. L Hench, J. K.West, Chem. Rev. 1990 90 33 72, 185.

[23] A. Fujishima, K. Honda, Nature 238 (1972) 37.

[24] R. W. Matthews, Water Res. 24 (1990) 653.

[25] J. A Navio, F. J Marchena, C.Cerrillos, F. J. Pablos, Photochem. Photobiol. A Chem.71 (1993) 97.

[26] A.V Vorontsov, L. Davydov, E.P. Reddy, C. Lion, E.V. Savinov, P.G. Smirniotis, New J. Chem. 32 (2001) 732.

[27] I.K. Konstantinou, T.A. Albanis, Appl. Catal. B: Environ. 42 (2003) 319.

[28] Z.X. Lu, L. Zhou, Z.L. Zhang, W.L. Z.X. Shi, Xie, H.Y.Xie, D.W. Pang, P. Shen , Langmuir 19 (2003) 8765.

[29] M.A. Fox, M.T. Dulay, Chem. Rev. 93 (1993) 341.

[30] P. Pichat, Marcel Dekker Inc., NewYork, Basel (2003) 77.

[31] A. Maldotti, A. Molinari, R. Amadelli, Chem. Rev. 102 (2002) 3811.

[32] Di Zhou, Hong Wang, Xi Yao, Li-Xia Pang, and Huan-Fu Zhou, J. Am. Ceram. Soc. 91 (2008) 39.

[33] Ryoji Takahashi, Satoshi Sato, Toshiaki Sodesawa, Masanori Suzuki, Nobuyuki Ichikuni, Microporous and Mesoporous Materials 66 (2003) 197.

[34] Akihiko Kudo and Masahiko Sekizawa, Chem. Commune. 2000, 1371–1372

[35] Lei Ge, Materials Chemistry and Physics 107 (2008) 465–470

[36] E. Keidel, Farben-Zeitung 1929, 34, 1242.

[37] C. F. Goodeve, J. A. Kitchener, Transactions of the Faraday Society 1938, 34, 570.

[38] S. P. Pappas, R. M. Fischer, Journal of Paint Technology, 46 (1974) 65.

[39] J. Plotnikow, Allgemeine Photochemie, Auflage ed., Verlag Walter de Gruyter & co., Berlin (1936).

[40] J. H. Carey, J. Lawrence, H. M. Tosine, Bull. Environ. Contam. Toxicol, 16 (1976) 697.

[41] A. L. Pruden, D. F. Ollis, J. Catal., 82 (1983) 404.

[42] C. Y. Hsiao, C. L. Lee, D. F. Ollis, J. Catal., 82 (1983) 418.

[43] T. Tatsuma, S. Tachibana, A. Fujishima, J Phys Chem. B105 (2001) 6987.

[44] N. Serpone, A. Salinaro, Pure Appl. Chem. 71 (1999) 303.

[45] M. Grätzel, Nature (London, U. K.) 414 (2001) 338.

[46] J. L. Gole, J. D. Stout, C. Burda, Y. Lou, X. Chen, J. Phys. Chem. B 108 (2004) 1230.

[47] H. Irie, S. Washizuka, Y. Watanabe, T. Kako, K. Hashimoto, J. Electrochem. Soc. 152 (2005) E351.

[48] O. Diwald, T. L. Thompson, T. Zubkov, E. G. Goralski, S. D. Walck, J. T. Yates, Jr., J. Phys. Chem. B 108 (2004) 6004.

[49] A. Ghicov, J. M. Macak, H. Tsuchiya, J. Kunze, V. Haeublein, L. Frey, P. Schmuki, Nano Lett. 6 (2006) 1080.

[50] Y. Nosaka, M. Matsushita, J. Nishino, A. Y. Nosaka, Sci. Technol. Adv. Mat. 6 (2005) 143.

[51] T. Sato, Y. Aita, M. Komatsu, S. Yin, J. Mater. Sci., 41 (2006) 1433.

[52] S. Yin, K. Ihara, M. Komatsu, Q. Zhang, F. Saito, T. Kyotani, T. Sato, Solid State Commun. 137(2006) 132.

[53] M. Sathish, B. Viswanathan, R. P. Viswanath, C. S. Gopinath, Chem. Mater., 17 (2005) 6349.

[54] C. H. Rhee, J. S. Lee, S. H. Chung, J. Mater. Res., 20 (2005) 3011.

[55] T. A. Egerton, M. Janus, A. W. Morawski, Chemosphere, 63 (2006) 1203.

[56] J. H. Park, S. Kim, A. J. Bard, Nano Lett., 6 (2006) 24.

[57] Y. Li, D.-S. Hwang, N. H. Lee, S.-J. Kim, Chem. Phys. Lett. 404 (2005) 25.

[58] R. Wang, K. Hashimoto, A. Fujishima, M. Chikuni, E. Kojima, A. Kitamura, M. Shimohigoshi, T. Watanabe, Nature 388 (1997) 431.

[59] H. M. Kang, X. H. Kang, Transaction of Tianjin University 2(2): (1996) 44.

[60] N.H. Ince, G. Tezcanli, R.K. Belen, I.G. Apikyan, Appl. Cat. B: Environ. 29 (2001) 167.

[61] X. Tao, W. Ma, T. Zhang, J. Zhao, Angew. Chem. Int. Ed. 40 (2001) 3014.

[62] W. Ma, J. Li, X. Tao, J. He, Y. Xu, J.C. Yu, J. Zhao, Angew. Chem. Int. Ed. 42 (2003) 1029.

[63] H. Kudo, I. Kato, Tsuji, Chem. Lett. 33 (2004) 1534.

[64] Di Valentin, G. Pacchioni, A. Selloni, Chem. Mater. 17 (2005) 6656.

[65] Stéphane Abanades, Patrice Charvin, Gilles Flamant, Chemical Engineering Science 62 (2007) 6323.

[66] B. Sasi, K. G. Gopchandran, Nanotechnology 18 (2007) 115613.

[67] M.I. Badawya, Montaser Y. Ghalyb, Tarek A. Gad-Allaha, Desalination 194 (2006) 166.

[68] Jong-Tae Jung, Jong-Oh Kim, Jae-Young Choi, Materials Science Forum 569 (2008) 29.

[69] J.C. Zhang, L.L. Gao, W.L. Cao, Chin. J. Inorg. Chem. 19 (2003) 934.

[70] He Rong, Qian Xue-feng, Yin Jie, Xi Hong-an, Bian Li-juan ,Zhu Zi-kang ,Colloids and Surfaces A: Phys. Eng. Aspects, 220 (2003) 151.

[71] Pang Qi, Shi Jianxin, Liu Yu, Xing Desong, Gong Menglian, Axe Ningsheng, Mater. Sci. Eng. B103 (2003) 57.

[72] Yin Hengbo, Yamamoto Tetsushi, Wada Yuji, Yanagida Shozo, Mater. Chem. Phys. 83 (2004) 66.

[73] Anderson Kris, Fernández Silvia Cortiñas, Hardacre Christopher, Marr Patricia C, Inorg. Chem. Commun. 7 (2004) 73.

[74] Kaskel Stefan, Schlichte Klaus, Kratzke Tobias J.Mol. Catal. A: Chem. 208 (2004) 291.

[75] D. W. Lee, B. K. Kim, Mater. Lett. 58 (2004) 378.

[76] R. Piticescu, Barbara Malic, Marija Kosec, A. Motoc, C. Monty, Iulia Soare, T. Kosmac , A. Daskobler , J. Euro. Ceram. Soc. 24 (2004)1941.

[77] A. Rouanet, G. Pichelin, C. Roucau, E. Snoeck, C. Monty. , Nanophase Materials Kluwer Academic Publishers, Dordrecht, The Netherlands (1994).

[78] B.L. Cushing, V.L. Kolesnichenko, C.J. O'Connor, Chem. Rev. 104 (2004) 3893.

[79] Y. Zhang, G. Li, Y. Wu, Y. Luo, and L. Zhang. J. Phys. Chem. B, 109 (2005) 5478.

[80] J. H. Harreld, W. Dong, and B. Dunn. Mater. Res. Bull., 33 (1998) 561.

[81] J. W. Long, K. E. Swider, R. M. Stroud, D. R. Rolison, Electrochem. Solid State Lett 3 (2000) 453.

[82] J. W. Long, A. L. Young, and D. R. Rolison. J. Electrochem. Soc. 150 A (2003) 1161.

[83] Amyn S. Teja, Pei-Yoong Koh, Progress in Crystal Growth and Characterization of Materials 55 (2009) 22.

[84] P.K. Khanna, Narendra Singh, Shobhit Charan, Materials Letters 61 (2007) 4725.

[85] Xingxue Wang, Sheng Meng, Xiali Zhang, Haitao Wang , Wei Zhong, Qiangguo Du , Chemical Physics Letters 444 (2007) 292.

[86] Xichen Cai, Kelechi C. Anyaogu, and Douglas C. Neckers, J. Am. Chem. Soc., 129, (2007) 11324.

[87] Srivatsan Sathyamurthy, Keith J. Leonard, Reza T. Dabestani, M. Parans Paranthaman, Nanotechnology 16 (2005) 1960.

[88] M. Galceran, M. C. Pujol, M. Aguil, F. D´ıaz, J Sol-Gel Sci Techn 42 (2007)79.

[89] V. Gombac , L. D. Rogatis , A. Gasparotto , G. Vicario , T. Montini , D. Barreca , G. Balducci , P. Fornasiero , E. Tondello , M. Graziani , Chemical Physics 339 (2007) 111.

[90] Mona Saif , M.S.A. Abdel-Mottaleb, Inorganica Chimica Acta 360 (2007) 2863.

[91] P. Borker, A.V. Salker, Mater. Sci. Eng. B 133 (2006) 55.

[92] H.M. Coleman, B.R. Eggins, J.A. Byrne, F.L. Palmer, E. King, Appl. Catal. B: Environ. 24 (2000) L1.

[93] C.S. Hong, Y.Wang, B. Bush, Chemosphere 36 (1998) 1653.

[94] Y. Ohko, I. Ando, C. Niwa, T. Tatsuma, T. Yamamura, T. Nakashima, Y. Kubota, A. Fujishima, Environ. Sci. Technol. 35 (2001) 2365.

[95] Y. Wang, C. Hong, Water Res. 34 (2000) 2791.

[96] I.K. Konstantinou, T.A. Albanis, Appl. Catal. B: Environ. 49 (2004) 1.

[97] H. Zollinger (Ed.), 2nd revised ed., VCH, 1991.

[98] A.G.S. Prado, L.B. Bolzon, C.P. Pedroso, A.O. Moura, L.L. Costa, Appl. Catal. B: Environ. 82 (2008) 219–224.

[99] W.Z. Tang, H. An, Chemosphere 31 (1995) 4158.

[100] O.J. Hao, H. Kim, P.C. Chiang, Environ. Sci. Technol. 30 (2000) 449.

[101] M. Sleiman, D. Vildozo, C. Ferronato, J.-M. Chovelon, Appl. Catal. B: Environ. 77 (2007) 1.

[102] Y.M. Slokar, A.M.L. Marechal, Dyes Pigm. 37 (4) (1998) 335.

[103] W.G. Kuo, Water Res. 26 (1992) 881.

[104] N.H. Ince, D.T. Gonenc, Environ. Technol. 18 (1997) 179.

[105] E. Forgacs, T. Cserhati, G. Oros, Environ. Int. 30 (2004) 953.

[106] I. Arslan, A.I. Balcioglu, J. Chem. Technol. Biotechnol. 76 (2001) 53.

[107] F.C. Wu, T.seng, R.L., Juang, R.S., Water Research 35 (2001) 613.

[108] N. Daneshvar, D. Salari, A.R. Khataee, J. Photochem. Photobiol. A: Chem. 162 (2004) 317.

[109] P. Reddy, A. Venugopal, M. Subrahmanyam, Appl. Catal. B: Environ. 69 (2007) 164.

[110] M. Saquib, M.A. Tariq, M. Faisal, M. Muneer, Desalination 219 (2008) 301.

[111] J. Sun, X. Wang, J. Sun, R. Sun, S. Sun, L. Qiao, J. Mol. Catal. A: Chem. 260 (2006) 241.

[112] C. Dominguez, J. Garcia, M.A. Pedraz, A. Torres, M.A. Galan, Catalysis Today 40 (1998) 85.

[113] T. Robinson, G. Mcmullan, R. Marchant, P. Nigam, Bioresource Technology 77 (2001) 247.

[114] V. Meshko, L. Markovska, M. Mincheva, A.E. Rodrigues, Water Research 35 (2001) 3357.

[115] Belgin Gözmena, Meral Turabikb, Journal of Hazardous Materials 164 (2009) 1487.

[116] Yuexu Lin, Shen Lin, Materials Letters 63 (2009) 1169.

[117] Lei Ge, Journal of Molecular Catalysis A: Chemical 282 (2008) 62.

[118] Sampa Chakrabarti , Basab Chaudhuri , Sekhar Bhattacharjee , Paramita Das, Binay Kanti Dutta , Journal of Hazardous Materials 154 (2008) 230.

[119] M.R. Sohrabi, Journal of Hazardous Materials 153 (2008) 1235.

[120] Chung-Hsin Wu, Journal of Hazardous Materials 153 (2008) 1254.

[121] K.M. Parida, N. Sahu, N.R. Biswal, B. Naik, A.C. Pradhan, Journal of Colloid and Interface Science 318 (2008) 231.

[122] N. Sobana, M. Swaminathan, Solar Energy Materials & Solar Cells 91 (2007) 727.

[123] J.C. Garcia, J.L. Oliveira, A.E.C. Silva, C.C. Oliveira, J. Nozaki , N.E. de Souza , Journal of Hazardous Materials 147 (2007) 105.

[124] Huihu Wang , Changsheng Xie , Wei Zhang , Shuizhou Cai , Zhihong Yang , Yanghai Gui , Journal of Hazardous Materials 141 (2007) 645.

[125] A. Valentine Rupa, D. Manikandan, D. Divakar, T. Sivakumar, Journal of Hazardous Materials 147 (2007) 906.

[126] Yin Zhao, Chunzhong Li, Xiuhong Liu, Feng Gu, Journal of Alloys and Compounds 440 (2007) 281.

[127] Chien-Tsung Wang, Journal of Non-Crystalline Solids 353 (2007) 1126.

[128] Theodora Papadama, Nikolaos P. Xekoukoulotakis, Ioannis Poulios, Dionissios Mantzavinos, Journal of Photochemistry and Photobiology A: Chemistry 186 (2007) 308.

[129] Yongqing Zhai, Shaoyang Zhang, Hui Pang, Materials Letters 61 (2007) 1863.

[130] Galina N. Kryukova , Galina A. Zenkovets , Alexei A. Shutilov ,Michael Wilde , Kerstin Gu¨nther , Dieter Fassler , Klaus Richter ,Applied Catalysis B: Environmental 71 (2007) 169–176

[131] Mohamed Mokhtar Mohameda, I. Othman, R.M. Mohamed, Journal of Photochemistry and Photobiology A: Chemistry 191 (2007) 153.

[132] Yu Zhiyong , M. Bensimon , V. Sarria , I. Stolitchnov , W. Jardim ,D. Laub , E. Mielczarski , J. Mielczarski , L. Kiwi-Minsker , J. Kiwi , Applied Catalysis B: Environmental 76 (2007) 185.

[133] Niyaz Mohammad Mahmoodi,, Mokhtar Arami , Nargess Yousefi Limaee , Kamaladin Gharanjig , Faramaz Doulati Ardejani , Colloids and Surfaces A: Physicochem. Eng. Aspects 290 (2006) 125.

[134] M. Muruganandham, M. Swaminathan, Journal of Hazardous Materials B135 (2006) 78.

[135] B. Neppolian, H.C. Choi, S. Sakthivel, B. Arabindoo, V. Murugesan, Chemosphere 46 (2002) 1173.

[136] C. Lizama, J. Freer, J. Baeza, H. Mansilla, Catal. Today 76 (2002) 235.

[137] A.A. Khodja, T. Sehili, J. Pilichowski, P. Boule, J. Photochem. Photobiol. A: Chem. 141 (2001) 231.

[138] N. Xu, Z. Shi, Y. Fan, J. Dong, J. Shi, M.Z.C. Hu, Ind. Eng. Chem. Res. 38 (1999) 373.

[139] N.L. Stock, J. Peller, K. Vinodgopal, P. Kamat, Environ. Sci. Technol. 34 (2000) 1747.

[140] A. Pandurangan, P. Kamala, S. Uma, M. Palanichamy, V. Murugesan, Indian J. Chem. Technol. 8 (2001) 496.

[141] I. Poulios, I. Tsachpinis, J. Chem. Technol. Biotechnol. 74 (1999) 349.

[142] A. Behnajady, N. Modirshahla, R. Hamzavi, J. Hazard. Mater. B 133 (2006) 226.

[143] ChangChun Chen, Ping Liu, ChunHu Lu, Chemical Engineering Journal 144 (2008) 509.

[144] B. Swarnalata, Y. Anjaneyulu, J. Mol. Catal. A: Chem. 223 (2004) 161.

[145] A. Akyol, M. Bayramoglu, J. Hazard. Mater. B 124 (2005) 241.

[146] M.J. Height, S.E. Pratsinis, O. Mekasuwandumrong, P. Praserthdam, Appl. Catal.B: Environ. 63 (2006) 305.

[147] C.C. Chen, J. Mol. Catal. A: Chem. 264 (2007) 82.

[148] A. Cybulski, J. Trawczy´nski, Appl. Catal. B: Environ. 47 (2004) 1.

[149] K.H. Wong, S. Tao, R. Dawson, P.K. Wong, Hazard. Mater. B 109 (2004) 149.

[150] J.C. Yu, W. Ho, J. Yu, S.K. Hark, K. Lu, Langmuir 19 (2003) 3889.

[151] Chwei-Huann Chiou, Cheng-Ying Wu, Ruey-Shin Juang , Chemical Engineering Journal 139 (2008) 322.

[152] M.A. Gondal, M.N. Sayeed, Z. Seddigi, Journal of Hazardous Materials 155 (2008) 83.

[153] Eduardo Bessa Azevedo, Francisco Radler de Aquino Neto, Ma´rcia Dezottic, Applied Catalysis B: Environmental 54 (2004) 165.

[154] Rog´erio Jos´e Ara´ujo L'Amoura, Eduardo Bessa Azevedo, Selma Gomes Ferreira Leite, M´arcia Dezotti, Separation and Purification Technology 60 (2008) 142.

[155] J. Luka , M. Klementova´ , P. Bezdic˘ka , S. Bakardjieva , J. S ubrt ,L. Szatma´ry , Z. Bastl , J. Jirkovsky , Applied Catalysis B: Environmental 74 (2007) 83.

[156] J. Arana, E. Pulido Melian, V.M. Rodrıguez L´opez, A. Pe˜na Alonso, J.M. Dona Rodrıguez, O. Gonzalez D´ıaz, J. Perez Pe˜na , Journal of Hazardous Materials 146 (2007) 520.

[157] N. Venkatachalam, M. Palanichamy, V. Murugesan, Journal of Molecular Catalysis A: Chemical 273 (2007) 177.

[158] Guo Zhifeng, Ma Ruixin, Li Guojun, Chemical Engineering Journal 119 (2006) 55.

[159] Beat Wawrzyniak, AntoniWaldemarMorawski, and Beata Tryba, International Journal of Photoenergy (2006) 1.

[160] Wang Zhengpeng, Cai Weimin, Hong Xiaoting, Zhao Xiaolian, Xu Fang, Cai Chuenguang, Applied Catalysis B: Environmental 57 (2005) 223.

[161] Andrzej Sobczy´nski, Lukasz Duczmal, Wojciech Zmudzi´nski, Journal of Molecular Catalysis A: Chemical 213 (2004) 225.

[162] Y. Tamaki, A. Furube, M. Murai, K. Hara, R. Kotoh, M. Tachiya, J. Am. Chem. Soc. 128 (2006) 416.

[163] C. Karunakaran, R. Dhanalakshmi, Int. J. Chem. Kinet. 41 (2009) 275.

[164] T.J. Kuo, C.N. Lin, C.L. Kuo, M.H. Hung, Chem. Mater. 19 (2007) 5143.

[165] F.D. Mai, C.S. Lu, C.W. Wu, C.H. Huang, J.Y. Chen, C.C. Chen, Sep. Purif. Technol. 62 (2008) 4236.

[166] C.C. Chen, J. Mol. Catal. A: Chem. 264 (2006) 82.

[167] A.H. Akyol, C. Yatmaz, M. Bayramoblu, Appl. Catal. B: Environ. 54 (2004) 19.

[168] Narayanasamy Sobana, Manickavasakam Muruganandam, Meenakshisundaram Swaminathan, Catalysis Communications 9 (2008) 262.

[169] M.C. Hidalgo, M. Maicu, J.A. Navı, G. Colo´n, Applied Catalysis B: Environmental 81 (2008) 49.

[170] N. Hadj Salah, M. Bouhelassa, S. Bekkouche, A. Boultif, Desalination 166 (2004) 347.

[171] J.R. Darwent, A. Mills, J. Chem. Soc., Faraday Trans. 2 78 (1982) 359.

[172] K. Sayama, K. Mukasa, R. Abe, Y. Abe, H. Arakawa, J. Photochem. Photobiol. A 148 (2002) 71.

[173] K.G. Kim, E.D. Jeong, P.H. Borse, S. Jeon, K. Yong, J.S. Lee, W. Li, S.H. Oh, Appl. Phys. Lett. 89 (2006) 064103.

[174] T. Arai, M. Yanagida, Y. Konishi, Y. Iwasaki, H. Sugihara, K. Sayama, Cat. Commun. 9 (2008) 1254.

[175] E. Stathatos, P. Lianos, C. Tsakiroglou, Micropor. Mesopor. Mater. 75(2004) 255.

[176] A. Kumbhar, G. Chumanov, J. Nanoparticle Res. 7 (2005) 489.

[177] M.R. Hoffmann, S.T. Martin, W. Choi, D.W. Bahnemann, Chem. Rev. 95 (1995) 69–96.

[178] S. Sakthivel, B. Neppolian, M.V. Shankar, B. Arabindoo, M. Palanichamy, V. Murugesan, Sol. Energy Mater. Sol. Cells 77 (2003) 65.

[179] M. Huang, C. Xu, Z. Wu, Y. Huang, J. Lin, J. Wu, Dyes Pigm. 77 (2008) 327.

[180] M.S.T. Gonclaves, A.M.F. Oliveira-Campose, E.M.M.S. Pinto, P.M.S. Plasencia, M.J.R.P. Queiroz, Chemosphere 39 (1999) 781.

[181] C. G. Silva, J. L. Faria, Journal of Molecular Catalysis A: Chemical 305 (2009) 147.

[182] E. Bizani, K. Fytianos, I. Poulios, V. Tsiridis, J. Hazard. Mater. 136 (2006) 85.

[183] I. Poulios and I. Aetopoulou, Environmental Technology 20 (1999), 479.

[184] J. Zhao, T. Wu, K. Wu, K. Oikawa, H. Hidaka, N. Serpone, Environ. Sci. Technol. 32 (1998) 2394.

[185] R.J. Davis, J.L. Gainer, G.O. Neal, I.W.Wu, Water Environ. Res. 66 (1994) 50.

[186] W.Z. Tang, H. An, Chemosphere 31 (1995) 4171.

[187] Feng Chen, Weiwei Zou, Wenwu Qu, Jinlong Zhang, Catalysis Communications 10 (2009) 1510.

[188] D.F. Ollis, E. Pelizzetti, N. Serpone, Environ. Sci. Technol. 25 (1991) 1522.

[189] U. Stafford, K.A. Gray, P.V. Kamat, J. Catal. 167 (1997) 25.

[190] M. Muneer, H.K. Singh, D.W. Bahnemann, Chemosphere 49 (2002) 193.

[191] H.R. Pouretedal, A. Norozi, M.H. Keshavarz, A. Semnani, J. Hazard. Mater. 162 (2009) 674.

[192] T. Sauer, G.C. Neto, H.J. José, R.F.P.M. Moreira, J. Photochem. Photobiol. A Chem. 149 (2002) 147.

[193] C. Guillard, J. Photochem. Photobiol. A Chem. 135 (2000) 65.

[194] M. Qamar, M. Saquib, M. Muneer, Dyes and Pigments 65 (2005) 1.

[195] M.A. Tariq, M. Faisal, M. Muneer, J. Hazard. Mater. 127 (2005) 172.

[196] I. Poulios, E. Micropoulou, R. Panou, K. Kostopoulou, Appl. Catal. B Environ. 41 (2003) 345.

[197] M.S.T. Goncalves, A.M.F. Oliveira-Compos, E.M.M.S. Pinto, P.M.S Plasencia, M.J.R.P. Queiroz, Chemosphere 39 (1999) 781.

[198] T. Velegraki, I.Poulios, M.C. Charalabaki, N. Kalogerakis, P. Samaras, D. Mantzavinos, Appl. Catal. B-Environ. 62 (2006) 159.

[199] Rajeev Jain, Menasha Shrivasta, Journal of Hazardous Materials 152(2008) 216.

[200] H. Yu, X. Zheng, Z. Yin, F. Tao, B. Fang, K. Hou, Chin. J. Chem. Eng. 15 (6) (2007) 802.

[201] C. Guillard, J. Disdier, C. Monnet, J. Dussaud, S. Malato, J. Blanco, M.I. Maldonado, J.M. Herrmann, Appl. Catal. B: Environ 46 (2) (2003) 319.

[202] W. Baran, A. Makowski, W. Wardas, Chemosphere 53 (2003) 87.

[203] C.H. Wu, H.W.Chang, J.M. Chern, J. Hazard. Mater. B 137 (2006) 336.

[204] O.E Kartal, M. Erol, H. Oguz, Chem. Eng. Technol. 24 (2001) 645.

[205] T. Velegraki, I. Poulios, M. Charalabaki, N. Kalogerakis, P. Samaras, D. Mantzavinos, Appl. Catal. B 62 (2006) 159.

[206] N. Daneshvar, M. Rabbani, J. Photochem. Photobiol. A168 (2004) 39.

[207] C. Karunakaran, S.Senthilvelan, Catal. Comm., 6 (2005) 159.

[208] F. Zhang, J. Zhao, T Shen, E. Pelizzeti, N. Serpone, Appl. Catal. B 15 (1998) 156.

[209] N. Daneshvar, D. Salari, A.R. Khataee, J. Photochem. Photobiol. A: Chem., 157 (2003) 111.

[210] S. Chakrabarti, B.K. Dutta, J. Hazard. Mater. B112 (2004) 269.

[211] S Tanaka, U.K Saha, Water Sci. Tech. 30(1994)47.

[212] N.T Dung, N.V. Khoa, J.M. Herrmann, Inter. J. Photo Energ. 7 (2005) 11.

[213] M. A.Gondal, M. N.Sayeed, Journal of Environmental Science and Health Part A 43 (2008) 70.

[214] A.K. Subramani, K. Byrappa, S. Ananda, K.M. Lokanatha Rai, C. Ranganathaiah M. Munner, R. Phillips, S. Das, Res. Chem. Intermed. 23 (1997) 233.

[215] H. Wei, Y. Wu, N. Lun, F. Zhao, J. Mater. Sci. 39 (2004) 1305.

[216] W. Ao, J. Li, H. Yang, X. Zeng, X. Ma, Powder Technol. 168 (2006) 148.

[217] Z. L. Lu, E. Lindner, H.A. Mayer, Chem. Rev. 102 (2002) 3543.

[218] N. Daneshvar, D. Salari, A.R. Khataee, J. Photochem. Photobiol. A: Chem. 162 (2004) 317.

[219] D. Li, H. Haneda, Chemosphere 51 (2003) 129.

[220] M.A. Gondal, A. Hameed, Z.H. Yamani, A. Al-Suwaiyan, Appl.Catal. A 268 (2004) 159.

[221] A. Mills, J.Wang, D.F. Ollis, J. Catal. 243 (2006) 1.

[222] H. Fu, C. Pan, W. Yao, Y. Zhu, J. Phys. Chem. B 109 (2005) 22432.

[223] A. Sobczynski, L. Duczma, W. Zmudzinski, J. Mol. Catal. A: Chem. 213 (2004) 225.

[224] V.Iliev, A.Mihaylova, L. Bilyarska, J. Mol. Catal. A: Chem. 184 (2002) 121.

[225] E. Bizani, K. Fytianos, I. Poulios, V. Tsiridis, J. Hazard. Mater. 136 (2006) 85.

[226] I.K.Konstantinou, T.A. Albanis, Appl. Catal. B: Environ. 49 (2004) 1.

[227] J. A. Lewis, Journal of the American Ceramic Society 83(2000) 2341.

[228] A. Mills, J.Wang, D.F. Ollis, J. Phys. Chem. B 110 (2006) 14386.

[229] A. Sclafani, J.M. Herrmann, J. Photochem. Photobiol. A: Chem. 113 (1998)181.

[230] F.B. Li, X.Z. Li, Chemosphere 48 (10) (2002) 1103.

[231] S.X. Liu, Z.P. Qu, X.W. Han, C.L. Sun, Catal. Today 93 (5) (2004) 877.

[232] D. Dvoranova,V. Brezova, M. Mazur, M. Malati, Appl Catal B: Environ 37 (2002) 91.

[233] Paola AD, Marci G, Palmisano L, Schiavello M, Uosaki K, Ikeda S, J Phys Chem B 106 (2002) 637.

Curriculum Vitae

Personal Data

Name : KHIZAR HAYAT

Date of Birth : 1st December, 1965

Nationality : Pakistani

Permanent Address

: Village Khanpur Wadhra, Tehsil Shahpur Sadar, District Sarghoda, Punjab, Pakistan

Present Address : P.O. Box 8265, King Fahd University of Petroleum & Minerals, Dhahran- 31261, Saudi Arabia

Contact No. : Mob# 00966-553396134

E-mail : khizar_z2@yahoo.com, khizar@kfupm.edu.sa

Education

2006-2011 **Doctor of Philosophy (Ph.D.) in Chemistry**

"Laser Induced Photo-Catalytic Applications of Nanoscale Materials for Degradation of Dyes and Phenol"

King Fahd University of Petroleum & Minerals, Dhahran, Saudi Arabia.

- **Major in Analytical Chemistry**
- **Minor in Physical Chemistry**

1990-1992 **Master of Philosophy (M. Phil.) in Chemistry**

"Superconductivity in Mn-doped Ca-Y-Ba-Cu-Oxide Ceramics"

Quaid-i-Azam University, Islamabad, Pakistan

- **Major in Physical Chemistry**

1988-1990 **Master of Science in Chemistry**

Quaid-i-Azam University, Islamabad, Pakistan

Publications

1. **Khizar Hayat**, M. A. Gondal , Mazen M. Khaled, Shakeel Ahmed (2010), Kinetic study of laser-induced photocatalytic degradation of dye (alizarin yellow) from wastewater using nanostructured ZnO, Journal of Environmental Science and Health Part A, VOL 45, ISSUE 11

2. M. Qamar, M.A. Gondal, **K. Hayat**, Z.H. Yamani, K. Al-Hooshani (2009), Laser-enhanced Degradation of Dye Derivative Eosin Yellowish Catalyzed by n-type WO_3 Semiconductor Catalyst, J. Hazardous Materials, V 170, 584-589.

3. M. A. Gondal, **K.Hayat,** Mazen M. Khaled, Z. H.Yamani and Shakeel Ahmed (2010), Photocatalytic Removal of Hazardous Dye from Water using Nanostructured WO3 , International Journal of Nano Particles, VOL 3, ISSUE 5

4. **K. Hayat**, M.A. Gondal, M.M. Khaled, S. Ahmed, Effect of Operational Key Parameters on Photocatalytic Degradation of Phenol using Nano Nickel Oxide Synthesized by Sol Gel Method, Journal of Molecular Catalysis A: Chemical (2010)

5. **K. Hayat,** M.A. Gondal, M.M. Khaled, S. Ahmed, A.M., Shemsi, Nano ZnO Synthesis by Modified Sol Gel Method and its Application in Heterogeneous Photocatalytic Removal of Phenol from Water, Applied Catalysis A, General (2010)

6. **Khizar Hayat**, M. A. Gondal, Mazen M. Khaled, Shakeel Ahmed, Laser induced Photocatalytic degradation of Safranin-O and the effect of different parameters using nanocrystalline WO3 (Accepted and in Press)

Conference papers

1. M. A. Gondal, **K. Hayat**, M. N. Sayeed (2009), Laser induced Photo-catalytic degradation of organic contaminants from water using semiconductor metal oxides, paper 3C-O646 6th world Congress on Oxidation Catalysis, 5-10th July, 2009 Lille, France

2. M A. Gondal, **K.Hayat**, Z. H.Yamani and S.Ahmed (2009) Removal of Hazardous Organic Dye from Water using Nanostructured Metal Oxides and Lasers, International Conference on Nanotechnology and Advanced Material (ICNOM 2009) Bahrain,4-7 May, 2009.

3. M. A. Gondal, M. N. Sayeed and **K. Hayat** (2009), Laser Enhanced Photo-catalytic Removal of Toxic Organic Matter (C_6H_5OH) from Waste Water using different Semiconductor Catalysts , Tiyabah International Conference on Chemistry, March, 21-23, 2009, Madina, Saudi Arabia.